Susceptibility to exertional heat illness

Lois Catherine Marie Gardner

Submitted in accordance with the requirements for the degree of Doctor of Philosophy

The University of Leeds
Faculty of Medicine and Health
School of Medicine
Leeds Institute of Biomedical and Clinical Sciences

February 2018

Declaration

The candidate confirms that the work submitted is her own and that appropriate credit has been given where reference has been made to the work of others.

Acknowledgements

Firstly, I would like to acknowledge The Colt Foundation for funding my doctorate and for taking an interest in my work throughout.

I would like to thank my supervisors Marie-Anne and Phil for their continued support and direction throughout my MSc and PhD and for providing me with the opportunity to present my research at national and international conferences.

I am grateful to Dorota for her guidance throughout the NGS analysis and to Clare Taylor for training us both on Fluidigm. Many thanks to Catherine for providing help willingly whenever I have needed it and to Rachel for our daily debrief sessions. Thanks to Essam for generously giving up his time to help me go through IVCT traces and to all past and present members of the MH unit who have offered their support. I would also like to thank Sarah for the laughs over the last four years and for watching me practice countless presentations!

I would like to thank Alastair Droop for his invaluable bioinformatics support and for introducing me to the world of high-performance computing. I am also grateful to the staff at the Leeds NGS facility for their technical assistance throughout my project.

Massive thanks to Carol and Dan at the INM, for all their hard work on the heat tolerance test and for happily providing additional patient information whenever I have asked for it. Thank you to Paul Allen, Jon Ramsey and Shane for their guidance during my time spent at UC, Davis and to Gaëlle for her warm welcome and for showing me the Californian sights.

Thank you to my family and friends for their constant reassurance and for helping me to maintain the work-life balance. Finally, and most importantly, I would like to thank Michael, for his unfailing support and for managing to keep a smile on my face throughout!

Abstract

Exertional heat illness (EHI) is a clinically important disorder, notifiable in military personnel, and is characterised by an inability to thermoregulate. Research investigating the genetic risk factors contributing to this potentially fatal condition is limited and the pathophysiology of EHI remains poorly understood. EHI shares a similar clinical manifestation to malignant hyperthermia (MH), a pharmacogenetic disorder associated with calcium dysregulation in skeletal muscle. Interestingly, 34% of the EHI patients in this study developed muscle contractures during an *in vitro* contracture test (IVCT), the gold-standard diagnostic test for MH susceptibility.

The coding regions of fifty genes relating to calcium homeostasis and energy metabolism were sequenced in sixty-four EHI patients using a next-generation sequencing (NGS) approach. Many of these genes have been previously implicated in MH, congenital myopathies and metabolic disorders. Seventy-nine rare (minor allele frequency ≤1%) and potentially pathogenic (CADD-score ≥15) non-synonymous variants were identified across twenty-four genes, potentially conferring susceptibility to EHI. Around 75% of MH susceptible individuals in the UK carry a diagnostic ryanodine receptor type-1 (*RYR1)* variant. Uncharacterised *RYR1* variants were identified in 38% of EHI patients in this study, 16% of which were annotated as rare and potentially pathogenic.

Global gene expression profiles were examined in a heterozygous RyR1 R163C mutant mouse model associated with EHI and MH to investigate the acute heat stress response. These mice demonstrated elevated basal O_2 consumption and increased expression of heat shock proteins (HSPs) after heat exposure. RNA-seq was also used to explore the exertional heat stress response in a cohort of EHI, MH and healthy control volunteers. Elevated HSPs were detected in the blood of MH individuals along with a basal reduction of key oxidative phosphorylation enzymes, both suggestive of oxidative stress. In contrast, increased expression of metabolic enzymes required for acetyl-coA synthesis were detected in both EHI and MH susceptible patients relative to controls.

This thesis highlights the likely role of calcium dysregulation and energy metabolism in the pathophysiology of this complex disorder.

List of Abbreviations

Abbreviation	Description
1000G	1000 Genomes Database
ACADM	Acyl-CoA dehydrogenase, medium chain
ACADVL	Acyl-CoA dehydrogenase, very long chain
AFA	Adaptive Focused Acoustics
AMPD1	Adenosine monophosphate deaminase 1
ANOVA	Analysis of variance
ANXA6	Annexin 6
ASP	Allele Specific Primer
ASPH	Aspartate beta-hydroxylase
ATP	Adenosine triphosphate
ATP2A1	ATPase, Ca++ transporting, cardiac muscle, fast twitch 1
BAQ	Base Alignment Quality
BH	Benjamini-Hochburg
BMR	Basal metabolic rate
BPM	Beats per minute
BWA MEM	Burrows–Wheeler aligner maximum exact matches
Ca^{2+}	Calcium ion
CACNA1S	Calcium channel, voltage-dependent, L type, alpha 1S subunit
CACNA2D1	Calcium channel, voltage-dependent, alpha 2/delta subunit 1
CACNB1	Calcium channel, voltage-dependent, beta 1 subunit
CACNG1	Calcium channel, voltage-dependent, gamma subunit 1
CADD	Combined Annotation Dependent Depletion
CALM1	Calmodulin 1 (phosphorylase kinase, delta)
CALR	Calreticulin
CAPN3	Calpain 3
Cas9	CRISPR associated protein 9
CASQ1	Calsequestrin 1
$Ca_v1.1$	Dihydropyridine receptor
CAV3	Caveolin 3
CCD	Central core disease
cDNA	complimentary DNA
CHERP	Calcium homeostasis endoplasmic reticulum protein
CLAMS	Comprehensive Lab Animal Monitoring System
CLCN1	Chloride channel, voltage-sensitive 1
CNM	Centronuclear myopathy
CPK	Creatine phosphokinase
CPT2	Carnitine palmitoyltransferase 2
CPVT	Catecholaminergic polymorphic ventricular tachycardia
CRAC	Ca^{2+} release-activated Ca^{2+}
CRISPR	Clustered Regularly Interspaced Short Palindromic Repeats
Cryo-EM	Cryogenic electron microscropy
DAVID	Database for Annotation, Visualization and Integrated Discovery
ddNTPs	dideoxynucleotide triphosphates
DIC	Disseminated intravascular coagulation
DNM2	Dynamin 2

EC	Excitation-contraction
ECACC	European Collection of Cell Cultures
ECCE	Excitation-coupled calcium entry
EDL	Extensor digitorum longus
EDTA	Ethylenediamine tetraacetic acid
EHI	Exertional heat illness
EHS	Exertional heat stroke
ELISA	Enzyme-linked immunosorbent assay
eQTL	Expression quantitative trait loci
ER	Exertional rhabdomyolysis
ETC	Electron transport chain
EVS	Exome Variant Server
ExAC	Exome Aggreation Consortium
FDR	False discovery rate
FKBP1A	FK506 binding protein 1A
gDNA	genomic DNA
GLM	Generalised linear model
GRCh37	Genome reference consortium human 37
GRCh38	Genome reference consortium human 38
GRCm38	Genome reference consortium mouse 38
GTEx	Genotype-Tissue Expression
GYS1	Glycogen synthase 1 (muscle)
GWAS	Genome-wide association study
H_2O_2	Hydrogen peroxide
HGMD	Human Gene Mutation Database
HI	Heat intolerant
HIC	Heat Illness Clinic
HOMER1	Homer homolog 1
HR	Heart rate
HRC	Histidine rich calcium binding protein
HRM	High resolution melting
HSD	Honest significant difference
HSF1	Heat shock factor 1
HSP	Heat shock protein
HSP90AA1	Heat shock protein 90kDa alpha (cytosolic)
HSPA4	Heat shock 70kDa protein 4
HSPB1	Heat shock 27kDa protein 1
HTT	Heat tolerance test
IDF	Israeli Defence Forces
IFC	Integrated fluidic circuits
IL	Interleukin
INDEL	Insertion or deletion
INM	Institute of Naval Medicine
IQR	Interquartile range
IVCT	*In vitro* contracture test
JMCs	Junctional membrane complexes
JPH1	Junctophilin 1
JPH2	Junctophilin 2
JSRP1	Junctional sarcoplasmic reticulum protein 1

K^+	Potassium ion
KDS	King Denborough Syndrome
LASSO	Least Absolute Shrinkage and Selection Operator
LFC	Log fold-change
LOAM	Late-onset axial myopathy
LOVD	Leiden Open Variation Database
LPIN1	Lipin 1
LSP	Locus Specific Primer
MAF	Minor allele frequency
MARC1	Medical Advanced Research Computer 1
MCU	Mitochondrial calcium uniporter
MH	Malignant hyperthermia
MHN	Malignant hyperthermia normal
MHS	Malignant hyperthermia susceptible
MHSh	Malignant hyperthermia susceptible to halothane only
MmD	Multi-minicore disease
MMPC	Mouse Metabolic Phenotyping Center
MoD	Ministry of Defence
MODREC	Ministry of Defence Research Ethics Committee
mRNA	Messenger RNA
MRS	^{31}P magnetic resonance spectroscopy
mtDNA	mitochondrial DNA
Na^+	Sodium ion
NAM	Native American Myopathy
NAO	National Audit Office
NCX	Na^+/Ca^{2+} exchanger
NEB	Nebulin
NGS	Next-generation sequencing
NHGRI	National Human Genome Research Institute
NHS	National health service
NO	Nitric oxide
NOS	Nitric oxide synthase
NTD	N-terminal domain
O_2^-	Superoxide
OH	Hydroxyl radical
$ONOO^-$	Peroxynitrite
ORAI1	ORAI calcium release-activated calcium modulator 1
OXPHOS	Oxidative phosphorylation
PANTHER	Protein Analysis Through Evolutionary Relationships
PBMC	Peripheral blood mononuclear cells
PCA	Principal component analysis
PCR	Polymerase chain reaction
PCr	Creatine phosphate
P_i	Inorganic phosphate
PolyPhen2	Polymorphism Phenotyping v2
PVALB	Parvalbumin
PYGM	Phosphorylase, glycogen, muscle (myophosphorylase)
RAM	Random access memory
RER	Respiratory exchange ratio

RFLP	Restriction fragment length polymorphism
RIN	RNA integrity numbers
RIN^e	RNA integrity numbers equivalent
rlog	regularised logarithm
RNS	Reactive nitrogen species
ROS	Reactive oxygen species
RQ	Respiratory quotient
RyR1	Ryanodine receptor type 1 channel
RYR1	Ryanodine receptor 1 (skeletal)
S100A1	S100 calcium binding protein A1
SAS	Special Air Service
SBS	Sequencing by synthesis
SCN4A	Sodium channel, voltage-gated, type IV, alpha subunit
SEPN1	Selenoprotein N, 1
SERCA	sarco/endoplasmic reticulum Ca2+-ATPase
SIFT	Sorting Intolerant From Tolerant
SLC8A1	Solute carrier family 8 (sodium/calcium exchanger), member 1
SLC8A3	Solute carrier family 8 (sodium/calcium exchanger), member 3
SNP	Single nucleotide polymorphism
SOCE	Store operated calcium entry
SR	Sarcoplasmic reticulum
SRL	Sarcalumenin
STA	Specific target amplification
STAC3	SH3 and cysteine rich domain 3
STIM1	Stromal interaction molecule 1
SYPL2	Synaptophysin-like 2
T_a	Ambient temperature
TAE	Tris Acetate EDTA
T_c	Core temperature
TLR-4	Toll-like receptor 4
TNF-α	Tumour necrosis factor alpha
TRDN	Triadin
TRIM72	Tripartite motif containing 72
TRPC	Transient receptor potential cation channel, subfamily C
TRPM6	Transient Receptor Potential Cation Channel, Subfamily M, Member 6
UCP	Uncoupling protein
UTR	Untranslated region
VLCAD	Very long-chain, acyl-CoA dehydrogenase
VO_2 max	Maximal oxygen consumption
WBC	White blood cell
WBGT	Wet bulb globe temperature
WES	Whole-exome sequencing
WGS	Whole-genome sequencing

Table of Contents

List of Figures

List of Tables

1 General Introduction

1.1 Exertional heat illness

1.1.1 Overview

Exertional heat illness (EHI) is a complex disorder whereby physiological and environmental factors are thought to interact to dysregulate thermal homeostasis (Muldoon *et al.*, 2007; Capacchione and Muldoon, 2009). The symptoms of EHI have been attributed to thermoregulatory failure caused by excessive metabolic heat production and ineffective heat dissipation (Epstein and Roberts, 2011). The subsequent rise in core temperature disrupts a wide range of physiological processes and can cause systematic damage to tissues (Capacchione and Muldoon, 2009). EHI can manifest as a spectrum of clinical phenotypes ranging from mild heat exhaustion through to severe and life-threatening cases of exertional heat stroke (EHS). Symptoms include hyperthermia, nausea, tachycardia, metabolic and respiratory acidosis, muscle cramps, rhabdomyolysis, elevated serum creatine phosphokinase (CPK), disruption of cerebral function, seizures, multi-organ failure, disseminated intravascular coagulation and death (Capacchione and Muldoon, 2009).

The major forms of EHI include heat syncope, exertional heat cramps, heat exhaustion and EHS, depending on the presenting clinical features. Heat syncope occurs when blood vessels dilate in an attempt to dissipate excess body heat, reducing blood pressure, which causes dizziness or fainting. This is often avoided by adhering to appropriate heat acclimatisation protocols. Heat cramps can either arise in isolation or as one of many symptoms during an EHI episode. Heat exhaustion is a mild manifestation of EHI, which can develop into EHS if left untreated (Glazer, 2005). Symptoms of heat exhaustion may include dizziness, weakness, headaches, nausea and general discomfort. EHS is the most severe form of EHI and arises once core temperature exceeds 40°C causing neurological impairment and in some cases multi-organ failure (Binkley *et al.*, 2002). The severity of EHI and the potential long-term neurological and physiological impact directly relates to the degree of hyperthermia sustained (Vicario, Okabajue and Haltom, 1986).

EHI often occurs in young, physically fit and otherwise healthy individuals, unlike classical heat stroke, which primarily develops in young children and the elderly. It is the unexplained and often recurrent cases of EHI that present the greatest likelihood of harbouring an underlying predisposition to the condition. The risk of developing EHI is

greater while exposed to hot and humid environmental conditions. EHI appears to be more common in males than females, for example 72.5% of all sport-induced heat illness cases treated in U.S. emergency departments between 2001-2009 were male (Disease Control and Prevention, 2011). This sex-specific difference in EHI prevalence has been associated with differences in subcutaneous fat content, aerobic fitness, sweating and the effect of oestrogen on thermoregulation (Kaciuba-Uscilko and Grucza, 2001; Iyoho, Laurel and Macfadden, 2017). It has also been suggested that thermoregulatory mechanisms are activated at a lower core temperature in women than in men, offering a protective effect against EHI (Knochel, 1996).

Both intrinsic and extrinsic factors are thought to contribute to the risk of developing EHI and therefore influence the severity of the final clinical phenotype (Epstein and Roberts, 2011). Intrinsic factors include genetics, fitness, acclimatization, illness, medication, and sleep quality. Extrinsic factors include exercise intensity and duration, clothing and equipment, ambient temp and relative humidity. EHI is predominantly observed in young and physically fit men when challenged with endurance exercise, commonly military personnel in hot climatic conditions (MoD, 2010; Armed Forces Health Surveillance Centre, 2015). EHI is a clinically important condition and a better understanding of the genetic factors contributing to this poorly understood disorder could help identify individuals at an increased risk of developing EHI. Prior knowledge of a genetic susceptibility to EHI is of considerable importance to military recruits, who are frequently deployed to countries with hot climates.

1.1.2 High profile cases

A British soldier died of exertional heat illness at Lucknow Barracks in Wiltshire in 2006. He was forced to endure an unlawful and unofficial physical punishment, known as ‘beasting’ (BBC NEWS, 2016). The army failed to identify and treat this fatal case of EHI. Years later, the deaths of three special forces soldiers from EHS while on a 16-mile selection march for the Special Air Service (SAS) reservists in 2013, again highlighted a lack of understanding into the diagnosis, treatment and prevention of this potentially fatal condition (BBC NEWS, 2015b; The Guardian, 2015). The victims were three of seventy-eight military personnel on selection exercises in the Brecon Beacons that day, with temperatures reaching 27˚C. EHI can often arise in temperate climates, where individuals have not acclimatised to heat. It is thought that the metabolic workload during these selection tests may have be higher than during standard military operations, due to the long duration and high intensity of the exercises (BBC NEWS,

2015a). A high profile inquest ruled the deaths a consequence of gross failures by the Ministry of Defence (MoD) on multiple levels (The Times, 2015), with two SAS instructors overseeing the selection test charged with neglect (BBC NEWS, 2015b, 2017). An EHI fatality made international headlines again in 2014 when a renowned travel journalist died while hiking on an assignment in a remote area of Uganda (Observer, 2014; Metro, 2015). Again, a lack of heat acclimatisation may have contributed to the development of EHS, along with limited access to medical aid and no access to hospital treatment. Civilian deaths have also been attributed to EHS, with cases more prevalent in endurance events (Disease Control and Prevention, 2011; Cooper *et al.*, 2016). Outside of the military, EHI is not a notifiable condition, so many cases go unrecorded.

1.1.3 Epidemiology of EHI

Figures produced by the UK armed forces' heat illness clinic (HIC), at the Institute of Naval Medicine (INM), estimate an annual incidence in the UK armed forces in excess of 500 military personnel, with ~145 being referred to the INM for heat tolerance testing (Roiz de Sa, pers. comm., 2016). The annual incidence of EHI cases in the British military peaked at 849 during summer campaigns in Iraq in 2003, with 161 of these requiring medical evacuation to the UK for further treatment (Ministry of Defence, 2017). A report produced by the National Audit Office (NAO) highlighted heat illness among the most commonly treated minor injuries or illnesses of military personnel (MoD, 2010). Further afield, the US armed forces reported more than 13,000 cases of EHI among military recruits between 2010-2014 including ~2,000 severe cases classified as EHS (Armed Forces Health Surveillance Centre, 2015). These figures highlight the international importance of this potentially life-threatening disorder and emphasise the need for research into the genetic susceptibility of EHI.

The incidence of EHI among U.S. high school athletes has been estimated at more than 9,000 cases a year, with risk increased during the summer months (Kerr *et al.*, 2013). In the United States, the highest incidence of EHI outside the military has been reported in American football players with 1 case of EHS reported per ~22,000 exposures, with approximately 24 deaths every ten years (Mueller and Cantu, 2009; Kerr *et al.*, 2013). Despite EHI being reported among the leading causes of mortality in young athletes, the epidemiology of this condition in the general population is limited (Maron *et al.*, 2009). The overall incidence of EHI is a challenge to estimate, as there are no consistent and well-documented records of EHI reactions outside of the military. The frequency of EHI

susceptibility may also be underestimated due to lower average levels of physical exertion in civilians relative to military personnel, thereby limiting risk. Therefore, the prevalence of EHI susceptibility in the general population remains unclear, with the genetic contribution to this complex disorder yet to be systematically explored.

1.1.4 Heat tolerance testing

Identification of individuals at increased risk of developing EHI has proved challenging, due to the limited understanding of EHI's complex aetiology and its varied presentation. Only two standardised heat tolerance tests (HTTs) are in routine use world-wide to determine the thermoregulatory capacity of military personnel. The tests developed by the UK's INM and the Israeli Defence Forces (IDF) have been modified to address the specific occupational and environmental demands of either the British or Israeli Armed Forces (Moran *et al.*, 2004; Moran, Erlich and Epstein, 2007; Kazman *et al.*, 2013; Roiz de Sa and House, 2015).

The UK HTT evaluates an individual's ability to reach thermal equilibrium, while working at a predefined relative intensity, in a temperature and humidity controlled chamber (Roiz de Sa and House, 2015). The chamber is set to 34°C (dry bulb temperature) with 40% relative humidity, producing a wet bulb globe temperature (WBGT) index of 27°C. Rectal temperature and sweat production are measured to assess the subject's thermoregulatory capacity. Healthy subjects are classified as those who are able to achieve a plateau in core temperature prior to reaching 39.5°C, while working at 60% of their maximal oxygen consumption (VO_2 max) on a treadmill. In contrast, the core temperature of heat intolerant individuals does not plateau and continues to rise. Once any subject reaches 39.5°C, the test is stopped and the individual is actively cooled.

Other HTTs have been developed within university sports physiology laboratories, but are not available for public use (Neal *et al.*, 2016). The INM adheres to strict guidelines on the physiological characterisation of EHI individuals (MoD, 2012; Roiz de Sa and House, 2015), ensuring that EHI classifications are consistent.

1.2 Exertional rhabdomyolysis

1.2.1 Overview

Exertional rhabdomyolysis (ER) is a frequent manifestation of EHI, but can also develop in the absence of hyperthermia. Mechanical and metabolic damage to skeletal muscle causes the breakdown of muscle cells, which releases cell contents including CPK and myoglobin into the bloodstream, which are biomarkers of this condition (Capacchione and Muldoon, 2009). It is important to note that these biomarkers are not specific to ER and can be elevated in several disorders affecting skeletal muscle. The risk factors for ER are similar to EHI, including exercise, heat, dehydration, muscle trauma, viral infections, alcohol and drug abuse (Voermans, Snoeck and Jungbluth, 2016). Myoglobinuria can develop as a complication of ER, and is defined as the presence of oxygen-carrying myoglobin molecules in the urine. Diagnosis of ER relies on the quantification of serum CPK concentrations, but there is no universal agreement regarding the normal range of CPK in blood, with baseline values dependent on ethnicity, sex and age (Neal *et al.*, 2009). ER is also often associated with myalgia and muscle cramps and can develop into a life-threatening condition if left untreated. Males appear to be at increased risk of developing ER compared to women, with male predominance reported at ~89% (Deuster *et al.*, 2013). Epidemiological data reveal that more than 12,000 episodes of ER are reported in the United States each year (Sinert *et al.*, 1994).

1.2.2 Pathophysiology of ER

Intracellular ion balance (low Na^+ Ca^{2+}, high K^+) is maintained by ion pumps and channels in the sarcolemmal membrane encasing skeletal muscle fibres. Muscle contraction and metabolic disturbance can cause damage to the sarcolemma, resulting in pump dysfunction. The subsequent rise in intracellular Na^+ and Ca^{2+} activates Ca^{2+} dependent proteases and phospholipases, which break down structural proteins releasing intracellular contents into the bloodstream (Voermans, Snoeck and Jungbluth, 2016). ER has been associated with several genetic conditions relating to human skeletal muscle, including muscular dystrophies, metabolic myopathies and disorders of calcium homeostasis (Figarella-Branger *et al.*, 1997; Melli, Chaudhry and Cornblath, 2005).

Around 30% of healthy individuals who present with rhabdomyolysis harbour *RYR1* mutations (Dlamini *et al.*, 2013). *RYR1* encodes the ryanodine receptor type 1 (RyR1), a Ca^{2+} release channel expressed in human skeletal muscle, required for skeletal muscle contraction. RyR1 forms a multi-protein complex, which coordinates Ca^{2+} release from the sarcoplasmic reticulum (SR) in a highly-regulated manner (Treves *et al.*, 2009; Boncompagni *et al.*, 2012; Tomasi *et al.*, 2012).

1.3 Association of EHI and ER with malignant hyperthermia

1.3.1 Malignant hyperthermia

Both EHI and ER have been associated with malignant hyperthermia (MH) on a phenotypic and genotypic level (Tobin *et al.*, 2001; Capacchione *et al.*, 2010; Dlamini *et al.*, 2013; Fiszer *et al.*, 2015). MH is a hypermetabolic disorder of skeletal muscle triggered by inhalational volatile anaesthetics, such as halothane and depolarising muscle relaxants, such as succinylcholine (Hopkins, 2008). The first documented case of MH was presented in 1960 (Denborough and Lovell, 1960), and since then the condition has been attributed to a disruption of calcium homeostasis, which causes an overload of cytosolic Ca^{2+}, resulting in myofilament activation and hyper-metabolism (Denborough, 1979; Fill *et al.*, 1990; Gillard *et al.*, 1991). In addition to massive Ca^{2+} release via RyR1 during a fulminant MH episode, a basal RyR1 Ca^{2+} leak is thought to contribute towards the pathogenesis of this condition (Yang *et al.*, 2007; Eltit *et al.*, 2012). Classic symptoms of MH can include hyperthermia, tachycardia, increased O_2 consumption, increased CO_2 production, acidosis, hyperkalaemia, muscular rigidity and rhabdomyolysis (Rosenberg *et al.*, 2015). MH is rare and has been described as an autosomal dominant condition. MH susceptibility has an estimated prevalence of between 1 in 2,000 and 1 in 10,000 (Monnier *et al.*, 2002; Miller, 2003); however, these may be conservative estimations, with only ~2% of the population exposed to inhalational anaesthetics each year and certain susceptible individuals not presenting with MH during every anaesthetic exposure (Robinson *et al.*, 2006). The clinical phenotype of MH is diverse, like EHI, and can present as a range of severities.

1.3.2 Genetics of MH

A substantial research effort over the last 20 years has advanced understanding of the genetic contribution to MH (Robinson *et al.*, 2006; Carpenter, Robinson, *et al.*, 2009;

Fiszer *et al.*, 2015); however, research into the genetic basis of EHI is only in its primary stages. To date, two genes have been explicitly implicated in MH, specifically *RYR1* and *CACNA1S* (Figure 1.1). These genes encode Ca^{2+} channels (RyR1 and $Ca_v1.1$) expressed in human skeletal muscle, which are central to excitation-contraction (EC) coupling. More recently, a *STAC3* variant p.W284S has been identified in families with Native American myopathy (NAM) and MH, although the variant has not yet been approved for the diagnosis of MH (Stamm *et al.*, 2008; Horstick *et al.*, 2013). SH3 and cysteine rich domain 3 (STAC3) binds to and regulates the RyR1-Cav1.1 complex, regulating Ca^{2+} release from the SR (Figure 1.1).

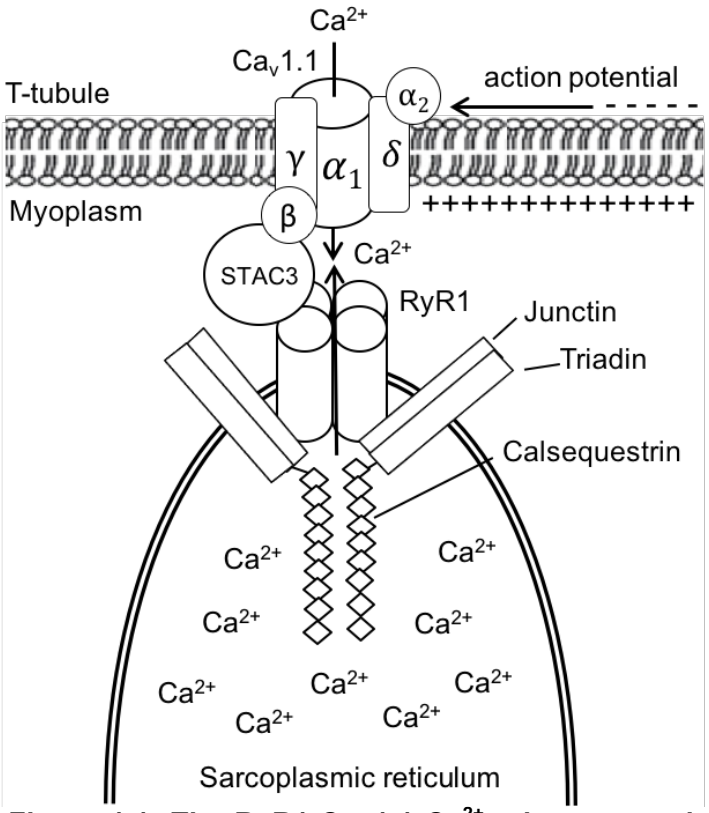

Figure 1.1: The RyR1-Cav1.1 Ca^{2+} release complex implicated in malignant hyperthermia including key regulatory proteins.

More than 200 heterozygous non-synonymous *RYR1* variants have been identified, only 42 of which have been functionally characterised (*European Malignant Hyperthermia Group*, 2017). This highlights the allelic heterogeneity of MH. Familial *RYR1* variants have been identified in 75.8% of the UK MH cohort (unpublished data) suggesting that additional genes may confer susceptibility to MH in a small proportion of families. The most common *RYR1* variant in the UK population is c.7300G>A, p.G2434R, accounting for ~50% of cases (Robinson *et al.*, 2006). This mutation has been shown to exhibit a milder phenotype relative to other functionally characterised *RYR1* variants (Carpenter,

Robinson, *et al.*, 2009). In some cases, multiple *RYR1* variants have been identified in one MH susceptible individual, indicating the genetic complexity of this condition (Fiszer *et al.*, 2015). Autosomal recessive inheritance of the *RYR1* p.R614C mutation, triggers porcine MH in response to stress, heat and halothane (Fujii *et al.*, 1991). The same mutation is conserved in humans and has been identified in the homozygous and heterozygous form in MH patients (Gillard *et al.*, 1991). The heat and halothane sensitive phenotype of MH pigs highlights the link between MH and EHI.

Less frequently, MH-associated genetic variants have been identified in *CACNA1S*, which encodes the α_1 pore-forming subunit of the dihydropyridine receptor ($Ca_v1.1$ complex) (Carpenter, Ringrose, *et al.*, 2009). $Ca_v1.1$ is a voltage-sensitive Ca^{2+} channel located in the sarcolemmal membrane, comprising five distinct subunits that allosterically interact with RyR1 regulating SR Ca^{2+} release (Proenza *et al.*, 2002). Only two genetic variants have been validated for diagnostic use, namely *CACNA1S* p.R1086H and p.R174W (Weiss *et al.*, 2004; Eltit *et al.*, 2012), accounting for 1.8% UK MH cases (unpublished data).

The genetic contribution to MH susceptibility is unaccounted for in ~22% of patients, suggesting that genes other than *RYR1* and *CACNA1S* may be responsible for MH in a subset of patients. Current hypotheses suggest that gene products which either interact with *RYR1* or are involved in the EC coupling mechanism or store-operated calcium entry (SOCE) could play a role in the pathophysiology of MH (Mickelson and Louis, 1996; Duke *et al.*, 2010; Rebbeck *et al.*, 2014). The dysregulation of calcium homeostasis has been shown to play a central role in the development of MH, therefore genes involved in this process in human skeletal muscle are fitting candidates to investigate the genetic cause of MH in unexplained cases.

1.3.3 *In vitro* contracture test diagnosis of MH

The current gold-standard diagnostic procedure for the identification of MH susceptible individuals is the *in vitro* contracture test (IVCT), which adopts a standardised protocol to quantify contractile responses to known RyR1 agonists, halothane and caffeine (EMHG, 1984; Hopkins *et al.*, 2015). *Ex vivo* muscle from MH susceptible patients produces abnormal muscle contractures upon exposure to these agents. The IVCT applies incremental concentrations of caffeine and halothane to freshly biopsied *vastus medialis* or *lateralis* muscle. Contracture of the electrically stimulated muscle is measured in tension (grams), with a conservative diagnostic threshold of a ≥0.2 g

baseline increase in force observed at 2% halothane and/ or 2mM caffeine (Figure 1.2). Pre-drug twitch height (g) is used as a measure of muscle viability (≥1 g).

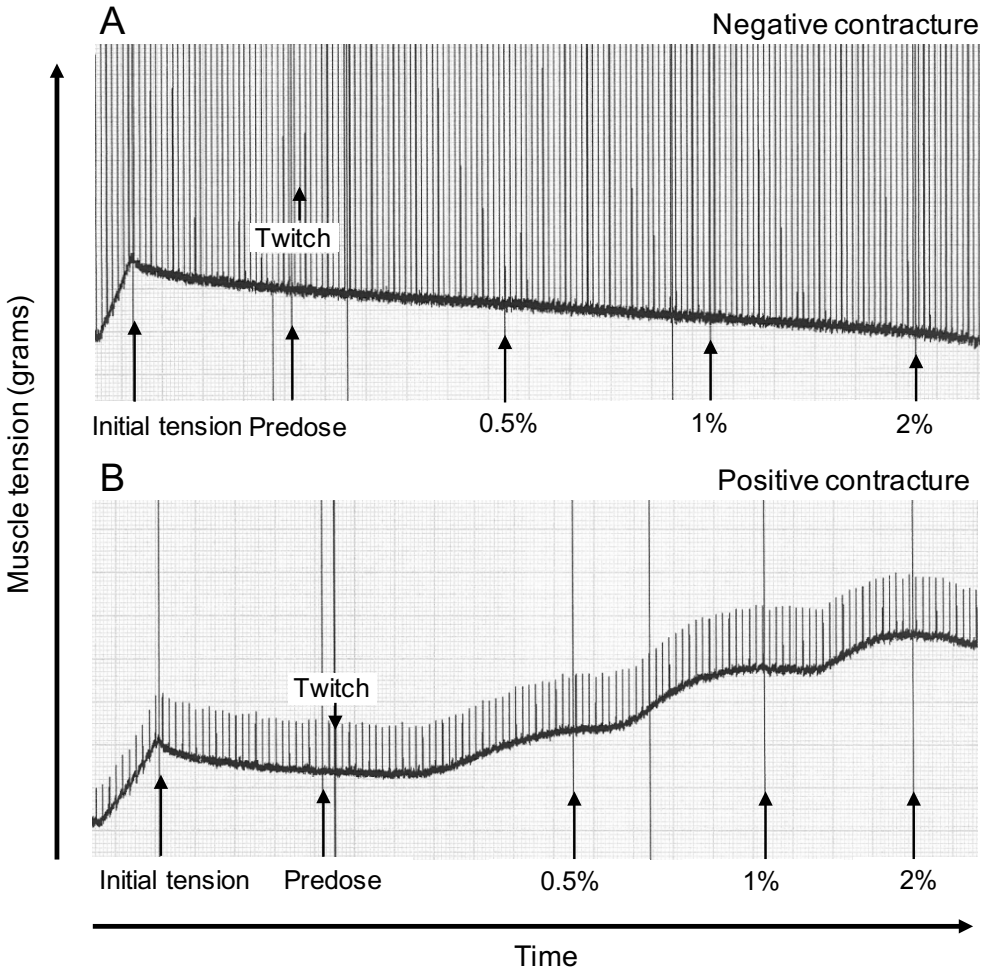

Figure 1.2: *In vitro* contracture test (IVCT) response to static halothane in a normal and MH susceptible patient sample. (A) This trace represents a normal response to incremental concentrations of halothane, with no increase in tension (g) detected. (B) This contrasting trace represents an abnormal contracture in response to 0.5% halothane.

Patients are either classified as MH susceptible to both agonists (MHShc), MH susceptible to halothane only (MHSh) or MH normal (MHN), depending on their contracture response. In recent years the invasive IVCT has been supported by and replaced with genetic screening of *RYR1* and *CACNA1S* where appropriate (Hopkins *et al.*, 2015). The UK MH Investigation Unit located at the University of Leeds is the only UK testing centre and routinely tests MH index cases and their family members. The unit also provides IVCT diagnoses and genetic testing for military personnel referred by the INM, which provides heat tolerance testing to the UK armed forces. Due to the proposed link between EHI and MH, UK military personnel who have experienced a

clinical EHI episode and subsequently fail two or more HTTs, or who have severe recurring exertional rhabdomyolysis, are offered an IVCT at the UK MH Investigation Unit. When EHI patients are referred for an IVCT an additional agonist ryanodine is applied to the muscle samples for research purposes. Biopsied muscle preparations are exposed to 1μM ryanodine and the time to onset of 0.2 g contracture is measured up to 30 minutes.

1.3.4 MH discordancy

Discordance between IVCT phenotype and *RYR1* genotype has been observed within 25.7% of UK MH families harbouring a familial *RYR1* variant (unpublished data). Discordant cases are defined as family members who are either phenotype positive (IVCT) and genotype negative (*RYR1*/ *CACNA1S* variant) or less frequently, phenotype negative and genotype positive. As family members with normal IVCT responses are not routinely genetically screened, there is an inevitable bias in the type of discordance reported. The existence of discordancy in MH families has complicated the move to replace the IVCT with predictive genetic testing. As a result, if a patient does not carry the familial variant they still require an IVCT to confirm their MHN status. MH discordancy was first reported 20 years ago, at a time when only known *RYR1* mutations were sequenced (Adeokun *et al.*, 1997; Fortunato *et al.*, 1999). Subsequent sequencing of the entire gene has uncovered additional *RYR1* variants within some MH families, disproving their discordancy (Robinson *et al.*, 2000, 2003). Discordant MH families highlight the genetic complexity of this condition, with the familial variant not segregating with IVCT classification. More than one pathogenic variant may confer susceptibility to MH in some families. The locus and allelic heterogeneity of MH, suggests that MH genetics is complex and may potentially involve modifying loci to account for the varied clinical and diagnostic phenotypes (Robinson *et al.*, 2003).

1.3.5 Treatment of MH

Fulminant MH reactions are treated with muscle relaxant dantrolene sodium, which inhibits extracellular Ca^{2+} entry via excitation-contraction coupling entry (ECCE) and increases the affinity of RyR1 to Mg^{2+} (Cherednichenko *et al.*, 2008; Choi, Koenig and Launikonis, 2017). Mg^{2+} inhibits RyR1 by competing with Ca^{2+} at the channel's activation site, while simultaneously binding to the inhibitory site (Steele and Duke, 2007). Dantrolene sodium is a potent drug and effectively reverses the effects of MH. MH

mortality rates have dramatically declined (<5%) since the introduction of dantrolene into the clinic in 1979 (Cannon, 2017). More recently, it has been proposed that dantrolene sodium could also be used to treat EHI and ER patients. A recent study attempted to evaluate the safety and efficacy of dantrolene sodium to treat EHI and concluded that use of dantrolene sodium increased the likelihood of full recovery (Hepner and Greenberg, 2017). There are currently no universal guidelines in place to standardise the administration of dantrolene sodium to treat EHI and ER.

1.3.6 MH association with EHI

MH has a similar clinical manifestation to EHI, suggesting that the pathophysiology of these conditions may be comparable (Muldoon *et al.*, 2004, 2008; Hopkins, 2007). Overlapping features include progressive hyperthermia, tachycardia, rhabdomyolysis, elevated serum CPK, mixed respiratory and metabolic acidosis, multi-organ failure, disseminated intravascular coagulation, and death (Capacchione and Muldoon, 2009). The link between MH and EHI was first proposed in 1991 when two members of the armed forces who had experienced EHI were classified MHSh by IVCT along with their relatives (Hopkins, Ellis and Halsall, 1991). This study provided the first evidence for an inherited skeletal muscle defect in EHI patients and although there has never been a controlled clinical study to link MH and EHI, several clinical case studies and genetic analyses have shown a clear relationship between the two disorders (reviewed in Hopkins, 2007; Muldoon et al., 2008; Thomas and Crowhurst, 2013).

In 1997, Ryan and Tedeschi published a case study of a 23-year-male who developed fatal EHS, featuring hyperthermia, muscular rigidity and cardiac arrest during moderate exercise. His nephew presented with MH while under anaesthesia, while the father of the EHS proband was classified MHShc by IVCT. His brother also complained of recurrent muscle cramps during exercise (Ryan and Tedeschi, 1997). In 2001, a 12-year-old child presented with MH while under anaesthesia and later developed a fatal EHS episode in mild weather after playing football. The post-mortem revealed a functionally characterised *RYR1* mutation, p.R163C, which was also identified in the patient's father (Tobin *et al.*, 2001).

More frequently, EHI has been associated with MH susceptibility through positive IVCT diagnoses. A case study was reported, describing a healthy 25-year-old male who presented with EHS featuring neurological impairment and ER (89,000 IU/L) while running 10-km. The patient developed rhabdomyolysis-associated acute renal failure

and was subsequently diagnosed as MHShc by IVCT along with 5 family members (Thomas and Crowhurst, 2013). Another clinical case study described a 21-year-old male with EHI featuring loss of consciousness during an 8-km military march. He also demonstrated symptoms consistent with rhabdomyolysis, including elevated CPK (19,040 IU/L) and discoloured urine. The patient subsequently received a muscle biopsy and was classified MHSh, signifying an abnormal sensitivity to halothane (Kochling *et al.*, 1998). A larger study presented IVCT data for 45 individuals who had previously developed symptoms consistent with EHI, with 19 of them subsequently demonstrating abnormal contracture responses during an IVCT. It is unclear how well characterised the study subjects were as the clinical features of each EHI episode were not provided (Figarella-Branger *et al.*, 1993).

The link between EHI clinical reactions and IVCT phenotypes has been further validated through genetic analyses. Specifically, by the identification of rare and likely pathogenic *RYR1* variants in EHI patients who produced abnormal contractures in response to halothane by IVCT (Fiszer *et al.*, 2015). It is important to note that none of the *RYR1* variants identified in these EHI patients had been functionally characterised for the diagnosis of MH. It is therefore not possible to confirm that these specific variants could cause a clinical episode of MH triggered by inhalational anaesthetics.

Molecular techniques have been used to investigate potential metabolic disturbances in EHS patients. Specifically, ^{31}P magnetic resonance spectroscopy (MRS) has been used to study human metabolism *in vivo*, assessing the bioenergetics of skeletal muscle during exercise (Bendahan *et al.*, 2001). Metabolites, including creatine phosphate (PCr), inorganic phosphate (P_i), adenosine triphosphate (ATP), glucose 6-phosphate and fructose 6-phosphate were measured in 26 EHS individuals, who had been classified MHShc by IVCT. Concentrations of these metabolites were normalised to resting PCr values, while intercellular pH was calculated from the chemical shift of P_i. Early intracellular acidosis was detected in the skeletal muscle of these patients in response to exercise, which has been attributed to an over-active glycogenolysis pathway. The same response was also detected in MH susceptible patients due to elevated cytosolic Ca^{2+} levels (Bendahan David *et al.*, 1998).

A combination of clinical, physiological and molecular evidence supports the link between EHI and MH. Despite the phenotypic and genotypic overlap between these conditions, the genetic risk factors remain unidentified in a large proportion of EHI cases. Genes related to calcium homeostasis in human skeletal muscle are prime candidates in the search for variants conferring susceptibility to EHI.

1.3.7 MH association with ER

Exertional rhabdomyolysis has also been frequently associated with the presence of *RYR1* variants (reviewed in Voermans, Snoeck and Jungbluth, 2016). A significant proportion of the familial *RYR1* variants identified in ER patients, have been previously associated with MH (Sambuughin *et al.*, 2009; Dlamini *et al.*, 2013). ER patients have also been frequently classified MH susceptible by IVCT (Wappler Frank *et al.*, 2001; Sambuughin *et al.*, 2009; Capacchione *et al.*, 2010). For example, Wappler and colleagues performed IVCTs on 12 ER individuals, 11 of whom demonstrated positive contractures in response to halothane (and caffeine in 10 of the cases) (Wappler Frank *et al.*, 2001). Three of these patients harboured an MH-associated *RYR1* variant, of which two have been functionally characterised and approved for MH susceptibility diagnosis (*RYR1* p.R163C and p.G341R).

Two unrelated ER cases featuring elevated CPK, muscle pain and cramps were both classified MHShc by IVCT, subsequently revealing a rare *RYR1* variant in common, p.R401C (Davis *et al.*, 2002). Although this variant has not been functionally characterised, it co-segregated with IVCT phenotype in both families. A separate ER study recruited six aerobically fit males of African American decent for IVCT diagnosis and genetic screening (Sambuughin *et al.*, 2009). All six individuals produced abnormal contractures in response to halothane, with one responding to caffeine below 2mM. Five of the study subjects shared the same *RYR1* variant, p.S1342G. Although this variant has been reported at a frequency of 0.0221 on the Exome Aggregation Consortium (ExAC) population database across all populations, the variant is enriched in the African population (MAF 0.2275). This suggests that this variant is not responsible for the ER phenotype in these individuals.

1.4 ER and metabolic myopathies

In addition to *RYR1*-related ER, the risk of developing this condition is also increased in the presence of the sickle cell trait and other heritable muscle disorders (Nelson *et al.*, 2016; Scalco *et al.*, 2016). These included several metabolic myopathies, such as disorders of glycogen and fatty acid metabolism, both of which have been previously associated with ER.

Mutations in *PYGM* cause an autosomal recessive glycogen storage disease known as McArdle's disease, which commonly features exertional rhabdomyolysis (Park *et al.*,

2016). The absence of glycogen phosphorylase prevents the breakdown of glycogen in skeletal muscle, causing fatigue, muscle pain, cramps, rhabdomyolysis and myglobinuria. A patient with fatty acid metabolism disorder known as very long-chain acyl-CoA dehydrogenase (VLCAD) deficiency presented with severe ER and required admission to the intensive care unit (Moniz *et al.*, 2017). Genetic analysis revealed compound heterozygosity with two mutations in *ACADVL.*

The sickle cell trait has also been shown to significantly increase the risk of developing rhabdomyolysis (Nelson *et al.*, 2016). For individuals who are heterozygous for the sickle cell mutation (*HBB* p.E6V) muscle damage can arise due to a reduced blow flow caused by exertional sickling (Anzalone *et al.*, 2010). Exertional sickling is exacerbated by dehydration and environmental heat exposure.

1.5 Other RyR1-related myopathies

RYR1 mutations have been implicated in several other disorders of skeletal muscle, including a number of congenital myopathies, such as central core disease (CCD) (Robinson *et al.*, 2006), multi minicore disease (MmD) (Zhou *et al.*, 2010), centronuclear myopathy (CNM) (Jungbluth *et al.*, 2007), late-onset axial myopathy (LOAM) (Jungbluth *et al.*, 2017) and King Denborough syndrome (KDS) (Dowling *et al.*, 2011). KDS is characterised by *RYR1*-associated dysmorphic and myopathic features in addition to MH susceptibility. In contrast to MH and EHI, congenital myopathies are often characterised by persistent muscle weakness, with clinical overlap reported between the conditions. MmD, CNM and LOAM are a genetically heterogeneous group of neuromuscular disorders and have been associated with mutations in more than one gene. *RYR1* however, is the major locus for CCD and KDS, with *RYR1* mutations reported to account for >90% of CCD cases (Robinson *et al.*, 2006; Wu *et al.*, 2006).

1.5.1 Central core disease

CCD is a rare and mild congenital myopathy featuring muscle weakness and is characterised by the presence of well-defined ‘cores’ along the centre of slow-twitch (type I) muscle fibres, which lack mitochondria and oxidative enzymes (Jungbluth, 2007) (Figure 1.3). CCD is predominantly inherited in an autosomal dominant manner, although recessive forms of the disease have been reported in rare cases (Ferreiro *et al.*, 2002).

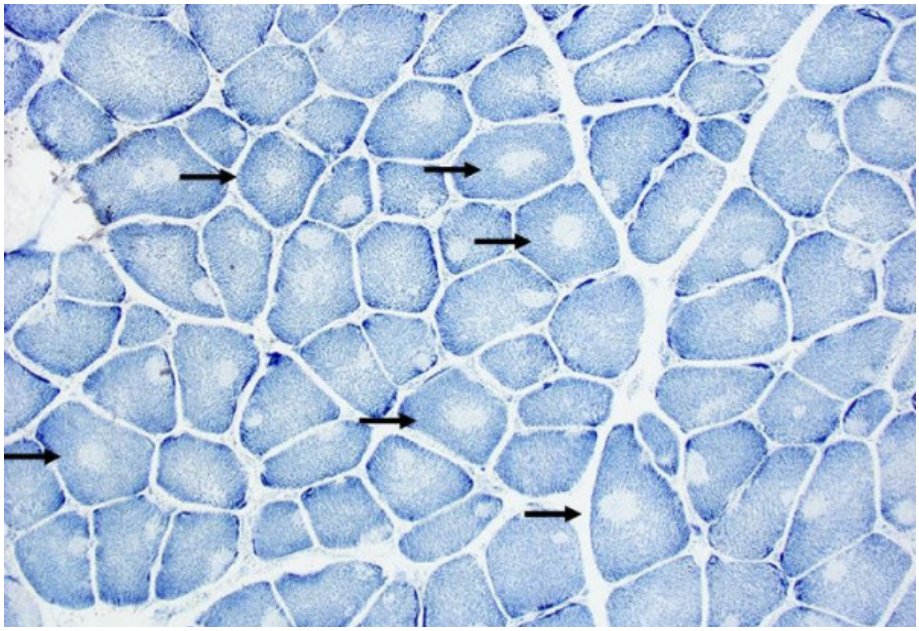

Figure 1.3: Histological appearance of central core disease (CCD). Characteristic 'cores' lacking mitochondria and oxidative enzymes are visible within the majority of muscle fibres (Jungbluth, 2007). Reproduced in accordance with the BioMed Central Ltd. Licence and under the terms of the Creative Commons Attribution License.

A comprehensive summary of *RYR1* variants associated with CCD was published in 2006 and reported 53 non-synonymous variants, with 10 of these identified in more than one family (Robinson *et al.*, 2006). Of these *RYR1* variants, 26 were also associated with an MH phenotype, either in combination with CCD or in additional MH cases (Robinson *et al.*, 2006; Zhou *et al.*, 2007). CCD was first reported in 1956, and was later associated with MH in 1973, when an IVCT positive patient with a family history of MH was diagnosed with CCD (Magee and Shy, 1956; Denborough, Dennett and Anderson, 1973). Clinical features of CCD include muscle atrophy, lower limb weakness, floppy infant syndrome and in some case skeletal deformities (Robinson *et al.*, 2006). It has been estimated that ~40% of CCD patients are asymptomatic, despite histopathological evidence of cores (Shuaib, Paasuke and W. Brownell, 1987).

The clinical features of CCD are thought to develop due to a disruption in Ca^{2+} release in skeletal muscle or as a consequence of a chronic basal RyR1 Ca^{2+} leak (Tong, McCarthy and MacLennan, 1999; Avila, O'Brien and Dirksen, 2001). A persistent Ca^{2+} leak in skeletal muscle is thought to cause damage to the muscle fibre core and reduce sensitivity for Ca^{2+} activation of RyR1. Certain CCD mutations, such as p.I4897T, have been shown to result in the uncoupling of sarcolemmal membrane depolarisation from RyR1 Ca^{2+} release (Avila, O'Brien and Dirksen, 2001; Kraeva *et al.*, 2013). The degree

of uncoupling observed is dependent on the specific *RYR1* mutation, supporting the varied clinical phenotypes reported in CCD patients (Du *et al.*, 2004).

1.6 RyR1 and calcium homeostasis in human skeletal muscle

1.6.1 The role of calcium

Ca^{2+} is the primary regulatory and signalling molecule of skeletal muscle, regulating a number of key processes including muscle contraction, bioenergetics and cell growth (Berchtold, Brinkmeier and Müntener, 2000). Ca^{2+} co-ordinates the contractile activity of skeletal muscle with ATP turnover by regulating glycogenolysis and the glycolytic pathway (anaerobic) along with pyruvate and fatty acid metabolism (aerobic) (Tate, Hyek and Taffet, 1991). Cytosolic Ca^{2+} is increased 100-fold from ~50 nM to ~5000 nM during skeletal muscle contraction (Rebbeck *et al.*, 2014). SR Ca^{2+} is buffered at ~1 mM and is depleted to ~100 μM after activation of RyR1 (Fryer and Stephenson, 1996).

1.6.2 The ryanodine receptor type-1

RyR1 is a large homotetrameric Ca^{2+} channel primarily expressed in skeletal muscle, which regulates Ca^{2+} release from the SR (Pessah, Waterhouse and Casida, 1985). RyR1 channels are localised to triad junctions where SR membranes are found in close proximity to regions of the sarcolemma known as transverse-tubules (t-tubules), which contain $Ca_v1.1$ channels (Flucher *et al.*, 1999). RyR1 is one of three mammalian isoforms of RyR, which are the largest known ion channels (Rossi *et al.*, 2002). RyR1 is also expressed at low levels in other tissues, including brain cells and peripheral blood mononuclear cells (PBMCs) (Furuichi *et al.*, 1994; Hosoi *et al.*, 2001). RyR2 is expressed primarily in cardiac muscle (Nakai *et al.*, 1990), whereas RyR3 is expressed more widely but is predominant in brain cells (McPherson and Campbell, 1990; Murayama and Ogawa, 1996). Due to the large size of these ion channels, their structures remain to be fully resolved. The structure of RyR1 has been resolved to 3.8 Å using single-particle electron cryomicroscopy (cryo-EM) (Yan *et al.*, 2015). Crystallised fragments of RyR1 have also been resolved, including a 2.5 Å N-terminal fragment of amino acids 1-599 (Amador *et al.*, 2009) and a 2.2Å fragment spanning the major phosphorylation site of RyR1, Ser2843 (Sharma *et al.*, 2012).

1.6.3 RyR1 mouse models

Mouse models of MH have predominantly focused on RyR1, with the aim of characterising MH-associated variants and their differential responses to various agonists, such as caffeine, halothane and heat. Four RyR1 mouse models have been developed to date, including p.R163C, p.Y522S, p.T4826I and p.I4896T (Table 1.1).

Table 1.1: Overview of RyR1 mouse models.

	RyR1 mouse models			
Clinical features	R163C	Y522S	T4826I	I4895T
Heat sensitivity	✓	✓	✓	✗
Anaesthetic sensitivity	✓	✓	✓	✗
Myopathic features	✗	✓	✓	✓

The *RYR1* p.R163C variant has been associated with a number of distinct clinical phenotypes including MH, CCD and EHI (Tobin *et al.*, 2001; Robinson *et al.*, 2002). A viable heterozygous *RYR1* p.R163C knock-in mouse was subsequently created, which developed fatal hypermetabolic reactions and full body contractures in response to both halothane and elevated environmental temperatures (42˚C) (Yang *et al.*, 2006). Despite the association with CCD, no myopathic features such as cores were detected in the mutant mice. Myotubes cultured from R163C heterozygous and homozygous mice, exhibited prolonged Ca^{2+} transients, due to delayed inactivation of $Ca_v1.1$ and enhanced ECCE (Estève *et al.*, 2010). Disrupted ECCE regulation was also observed in heterozygous R163C adult skeletal muscle fibres and isolated SR membranes, with higher cytosolic Ca^{2+} measured at rest (Feng *et al.*, 2011). Elevated Ca^{2+} was also detected within the mitochondrial matrix, which coincided with increased reactive oxygen species (ROS) production and reduced expression of mitochondrial proteins (Giulivi *et al.*, 2011). These mice also demonstrated compromised energy metabolism, including impaired fatty acid oxidation, glycolysis and oxidative phosphorylation. This represented an insulin-resistance like phenotype, which suggested a metabolic adaptation to disturbed basal bioenergetics.

A similar temperature and anaesthetic-induced hypermetabolic phenotype is observed in heterozygous *RYR1* p.Y522S mice (Chelu *et al.*, 2006). This *RYR1* mutation has been previously identified in both MH and CCD patients. The mutant mice developed fatal hyperthermia, rhabdomyolysis, whole-body muscle contractures, but in contrast to the R163C mice, resting cytosolic Ca^{2+} levels were not affected. Initially no central cores were detected in this mouse model, but subsequently studies have reported core regions lacking mitochondria, caused by localised mitochondrial damage and swelling

(Boncompagni *et al.*, 2009). The temperature sensitivity of the *RYR1* p.Y522S mouse is thought to be caused by a Ca^{2+} leak, which increases the production of reactive nitrogen species (RNS), which in turn results in the S-nitrosylation of RyR1 (Durham *et al.*, 2008). This post-translational modification of RyR1 increase its temperature sensitivity for activation, therefore triggering massive Ca^{2+} release from RyR1 on exposure to high environmental temperatures. The effect of RyR1 S-nitrosylation is two-fold as it also enhances Ca^{2+} activation of the channel (Aracena *et al.*, 2003). Exercise has also been shown to stimulate RyR1 S-nitrosylation, generating leaky channels, thus reducing work capacity during sustained exercise (Bellinger *et al.*, 2008).

RYR1 p.T4826I confers susceptibility to MH only, and has not been associated with a clinical diagnosis of CCD (Brown *et al.*, 2000). Both homozygous and heterozygous T4826I knock-in mice are viable and exhibit sex- and dose-dependent responses to halothane and heat (Yuen *et al.*, 2012). Male homozygous mice demonstrate the greatest sensitivity to temperature and anaesthetic triggers. Male T4826I homozygotes also reveal late-onset disordered muscle morphology, contrary to the human phenotype (Yuen *et al.*, 2012).

Finally, an *RYR1* mutation, p.I4895T, which has been found exclusively in CCD patients, causes a progressive congenital myopathy in heterozygous mice (Zvaritch *et al.*, 2007; Loy *et al.*, 2010). The *RYR1* p.I4895T mutation in the homozygous form is lethal in perinatal mice, who display severe developmental defects, paralysis and die of respiratory failure (Zvaritch *et al.*, 2007). Heterozygous mice present with muscle weakness and atrophy, featuring central cores. This myopathic phenotype has been attributed to reduced SR Ca^{2+} release rather than chronic Ca^{2+} leak, but the mechanism contributing to the development of cores in unclear (Loy *et al.*, 2010). It has been hypothesised that heterogeneity of normal and mutant RyR1 channels, causes irregular contractions across myofibrils, resulting in damage and core development (Zvaritch *et al.*, 2009).

1.6.4 The excitation-contraction coupling mechanism

RyR1 Ca^{2+} release is tightly regulated by a process known as EC coupling, which converts an action potential stimulus into the mechanical contraction of skeletal muscle fibres (Rebbeck *et al.*, 2014). A schematic representation of the EC coupling mechanism is presented in Figure 1.4. Specifically, acetylcholine is released across the neuromuscular junction, which propagates an action potential along the sarcolemmal

membrane. This depolarises the membrane, triggering voltage-sensitive $Ca_v1.1$ channels to undergo conformational changes and allosterically interact with RyR1 channels. Ca^{2+} is released from the SR via RyR1, which binds to troponin, exposing the myosin-binding sites within the actin filaments. Cross-bridges subsequently form between the actin and myosin filaments causing skeletal muscle to contract. Finally, Ca^{2+} is driven back into the SR via sarco/endoplasmic reticulum Ca^{2+} ATPases (SERCA) pumps, restoring cytosolic Ca^{2+} back to baseline levels and allowing muscle relaxation to occur (Calderón, Bolaños and Caputo, 2014). Due to the highly regulated and sequential nature of EC coupling, all proteins within this pathway are candidates for the investigation of both MH and EHI.

1.6.5 RyR1 regulatory proteins

1.6.5.1 STAC3

STAC3 encodes a protein, which has been co-localised to the RyR1-$Ca_v1.1$ complex at the triad junction between the sarcolemma and SR (Horstick *et al.*, 2013). The specific mechanism by which STAC3 regulates the RyR1-$Ca_v1.1$ complex remains unknown. In 2013, a homozygous mutation in *STAC3* (p.W284S) was implicated in patients with Native American myopathy (NAM) and MH susceptibility (Stamm *et al.*, 2008; Horstick *et al.*, 2013). Native American myopathy (NAM) was first identified in 1987 as an autosomal recessive congenital myopathy characterised by weakness, cleft palate, ptosis, short stature, MH susceptibility (Bailey and Bloch, 1987). Despite its name, NAM was recently identified in an individual of Turkish decent (Grzybowski *et al.*, 2017). The Turkish NAM patient was a compound heterozygote, harbouring two variants in *STAC3* in *trans* (p.K288* and a splice variant skipping exon 4).

STAC3 is now routinely screened in patients referred to the UK MH Investigation Unit, with a family history of MH. Recently, a heterozygous *STAC3* variant (p.N281S) was identified in two unrelated patients with a family history of MH, but the clinical significance of this variant is currently unknown (unpublished data). Neither of the individuals revealed any phenotypic or histopathological features consistent with a myopathy.

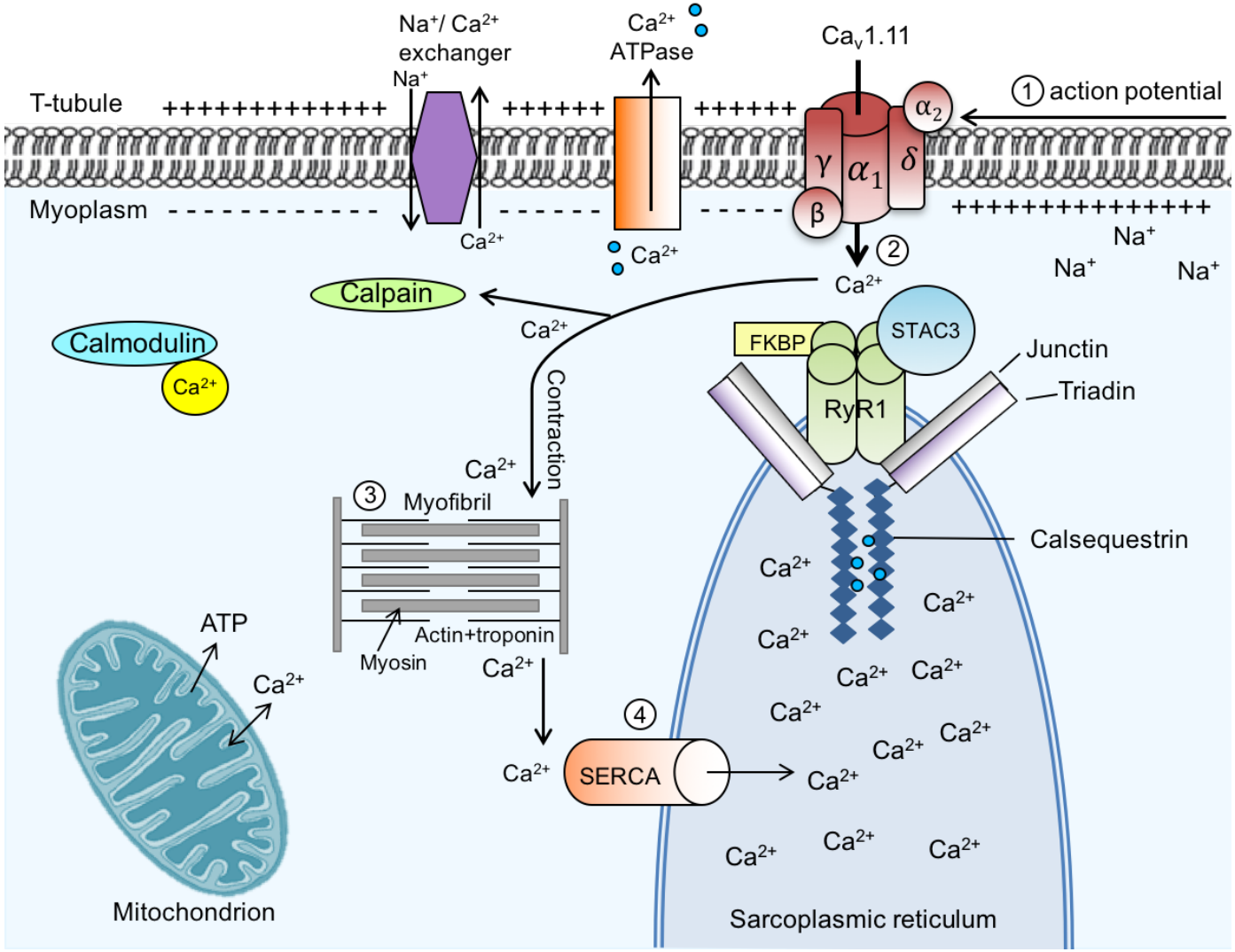

Figure 1.4: Schematic of excitation-contraction (EC) coupling in human skeletal muscle. (1) Depolarisation of sarcolemmal membrane by action potential (2) voltage-activation of $Ca_v1.1$ stimulating Ca^{2+} release by RyR1 (3) Ca^{2+} induced muscle contraction (4) refilling of SR Ca^{2+} stores by SERCA pump.

1.6.5.2 Calsequestrin-1

In contrast to STAC3, the majority of RyR1 regulatory proteins have been localised to the SR lumen. *CASQ1*, encodes a SR luminal Ca^{2+} binding protein, known as calsequestrin-1 (CASQ1), which has been shown to regulate RyR1 (Kawasaki and Kasai, 1994). *CASQ1* was first identified as a candidate gene for MH and EHI in 2009, when CASQ null male mice experienced hypermetabolic reactions featuring hyperthermia, severe rhabdomyolysis and whole-body contractures in response to both 2% halothane and 41°C environmental temperatures (Paolini *et al.*, 2007; Dainese *et al.*, 2009; Protasi, Paolini and Dainese, 2009). The spontaneous death rate was also significantly higher in male CASQ knockout mice. The direct importance of CASQ1 was confirmed when introduction of CASQ1 *in vivo* was able to rescue the null phenotype, restoring Ca^{2+} transients (Tomasi *et al.*, 2012).

Non-synonymous *CASQ1* variants have since been implicated in two similar autosomal dominant conditions, tubular aggregate myopathy and vacuolar myopathy with CASQ1 aggregates (Rossi *et al.*, 2014; Di Blasi *et al.*, 2015; Barone *et al.*, 2017). Interestingly, both conditions feature exercise-induced muscle cramps and weakness. Mutations in the *CASQ2* gene expressed in cardiac muscle have also been associated with an exercise- and stress-induced condition, known as catecholaminergic polymorphic ventricular tachycardia (CPVT) (Lahat *et al.*, 2001). This is an autosomal recessive condition, characterised by arrhythmia, recurrent syncope, seizures and sudden death. CPVT is also caused by mutations in *RYR2* and *TRDN* (Lahat, Pras and Eldar, 2003; Rooryck *et al.*, 2015).

CASQ1 has a high Ca^{2+} buffering capacity, particularly once formed into elongated polymers in the presence of high SR luminal Ca^{2+} (~1 mM) (Wang *et al.*, 1998). CASQ1 has been shown to act as a Ca^{2+} sensor, inhibiting RyR1 at low Ca^{2+} concentrations via the triadin-1 and junctin complex (Zhang *et al.*, 1997; Beard *et al.*, 2002; Györke *et al.*, 2004). In contrast, CASQ1 increased RyR1 activity when bound directly to purified RyR1 channels, highlighting the need for triadin/ junctin anchor proteins to elicit the inhibitory effect (Beard *et al.*, 2002).

1.6.5.3 The junctin/ triadin complex

Both junctin and triadin are transmembrane proteins, which have been co-localised to the triad junction where they interact with and regulate RyR1 (Carl *et al.*, 1995; Jones *et*

al., 1995; Zhang *et al.*, 1997). Like *CASQ1*, mutations in the gene which encodes triadin (*TRDN*) has been associated with CPTV, causing cardiac arrhythmias and sudden death. This illustrates the importance of these genes in the Ca^{2+} handling properties of cardiac muscle (Roux-Buisson *et al.*, 2012). Both proteins contain binding sites for RyR1 and CASQ1, but they are thought to have distinct functional properties, interacting with RyR1 at different sites (Wei *et al.*, 2009). Conflicting evidence has been presented regarding their role in mediating the Ca^{2+} dependent inhibition of RyR1 by CASQ1.

Wei and colleagues demonstrated that junctin alone mediates CASQ1-RyR1 cross-talk using artificial bilayers (Wei *et al.*, 2009); however, *ex vivo* and *in vitro* experiments using junctin and triadin null mice revealed that ablation of triadin had a more marked effect on CASQ1-dependent SR architecture and Ca^{2+} regulation than junctin (Boncompagni *et al.*, 2012). Both junctin and triadin null mice revealed significantly elevated myoplasmic Ca^{2+} levels at rest (Shen *et al.*, 2007; Yuan *et al.*, 2007). Cell-free experimental models using artificial bilayers and purified proteins showed that junctin and triadin activate RyR1 in the absence of CASQ1. The subsequent addition of CASQ1 to junctin/ triadin bound RyR1, inhibited activity of the Ca^{2+} release channel (Wei *et al.*, 2009). Overexpression of triadin in ventricular myocytes significantly increased Ca^{2+} transients (Terentyev *et al.*, 2005). Although the amplitude of Ca^{2+} transients were significantly reduced in triadin null mice, this related to reduced SR Ca^{2+} content due to an RyR1 calcium leak (Shen *et al.*, 2007; Boncompagni *et al.*, 2012). Disrupted Ca^{2+} homeostasis in triadin null myotubes was not as pronounced as detected in alternative *in vitro* systems, indicating a compensatory response in triadin null mice (Shen *et al.*, 2007). In contrast, the junctin null mouse demonstrated enhanced RyR1 Ca^{2+} release, confirming the importance of junctin in the inhibition of RyR1 (Yuan *et al.*, 2007). It remains unknown whether the ablation of junctin positively regulates RyR1 directly or by direct binding of CASQ1 to RyR1.

The contrasting literature on triadin, junction and calsequestrin-1, which reveal the differential functional properties of the proteins dependent on the presence of other regulators of RyR1 and the experimental model used, highlights the complexity RyR1 regulation.

1.6.6 The inhibitory effect of Mg^{2+} on RyR1

In contrast to the Ca^{2+}-dependent activation of RyR1, the channel is inactivated by the direct binding of Mg^{2+} (Steele and Duke, 2007). Mg^{2+} is thought to bind to inhibitory sites

(I-sites) on RyR1, whilst simultaneously competing with Ca^{2+} at the activation sites (A-sites). Previous studies have suggested that certain mutations in *RYR1* alter Mg^{2+} regulation of RyR1, conferring susceptibility to MH (Steele and Duke, 2007). The importance of Mg^{2+} is further substantiated by the potent antagonistic properties of dantrolene sodium on RyR1, which increases the channel's affinity to Mg^{2+} (Choi, Koenig and Launikonis, 2017). Due to the significant role Mg^{2+} plays in Ca^{2+} homeostasis, it is important to consider the potential impact of mutations in skeletal muscle Mg^{2+} channels. *TRPM6* encodes a Mg^{2+} channel expressed in the sarcolemmal membrane of skeletal muscle fibres and therefore regulates the cytosolic Mg^{2+} concentration (Schlingmann *et al.*, 2007). Magnesium deficiencies have been detected in military personnel, for example a 17-year-old who presented with aching muscle and cramps during exercise (Bilbey and Prabhakaran, 1996). Both homozygous and heterozygous *TRPM6* mutations have also been identified in families with hypomagnesemia with secondary hypocalcaemia, who presented with seizures and tetany (Walder *et al.*, 2002). This highlights the importance to maintain a balance between Ca^{2+} and Mg^{2+} and the direct impact of *TRPM6* mutations on RyR1 Ca^{2+} release.

1.6.7 Store operated calcium entry

Intracellular Ca^{2+} concentrations in skeletal muscle are maintained by extracellular Ca^{2+} entry to support sustained Ca^{2+} transients, which can be activated by both Ca^{2+} SR store depletion and by the EC coupling mechanism (Kurebayashi and Ogawa, 2001; Cherednichenko *et al.*, 2004; Lyfenko and Dirksen, 2008) (Figure 1.5). The former is known as SOCE and involves two Ca^{2+} channels in the sarcolemmal membrane (Orai1 and TRPC) and a Ca^{2+} calcium sensing molecule in the SR membrane (STIM1).

STIM1 encodes Stromal Interaction Molecule 1 (STIM1), which detects SR Ca^{2+} store depletion and interacts with and activates Orai1 Ca^{2+} channels, transient receptor potential cation (TRPC) channels and heteromeric complexes of Orai1 and TRPC (Worley *et al.*, 2007; Liao *et al.*, 2008). Extracellular Ca^{2+} entry is required to replenish Ca^{2+} stores in order to prevent contractile decline during prolonged stimulation (Pan *et al.*, 2002). SOCE was not detected in mouse myotubes lacking functional STIM1 proteins, preventing the refilling of SR Ca^{2+} stores (Stiber *et al.*, 2008). The absence of functional STIM1 causes a lethal skeletal myopathy in perinatal mice, with only heterozygous mice surviving (Stiber *et al.*, 2008). *Ex vivo* extensor digitorum longus (EDL) muscle extracted from these heterozygous mice fatigued significantly faster than wild-type mice.

In contrast, enhanced SOCE has been observed in CASQ1 knock-down skeletal muscle fibres (Zhao *et al.*, 2010). Both RyR1 mutant (p.Y524S) and CASQ1 null mice also demonstrated accelerated activation of SOCE, contributing to the hypermetabolic phenotype observed in these mouse models (Yarotskyy, Protasi and Dirksen, 2013). CASQ1 is thought to suppress SOCE by binding to STIM1 at low luminal Ca^{2+} concentrations, preventing its interaction with Orai1/ TRPC channels (Shin *et al.*, 2003; Wang *et al.*, 2015). The anaesthetic and heat-sensitive phenotype observed in CASQ1 null mice is therefore thought to be due to the lack of inhibition of both RyR1 and STIM1.

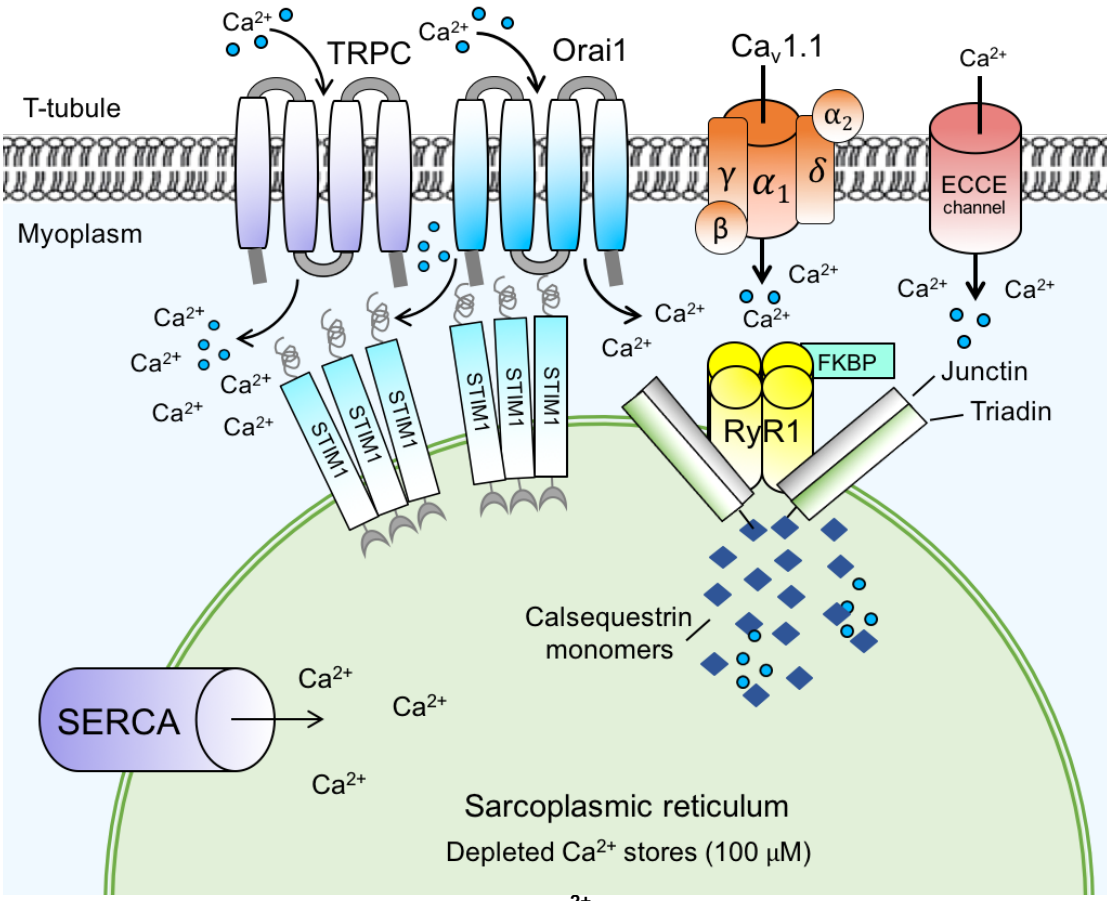

Figure 1.5: Schematic of extracellular Ca^{2+} entry via store-operated calcium entry (SOCE) channels and excitation-coupled calcium entry (ECCE) channels to replenish intracellular Ca^{2+}. SOCE channels (TRPC and Orai1) are activated by SR Ca^{2+} store depletion, sensed by STIM1. ECCE channels ($Ca_v1.1$ and ECCE) are stimulated by membrane depolarisation.

1.6.8 Excitation-coupled calcium entry

ECCE represents a distinct pathway to SOCE that is not dependent on SR Ca^{2+} store depletion for activation but rather requires sustained or repetitive membrane

depolarisation in the presence of RyR1 and Cav1.1 (Cherednichenko *et al.*, 2004) (Figure 1.5). The mechanism of ECCE is yet to be fully elucidated, although Ca^{2+} is thought to enter the cytosol via $Ca_v1.1$ and potentially an additional ECCE channel, which remains to be identified (Bannister, Pessah and Beam, 2009). Interestingly, ECCE was enhanced in myotubes harbouring functionally characterised *RYR1* MH mutations (p.R615C, p.R2163C and p.T4826I) relative to myotubes harbouring wild-type *RYR1* (Yang *et al.*, 2007). The ECCE mechanism has also been implicated in the anaesthetic and heat-sensitive phenotype displayed by RyR1 p.R163C knock-in mice (Cherednichenko *et al.*, 2008). Specifically, heterozygous and homozygous myotubes isolated from the *RYR1* p.R163C mice revealed significantly elevated ECCE rates, which could be regulated by addition of dantrolene sodium. These studies highlight the importance of ECCE in the pathophysiology of MH and potentially EHI.

1.7 Mitochondrial dysfunction in disease

1.7.1 Energy metabolism and ROS

The mitochondrion is the powerhouse of energy metabolism, as the site of oxidative phosphorylation (OXPHOS), the major ATP synthesis pathway. During OXPHOS, H^+ pumps located within the inner mitochondrial membrane, known as complexes I-IV, reduce substrates to create an electrochemical membrane gradient, driving ATP synthesis via complex V (ATP synthase) (Senior, 1988). ROS are produced as intermediary by-products during the reduction of O_2 to H_2O in the mitochondrial respiratory chain (Murphy, 2009). Examples of mitochondrial ROS include superoxides (O_2^-), hydrogen peroxides (H_2O_2) and hydroxyl radicals (OH) (Jensen, 1966; Chance, Sies and Boveris, 1979). Surprisingly, these reactive molecules are required in small quantities for localised cellular signalling, but at higher levels are damaging to proteins, lipid and DNA, causing a range of pathologies (Brunelle *et al.*, 2005; Hamanaka and Chandel, 2010). If aerobic metabolism becomes unbalanced with mitochondrial antioxidant production (glutathione reductase, superoxide dismutase and catalase), the subsequent ROS production can cause widespread oxidative stress (Aruoma, 1998; Marí *et al.*, 2009). ROS has been associated with cancer, diabetes, rheumatoid arthritis, cardiovascular disease and neurodegenerative diseases, including Alzheimer's disease and Parkinson's disease (Valko *et al.*, 2007).

1.7.2 Calcium, heat and ROS

The physiological and biochemical functions of Ca^{2+} are diverse. Mitochondrial Ca^{2+} is a critical regulator of energy metabolism and ultimately cell survival and therefore Ca^{2+} homeostasis within these organelles is vital for effective ATP production (McCormack and Denton, 1993). Ca^{2+} stimulates several metabolic pathways, although is predominately involved in the regulation of the Krebs cycle and OXPHOS (Tate, Hyek and Taffet, 1991). Despite its central regulatory role in mitochondrial function, Ca^{2+} overload in the mitochondrial matrix can drive ROS production (Görlach *et al.*, 2015). It is hypothesised that elevated mitochondrial Ca^{2+}, which drives ATP synthesis, increases the metabolic rate and in turn enhances electron transport chain (ETC) electron leakage and ROS generation (Brookes *et al.*, 2004). It has also been suggested that if mitochondria are overloaded with Ca^{2+}, then ROS production may rise independently of the metabolic rate (Peng and Jou, 2010).

Conversely, ROS has been shown to regulate cellular Ca^{2+} levels by altering the activity of Ca^{2+} channels, pumps and exchangers (Görlach *et al.*, 2015). Interestingly, ROS has been shown to directly enhance the activity of RyRs by oxidising thiol groups (Cooper *et al.*, 2013). In contrast, ROS have been shown to inhibit SERCA pumps by preventing ATP binding, limiting Ca^{2+} uptake into the SR stores (Cook *et al.*, 2012). The crosstalk between mitochondrial Ca^{2+}, energy metabolism and ROS production highlights the complexity of mitochondrial function and the importance of Ca^{2+} balance within the mitochondrial matrix.

Heat stress also stimulates ROS production, particularly O_2^-, while simultaneously down-regulating the antioxidant, superoxide dismutase (Mujahid *et al.*, 2006; El-Orabi *et al.*, 2011; Li *et al.*, 2017). Heat stress has been shown to directly inhibit mitochondrial ATP synthesis by inactivating complex I of the of the ETC, with elevated ROS levels inhibiting complexes I, II and IV (Downs and Heckathorn, 1998; Lin *et al.*, 2002; Huang *et al.*, 2015). This heat-induced inhibition of the ETC reduces oxygen uptake, which further accelerates ROS production (Boveris, Oshino and Chance, 1972). ROS can cause widespread cellular damage, ultimately triggering mitochondrial apoptotic pathways.

1.7.3 RNS

Reactive nitrogen species (RNS) are derivatives of nitric oxide (NO) and include the reaction of O_2^- with NO to form peroxynitrite ($ONOO^-$). Similarly to ROS, both Ca^{2+} and heat can stimulate nitric oxide synthase (NOS), which catalyses the formation of NO (Hall *et al.*, 1994). NO subsequently inhibits the activity of cytochrome c oxidase (ETC complex IV), blocking oxygen utilisation and ATP synthesis (Cleeter *et al.*, 1994). Formation of mitochondrial $ONOO^-$ causes oxidative stress, mainly by inhibiting complexes I, III and V of the ETC, ultimately causing cellular damage (Radi, Cassina and Hodara, 2002). Research suggests that hyperthermia-induced NO can offer a protective effect to heat shock by initiating a systemic stress response (Matsumoto *et al.*, 1999).

1.7.4 Metabolic myopathies and exercise intolerance

Metabolic myopathies represent a diverse group of metabolic disorders, primarily affecting skeletal muscle function. Metabolic myopathies are commonly autosomal recessive conditions, which can be categorised into disorders of fatty acid metabolism, glycogen storage and mitochondrial function (Berardo, DiMauro and Hirano, 2010). The clinical features and severity of each condition are dependent on the specific enzymatic defect and which metabolic pathway is affected, although an exercise intolerance phenotype is common to all three groups.

Disorders of fatty acid metabolism prevent the utilisation of certain fats as an energy source and range from mild adult myopathic conditions to lethal neonatal forms. Myopathic forms typically manifest during aerobic exercise as slow-onset muscle pain and weakness, featuring recurrent rhabdomyolysis. Examples include carnitine palmitoyltransferase II (CTPII) deficiency and very long-chain acyl-CoA dehydrogenase (VLCAD) deficiency (Corti *et al.*, 2008; Laforêt *et al.*, 2009). In contrast, glycogen storage diseases either inhibit the breakdown or synthesis of glycogen and manifest during high-intensity exercise. Cases often present with fast-onset exercise-induced cramps and pain, including myoglobinuria. An example includes McArdle's disease, which arises from the deficiency of myophosphorylase, an enzyme required for the breakdown and utilisation of glycogen (McArdle, 1951; Nogales-Gadea *et al.*, 2015). Finally, mitochondrial myopathies arise from deficiencies of a variety of mitochondrial enzymes and therefore can manifest with a range of symptoms, including weakness and

premature fatigue. Mitochondrial diseases also cause a notable reduction in VO_2 max capacity and reduced ATP production (Chaussain *et al.*, 1992; Shepherd *et al.*, 2006).

1.8 Thesis aims

This thesis aims to investigate the genetic susceptibility to EHI and to explore the pathophysiological mechanisms underlying the EHI phenotype. This research offers a unique opportunity to explore the phenotypic and genotypic link between EHI and MH in a clearly defined cohort of patients. This thesis also aims to characterise the heat stress response in both heat-sensitive *RYR1* mice and human EHI patients. This work will attempt to elucidate key mechanisms and pathways underlying the hypermetabolic episodes triggered by heat stress. The long-term aim is to develop a genetic test for military use to identify members of the armed forces at increased risk of developing EHI.

1.9 Thesis objectives

1.9.1 Investigate the genetic susceptibility to EHI

The primary objective of this thesis is to identify rare, non-synonymous variants predicted to modify protein function, with the potential to predispose individuals to EHI. The coding region of fifty genes relating to calcium homeostasis in skeletal muscle, energy metabolism and congenital myopathies will be sequenced in a cohort of sixty-four individuals with a clinical history of EHI. The EHI cohort are predominantly UK military personnel who have been diagnosed as heat intolerant by HTT. Rare and potentially deleterious variants will then be screened across a cohort of individuals with a family history of MH who have been characterised by IVCT. Genetic data will then be correlated with phenotypic data, including clinical EHI symptoms, HTT output and quantitative IVCT responses.

1.9.2 Characterise the heat stress response in RyR1 mutant mice

RyR1 mutant and wild-type mice will be subjected to environmental heat stress in whole-body calorimetry chambers prior to recovery at room temperature for up to 24-hours. RNA-seq will be used to quantify global gene expression profiles to identify differentially expressed genes between the two genotypes. Quantitative PCR will also be used to explore differential expression of candidate genes.

1.9.3 Explore differential heat stress responses in EHI, MH and control volunteers

An RNA-seq approach will also be used to examine the global heat stress response in a cohort of individuals clinically classified as EHI or MH susceptible, in addition to a group of age, sex and fitness-matched controls. All volunteers will complete the INM's standardised HTT and have blood extracted prior to, 2-hours post and 24-hours post testing. Again, RNA-seq data will be modelled to identify a signature of differentially expressed genes between the status groups.

2 Identifying genetic variants in association with exertional heat illness

2.1 Introduction

The genetic contribution to EHI is poorly understood and the genetic characterisation of EHI individuals has been limited to individual case studies. Due to the diverse clinical presentation of EHI, research to date has focused on patients with specific features such as exertional rhabdomyolysis. The first clinical case linking EHI with MH was reported by Tobin *et al*. 2001, with a 12 year old presenting with MH after exposure to general anaesthetic, sevoflurane (Tobin *et al.*, 2001). The patients' core temperature reached 39.4˚C, his heart rate (HR) rose to 150 bpm and serum creatine phosphokinase (CPK) levels peaked at 9,049 IU/L. The patient experienced a fatal EHI episode 8 months later, while playing football. The ambient temperature was 26˚C and his rectal temperature reached 42.2˚C. The EHI episode featured muscle weakness and stiffness, seizure and cardiac arrest. Genetic analysis revealed a heterozygous variant in *RYR1* (p.R163C) in the patient and his father. *RYR1* p.R163C was the first familial variant associated with EHI, a phenotype which has also been replicated in a knock-in mouse model (Yang *et al.*, 2006). The proposed link to MH saw subsequent genetic analyses focus on *RYR1*, which were constrained by the financial and technical limitations of sequencing technologies.

Variants in *RYR1* have also been implicated in cases of environmental heat stroke. For example, a heterozygous non-synonymous *RYR1* variant and duplication (p.R4645Q and p.L4320_R4322dup) were identified in a post-mortem genetic analysis of a 2-year-old child who developed a fatal case of heat stroke after prolonged exposure to ambient temperatures measuring 43.6°C (Nishio *et al.*, 2009). The same genetic alterations have also been identified independently in unrelated MH susceptible individuals with high CPK levels (Ibarra *et al.*, 2006). A separate case study reported heterozygous *RYR1* variant p.R3983C in recurrent cases of heat illness in 2 unrelated children (Groom *et al.*, 2011). One of the children also experienced an MH reaction under anaesthesia and later tested as positive to both RyR1 agonists, caffeine and halothane during an IVCT. Both children often developed hyper-metabolic symptoms while harbouring viral infections.

RYR1-related exertional rhabdomyolysis (ER) has been widely reported in the literature, with *RYR1* variants accounting for around 30% of cases (Voermans, Snoeck and Jungbluth, 2016). Both functionally characterised MH mutations and *RYR1* variants of

unknown significance have been reported in patients presenting with ER with or without evidence of EHI. For example, a seemingly healthy 27 year old male developed EHI featuring rhabdomyolysis was later was shown to carry an uncharacterised homozygous variant, *RYR1* p.R830W. Both of his parents were asymptomatic and heterozygous for the same variant (Snoeck *et al.*, 2015). Dlamini and colleagues screened *RYR1* in 39 unrelated families in the United Kingdom or The Netherlands diagnosed with ER, with no features of EHI. Nine heterozygous *RYR1* variants were identified in 14 of the families (Dlamini *et al.*, 2013). A number of the variants were observed in more than one family, for example *RYR1* p.K1393R was identified in 2 unrelated individuals, and had been previously identified in Swedish MH index cases (Broman *et al.*, 2009).

In some instances, patients suffering with ER have also presented with MH while under anaesthesia (Capacchione *et al.*, 2010). The otherwise fit and healthy 30 year old male reported by Capacchione and colleagues harboured a heterozygous variant in *RYR1*, p.S1342G, along with variants in *PYGM*, *AMPD1* and *CASQ1*. The significance of these remain unknown. The individual later underwent an IVCT and demonstrated a positive contracture in response to halothane. The same heterozygous variant (*RYR1* p.S1342G) has also been associated with a number of recurrent ER cases featuring myalgia either independently or in combination with additional *RYR1* variants (Sambuughin *et al.*, 2009). All reported cases carrying *RYR1* p.S1342G were males of African American origin, aged between 21 and 41 years old.

An interesting case of identical twin brothers was reported both of whom carried a functionally characterised heterozygous MH mutation, *RYR1* p.R2452C (Potts *et al.*, 2014). Both siblings had experienced recurrent ER featuring muscle cramps, myalgia and persistently high CPK levels. Both complained of exercise intolerance due to severe cramps, which developed into an inability to tolerate even low levels of exertion. The first twin underwent an IVCT, and demonstrated positive contractures in response to both caffeine and halothane (MHShc). The second twin reported previous complications under general anaesthesia, including cardiac arrest, but only went on to receive an MH susceptible diagnosis by genetic testing.

Three apparently unrelated families who presented clinically with either MH or ER were reported to share the same heterozygous *RYR1* variant, p.R401C. All three index cases and select family members demonstrated abnormal responses to both caffeine and halothane during their IVCT. There have also been individuals who have experienced both ER and MH. For example, two unrelated MH patients developed ER, which was characterised by myalgia and cramps (Davis *et al.*, 2002).

Less commonly, EHI has been associated with other defects of human skeletal muscle, such as CCD. A child carrying heterozygous *RYR1* variant p.G4820R experienced a fatal EHI episode, featuring increased heart rate, muscle stiffness, jaw clenching, seizures and a core temperature reaching 42.7˚C (Lavezzi *et al.*, 2013). Unsuspecting of a susceptibility to MH, the patient was given succinylcholine, a muscle relaxant, which is a potent trigger of MH. The patient and two of his siblings all shared the same *RYR1* variant. This genetic variant was inherited from their father, who was classified MHShc by IVCT, with histology diagnosing CCD.

Interestingly, variants in other genes involved in the excitation-contraction (EC) coupling mechanism have been associated with an exercise intolerance phenotype. These conditions are predominantly autosomal recessive. For example, variants in *TRDN* have been associated with ventricular tachycardia featuring muscle weakness (CPVT5) (Roux-Buisson *et al.*, 2012). CPVT5 is characterised by exercise or stress-induced syncope or sudden death and skeletal muscle weakness. Triadin is an SR membrane protein, which forms part of the RyR1 complex and anchors calsequestrin to the junctional SR modulating calcium release (Kobayashi *et al.*, 2000; Györke *et al.*, 2004). Deletions, nonsense mutations and non-synonymous variants in *TRDN* have been implicated in CPVT5, for example p.T59R (Roux-Buisson *et al.*, 2012). CPTV5 is genetically heterogeneous and additional genes have been identified as causative, including the cardiac forms of the ryanodine receptor and calsequestrin (*RYR2* and *CASQ2*) (Ylänen *et al.*, 2010).

Mutations in *ATP2A1* cause Brody's myopathy, which is characterised by delayed muscle relaxation, muscle stiffness triggered by exercise, cramps and myalgia (Vattemi *et al.*, 2010; Voermans *et al.*, 2012). *ATP2A1* encodes a sarco/endoplasmic reticulum Ca^{2+}-ATPase (SERCA) pump, which transports Ca^{2+} into the SR lumen allowing cytosolic Ca^{2+} to return resting levels. A number of genetic alterations have been associated with this rare condition, including non-synonymous variants, nonsense variants, deletions and translocations. Patients who do not carry *ATP2A1* variants have been classified as a genetically distinct from Brody's myopathy patients and were re-classified as having a condition known as Brody's syndrome (Voermans *et al.*, 2012; Guglielmi *et al.*, 2013). Compound heterozygous mutations, *ATP2A1* p.I235N and p.Q982K, cause ablation of SERCA1, which causes the compensatory upregulation of SERCA2 (*ATP2A2*) in both slow and fast-twitch muscles (Sambuughin *et al.*, 2014). Literature to date suggests that the two conditions are genetically heterogenous and are yet to be fully elucidated.

Another condition characterised by delayed muscle relaxation is myotonia congenita, which has been associated with mutations in *CLCN1* (Duno et al., 2004). Myotonia congenita can feature delayed skeletal relaxation, muscle stiffness and weakness and hypertrophic muscle. Both autosomal dominant and recessive forms of the disorder have been described, known as Thomsen disease and Becker disease, respectively (Zhang *et al.*, 1996). *CLCN1* encodes a voltage-gated chloride channel, which regulates the electric excitability of the skeletal muscle membrane. More than 130 mutations in the *CLCN1* gene have been reported in association with myotonia congenital (Ferradini *et al.*, 2017).

Alternatively, genetic variants in genes related to energy metabolism have been associated with autosomal recessive conditions featuring an exercise intolerance phenotype. Variants in *ACADVL* cause very long-chain acyl-CoA dehydrogenase (VLCAD) deficiency (Andresen *et al.*, 1999; Laforêt *et al.*, 2009; Oliveira *et al.*, 2013). Three forms of autosomal recessive VLCAD deficiency have been described, one of which is a rare adult-onset form characterised by exercise intolerance, ER, myalgia and myoglobinuria. VLCAD is a mitochondrial enzyme required for the breakdown of fatty acids. A number of homozygous and compound heterozygous mutations have been implicated in the late-onset form including *ACADVL* p.L500del, which was identified in two symptomatic siblings from a consanguineous family (Oliveira *et al.*, 2013).

Genetic variants in *PYGM* cause McArdle's disease, a rare autosomal recessive condition caused by a deficiency in the myophosphorylase enzyme. This metabolic enzyme encoded by *PYGM* is required to convert glycogen to glucose-1-phosphate to be utilised as an energy source in human skeletal muscle (Tsujino, Shanske and DiMauro, 1993). McArdle's is also known as glycogen storage disease type V and is characterised by premature muscle fatigue, sometimes featuring rhabdomyolysis and myoglobinurea (Leite, Oliveira and Rocha, 2012). More than 147 *PYGM* mutations have been reported in association with this glycogen storage disease (Nogales-Gadea *et al.*, 2015).

Mutations in a second gene encoding a metabolic enzyme, *CPT2,* cause a deficiency with a similar clinical phenotype. Carnitine palmitoyltransferase II (CPTII) is a mitochondrial enzyme required for the transport of long-chain fatty acids across the inner mitochondrial membrane prior to their β-oxidation. Therefore, mutations in *CPT2* prevent the utilisation of certain fats for energy (Tong *et al.*, 1997). There are 3 forms of CPTII deficiency: a lethal neonatal form (MIM #608836), a life-threatening infantile form (MIM #600649) and an adult-onset myopathic form (MIM #255110). The myopathic form of

CPTII deficiency is a rare, autosomal recessive condition, characterised by myalgia, muscle weakness and rhabdomoylsis. In contrast to the severe early-onset CPTII deficiencies, patients with the myopathic form remain asymptomatic between episodes, with episodes triggered by exercise, stress, elevated ambient temperatures, viral infection or fasting (Sigauke *et al.*, no date; Bonnefont *et al.*, 2004). More than 70 mutations have been associated with CPTII deficiency. *CPT2* mutations such as p.S113L and p.P50H are common within the Caucasian population (Deschauer, Wieser and Zierz, 2005).

Finally, genetic variants in *AMPD1* have been associated with an enzyme deficiency characterised by exercise intolerance (Morisaki *et al.*, 1992; Gross *et al.*, 2002; Toyama *et al.*, 2004). *AMPD1* encodes adenosine monophosphate deaminase 1, which is involved in energy production within skeletal muscle, converting AMP to IMP. AMPD1 deficiency is considered the most common metabolic disorder seen in Caucasian populations, affecting 2% of individuals. Historically, all cases were thought to inherit two copies of the *AMPD1* p.Q45* and p.P77L mutations, in *cis* (Morisaki *et al.*, 1992). More recent literature however has implicated a number of additional variants, such as *AMPD1* p.K316I and p.M340I (Toyama *et al.*, 2004).

This chapter will present the genotypic and phenotypic characterisation of a cohort EHI patients, who have presented clinically with either EHI or exertional rhabdomyolysis. These individuals were phenotypically classified by a standardised heat tolerance test (HTT) and *in vitro* contracture test (IVCT) to better define their condition. All patients were also genetically screened using a custom 50-gene panel, including genes related to Ca^{2+} and energy metabolism.

2.2 Materials and Methods

2.2.1 Samples

The EHI cohort (Table 2.1) comprised sixty-four patients referred to the Malignant Hyperthermia Investigation Unit, University of Leeds, where genetic and functional (IVCT) tests are routinely used to diagnose MH susceptibility. Fifty-nine patients were military personnel referred by the INM, while five were civilians referred to the Leeds MH Unit after presenting clinically with EHI. Four civilians were referred to the Leeds MH Unit via the national health service (NHS) and the fifth civilian underwent heat tolerance testing at the University of Portsmouth (laboratory of Professor Mike Tipton). Two

military EHI patients were referred historically prior to the development of a HTT at the INM. Of the fifty-eight EHI referrals who underwent heat tolerance testing, fifty-two failed to thermoregulate. The six individuals who passed the HTT had all experienced either EHI reactions featuring exertional rhabdomyolysis or exertional rhabdomyolysis, warranting further investigation.

The EHI subjects were predominately male, young, fit and otherwise healthy due to their military occupation. Reports detailing the EHI clinical reactions and heat tolerance test responses were provided by the INM, while IVCTs were conducted by staff at the UK MH Investigation Unit and data were archived with both hard and electronic copies available. Sensitivity to caffeine and halothane were measured through muscle contracture force (grams) in response to incremental concentrations of each agonist. Differences in contracture strength were recorded at either 2% halothane or 2 mM caffeine for the 22 IVCT positive EHI patients and 46 MH patients for comparison. Muscle twitch was recorded for all patients with an IVCT result as a measure of muscle viability and strength, with pre-drug twitch ≥1 g representing viable muscle. The values were re-measured and scaled from the original IVCT traces with help from Dr. Aboelsaod at the UK MH Investigation Unit.

Table 2.1: Overview of exertional heat illness cohort. Information includes IVCT classification, number of individuals, age at biopsy, sex, occupation and whether heat tolerance testing was conducted.

IVCT	Individuals	Age at biopsy	Male/ Female	Military	Civilian	HTT
MHN	41	17-34	M	38	3	37
MHSh	18	20-34	M/ F	17	1	17
MHShc	4	20-28	M	4	–	4
No IVCT	1	N/A	M	–	1	–
ALL	64	17-34	63M / 1F	59	5	58

Genomic DNA (gDNA) samples extracted from the 64 EHI patients were included in the targeted next-generation sequencing (NGS) study. Ethical approval was granted by the Leeds Healthcare St James's University Hospital NHS Trust Clinical Research (Ethics) Committee (10/H1306/70), with all patients providing written consent for peripheral blood and muscle samples to be stored for research purposes. Family members of EHI index cases were also included in the 50-gene sequencing study, where available, in order to perform segregation studies. Specifically, 10 individuals from 3 EHI families were sequenced alongside the 64 EHI patients. In addition, 1,123 non-EHI samples were screened by Fluidigm SNP Type™ genotyping assays using Dynamic Array integrated

fluidic circuits (IFCs) (Table 2.2). The samples comprised 658 MHSh/hc and 180 MHN patients diagnosed by IVCT and 285 unrelated British Caucasian DNA samples (European Collection of Cell Cultures (ECACC)). The MHSh/hc samples represented 636 independent families from the Leeds MH Investigation Unit, including MH susceptible probands where available or an MHSh/hc relative. The MHN samples comprised 112 MHN relatives of MH susceptible index cases and 68 MHN individuals who had experienced a clinical reaction under anaesthesia. Fifty-five EHI samples from the cohort of sixty-four were used as positive controls in the Fluidigm genotyping screen.

Table 2.2: Non-EHI samples screened using the custom Fluidigm variant genotyping screen.

Group	Total	Unrelated	IVCT
MHSh/hc	658	636	✓
MHN	180	176	✓
UK POP	285	285	✗

2.2.2 Targeted next-generation sequencing

2.2.2.1 DNA preparation

DNA was extracted from peripheral whole blood samples using a salt precipitation method, which was performed by staff at the Leeds MH Unit. Briefly, erythrocyte lysis was achieved by adding a buffer containing 155 mM NH_4 Cl, 10 mM $KHCO_3$ and 1.0 mM EDTA to whole blood in a 3:1 ratio. Leukocytes were pelleted and then lysed with 3 mL of a solution containing 2% sodium dodecyl sulphate and 25 mM EDTA. Protein was precipitated using 10 M ammonium acetate and pelleted, while DNA remained in the supernatant. DNA was precipitated using isopropanol, pelleted and washed in 70% ethanol. Extracted gDNA was diluted to 500 ng/µl in Tris-EDTA (10 mM Tris-HCl, 1 mM disodium EDTA, pH 8.0) and stored at -80°C. DNA concentration and quality was re-checked prior to library preparation using the NanoDrop™ 1000 spectrophotometer, ensuring all samples had a 260/280 absorbance ratio of ~1.8. DNA was diluted to 50 ng/µl in Tris-EDTA, pH 8.0 to allow accurate quantification and visualisation. DNA integrity was checked by agarose gel electrophoresis prior quantification. Gels were formed by dissolving molecular grade agarose tablets (Bioline) in 1X Tris Acetate EDTA (TAE) buffer to a final concentration of 1% (plus 0.5 µg/ml EtBr). 1X TAE buffer contained 40 mM Tris, 20 mM acetic acid and 1 mM EDTA. Samples were mixed in a

1:5 ratio [v/v] with 6x loading buffer (New England Biolabs), loaded onto the gel alongside a Quick-Load® 100 bp DNA Ladder (New England Biolabs) and run at 120V for 1 hour. The gel was visualised on a UV gel imaging system (Syngene).

DNA concentrations were measured using the Quant-iT™ dsDNA High-Sensitivity Assay kit (Invitrogen™), according to manufacturer's instructions. DNA standards were prepared ranging between 0-100 ng/µl. Quanti-iT™ dsDNA HS reagent was diluted 1:200 in Quanti-iT™ dsDNA HS buffer. 200 µl working solution and 2 µl DNA sample was added to each well. Fluorescence was measured using a FLUOstar Galaxy microreader (BMG LABTECH) following the manufacturer's instructions (excitation/ emission at ~480/530). All gDNA samples were then diluted to a working concentration of 5 ng/µl for HaloPlex™ target enrichment.

2.2.3 HaloPlex™ target enrichment

HaloPlex™ target enrichment (Agilent Technologies, Santa Clara, CA, USA) was performed per the manufacturer's protocol (HaloPlex™ Target Enrichment System for Illumina Sequencing Version D.3, December 2012). The system relies on a combination of restriction digestion, customised probe hybridisation, magnetic bead capture, and polymerase chain reaction (PCR) amplification to create a targeted HaloPlex™ library for downstream sequencing applications (Figure 2.1). In brief, 200ng gDNA was fragmented using combinations of 8 restriction enzymes and then hybridised to custom HaloPlex™ oligonucleotide probes complimentary to the 353 target exons. The individual gDNA libraries were barcoded using 8-nucleotide indexing primer cassettes to allow subsequent pooling of samples for sequencing. Each fragment of circularised target DNA comprised a unique nucleotide index, an Illumina sequencing motif and biotinylated target specific probe. The target DNA was then captured on streptavidin magnetic beads (HaloPlex™) and ligated to seal the circularised DNA fragments. The captured DNA fragments were amplified by PCR and purified with AMPure® XP beads (Agencourt). The target libraries were validated and quantified (fmol/ µl) using Agilent's High Sensitivity DNA assay kit and run on the 2100 Bioanalyzer (Agilent technologies, Santa Clara, CA). Molar concentrations of enriched target DNA (175-625 bp) were calculated and equimolar amounts of each HaloPlex™ library (100 fmol) were combined into a single indexed pool for sequencing.

HaloPlex™ SureDesign was used to create a custom oligonucleotide probe library to target 1091 exons of 50 genes related to calcium homeostasis, energy metabolism and

MH-related myopathies. These included 5 genes that encode RyR1 and the $Ca_v1.1$ complex (Table 2.3), 6 genes associated with an exercise intolerance phenotype (Table 2.4) and 39 additional genes involved in calcium homeostasis and energy metabolism (Table 2.5).

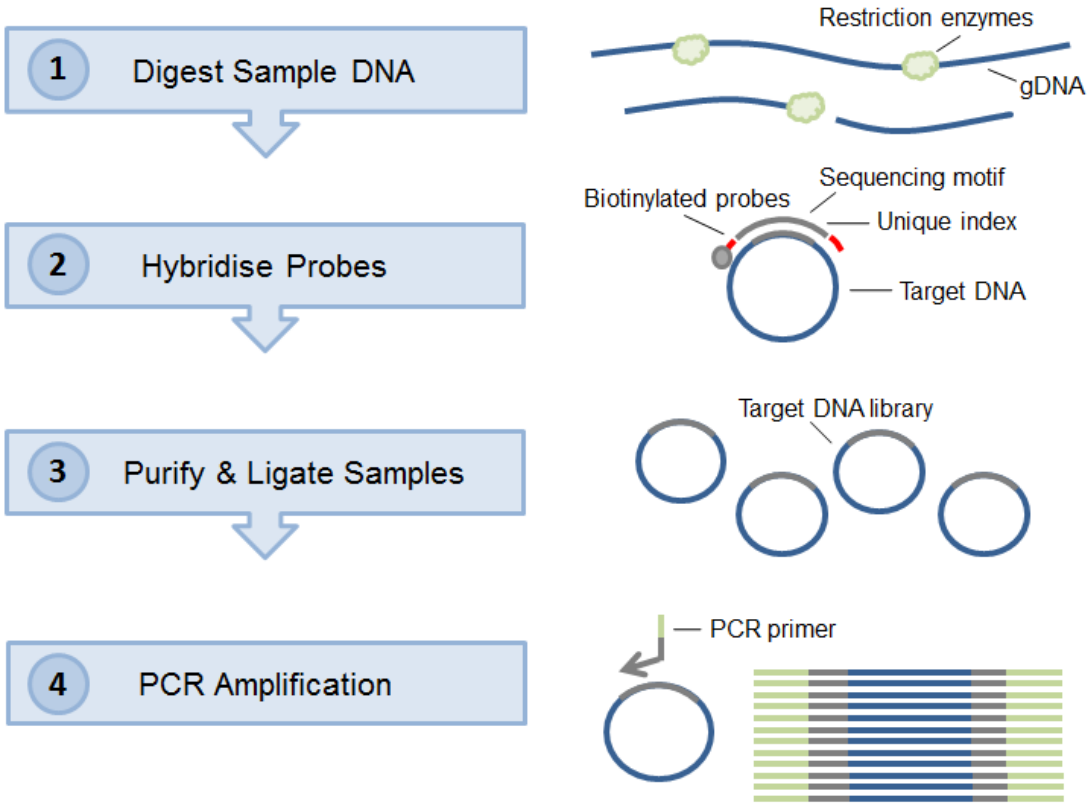

Figure 2.1: Schematic representation of Agilent's HaloPlex™ target enrichment system. Custom designed probes specific to target regions are hybridised to gDNA, purified, and PCR amplified resulting in libraries of target DNA. Schematic based on manufacturer's protocol workflow, adapted and redrawn (HaloPlex™ Target Enrichment System for Illumina Sequencing Version D.3, December 2012).

Table 2.3: Summary of genes encoding RyR1 and the $Ca_v1.1$ complex. This table includes information regarding number of exons, predicted coverage of HaloPlex™ target enrichment, protein function and disease associations reported in the literature.

Gene	Protein product	Exons	Coverage	Function	Disease association
CACNA1S OMIM: 114208	calcium channel, voltage-dependent, L type, alpha 1S subunit	44	99.88%	Alpha 1S subunit of the voltage-gated Ca^{2+} channel ($Ca_v1.1$). This pore-forming subunit contains the voltage sensor.	(Eltit *et al*., 2012; Weiss *et a*l., 2004)
CACNA2D1 OMIM: 114204	calcium channel, voltage-dependent, alpha 2/delta subunit 1	44	99.87%	Alpha 2/delta subunit of the $Ca_v1.1$ complex. This subunit regulates calcium current density and kinetics of the channel.	N/A
CACNB1 OMIM: 114207	calcium channel, voltage-dependent, beta 1 subunit	16	99.91%	Beta-subunit of the $Ca_v1.1$ complex, which modulates peak calcium current, voltage dependence and involved in the interaction between $Ca_v1.1$ and RyR1.	N/A
CACNG1 OMIM: 114209	calcium channel, voltage-dependent, gamma subunit 1	4	100.00%	Gamma-subunit of the $Ca_v1.1$ complex modulates membrane trafficking, current kinetics and gating properties of the channel.	N/A
RYR1 OMIM: 180901	ryanodine receptor 1 (skeletal)	106	99.86%	Calcium release channel in the sarcoplasmic reticulum that triggers muscle contraction following depolarisation of T-tubules.	Malignant hyperthermia/ central core disease/ multi-minicore disease (Robinson *et al.*, 2006; Zhou *et al.*, 2010)

Table 2.4: Summary of genes investigated associated with an exercise intolerance phenotype. This table includes information regarding number of exons, predicted coverage of HaloPlex™ target enrichment, protein function and disease associations reported in the literature.

Gene	Protein product	Exons	Coverage	Function	Disease association
AMPD1 OMIM: 102770	adenosine monophosphate deaminase 1	16	100.00%	Involved in energy production within skeletal muscle (conversion of AMP to IMP).	Adenosine Monophosphate Deaminase 1 Deficiency (Gross *et al.*, 2002)
ATP2A1 OMIM: 108730	ATPase, Ca++ transporting, cardiac muscle, fast twitch 1	25	100.00%	SERCA pump transports calcium from the cytosol to the sarcoplasmic reticulum lumen.	Brody's myopathy (delayed muscle relaxation) (Vattemi *et al.*, 2010)
CLCN1 OMIM: 118425	chloride channel, voltage-sensitive 1	25	100.00%	Chloride channel regulates the electric excitability of the skeletal muscle membrane.	Myotonia congenita (delayed muscle relaxation) (Duno *et al.*, 2004).
CPT2 OMIM: 600650	carnitine palmitoyltransferase 2	5	94.91%	Nuclear protein which is transported to the mitochondrial inner membrane and involved in fatty acid oxidation.	Myopathic form of CPT II deficiency (Vladutiu *et al.*, 2000)
PYGM OMIM: 608455	phosphorylase, glycogen, muscle	20	99.44%	Myophosphorylase breaks down glycogen to glucose-1-phosphate.	McArdle's disease (glycogen storage) (Nogales-Gadea *et al.*, 2015)
TRDN OMIM: 603283	Triadin	48	99.48%	Forms complex with RyR1 and anchors calsequestrin to the junctional SR modulating calcium release.	Ventricular tachycardia, muscle weakness (CPVT5) (Roux-Buisson *et al.*, 2012)

Table 2.5: Summary of additional genes included in HaloPlex™ panel. This table includes gene name, OMIM ID and description along with number of exons, predicted coverage of HaloPlex™ target enrichment and protein function.

Gene	OMIM ID	Protein product	Exons	Coverage	Function
ACADM	OMIM: 607008	Acyl-CoA dehydrogenase, medium chain	16	99.68%	Involved in fatty acid oxidation within the mitochondria.
ACADVL	OMIM: 609575	Acyl-CoA dehydrogenase, very long chain	7	100.00%	Involved in fatty acid oxidation within the mitochondria.
ANXA6	OMIM: 114070	Annexin 6	29	99.86%	Ca^{2+}-binding protein which regulates release of Ca^{2+} from intracellular stores.
ASPH	OMIM: 600582	Aspartate beta-hydroxylase	37	99.99%	Role in Ca^{2+} homeostasis regulating Ca^{2+} release from sarcoplasmic reticulum (SR).
CALM1	OMIM: 114209	Calmodulin 1	6	100.00%	Member of the EF-hand calcium-binding protein family.
CALR	OMIM: 109091	Calreticulin	9	100.00%	Ca^{2+}-binding chaperone involved in Ca^{2+}homeostasis.
CAPN3	OMIM: 114240	Calpain 3	30	100.00%	Ca^{2+}-sensitive intracellular protease.
CASQ1	OMIM: 114250	Calsequestrin 1	12	100.00%	Ca^{2+}-binding protein acts as an internal Ca^{2+} store in muscles.
CAV3	OMIM: 601253	Caveolin 3	4	100.00%	Scaffolding protein in muscle cell walls.
CHERP	N/A	Calcium homeostasis endoplasmic reticulum protein	18	100.00%	Involved in calcium homeostasis, growth and proliferation.
DNM2	OMIM: 602378	Dynamin 2	22	99.98%	GTP-binding protein involved in producing microtubule bundles.
FKBP1A	OMIM: 186945	FK506 binding protein 1A	7	99.01%	Coordinates multi-protein RYR1 complex formation.
GYS1	OMIM: 138570	Glycogen synthase 1 (muscle)	15	100.00%	Catalyzes addition of glucose monomers to the glycogen molecule.
HOMER1	OMIM: 604798	Homer homolog 1	9	99.29%	Scaffold protein that bind to and regulates RyR1.
HRC	OMIM: 142705	Histidine rich calcium binding protein	6	100.00%	Luminal SR protein, binds to the cytoplasmic domain of triadin.
HSP90AA1	OMIM: 140571	Heat shock protein 90kDa alpha (cytosolic)	10	99.83%	Molecular chaperone that is expressed under conditions of stress and promotes proper folding of specific target proteins.
HSPA4	OMIM: 601114	Heat shock 70kDa protein 4	21	100.00%	Molecular chaperone that is expressed under conditions of stress.
HSPB1	OMIM: 602195	Heat shock 27kDa protein 1	2	100.00%	Involved in stress resistance and actin organization and is induced by environmental stress.
JPH1	OMIM: 605226	Junctophilin 1	6	99.79%	Forms junctional membrane complexes (JMCs) linking the plasma membrane with the SR vital for RyR1-mediated calcium release.
JPH2	OMIM: 605267	Junctophilin 2	7	99.84%	Forms junctional membrane complexes (JMCs), which is central to RyR1-mediated calcium release.
LPIN1	OMIM: 605518	Lipin 1	33	98.82%	Plays important role in controlling the metabolism of fatty acids.

Table 2.5 (continued)

Gene	OMIM ID	Protein product	Exons	Coverage	Function
NEB	OMIM: 161650	Nebulin	183	91.25%	Component of the cytoskeletal matrix co-exists with thick/thin filaments of skeletal muscle.
ORAI1	OMIM: 610227	ORAI calcium release-activated calcium modulator 1	2	99.07%	Mediates Ca^{2+} influx following depletion of intracellular Ca^{2+} stores, detected by STIM1.
PVALB	OMIM: 168890	Parvalbumin	19	100.00%	High affinity Ca^{2+}-binding protein involved in muscle relaxation.
S100A1	OMIM: 176940	S100 calcium binding protein A1	3	100.00%	Ca^{2+}-binding protein associated with cardiomyopathies.
SCN4A	OMIM: 603967	Sodium channel, voltage-gated, type IV, alpha subunit	24	99.96%	Voltage-gated Na^{+} channels that propagate action potentials in skeletal muscle.
SEPN1	OMIM: 606210	Selenoprotein N, 1	14	98.22%	Protects against oxidative stress and binds Ca^{2+}, associated with multi-minicore disease and congenital muscular dystrophy.
SLC8A1	OMIM: 182305	Solute carrier family 8 (sodium/calcium exchanger), 1	19	100.00%	Not expressed in skeletal muscle, so excluded from analysis.
SLC8A3	OMIM: 607991	Solute carrier family 8 (sodium/calcium exchanger), 3	11	100.00%	Rapidly transports Ca^{2+} across plasma membrane during EC coupling to restore Ca^{2+} levels.
SRL	OMIM: 604992	Sarcalumenin	8	100.00%	Ca^{2+}-binding protein in SR, which helps buffer Ca^{2+}.
STAC3	OMIM: 615521	SH3 and cysteine rich domain 3	12	100.00%	Skeletal muscle-specific T-tubule protein is required for myotubule formation and myogenic differentiation.
STIM1	OMIM: 605921	Stromal interaction molecule 1	27	99.46%	Mediates Ca^{2+} influx after sensing depletion of intracellular Ca^{2+} stores by gating ORAI1.
SYPL2	N/A	Synaptophysin-like 2	6	99.95%	Involved in communication between the T-tubular and junctional sarcoplasmic reticulum (SR) membranes.
TRIM72	OMIM: 613288	Tripartite motif containing 72	7	100.00%	Muscle-specific protein that plays a central role in cell membrane repair.
TRPC1	OMIM: 602343	Transient receptor potential cation channel, C, 1	13	99.08%	Forms a non-selective channel permeable to Ca^{2+} and other cations. Activated by intracellular Ca^{2+} store depletion.
TRPC2	N/A	Transient receptor potential cation channel, C, 2	18	100.00%	Pseudogene. Excluded from analyses.
TRPC3	OMIM: 602345	Transient receptor potential cation channel, C, 3	14	100.00%	Forms a non-selective channel permeable to calcium and other cations. Activated by intracellular calcium store depletion.
TRPM6	OMIM: 607009	Transient receptor potential cation channel, M, 6	45	99.55%	Essential ion channel that is crucial for magnesium homeostasis.

2.2.4 Illumina® MiSeq®

The enriched HaloPlex™ libraries were sequenced on-site using Illumina's MiSeq® platform, producing 150-bp paired-end reads totalling 13457 amplicons per sample. This NGS platform supports high-throughput sequencing by clonal bridge amplification and sequencing by synthesis (SBS) technology (Bentley *et al.*, 2008). Specifically, DNA fragments are hybridised to oligonucleotides on the flow cell which are complimentary to the Illumina adapters incorporated into each fragment. Clusters of identical fragments are produced by bridge amplification as shown in Figure 2.2. The nucleotide base of each read is determined as the complementary strand is synthesised, whereby fluorescently tagged nucleotides are incorporated and imaged in real-time to capture the sequence. This high-throughput technology allows target genes to be sequenced in all samples in parallel across one MiSeq® flow cell. The sequencer de-multiplexes the reads using the unique indexes, which generates a forward and reverse FASTQ file for each sample.

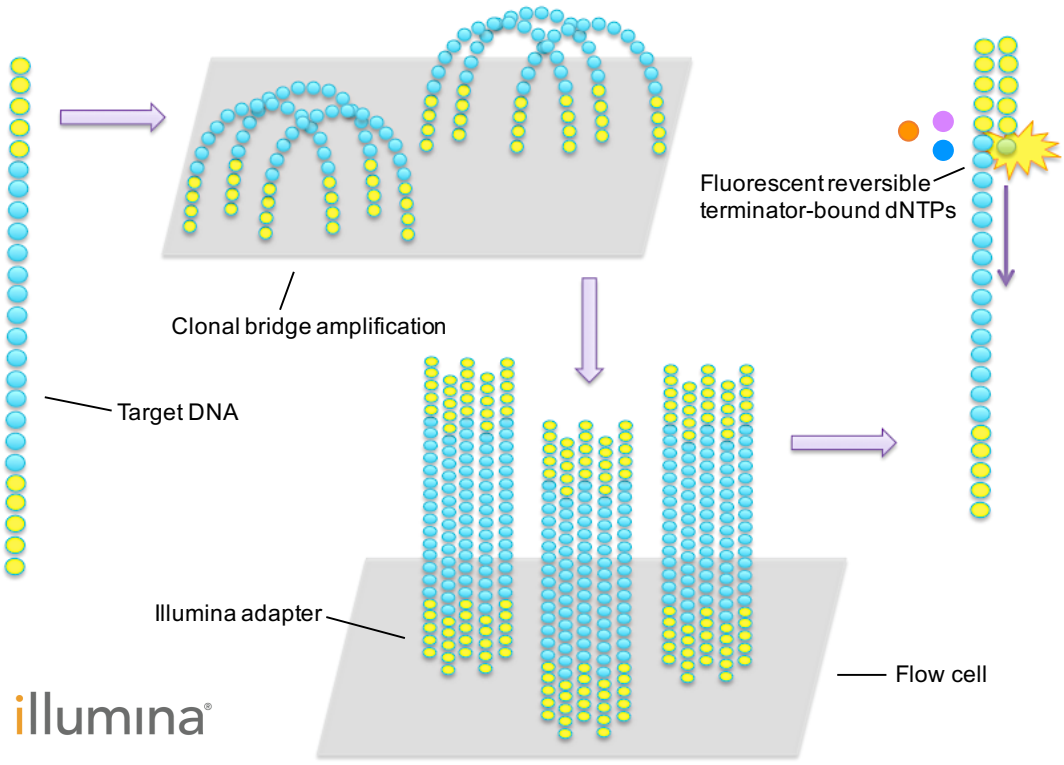

Figure 2.2: Overview of Illumina next-generation sequencing technologies used across their platforms.

2.2.5 HaloPlex™ NGS data analysis

An overview of the data analysis pipeline is shown in (Figure 2.3). The sequence data were analysed using SureCall (Agilent Technologies), purpose-built software, which offers an integrated pipeline to pre-process, align, categorise and annotate genetic data. In brief, default settings were used to upload raw FASTQ files, after which the reads were trimmed to remove sequencing adapters and low-quality bases. Sequence data were selectively aligned to the target regions using a custom design annotation based on the human reference genome (assembly GRCh37/hg19) and the Burrows–Wheeler aligner maximum exact matches (BWA MEM) algorithm. Genetic variants were called using the SAMtools Base Alignment Quality (BAQ) SNP Caller (Li *et al.*, 2009). Non-synonymous variants were selected by filtering for category I and II sequence variations (Table 2.6) and manually checked to remove false-positive calls picked up by the default software parameters. All remaining variants had a read depth ≥10 with the variant detected on both forward and reverse reads.

Figure 2.3: NGS variant filtering pipeline. Non-synonymous variants were identified and annotated with population frequency and in silico pathogenicity predictions to prioritise variants for further analyses.

The filtered variants were exported from SureCall, which extracts known annotations from various databases and online tools to guide interpretation. Minor allele frequencies (MAF) were provided from the 1000 Genomes (1000G) and dbSNP databases and were calculated using all populations (Sherry *et al.*, 2001; 1000GenomesProject, 2012). Additional minor allele frequencies were extracted manually from the Exome Aggregation Consortium (ExAC) and used for subsequent filtering steps (Lek *et al.*, 2016). The ExAC data set comprises 60,706 unrelated individuals of European, South Asian, East Asian, Latino or African descent. Variant frequencies taken from the ExAC browser were calculated from allele counts across all populations.

Table 2.6: Genetic variant categorisation using SureCall software. Non-synonymous variants will be classified as either category I or II depending on reported pathogenicity in the literature and on relevant databases.

SureCall software variant filtering criteria
Category I:
- Known in literature to be clinically significant and causative
- Evidence for pathogenicity in locus-specific databases
- Is associated with disease in GWAS catalog
- Is associated with a tumor site in COSMIC
- Is validated in clinical study in NCBI SNP
- Annotated pathogenic in NCBI SNP database
- Is non-synonymous coding variant in stop
- Is non-synonymous coding variant
- Sequence changes seen multiple times in different samples
Category II:
- Introduction of a stop codon
- In-frame exon deletion
- Mutates the initiation codon (ATG)
- Missense mutation of the normal stop codon
- Annotated probable pathogenic in NCBI SNP database
- Deletes nucleotide(s) that lead(s) to a shift of reading frame
- Deletes exon which results in shift of reading frame
- Results in codon change
- Results in codon insertion/ deletion
- Any missense mutation
- Nonsense or a frame shift mutation
- Is non-synonymous coding variant in start

Sorting Intolerant From Tolerant (SIFT) scores (Sim *et al.*, 2012) and Polyphen2: Polymorphism Phenotyping scores (Adzhubei *et al.*, 2010) were calculated and provided by the SureCall software. SIFT and Polyphen2 scores predict the functional effect of variants at protein-level. More specifically SIFT scores use the level of conservation of an amino acid to predict whether a substitution will be tolerated or not. Alternatively,

PolyPhen-2 predicts impact of an amino acid substitution on the structure, stability and function of the protein.

An additional *in silico* pathogenicity prediction tool known as Combined Annotation Dependent Depletion (CADD) was used as the primary pathogenicity annotation (Kircher *et al.*, 2014). The CADD tool incorporates 63 *in silico* pathogenicity annotations to score (C-score) and rank the 8.6 billion possible substitutions in the human reference genome (GRCh37), offering a robust measure to prioritise variants for follow-up. Pathogenicity C-scores were calculated using CADD v1.3 (last accessed 20.02.17).

Non-synonymous variants identified in EHI patients with a MAF ≤1% (ExAC) and a C-score of ≥15 were selected for further investigation. Due to the unknown prevalence of EHI susceptibility in the general population an allele frequency of 1% was chosen to include all rare variants. C-scores of 15 or greater represent the 5% most deleterious substitutions in the human genome and therefore was suggested as an appropriate threshold by the CADD tool developers. Available resources were used to check for disease associations in published literature, primarily the Human Gene Mutation Database (HGMD®) and the Leiden Open Variation Database (LOVD) (Fokkema *et al.*, 2011; Stenson *et al.*, 2014).

2.2.6 Sequencing gaps in *RYR1* coverage identified in NGS data

2.2.6.1 Long-range PCR

Recurrent gaps in *RYR1* coverage were sequenced using a NGS long-PCR approach. PCR oligonucleotide primers were designed (previously by Dr. Dorota Miller) to produce amplicons of between 3.7-5.7-kb covering the 7 regions of *RYR1* with gaps detected in coverage (Table 2.7). Long-range PCR was performed generating 7 *RYR1* amplicons per sample using the SequalPrep™ Long PCR kit, which accurately amplifies fragments up to 15-kb long. The reagents were added according to manufacturer's instructions and thermal cycler conditions were optimised for long PCR fragments, including 2 minutes at 94°C, 10 seconds at 94°C, 30 seconds at 60°C, 6 minutes at 68°C (steps 2-4 repeat for 35 cycles), 5 minutes at 72°C. PCR products were then visualised by agarose gel electrophoresis, as described in section 2.2.2.1.

Table 2.7: Primer sequences for *RYR1* long-range PCR amplicons.

Primer ID	Exons	Size	Sequence
RYR1_FR4_F	Ex 12 - 16	5606bp	5'-CCAGTGCCTAGAACAGAGCC-3'
RYR1_FR4_R			5'-GCAACAGGAACTTGTAGGGC-3'
RYR1_FR9_F	Ex 35 – 38	3762bp	5'-GACCTGGGTGGATCTTAAGGAG-3'
RYR1_FR9_R			5'-CTATCTACCCCTCCCTTGCATCT-3'
RYR1_FR11_F	Ex 43 – 49	4036bp	5'-GTCTCTGACTGAGCCCCTTCT-3'
RYR1_FR11_R			5'-GAGATTTCTACGGGGACGCT-3'
RYR1_FR12_F	Ex 50 – 58	4004bp	5'-GCATCCATATGCCCATTTACTC-3'
RYR1_FR12_R			5'-TAGGTGAGTCTGGTCTGCAGAA-3'
RYR1_FR14_F	Ex 64 – 67	4937bp	5'-GAGGAAGTACCCCTCACTTTCA-3'
RYR1_FR14_R			5'-GAAACCAGGAGGAAGAGTCAGA-3'
RYR1_FR17_F	Ex 85 – 89	5703bp	5'-TGCTTTCTGGCATACAATAGGA-3'
RYR1_FR17_R			5'-CGGTTCTCATCTGTGTTAATGC-3'
RYR1_FR22_F	Ex 97 – 101	5034bp	5'-GACAGCTCTGATCCCTCTGG-3'
RYR1_FR22_R			5'-ATGCATCAGCTTGCCAAACT-3'

2.2.6.2 Agencourt® AMPure® XP sample purification

Long-range PCR products were purified using the Agencourt® AMPure® XP system (Agencourt Bioscience Corp., Beverly, MA) according to the manufacturer's protocol (Agencourt® AMPure® XP protocol 000387v001). In brief, AMPure® XP paramagnetic beads were added at 1.8X the total volume of PCR product, binding DNA fragments ≥100-bp. The DNA-bead complexes were separated from contaminants using an Agencourt® SPRIPlate 96 Super Magnet Plate and washed twice with 200 µl 70% ethanol. Samples were removed from the magnetic plate and eluted with Ambion™ nuclease-free water. Finally, the eluates were returned to the magnetic plate and the purified gDNA samples were transferred to a clean 96-well plate.

2.2.6.3 PCR product quantification

The purified PCR products were quantified using the Quant-iT™ High-Sensitivity dsDNA Assay Kit (Invitrogen™), which detects double-stranded DNA in the range of 0.2-100 ng. Concentrations were calculated using a FLUOstar Omega microreader (BMG LABTECH) and equimolar amounts of DNA were pooled (10 fmol each) to create one PCR product pool per sample comprising 7 *RYR1* fragments (70 fmol total DNA in 50 µl nuclease-free water (1.4 nM).

2.2.6.4 Covaris® DNA fragmentation

Pooled PCR products were sheared to produce ~200-bp fragments using the Covaris® E220 focused-ultrasonicator according to the manufacturer's instructions. In brief, samples were transferred to Covaris® microTUBES and fragmented using Adaptive

Focused Acoustics™ (AFA) technology, whereby bursts of high-frequency acoustic energy are released from a Covaris® focused-ultrasonicator. Settings included 1.75 peak power, 10% duty factor, 200 cycles, 17.5 average power and 120 second per sample.

2.2.6.5 NEBNext® Ultra™ DNA Library Preparation

Indexed libraries of target DNA were created using the NEBNext® Ultra™ DNA Library kit in combination with NEBNext® Multiplex Oligos for Illumina® according to the manufacturer's protocol. In brief, DNA fragments were repaired to produce DNA with 5' phosphorylated, 3' dA-tailed ends. NEBNext® adaptors were ligated to the DNA fragments via dT overhangs prior to size selection with AMPure® XP beads. Unique index sequences were incorporated during a PCR amplification step and purified again using AMPure® XP beads. The size distribution and concentration of the libraries were checked using the High Sensitivity D1000 ScreenTape system and Agilent's 2200 TapeStation, according to the manufacturer's instructions.

2.2.6.6 Illumina® MiSeq® NGS

The purified libraries were pooled and sequenced on-site using Illumina's MiSeq® platform producing 150-bp paired-end reads, as described in section 2.2.4, Sequenced reads were de-multiplexed to create a forward and reverse FASTQ file for each sample.

2.2.6.7 NEBNext® Ultra™ NGS data analysis

Sequence data were analysed using the SureCall software (Agilent Technologies). The same analysis pipeline was used as for the HaloPlex™ NGS data analysis (see section 2.2.5 for details). Non-synonymous variants detected in the regions of *RYR1* of not covered by HaloPlex™ target enrichment were annotated with MAF from the ExAC database (Lek *et al.*, 2016) and *in silico* pathogenicity C-scores ((Kircher *et al.*, 2014).

2.2.7 Fluidigm® high throughput variant screen

2.2.7.1 Sample purification using the Agencourt® AMPure® XP system

Due to long-term storage of samples at the Leeds MH Investigation Unit, the 658 MHSh/hc and 180 MHN samples were bead cleaned prior to genotyping to ensure

uniform DNA quality (260:280 ratio 1.5-1.8). It was not necessary to purify the 285 commercial UK populations samples manufactured by ECACC and purchased from Sigma-Aldrich. Sample purification was performed using the Agencourt® AMPure® XP system (Agencourt Bioscience Corp., Beverly, MA) according to the manufacturer's protocol (Agencourt® AMPure® XP protocol 000387v001), described previously (Section 2.2.6.2).

2.2.7.2 Fluidigm® specific target amplification (STA)

Specific target amplification (STA) is multiplex PCR performed to amplify ~50 bp fragments around the target region to provide sufficient template molecules for use on Fluidigm's IFCs (Figure 2.4).

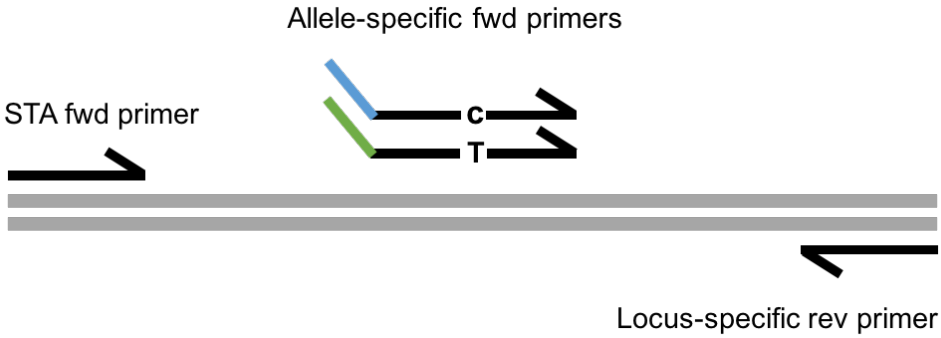

Figure 2.4: Figure illustrating optional specific target amplification (STA) prior to Fluidigm genotyping. Target regions amplified using STA forward primers and locus-specific reverse primers.

Only the MHSh/hc and MHN samples were subjected to STA due to the low gDNA concentration of many samples after AMPure® bead purification. STA was performed according to the manufacturer's protocol (Fluidigm SNP Genotyping Analysis User Guide PN 68000098 O1). In brief, SNP Type™ STA primer assays and SNP Type™ Locus Specific Primer (LSP) assays were pooled to create a 10X primer pool with primers at a final concentration of 500 nM (Primer sequences provided in appendix A). This 10X primer pool was combined with Qiagen 2X Multiplex PCR Master Mix and Ambion™ nuclease-free water to produce an STA pre-mix (3.75 µl per sample) and added to 1.25 µl gDNA ready for PCR amplification (5 µl per sample). Thermal cycler conditions comprised a 15-minute hold at 95˚C and 14 cycles of 15-seconds at 95˚C and 4-minutes at 60˚C. The STA products were diluted 1:80 in DNA suspension buffer and stored at -20˚C.

2.2.7.3 Fluidigm® SNP Type™ genotyping on the Dynamic Array™ IFCs

An overview of the Fluidigm® SNP Type™ genotyping chemistry has been presented in Figure 2.5. Fluidigm® SNP Type™ genotyping (Fluidigm Corporation, San Francisco, CA) was completed on the 1,123 non-EHI samples as described in Table 2.2. Fifty-five EHI samples were also screened acting as positive controls. SNP Type™ genotyping was carried out according to the manufacturer's protocol (Fluidigm® SNP™ Genotyping Analysis User Guide PN 68000098 O1). In brief, SNP Type™ allele-specific primers (ASP1/ ASP2) (7.5 µM final concentration) were combined in a 96 well plate with SNP Type™ LSP assays (20 µM final concentration) and DNA Suspension Buffer and mixed with 2X Assay Loading Reagent and Ambion™ nuclease-free water to produce a 10X assay mix (5 µl per assay) (Primer sequences provided in appendix A). Sample mixes were prepared by combining Biotium 2X Fast Probe Master Mix, 20X SNP Type Sample Loading Reagent, 60X SNP Type Reagent, ROX reference dye and Ambion™ nuclease-free water with 2.5 µl gDNA in a 96 well plate (6 µl per sample mix). The 10X Assay Mix (4 µl) and Sample Mix (5 µl) were loaded onto the Dynamic Array IFC and run on the BioMark™ HD System using the SNP Type 96x96 v1 thermal cycling protocol labelled with universal probes containing fluorophores SNP Type-FAM and SNP Type-HEX.

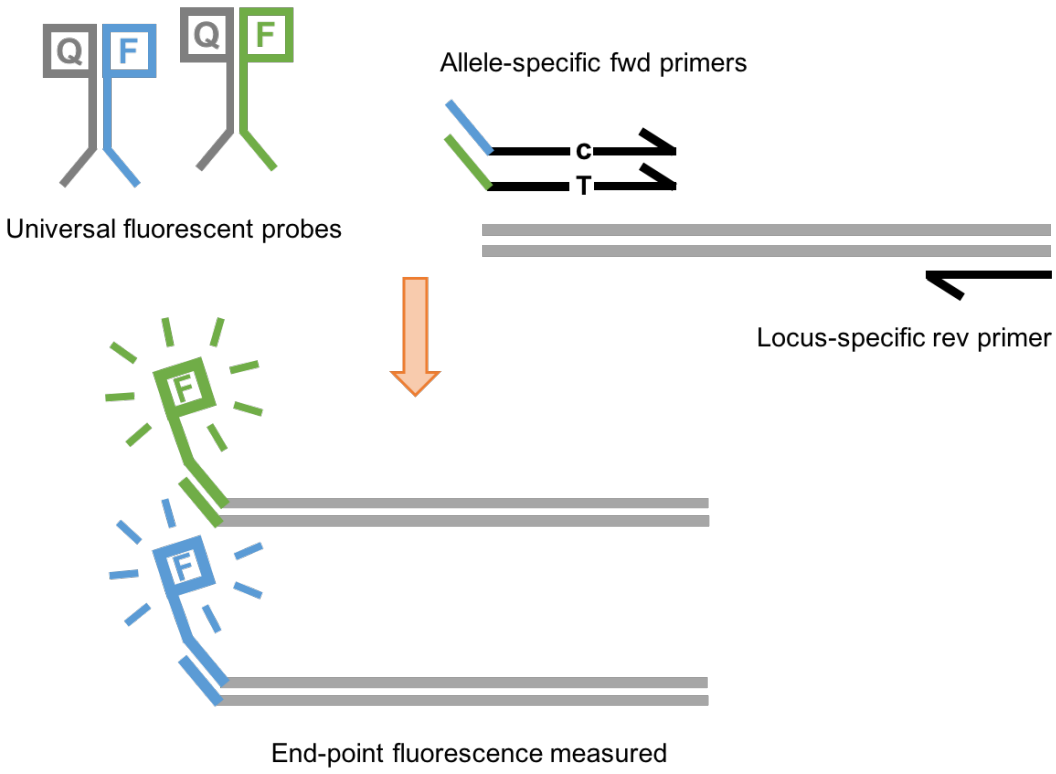

Figure 2.5: Schematic representation of allele-specific SNP Type™ genotyping chemistry developed by Fluidigm®.

2.2.7.4 SNP Genotyping Analysis

Data were analysed using Fluidigm's custom-built SNP Genotyping Analysis software. Fluorescence emitted from FAM and HEX labelled allele-specific amplicons were quantified and values were plotted to assign genotypes for each variant. Genotype calls were manually checked and amended if necessary. Final genotypes were saved and exported into Excel spreadsheets to merge data across SNPtype arrays. Specificity of Fluidigm® assays were calculated by dividing the number of true negative genotypes by the sum of true negative and false positive genotypes.

2.2.8 Confirmation of positive variant calls using alternative methods

2.2.8.1 PCR amplification

PCR oligonucleotide primers were designed using Primer-BLAST (NCBI) to produce amplicons of between 300-600-bp covering the regions of interest (Table 2.8) for downstream applications including restriction enzyme digestion and Sanger sequencing. Positive genotypes were confirmed for 18 non-synonymous variants included in the Fluidigm variant screen across 17 PCR amplicons. Primer sequences were checked for single nucleotide polymorphisms (SNPs) to exclude the potential of preferential amplification of the common allele resulting in a false negative result.

PCR was performed using 0.625 units of DreamTaq DNA polymerase (ThermoFisher Scientific), 1X DreamTaq buffer, 200 µM dNTPs, 0.4 µM of each forward and reverse primers, ~20 ng gDNA and nuclease-free water to 25 µl. Temperature gradients were used to determine optimal annealing conditions for all primers pairs. Final thermal cycler conditions included 5 minutes at 95°C (denaturation), 30 seconds at 95°C (denaturation), 30 seconds at 61°C (annealing), 1 minute at 72°C (extension) (steps 2-4 repeat for 30 cycles) and 5 minutes at 72°C (final elongation). PCR products were visualised by agarose gel electrophoresis on gels made with 1% agarose, 1X TAE buffer and 1 µg/mL EtBr. Samples were diluted with 6X loading buffer loaded onto the gels alongside a 100 bp DNA Ladder and run at 120V for 1 hour (described in detail in section 2.2.2.1).

Table 2.8: Primer sequences for Fluidigm confirmations. Positive Fluidigm genotyping results were confirmed for 18 variants across 17 PCR amplicons.

Primer ID	Sequence	Product size
AMPD1_R104H_F	5'-GCCTATTCTGCTGGGAGTGG-3'	476-bp
AMPD1_R104H_R	5'-GAGTGGCAAGGACCAACTCA-3'	
AMPD1_M340I_F	5'-TCACTTTGTCCCAACGCAGT-3'	463-bp
AMPD1_M340I_R	5'-GGGACAGGTGACAATGAGCA-3'	
ATP2A1_Ex14_F*	5'-TCTGTCTATTGCTCCCCAGC-3'	485-bp
ATP2A1_Ex14_R*	5'-AGGTAGGAAATGATCCGGGTG-3'	
ATP2A1_D650N_F	5'-CAGACGGACCTGACATTCGT-3'	381-bp
ATP2A1_D650N_R	5'-TCTCCGTGGACACTAAGGCT-3'	
CACNA1S_G258D_F	5'-TTCACTGTCACCGTCTGCTC-3'	376-bp
CACNA1S_G258D_R	5'-GACCCACCCAGTAAAGGACG-3'	
CACNA1S_R683C_F	5'-GCTCCCTTCCACCTACAACC-3'	355-bp
CACNA1S_R683C_R	5'-TTGTCTCTGTTCTTGCCCCC-3'	
PYGM_R427W_F	5'-GCTTCCTCAACGTGAGTCCG-3'	513-bp
PYGM_R427W_R	5'-GCTTGTAAGAATGACGCCACC-3'	
RYR1_R1622Q_F	5'-ATGTGTGTCTCTCTGCCCTC-3'	512-bp
RYR1_R1622Q_R	5'-CCTTGGGGTATTGTCTGGGT-3'	
RYR1_S2776F__F	5'-AAGAAATACGACCCGGAGCT-3'	1,141-bp
RYR1_S2776F_R	5'-CTCCCTGGCCTTCTCTATCG-3'	
RYR1_T3711M_F	5'-CCAGCTCCTGGCTTGAGTAG-3'	373-bp
RYR1_T3711M_R	5'-GATCCGTCTGTCTTGGGCTC-3'	
RYR1_H3981Y_F	5'-TTGAAGAGCAGGGCAAGAGG-3'	385-bp
RYR1_H3981Y_R	5'-ACAAACTGACCAAAGGGGCA-3'	
RYR1_I3253T_F	5'-GGTAGTTGGGTTGGAGGGTG-3'	460-bp
RYR1_I3253T_R	5'-ATGCCCAGGTTGTTGACGAT-3'	
RYR1_R3366H_F	5'-CAAGGTTAGGGTCAGGCTGG-3'	370-bp
RYR1_R3366H_R	5'-GTTGTCCACGTAGCGGATGA-3'	
RYR1_D4505H_F	5'-TGAGCCTCAGTTTCCCCTCT-3'	411-bp
RYR1_D4505H_R	5'-TTACTCAGAGCCCCTCCTCC-3'	
SRL_R398C_F	5'-TTGGCCCCTCTCATCAATGT-3'	461-bp
SRL_R398C_R	5'-TCCAGAAAGCAACCTCCCAT-3'	
TRDN_S339N_F	5'-CCACTAGTCTGTTATGAAGGTGCT-3'	551-bp
TRDN_S339N_F	5'-TACGTTTTGAGGGGGAAAAGCC-3'	
TRPM6_M1088R_F	5'-TGTATTGGGTAACTGCCGGT-3'	301-bp
TRPM6_M1088R_R	5'-ACCCTCTTCTTGGTCGTGAG-3'	

*Primer pair ATP2A1_EX14 covers *ATP2A1* p.T538M and p.P540L.

2.2.8.2 Restriction fragment length polymorphism (RFLP)

Restriction fragment length polymorphism (RFLP) analysis was used to genotype 35 family members from 4 unrelated families for a heterozygous *RYR1* variant (c.8327C>T p.S2776F). The non-synonymous variant alters a recognition sequence for the restriction endonuclease AvaII preventing the enzyme cutting the DNA at this restriction site (5'…G▼GWCC…3' 3'…CCWG▲G…5'). AvaII restriction sites within the 1,141 bp fragment of *RYR1* (PCR primers provided in Table 2.8) were identified using http://www.restrictionmapper.org/. In the absence of a variant the endonuclease is predicted to cut at 5 sites across the PCR product producing fragments of 349 bp, 118 bp, 111 bp, 380 bp, 41 bp and 142 bp. *RYR1* c.8327C>T p.S2776F alters the third

recognition site, preventing the endonuclease cutting, producing a larger uncut 491 bp fragment.

The restriction digest was set up, including 1 µl PCR product, 1 µl AvaII endonuclease (NEB), 2 µl CutSmart buffer and 16 µl nuclease-free water and incubated at 37°C for 1 hour. Restriction digests for each patient DNA sample were visualised by gel electrophoresis as described in chapter 2.2.2.1 (1% agarose dissolved in 1X TAE plus 1 µg/mL EtBr run at 120V for 1 hour).

2.2.8.3 Sanger sequencing

Sanger sequencing is a method that incorporates fluorescently-labelled chain-terminating dideoxynucleotide triphosphates (ddNTPs) into DNA strands randomly terminating replication. The resulting fluorescently-labelled DNA strands are separated by size using capillary electrophoresis and fluorescence is measured by a genetic analyser.

ExoSAP-IT™ was used to enzymatically remove contaminants from PCR products prior to Sanger sequencing. Specifically, 2 µl ExoSAP-IT was added to 5 µl PCR product and incubated for 30 minutes at 37°C followed by 15 minutes at 80°C. Subsequently, 2 µl clean PCR product was combined with 1 µl BigDye®, 1 µl halfBD™, 1 µl of either forward or reverse primer (separate reactions) diluted to 3.2 µM and 5 µl nuclease-free water. The sequencing reactions were then incubated at 96°C for 5 minutes, 96°C for 30 seconds, 58°C for 20 seconds, 60°C for 4 minutes (steps 2-4 repeated for 30 cycles). DNA precipitation was performed at room temperature. To the sequenced product 1 µl ammonium acetate (Sigma Aldrich) and 25 µl 95% ethanol was added and left at room temperature for 20 minutes to allow the products to precipitate. The samples were centrifuged for 30 minutes at 2250 g at 4°C to pellet the DNA, followed by 1 minute at 700 g inverted to aspirate the ethanol. The pellets were washed with 70 µl of 70% ethanol and centrifuged at 2250 g for 10 minutes, followed by 1 minute at 700 g inverted. Pelleted were air-dried at room temperature and resuspended in 10 µl Hi-Di™ Formamide (Applied Biosystems™). Samples were run on the ABI 3130xl on-site and sequencing traces were analysed using 4Peaks (Mekentosj, Amsterdam). Sanger sequencing for a number of samples was outsourced to Source BioScience (Nottingham, UK), with 5 µl PCR product and 5 µl of each 3.2 µM forward and reverse primer shipped to the company.

2.2.8.4 High-resolution melting analysis

High-resolution melting (HRM) analysis was completed to confirm positive genotype calls identified by high throughput Fluidigm® SNP Type™ genotyping. HRM analysis was performed by Dr Dorota Miller at the Leeds MH Unit. In brief, DNA samples were diluted to 10 ng/μL. Each PCR reaction contained 1 μL DNA sample, 5 μL 2X PCR MasterMix (Acqua Science), 1 μL 10X LCGreen® Plus+ (BioFire Defense), 0.4 μL of each 10 μM primer and 2.2 μL water. Fluidigm STA forward and locus-specific reverse primers were used for HRM (Appendix A). Thermal cycler conditions included 15 minutes at 95°C (denaturation), 45 cycles of 10 seconds at 95°C (denaturation), 15 seconds at 54-62°C (annealing), 15 seconds at 72°C (extension), followed by 1 cycle of 30 seconds at 94°C (0.1°C/sec ramp), 5 minutes at 25°C (hold). Samples were then placed into the LightScanner® Instrument and run using the following parameters: 70°C start temperature, 96°C end temperature and 67°C hold temperature. Data were analysed using the LightScanner® software.

2.3 Results

2.3.1 Exertional heat illness phenotypes

2.3.1.1 EHI clinical reactions

Descriptions of the clinical reactions of all 64 EHI patients were summarised and included number of episodes, core temperature (°C) if recorded, clinical features, complications and other potentially contributing factors (Table 2.9). EHI episodes of the 59 UK military personnel and 5 civilians referred to the Leeds MH Unit were diverse with individuals presenting a spectrum of clinical features. The clinical reactions reported in Table 2.9 may not provide an exhaustive list of symptoms experienced by each patient as they rely on accounts provided by medical staff at military establishments and the patients recalling the event themselves.

Collapse was a prominent feature observed in 47 of the EHI cases, with loss of consciousness experienced in 30 of these. Twenty-four of the patients who lost consciousness during their EHI reaction did not go on to develop any complications. The 6 patients who did experience complications in addition to loss of consciousness suffered complications including renal failure, seizures, multi-organ failure, lactic

acidosis, disseminated intravascular coagulation (DIC) and cardiac arrest. These complications all arose as a result of severe rhabdomyolysis.

Thirty-two of the EHI cohort presented with symptoms consistent with rhabdomyolysis, equating to 50% of all EHI referrals to the UK MH Investigation Unit. Four of these patients experienced ER exclusively with no other features of EHI documented. Two of these also displayed evidence of myoglobinuria, but none of the four ER cases developed into a life-threatening condition. The remaining 28 patients with rhabdomyolysis also presented with other symptoms of EHI, including high core temperature, collapse and impairment to neurological function. Serum CPK levels were documented for 25 patients who presented with rhabdomyolysis and ranged between 1,289 and >100,000 IU/L, although accuracy of CPK reporting differed between patients. The range of CPK values observed were similar between IVCT positive (MHShc/ MHSh) and IVCT negative (MHN) subgroups.

A total of 13 severe cases of EHI resulted in complications including renal failure, multi-organ failure, myoglobinuria, metabolic acidosis, disseminated intravascular coagulation, seizures and cardiac arrest. Again, all but one of these cases was a result of severe rhabdomyolysis, commonly featuring high CPK levels (5,510- >100,000 IU/L). The case reported with no evidence of rhabdomyolysis was a civilian who was found collapsed during a 10-mile race. He later developed life-threatening heatstroke with multi-organ failure.

Measurement of core temperature at the time of presentation was limited and was only provided in 21 cases. Of those reported, core temperatures (ºC) ranged between 38.5ºC and 44ºC during the clinical presentation of EHI. Seven of the EHI patients reported additional factors that may have contributed to the development of EHI, including dehydration, fatigue and one case each of myocardial hypertrophy and a mild non-specific myopathy. Overall, the severity of clinical presentation did not correlate with an MHShc, MHSh or MHN classification by IVCT as all subgroups displayed a similar spectrum of symptoms (Table 2.9).

Table 2.9: Clinical features of EHI reactions seen across the EHI cohort. Four patients were referred for exertional rhabdomyolysis (ER).

ID	IVCT	EHI cases	Core temp (ºC)	Collapse	Loss of consciousness	Rhabdomyolysis, CK (IU/L)	Complications	Other factors	HTT
1	MHShc	2	39.1ºC	✓	✓	✓	-	-	Passed
2	MHShc	2	41ºC	✓ (1/2)	✓ (1/2)	-	-	-	Failed
3	MHShc	1	42ºC	✓	✓	-	-	-	Failed
4	MHShc	1	-	✓	-	✓ CK 48,986	-	-	Failed
5	MHSh	1	41ºC	✓	✓	-	-	-	N/A
6	MHSh	3	-	✓	✓	-	-	-	Failed
7	MHSh	1	40.7ºC	✓	✓	✓ CK 11,000	-	-	Failed
8	MHSh	1	-	✓	-	✓ CK 15,000	-	-	Failed
9	MHSh	3	-	✓	✓	-	-	-	Failed
10	MHSh	1	-	-	-	✓ Cramps, hyponatremic	Renal failure, chicken pox	-	Failed
11	MHSh	2	-	-	-	✓ ER, Cramps	Myoglobinuria	-	Passed
12	MHSh	1	40.7ºC	✓	✓	✓ CK >100,000	Renal failure	-	Failed
13	MHSh	2	-	✓	✓	-	-	-	Failed
14	MHSh	1	39.1ºC	✓	✓	✓ Cramps	Renal failure	Myocardial hypertrophy	Failed
15	MHSh	2	-	-	-	✓ ER, CK >10,000	-	-	Passed
16	MHSh	1	-	✓	-	Post-exercise ache in kidneys	-	-	Failed
17	MHSh	2	-	-	-	✓ CK 27,000	-	-	Failed
18	MHSh	1	-	✓	-	-	-	-	Failed
19	MHSh	2	-	-	-	-	-	-	Failed
20	MHSh	1	-	-	-	-	-	-	Failed
21	MHSh	2	-	-	-	-	-	-	Failed
22	MHSh	1	-	-	-	✓	-	-	Failed
23	MHN	1	-	-	-	✓ CK >30,000	Renal failure	-	N/A
24	MHN	1	-	✓	-	-	-	-	Failed
25	MHN	1	-	✓	✓	-	-	-	Failed
26	MHN	1	38.9ºC	✓	-	✓ CK 15,000	-	Dehydration	Failed
27	MHN	2	-	✓	✓	✓ CK >20,000	-	-	Failed
28	MHN	1	-	✓	-	-	Multi-organ failure	-	N/A

Table 2.9 (continued)

ID	IVCT	EHI cases	Core temp (ºC)	Collapse	Loss of consciousness	Rhabdomyolysis, CK (IU/L)	Complications	Other factors	HTT
29	MHN	1	39.5ºC	✓	-	✓ CK 63,000	Renal failure, metabolic acidosis, myglobinurea	-	N/A
30	MHN	1	-	✓	-	-	-	-	Failed
31	MHN	1	42ºC	✓	✓	-	-	Alcohol consumption	Failed
32	MHN	3	-	✓	-	-	-	-	Failed
33	MHN	6	-	✓	✓ (1/6)	-	-	-	Failed
34	MHN	1	41.6ºC	✓	✓	✓ CK 5,510	Intensive care for several days	-	Failed
35	MHN	1	-	✓	✓	-	-	-	Failed
36	MHN	1	-	-	-	✓ ER	-	-	Failed
37	MHN	1	-	✓	✓	-	-	Fatigue and dehydration	Failed
38	MHN	3	40ºC	✓	-	✓ CK 32,000	-	-	Failed
39	MHN	1	-	✓	✓	-	-	-	Failed
40	MHN	1	-	-	-	-	-	-	Failed
41	MHN	1	40ºC	✓	-	-	-	-	Failed
42	MHN	1	-	-	-	✓ ER, CK 60,000	Myoglobinuria	-	Passed
43	MHN	2	-	-	-	-	-	Dehydration	Failed
44	MHN	2	-	✓	✓ (1/2)	-	-	-	Failed
45	MHN	1	-	✓	✓	-	-	-	Failed
46	MHN	1	-	✓	✓	-	-	-	Failed
47	MHN	2	-	✓	✓	Cramps	-	-	Failed
48	MHN	1	>40ºC	✓	✓	✓ CK 10,000	Seizure, renal failure	-	Failed
49	MHN	1	44ºC	✓	✓	✓ CK >10,000	-	-	Failed
50	MHN	1	-	✓	✓	-	-	-	Failed
51	MHN	21	-	-	-	-	-	-	Failed
52	MHN	1	-	✓	✓	✓CK 3,848	-	-	Failed
53	MHN	1	-	✓	-	-	-	-	Failed
54	MHN	1	38.5ºC	✓	-	✓CK, 1,289	-	-	Failed

Table 2.9 (continued)

ID	IVCT	EHI cases	Core temp (ºC)	Collapse	Loss of consciousness	Rhabdomyolysis, CK (IU/L)	Complications	Other factors	HTT
55	MHN	1	39ºC	✓	✓	✓ CK 24,210	-	Non-specific myopathy	Passed
56	MHN	1	39.6ºC	✓	-	✓ CK 2,000	-	-	Failed
57	MHN	1	-	✓	-	✓ CK 47,000	Renal failure	-	Failed
58	MHN	1	-	✓	✓	✓ Cramps CK >10,000	-	Post-exertion headaches	Passed
59	MHN	1	40ºC	✓	-	✓Cramps CK 4836	-	-	Failed
60	MHN	1	-	-	-	-	-	-	Failed
61	MHN	1	42ºC	✓	✓	✓ CK 7,000	Renal failure	-	Failed
62	MHN	1	-	-	-	-	-	-	Failed
63	MHN	1	40ºC	✓	✓	✓ CK >100,000	Seizures, multi-organ failure, lactic acidosis, DIC, cardiac arrest	-	N/A
64	N/A	1	42.5ºC	-	-	-	-	Alcohol consumption	N/A

2.3.1.2 Heat tolerance tests

The INM provided HTT reports for each EHI referral, including a summary of test parameters, peak rectal temperature (°C), rate of rise of core temperature (°C/hr), relative sweat rate (L/hr/m^2), VO_2 max (mL/min/kg) and HR (beats per minute). Carol House (INM) provided additional HTT details including core temperature (°C) values recorded at 5-minute intervals during the HTT. The average fitness capacity (VO_2 max) of EHI referrals who demonstrated normal IVCT responses was significantly higher than those who displayed abnormal IVCT responses (p= 0.12) (Figure 2.6). VO_2 max scores for the EHI patients who were classified MHN ranged between 35-66 ml/min/kg, representing a range of fitness capacities. The distribution of EHI patients who were classified MHSh/hc was smaller, and ranged between 34-55 mk/min/kg. Plotting individual EHI patients revealed normally distributed VO_2 max scores within each group and overlap between those who were classified MHN and MHSh/hc. Both MHN and MHSh/hc status groups contained one sample each with a particularly low VO_2 max capacity, 35 (patient 54) and 34 ml/min/kg (patient 12), respectively.

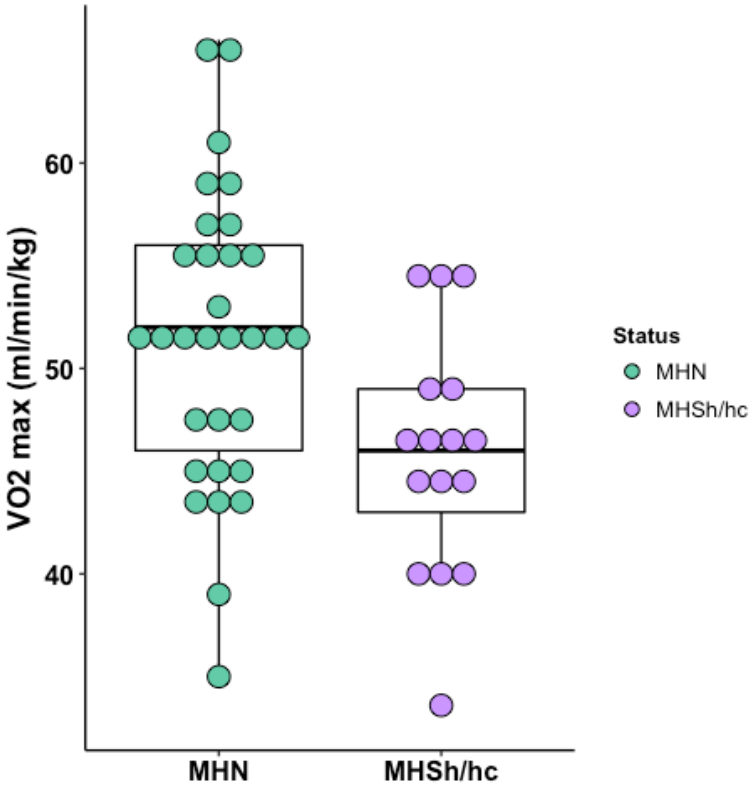

Figure 2.6: Distributions of VO_2 max capacity in the EHI cohort as a measure of fitness. EHI patients have been categorised according to their IVCT classification. Boxplots represent the median, interquartile ranges (IQRs) and 1.5X the IQR (whiskers).

There were no significant differences observed between the sweat rates of EHI patients who were later classified as MHN or MHSh/hc (Figure 2.7). The median sweat rate of MHSh/hc EHI individuals was slightly lower than MHN. Sweat rates were also presented relative to VO_2max, to account for differences in workload during the HTT (Figure 2.7). Again, no differences were detected between the groups. The range of relative sweat rates of both MHN and MHSh/hc classified patients were similar and measured between 0.8-2.25 L/hr/m^2. Both status groups had an outlier sample with a higher sweat rate than all other samples.

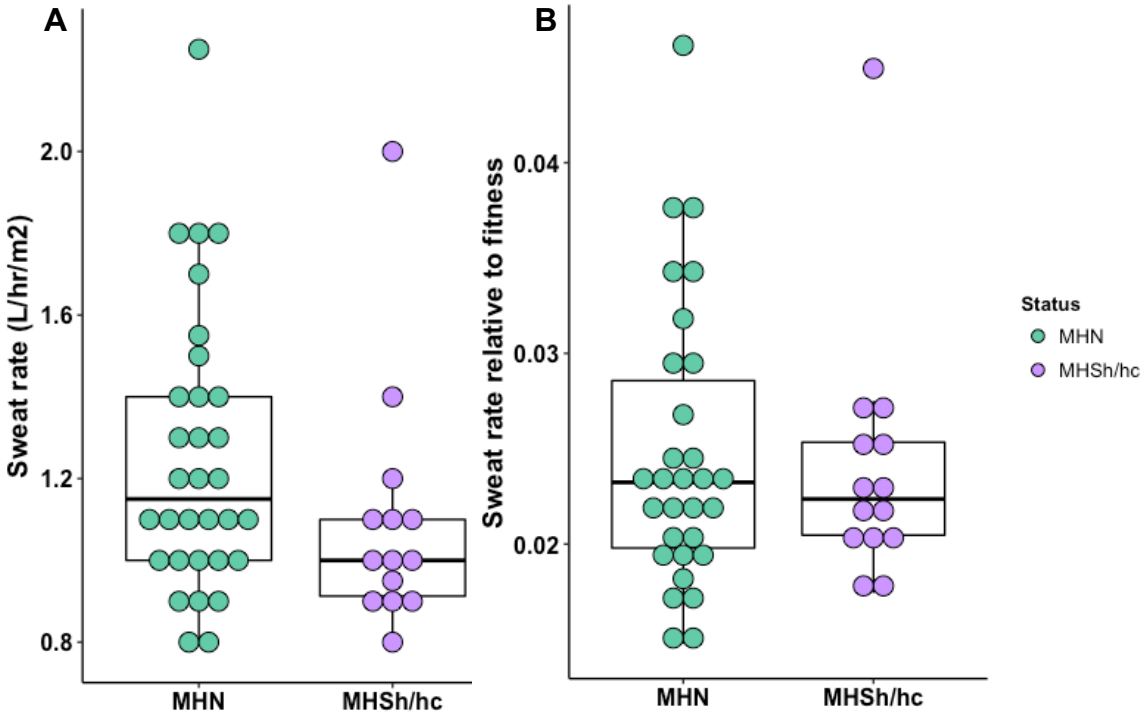

Figure 2.7: Distribution of relative sweat rates in the EHI cohort during the heat tolerance test. EHI patients have been categorised according to their IVCT classification. (A) Sweat rates relative to surface area (B) Relative sweat rates normalised to Vo_2max (a proxy for workload). Boxplots represent the median, interquartile ranges (IQRs) and 1.5X the IQR (whiskers).

Interestingly, no correlation was observed between the individual sweat rates of EHI patients and their VO_2 max scores (Figure 2.8). For the EHI patients with high VO_2 max capacities, working at a higher absolute workload during the HTT, sweat rates were no higher to compensate for increased heat production. One EHI referral (patient 25) was an exception, with a high VO_2 max of 65 ml/min/kg and a high sweat rate of 2.25 L/hr/m^2, to maintain thermal equilibrium.

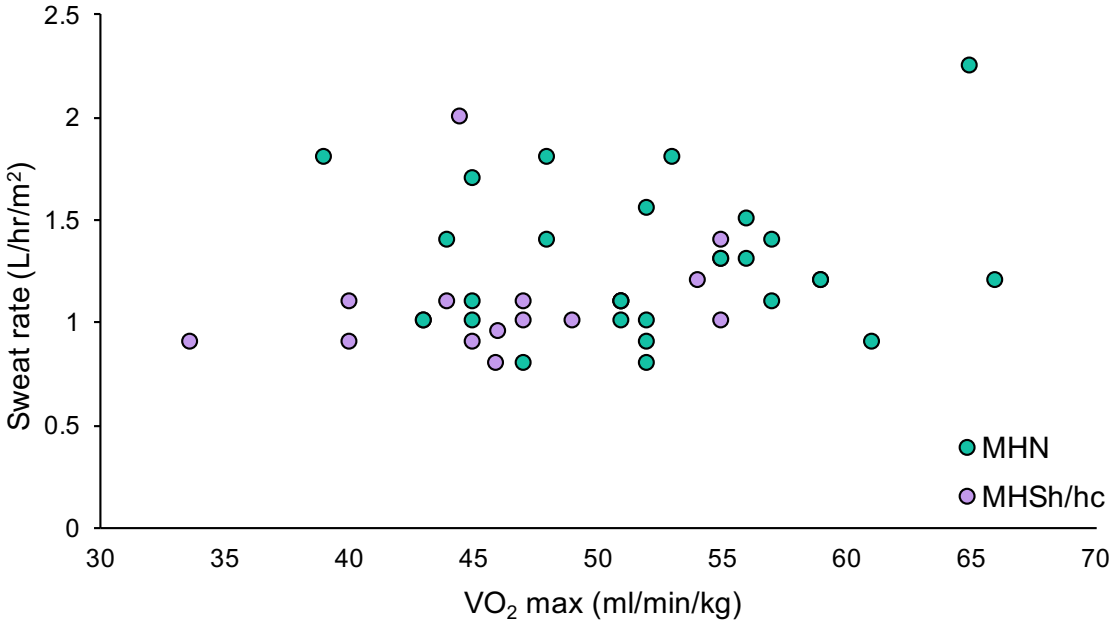

Figure 2.8: Individual sweat rates of EHI individuals plotted against VO_2 max scores. EHI patients have been categorised according to their IVCT classification.

Individual rectal temperatures were measured throughout each HTT and plotted and classified according to subsequent IVCT responses (Figure 2.9). The majority of EHI individuals failed to thermoregulate regardless of their subsequent IVCT classification. Six individuals passed the HTT and were able to maintain thermal homeostasis (highlighted with an asterisk in Figure 2.9), but due to a history of recurrent rhabdomyolysis, were all referred for an IVCT. Three of these individuals demonstrated abnormal contracture responses to halothane and caffeine despite their ability to thermoregulate (EHI patients 1, 11, & 15). The remaining three with normal HTTs were also classified MHN (EHI patients 42, 55, 58). In contrast, for the EHI referrals who failed to thermoregulate, a mixture of IVCT responses were observed.

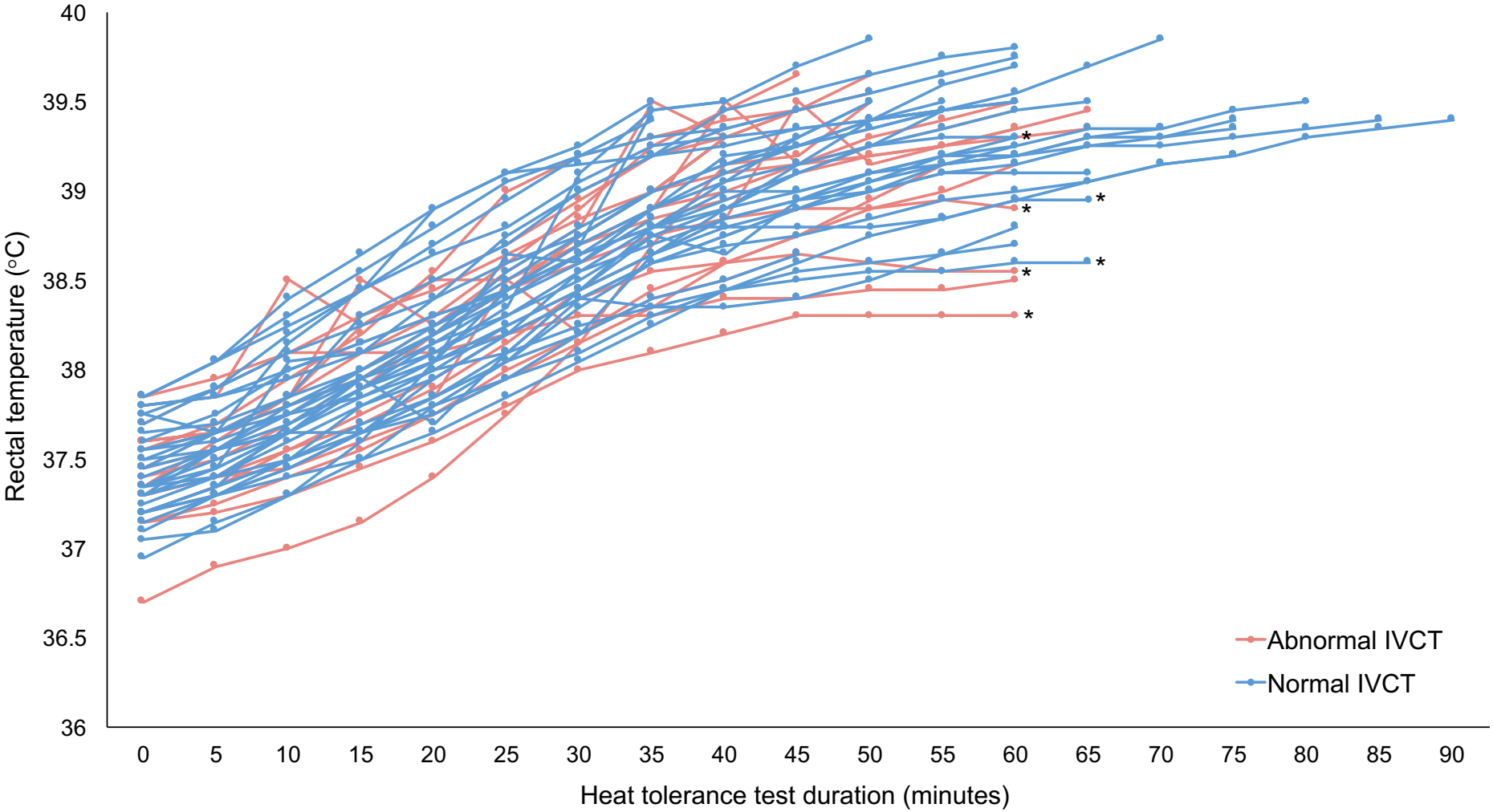

Figure 2.9: Rectal temperature of EHI military recruits during heat tolerance test. EHI patients have been categorised according to their IVCT classification. Individuals marked with an asterisk demonstrated normal thermoregulation and were referred due to recurrent exertional rhabdomyolysis.

2.3.1.3 *In vitro* contracture tests

IVCT muscle contractures were recorded by staff at the Leeds MH Investigation Unit, in response to incremental concentrations of caffeine and halothane. IVCT traces and diagnostic information were archived with both hard and electronic copies available. IVCT results comprised three discreet tests on *ex vivo vastus medialis* muscle and included static and dynamic halothane and static caffeine. Interestingly, 35% of the EHI cohort produced abnormal contracture responses. The IVCT responses were varied, with 4 patients responding to both caffeine and halothane (MHShc), 18 patients showing an abnormal response to halothane only (MHSh) and 41 patients responded to neither triggering agent (MHN). In addition to a diagnostic classification at a predefined threshold of 2% halothane or 2mM caffeine, IVCTs can also offer a quantitative phenotype. The 2% halothane contractures (g) of 22 IVCT positive EHI patients and 46 MH patients were measured and plotted, revealing no statistically significant differences between the groups (Figure 2.10).

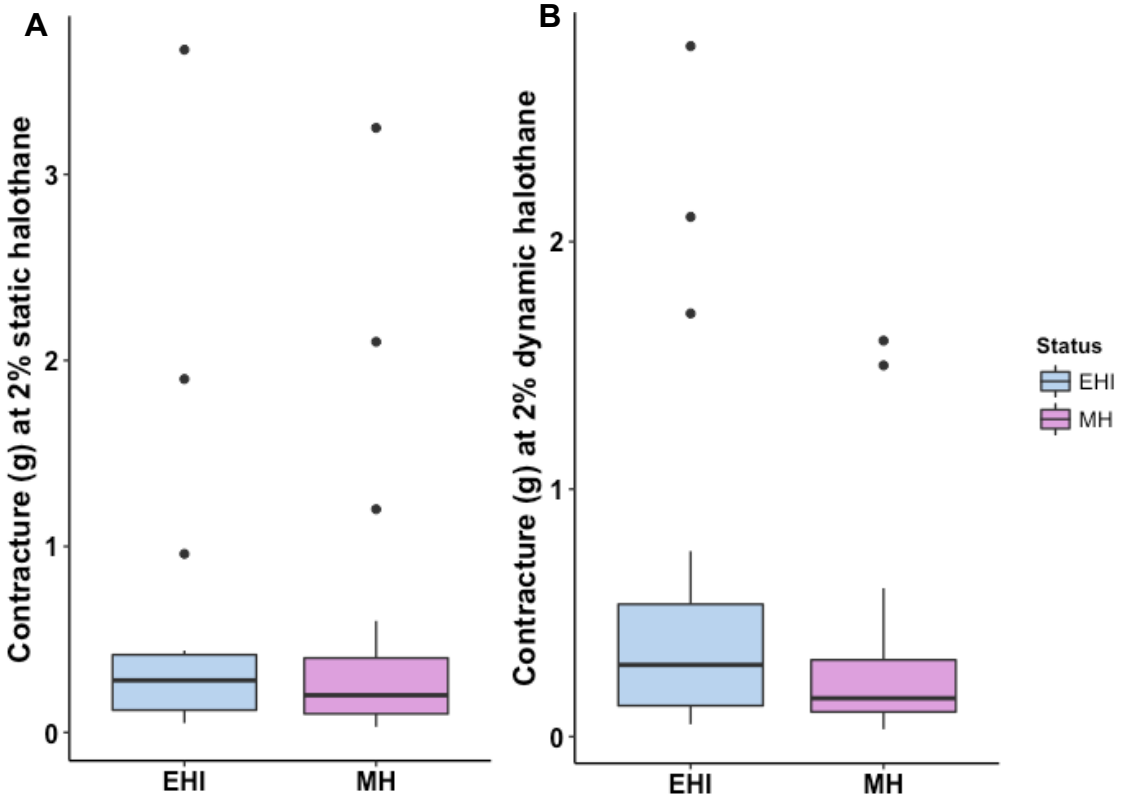

Figure 2.10: Skeletal muscle contractures (g) in response to 2% halothane between clinically classified EHI and MH patients. Halothane exposure to static *ex vivo vastus medialis* muscle (B) Halothane exposure to *vastus medialis* muscle under dynamic tension cycles. Contractures are measured from lowest tension (g) to tension at 2% halothane. Boxplots represent the median, interquartile ranges (IQRs) and 1.5X the IQR (whiskers).

Both status groups contained outliers who produced very strong contractures at 2% static and dynamic halothane. Specifically, EHI patients 2, 4 and 21 demonstrated strong reactions on the static test and EHI patients 2, 4 and 17 on the dynamic test.

Pre-drug twitch (g) was used as a measure of muscle viability and was taken as a mean average of the static and dynamic halothane and static caffeine muscle preparations. IVCT muscle viability (twitch) was significantly reduced in EHI patient samples relative to the MH sample cohort used for comparison (Mann-Whitney U Test, p=0.018) (Figure 2.11). Some samples did not meet the 1 g threshold required for a reliable diagnosis.

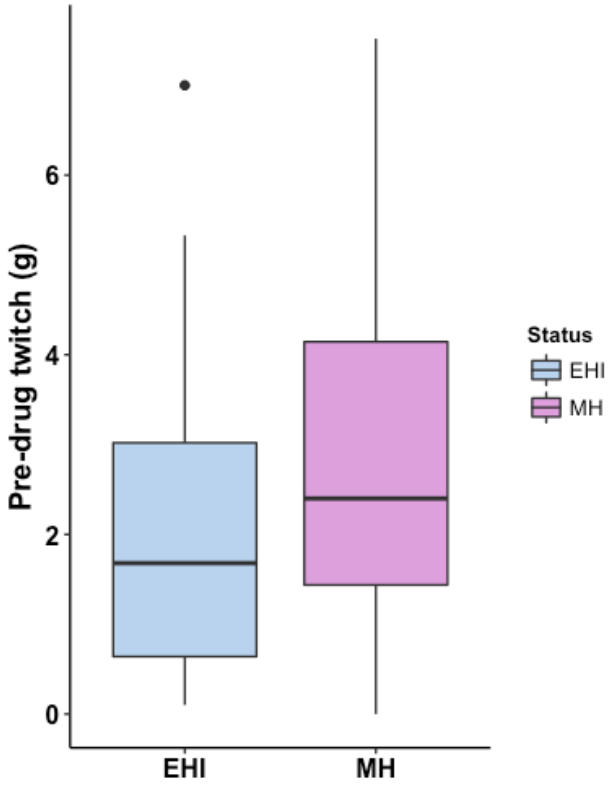

Figure 2.11: Pre-drug twitch (g) between EHI and MH *ex vivo* muscle, as a measure of muscle viability. Boxplots represent the median, interquartile ranges (IQRs) and 1.5X the IQR (whiskers).

Only four EHI referrals developed contractures ≥0.2 g in response to 2mM caffeine, with an additional individual producing a slight contracture at 2mM, below the 0.2 g threshold. Caffeine contracture strengths ranged between 0.06 and 0.78 g. Around 93% of MH susceptible individuals with a family history of anaesthetic-induced MH demonstrate a sensitivity to caffeine in addition to halothane. Therefore, a lack of caffeine sensitivity in EHI patients contrasts with IVCT responses observed in MH susceptible individuals. Contractures to 1 μM ryanodine within a 30-minute period were only detected in 3 EHI individuals (patient ID 2,4 and 23). Interestingly, patient 23 did not develop contractures

on exposure to either halothane or caffeine. It is important to note the ryanodine test is performed last and the mean average pre-drug twitch (g) across the EHI cohort was only 0.54 grams, with only 10 muscle samples reaching the viability threshold of 1 g. The three EHI patients who responded to ryanodine recorded pre-drug twitches between 2.85 and 3.9 grams.

2.3.2 Exertional heat illness genotypes

HaloPlex™ target libraries were successfully created and sequenced for all 64 EHI patients. An example of library quantification using Agilent's Bioanalyzer system has been presented in Figure 2.12.

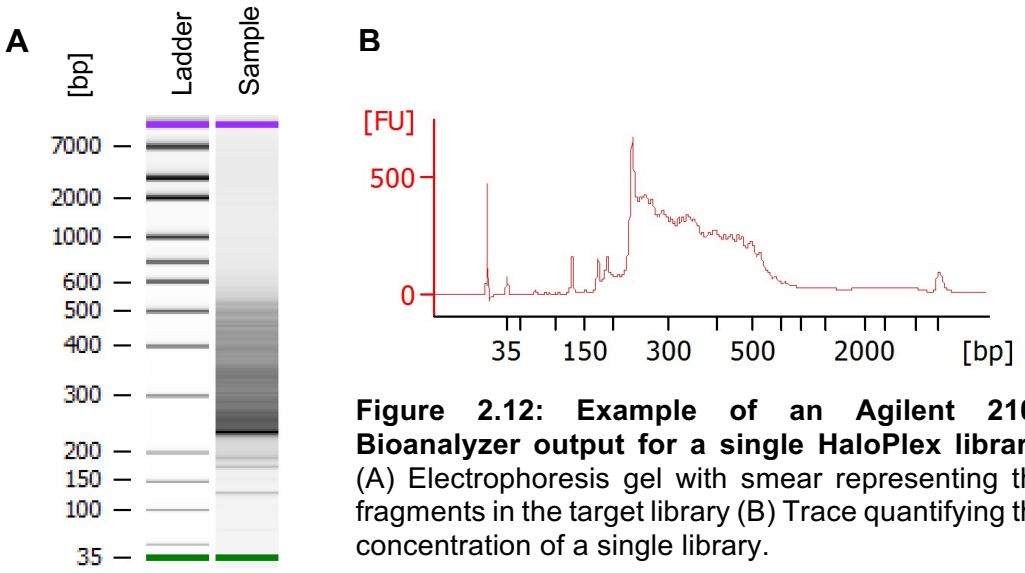

Figure 2.12: Example of an Agilent 2100 Bioanalyzer output for a single HaloPlex library. (A) Electrophoresis gel with smear representing the fragments in the target library (B) Trace quantifying the concentration of a single library.

The coding region of *RYR1* had been previously sequenced in 27 patients from the EHI cohort (Dr Dorota Miller), and therefore gaps in HaloPlex *RYR1* coverage only remained in 37 EHI individuals. Long-PCR and NEB-next ultra NGS was successfully performed for 7 *RYR1* regions in 35 EHI patients (Figure 2.13). Long-PCR failed for two EHI patients (ID 7 and 28), due to degraded DNA, therefore the presence of *RYR1* variants in these regions cannot be ruled out for these two individuals.

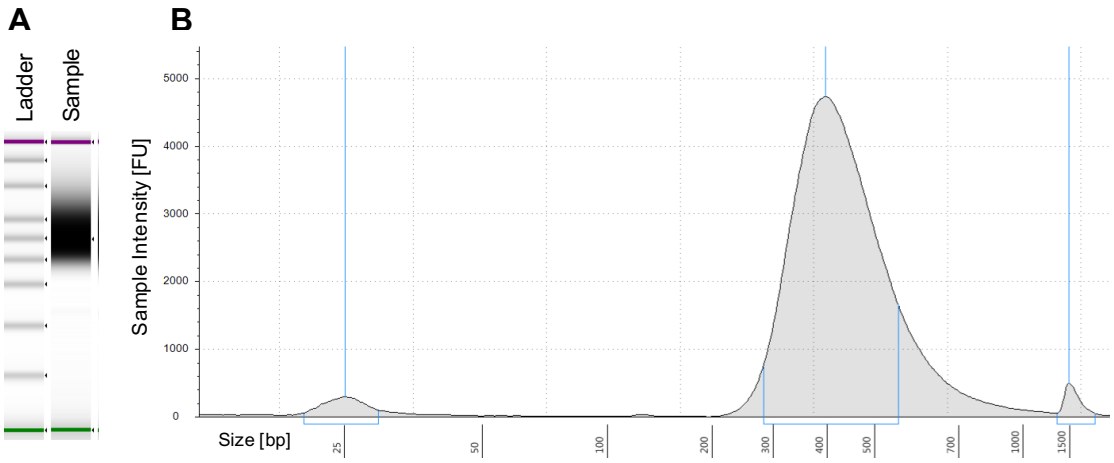

Figure 2.13: Example of an *RYR1* NEBnext® library quantification using an Agilent ScreenTape. (A) Electrophoresis gel with representing the fragments of NEBnext® library (B) Trace quantifying the concentration of a single library.

2.3.2.1 NGS summary

The custom HaloPlex™ 50 gene panel was designed to produce 13,547 amplicons per sample, predicting an average coverage of 98.71% across the coding regions of the 50 genes. Due to a range in quality of target-enriched libraries across the EHI cohort, the coverage and read depth within these regions varied between patients, but all samples had an average read depth >50. Quality reports were checked for gaps in read coverage observed across all samples in *RYR1* and *CACNA1S* genes (Table 2.10), with the aim to obtain full coverage of these key genes. Exon 91 is routinely covered by Sanger sequencing due to issues obtaining NGS coverage of GC rich regions. High GC content alters probe hybridisation and PCR efficiency.

Eleven exons across *RYR1* and *CACNA1S* contained regions of low read depth (<20 reads), with 7 exons of *RYR1* revealing short sections of sequence with no coverage (total 162 amino acids). Gaps in *RYR1* and *CACNA1S* were given priority to sequence in the first instance due to their association with MH. *RYR1* is a large gene comprising 106 exons (5038 amino acids), so the 7 regions highlighted for NEBNext® Ultra™ NGS represented 3.2% of the gene. In the remaining 48 genes, 120 exons were identified containing regions with read depth below 20 (read depth >10 required), but gaps in coverage have not been reported and were not covered with additional sequencing.

Table 2.10: Summary of low NGS coverage in *RYR1* and *CACNA1S* genes. Coverage has been presented as percentage of exon with a read depth <20.

Gene	Transcript	Exon	% <20	Coverage
CACNA1S	NM_000069	Exon 21	19.54	Read depth 8 for last 16 bases of exon
RYR1	NM_000540	Exon 12	15.7	Gaps or low read depth aa. 399-414*
RYR1	NM_000540	Exon 34	12.91	Read depth 16 for part of exon
RYR1	NM_000540	Exon 38	96.58	Gaps or low read depth aa 2080-2091*
RYR1	NM_000540	Exon 48	35	Gap for last 10 aa of exon aa 2602-11*
RYR1	NM_000540	Exon 58	30.43	Gaps or low read depth aa. 2965-2977*
RYR1	NM_000540	Exon 65	12.31	Gaps or low read depth aa. 3165-3197*
RYR1	NM_000540	Exon 66	0.9	Read depth 16 for 3 bases in middle of exon
RYR1	NM_000540	Exon 85	6.82	Read depth 1 or gap aa. 3925-96*
RYR1	NM_000540	Exon 91	54.06	Gaps aa. 4279-88, 4367-90, 4427-39, 4476-79
RYR1	NM_000540	Exon 101	29.85	Read depth 10 or gap aa. 4843-55*

* Gaps in exons sequenced by NEBNext® Ultra™NGS.

A total of 203 different non-synonymous variants were detected across the EHI cohort, in 39 of the 50 target genes. Of these, 79 were rare and potentially pathogenic, with a reported MAF ≤1% on the ExAC database (last accessed 29.06.16) and a C-score ≥15. Nine variants were previously unreported on available databases and in the literature. Fourteen EHI patients did not reveal any rare (MAF ≤1%) or potentially deleterious (C-score ≥15) variants across the 50 genes investigated.

2.3.2.2 *RYR1* and the genes of the $Ca_v1.1$ complex

Sequencing revealed 33 non-synonymous variants in the genes coding for RyR1 (*RYR1*) and the $Ca_v1.1$ complex (*CACNA1S*, *CACNA2D1*, *CACNB1* and *CACNG1*) (Table 2.11). Specifically, 18 variants were identified in *RYR1* and 15 in the four $Ca_v1.1$ complex genes. The 18 variants in *RYR1* were distributed across the gene, with 9 variants clustering between amino acids 3000-4000. The 10 genetic variants identified in *CACNA1S* were distributed evenly across the gene, as were the variants in *CACNA2D1*. Only 1 variant was found in *CACNG1*, with no variants uncovered in *CACNB1*. Most patients were heterozygous for the variants detected, but 3 common variants were found in both heterozygous and homozygous forms (Table 2.11). These included *CACNA1S* p.A69G (MAF 0.0372), *CACNA1S* p.L458H (MAF 0.2428) and *CACNG1* p.G196S (MAF 0.1196).

Twenty-two of the variants were rare (MAF ≤0.01 (1%)), with 19 of these also predicted to elicit a pathogenic effect (C-score ≥15). These included 12 in *RYR1*, 4 in *CACNA1S* and 3 in *CACNA2D1*. Fourteen of these variants were selected for the Fluidigm

genotyping screen based on population frequency (MAF ≤1%) and *in silico* pathogenicity predictors (C-score ≥15), highlighted in Table 2.11. Genotypes were already available for variant *RYR1* p.R3539H due to routine screening of MH probands at the Leeds MH Unit. *CACNA2D1* p.T50I and *RYR1* p.R492H had not been reported previously on the ExAC, 1000G and Exome variant server (EVS) population databases, but *RYR1* p.R492H had been reported by the ClinSeq project (National Human Genome Research Institute (NHGRI)). The MAFs reported on the ExAC database were calculated using all population groups including European (Finnish), European (Non-Finnish), East Asian, South Asian, Latino, African and other.

Thirteen of the variants presented in Table 2.11 were seen more than once in the EHI cohort, two of which were observed at a significantly ($p \leq 0.05$) higher frequency than expected based on population frequency (ExAC database). Firstly, *CACNA1S* p.S606N was identified in 4 of the 64 EHI patients (6.25%), while having an expected genotype frequency of 1.74% (MAF ExAC 0.0088). A 2-tailed chi-squared test was performed with Yates' correction and revealed the genotype frequency to be significantly higher in the EHI cohort than expected ($p= 0.02$). This rare variant was also predicted to elicit a pathogenic effect using *in-silico* predictors, with a C-score of 26.8. The EHI patients carrying this variant displayed varied responses by IVCT, with 1 negative (patient 42) and 3 positive contractures (patients 10, 15 and 27). Two of these EHI patients that demonstrated positive contractures carried an additional variant in *RYR1* (p.I3253T and p.E3583Q), listed in Table 2.11. The second variant *CACNA1S* p.L458H was common (MAF ExAC 0.2428), but despite this was found at a significantly higher frequency in the EHI cohort than expected ($p= 0.04$, 2-tailed chi-squared test with Yates' correction). Twenty-five of the patients carrying this genetic variant displayed a normal response by IVCT (MHN), 8 showed an abnormal response to halothane only (MHSh) and 1 developed a contracture in response to halothane and caffeine (MHShc).

Of the variants annotated as rare and pathogenic only two were seen more than once in the EHI cohort, *CACNA1S* p.S606N and *CACNA2D1* p.D1045A (MAF ExAC 0.0028, C-score 22.2). *CACNA2D1* p.D1045A was observed 2 EHI individuals, 1 classified MHSh by IVCT (patient 17) and the other MHN (patient 43). The EHI patient carrying *CACNA2D1* p.D1045A who demonstrated a positive IVCT also harboured a common *RYR1* variant (p.E3583Q), which had a MAF on the ExAC of 0.0149 and a C-score of 13. Eleven EHI patients carried a rare and predicted pathogenic variant in the *RYR1* gene, eight of which displayed a positive contracture by IVCT (7 MHSh and 1 MHShc), two who showed normal responses (MHN) and 1 patient who was sequenced without an IVCT.

Table 2.11: Non-synonymous variants identified in *RYR1* and genes of the $Ca_v1.1$ complex.

Gene	Variant ID	DNA change	AA change	Genotype	MAF (ExAC)	C-score	EHI	IVCT	
CACNA1S	rs12406479	c.206C>G	p.A69G	1 Hom/ 2 Het	0.0372	24.6	3	2 MHN, 1 MHSh	
CACNA1S	rs35534614	c.773G>A	p.G258D	Het	0.0074	23.2	1	1 MHN	*
CACNA1S	rs12742169	c.1373T>A	p.L458H	12 Hom/ 23 Het	0.2428	19.42	35	25 MHN, 9 MHSh/hc	
CACNA1S	rs150590855	c.1493G>A	p.R498H	Het	0.000238	35	1	1 MHN	*
CACNA1S	rs142356235	c.1817G>A	p.S606N	Het	0.0088	26.8	4	1 MHN, 3 MHSh	*
CACNA1S	rs35708442	c.2047C>T	p.R683C	Het	0.0031	34	1	1 MHShc	*
CACNA1S	rs3850625	c.4615C>T	p.R1539C	Het	0.1172	34	10	6 MHN, 4 MHSh/hc	
CACNA1S	rs13374149	c.4973G>A	p.R1658H	Het	0.0656	23.2	2	1 MHN, 1 MHSh	
CACNA1S	rs12139527	c.5399T>C	p.L1800S	Het	0.1549	27.7	14	9 MHN, 5 MHSh/hc	
CACNA1S	rs149547196	c.5515C>T	p.P1839S	Het	0.0023	2.863	1	1 MHN	
CACNA2D1	−	c.149C>T	p.T50I	Het	−	24.9	1	1 MHN	*
CACNA2D1	rs79030053	c.920A>T	p.N307I	Het	0.0044	4.924	2	2 MHSh	
CACNA2D1	rs78086631	c.2126G>A	p.S709N	Het	0.0027	17.75	1	1 MHN	
CACNA2D1	rs35131433	c.3134A>C	p.D1045A	Het	0.0028	22.2	2	1 MHN, 1 MHSh	*
CACNG1	rs1799938	c.586G>A	p.G196S	4 Hom/ 9 Het	0.1196	24.6	13	7 MHN, 6 MHSh	
RYR1	rs199826952	c.1475G>A	p.R492H	Het	−	27.6	1	1 MHShc	*
RYR1	rs746904839	c.2635G>A	p.E879K	Het	0.000008	33	1	1 MHN	
RYR1	rs34694816	c.4024A>G	p.S1342G	Het	0.0221	9.927	2	2 MHSh	
RYR1	rs146429605	c.4711A>G	p.I1571V	Het	0.0013	3.864	1	1 MHShc	
RYR1	rs780579604	c.4865G>A	p.R1622Q	Het	0.0002	28.4	1	1 MHSh	*
RYR1	rs34934920	c.5360C>T	p.P1787L	Het	0.0196	22.7	2	2 MHN	
RYR1	rs35364374	c.6178G>T	p.G2060C	Het	0.0694	21.2	12	3 MHSh, 9 MHN	
RYR1	rs147707463	c.8327C>T	p.S2776F	Het	0.0007	23.7	1	1 MHSh	*
RYR1	rs375626634	c.9758T>C	p.I3253T	Het	0.00004	20	1	1 MHSh	*
RYR1	rs200375946	c.9800C>T	p.P3267L	Het	0.00006	23.5	1	1 MHN	
RYR1	rs137932199	c.10097G>A	p.R3366H	Het	0.0009	23.9	1	1 MHShc	*
RYR1	rs143987857	c.10616G>A	p.R3539H	Het	0.0018	26.1	1	1 MHSh	**
RYR1	rs55876273	c.10747G>C	p.E3583Q	Het	0.0149	13	4	2 MHN, 2 MHSh	
RYR1	rs375915752	c.11117C>T	p.T3711M	Het	0.000008	24.3	1	1 MHShc	*
RYR1	rs4802584	c.11251C>G	p.Q3756E	Het	0.0337	11.43	2	1 MHN, 1 MHSh	
RYR1	rs147136339	c.11798A>G	p.Y3933C	Het	0.009	24.1	1	1 MHSh	
RYR1	rs148772854	c.11926C>T	p.H3981Y	Het	0.0013	24.5	1	1 MHSh	*
RYR1	rs150396398	c.13498G>C	p.D4505H	Het	0.0061	23.4	1	1 MHN	*

* Fourteen rare (MAF ≤1%) and potentially pathogenic (C-score ≥15) variants were included in the Fluidigm genotyping screen.

** This variant was excluded from the Fluidigm screen as genotyping had already been completed for Leeds MH Unit samples.

Of the 22 EHI patients who showed a positive contracture by IVCT (MHShc or MHSh), 10 carried a variant in the *RYR1* gene (Table 2.12). These 10 EHI individuals revealed 14 different *RYR1* variants between them with 4 patients carrying combinations of two *RYR1* variants. This left 12 EHI patients displaying a positive contracture who did not harbour an *RYR1* variant which could account for their IVCT response. More specifically, 12 of the 22 EHI patients presented with evidence of exertional rhabdomyolysis, a condition previously associated with *RYR1* mutations (Voermans, Snoeck and Jungbluth, 2016). Only 5 of these individuals carried an *RYR1* variant, meaning that 7 of the EHI patients with features of exertional rhabdomyolysis did not have an *RYR1*-related condition.

Table 2.12: *RYR1* variants in EHI patients with positive IVCT contractures.

ID	IVCT	Rhabdomyolysis	RYR1 variant
1	MHShc	✓	–
2	MHShc	✗	–
3	MHShc	✗	p.R492H
4	MHShc	✓	p.R3366H, p.T3711M, Y3933C, p.G2050C, p.I1571V
5	MHSh	✗	p.R1622Q
6	MHSh	✗	–
7	MHSh	✓	p.R3534H
8	MHSh	✓	–
9	MHSh	✗	–
10	MHSh	✓	p.I3253T
11	MHSh	✓	p.S1342G
12	MHSh	✓	–
13	MHSh	✗	p.Q3756E
14	MHSh	✓	p.S1342G + p.H3981Y
15	MHSh	✓	–
16	MHSh	✓	–
17	MHSh	✓	p.E3583Q
18	MHSh	✗	–
19	MHSh	✗	p.S2776F + p.E3583Q
20	MHSh	✗	–
21	MHSh	✗	–
22	MHSh	✓	–

2.3.2.3 Fluidigm® SNP Type™ genotyping of variants in *RYR1* and genes of the Cav1.1 complex

Fluidigm® SNP Type™ genotyping assays were designed for 14 rare (MAF ≤1%) and potentially deleterious (C-score ≥ 15) non-synonymous variants across *RYR1* and

genes of the $Ca_v1.1$ complex, with functioning assays successfully produced for 13 of these variants. Figure 2.14 shows examples of 2 Fluidigm® SNP Type™ genotyping plots (*CACNA2D1* p.D1045A and *RYR1* p.D4505H) and highlights the clear distinction between the two genotype groups (heterozygous EHI positive controls shown in blue and samples homozygous for the wild-type allele shown in red).

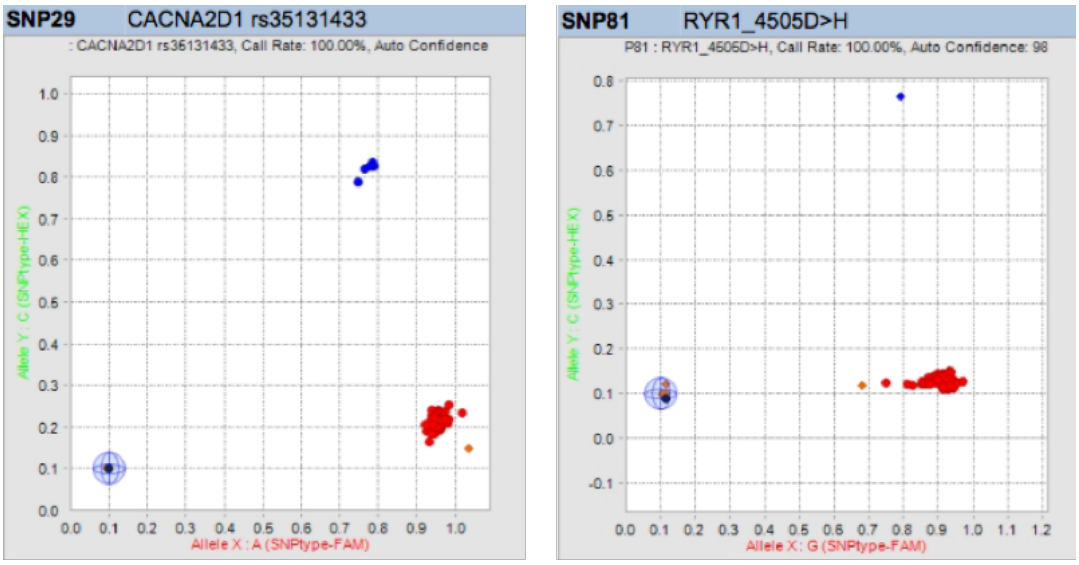

Figure 2.14: Examples of Fluidigm SNP Type genotyping plots. Red markers indicate samples positive for the wild-type allele. Blue markers indicate heterozygous samples positive for both the wild-type and variant allele. No template controls are black and highlighted by the sphere.

Specificity of each assay was calculated revealing five assays with 100% specificity and the remaining eight assays with a specificity greater than 99.5% (Table 2.13). Four variants were flagged by Fluidigm as producing non-standard assays with high GC content (>65%); however, this assay quality measure did not correlate with assay sensitivity or specificity. The genotyping assay synthesised for novel variant *CACNA2D1* p.T50I did not produce clear genotype calls so data were excluded from analyses. NGS data for this EHI patient were good quality with a read depth of 208 covering the location of the variant, so it is unlikely to be a false positive variant. All remaining assays clearly distinguished between homozygous and heterozygous genotypes, with EHI positive controls confirming NGS results. Fluidigm genotyping results for these genes have been presented in Table 2.14, with Sanger sequencing and melt-curve results presented in brackets. Non-EHI individuals screened per group included 658 MHShc, 180 MHN and 285 UK population samples with the number of observations across the EHI cohort representative of NGS data.

Table 2.13: Specificity of Fluidigm SNP Type genotyping assays for selected variants in *RYR1* and genes of the $Ca_v1.1$ complex.

Fluidigm assay	True negative	False positive	Specificity
CACNA1S c.773G>A p.G258D	1169	3	99.74%
CACNA1S c.1493G>T p.R498H	1186	0	100%
CACNA1S c.1817G>A p.S606N	1151	2	99.83%
CACNA1S c.2047C>T p.R683C	1186	1	99.92%
CACNA2D1 c.3134A>C p.D1045A	1171	3	99.74%
RYR1 c.1475G>A p.R492H	1186	0	100%
RYR1 c.4865G>A p.R1622Q	1186	0	100%
RYR1 c.8327C>T p.S2776F	1178	0	100%
RYR1 c.9758T>C p.I3253T	1186	1	99.92%
RYR1 c.10097G>A p.R3366H	1179	4	99.66%
RYR1 c.11941C>T p.H3981Y	1181	4	99.66%
RYR1 c.11132C>T p.T3711M	1185	0	100%
RYR1 c.13513G>C p.D4505H	1178	1	99.92%

Six of the variants *CACNA1S* p.R498H and p.R683C and *RYR1* p.R492H, p.R1622Q p.I3253T and p.H3981Y were only detected once on the Fluidigm genotype screen in the original EHI patient. One rare *RYR1* variant was detected in only EHI and MHSh/hc samples (p.T3711M) and confirmed by Sanger sequencing. Heterozygous variant *RYR1* p.R3366H was detected and confirmed in EHI, MHSh/hc and MHN patients, but the 3 heterozygous genotypes identified in the UK population samples were not confirmed by Sanger sequencing. Although heterozygous variant *CACNA1S* p.S606N was identified in all groups, it was found at a significantly higher frequency in the EHI and MH population than expected based on the MAF reported on the ExAC database (p= <0.0001, 2-tailed chi-squared test with Yates' correction). The remaining 4 variants were detected in 9 or more individuals, including at least 1 UK population sample. Heterozygous variant *RYR1* p.D4505H was identified in 3 MHShc samples of New Zealand origin (Stowell, pers. comm., 2017) in addition to the 9 confirmed observations in this study (1 EHI, 7 MHSh/hc and 1 UK population sample).

Table 2.14: Fluidigm genotype screen results for variants meeting criteria identified in *RYR1* and genes of the $Ca_v1.1$ complex. Thirteen rare (MAF ≤1%) and potentially pathogenic (C-score ≥15) variants successfully screened by Fluidigm high throughput genotyping. All variants were heterozygous and observed in independent families. Fluidigm results were confirmed using Sanger sequencing or melt-curve analysis (presented in brackets for comparison).

Gene	DNA change	AA change	EHI	MHSh/hc	MHN	UK POP
CACNA1S	c.773G>A	p.G258D	1 (1)	12 (9)	1 (1)	7 (7)
CACNA1S	c.1493G>T	p.R498H	1 (1)	–	–	–
CACNA1S	c.1817G>A	p.S606N	4 (4)	24 (24)	3 (3)	7 (5)
CACNA1S	c.2047C>T	p.R683C	1 (1)	1 (0)	–	–
CACNA2D1	c.3134A>C	p.D1045A	2 (2)	10 (7)	2 (2)	4 (4)
RYR1	c.1475G>A	p.R492H	1 (1)	–	–	–
RYR1	c.4865G>A	p.R1622Q	1 (1)	–	–	–
RYR1	c.8327C>T	p.S2776F	1 (1)	6 (6)	1 (1)	1 (1)
RYR1	c.9758T>C	p.I3253T	1 (1)	1 (0)	–	–
RYR1	c.10097G>A	p.R3366H	1 (1)	7 (6)	1 (1)	3 (0)
RYR1	c.11941C>T	p.H3981Y	1 (1)	3 (0)	1 (0)	–
RYR1	c.11132C>T	p.T3711M	1 (1)	1 (1)	–	–
RYR1	c.13513G>C	p.D4505H	1 (1)	8 (7)	–	1 (1)

Assay failed for variant *CACNA2D1* c.149C>T p.T50I so was excluded from table.

Five of the six non-EHI MH susceptible individuals carrying *RYR1* variant p.S2776F (MAF ExAC 0.0007, C-score 23.7) carried an additional variant in the *RYR1* gene. Interestingly, four of these from the MHSh/hc group carried the same functionally characterised variant *RYR1* p.T2206M (MAF ExAC 0.00003), presented in Table 2.15. The fifth MH susceptible individual from UK cohort carried *RYR1* p.E3104K (MAF ExAC 0.00002) in addition to *RYR1* p.S2776F. EHI patient 19, who carried *RYR1* p.S2776F did not possess the same *RYR1* variant combination as the 4 non-EHI MHSh/hc families but revealed a second more common variant (*RYR1* p.E3583Q, ExAC 0.0149).

Table 2.15: Additional *RYR1* variants identified in MHSh/hc patients carrying *RYR1* p.S2776F detected on the Fluidigm genotype screen. Sequencing was performed by the Leeds NHS Genetics Laboratory or Leeds MH Unit. All variants were identified in the heterozygous form.

IVCT	Additional *RYR1* variant
1 x EHI MHSh patient	*RYR1* c.10732G>C p.E3583Q
4 x non-EHI MHSh/hc individuals	*RYR1* c.6617C>T p.T2206M
1 x non-EHI MHShc individual	*RYR1* c.9310G>A p.E3104K
1 x non-EHI MHSh individual	No additional variant
1 x non-EHI MHN individual	Not screened
1 x non-EHI with no IVCT diagnosis	Not screened

To investigate whether the two *RYR1* variants (p.S2776F & p.T2206M) were in *cis*, the family members of the four non-EHI MHSh/hc patients identified with the combination were sequenced (Table 2.16). The two variants were always present in the same individuals, with 10 MHSh/hc individuals carrying both variants. There was one MHN individual from family 3 who possessed both genetic variants, but the remaining 25 MHN individuals were variant negative. Genetic confirmation of *RYR1* p.S2776F was not possible for 1 MHShc individual in family 4 due to degraded DNA.

Table 2.16: Family follow-up of two *RYR1* variants in four independent MH families. A combination of two *RYR1* variants and their co-segregation with IVCT status in four non-EHI MHShc families.

Family	Status	*RYR1* p.S2776F	*RYR1* p.T2206M
Family 1:	3 MHSh/hc	✓	✓
	13 MHN	✗	✗
Family 2:	5 MHSh/hc	✓	✓
	5 MHN	✗	✗
Family 3:	1 MHSh	✓	✓
	1 MHN	✓	✓
	4 MHN	✗	✗
Family 4:	1 MHShc	✓	✓
	1 MHShc	?	✓
	3 MHN	✗	✗

2.3.2.4 Very rare and potentially deleterious variants identified in RYR1 and genes of the $Ca_v1.1$ complex

Of particular interest, nine non-synonymous variants annotated as very rare (MAF ExAC ≤0.1%) and potentially deleterious (C-score ≥15) were identified in *RYR1* and genes of the $Ca_v1.1$ complex (Table 2.17). Rare variants were enriched in the EHI cohort, five of which were identified in IVCT positive EHI patients (p.R492H, p.R1622Q, p.S2776F, p.R3366H and p.T3711M).

Table 2.17: Very rare (MAF ≤0.1%) and potentially deleterious (C-score ≥15) non-synonymous variants identified in RYR1 and genes of the $Ca_v1.1$ complex.

Gene	Variant ID	DNA change	AA change	MAF (ExAC)	C-score	EHI
CACNA1S	rs150590855	c.1493G>A	p.R498H	0.000238	35	1
CACNA2D1	N/A	c.149C>T	p.T50I	N/A	24.9	1
RYR1	rs199826952	c.1475G>A	p.R492H	N/A	27.6	1
RYR1	rs746904839	c.2635G>A	p.E879K	0.000008	33	1
RYR1	rs780579604	c.4865G>A	p.R1622Q	0.0002	28.4	1
RYR1	rs147707463	c.8327C>T	p.S2776F	0.0007	23.7	1
RYR1	rs200375946	c.9800C>T	p.P3267L	0.00006	23.5	1
RYR1	rs137932199	c.10097G>A	p.R3366H	0.0009	23.9	1
RYR1	rs375915752	c.11117C>T	p.T3711M	0.000008	24.3	1

2.3.2.5 Genes associated with an exercise intolerance phenotype

Six additional genes were investigated due to their previous association with an exercise intolerance phenotype. The reported mutations to date cause six distinct rare autosomal recessive genetic disorders, including *AMPD1* deficiency (*AMPD1*), Brody's myopathy (*ATP2A1*), myotonia congenita (*CLCN1*), myopathic form of CPTII deficiency (*CPTII*), McArdle's disease (*PYGM*) and ventricular tachycardia with muscle weakness (*TRDN*) (Vladutiu *et al.*, 2000; Gross *et al.*, 2002; Duno *et al.*, 2004; Vattemi *et al.*, 2010; Roux-Buisson *et al.*, 2012; Nogales-Gadea *et al.*, 2015). The individuals reported in the literature all harboured either homozygous or compound heterozygous mutations in one of the genes.

Sequencing the coding region of these genes revealed 31 non-synonymous variants, 15 of which were both rare and heterozygous (MAF ≤1%) with 13 also annotated as pathogenic (C-score ≥15) (Table 2.18). Two of these, namely *AMPD1* p.M340I and *ATP2A1* p.T538M, were found in the same EHI MHSh individual (patient 20).

Table 2.18: Non-synonymous variants identified in genes associated with exercise intolerance.

Gene	Variant ID	DNA change	AA change	Genotype	MAF (ExAC)	C-score	EHI	IVCT	
AMPD1	rs17602729	c.133C>T	p.Q45*	Het	0.0871	36	11	4 MHSh/ 7 MHN	
AMPD1	rs139512772	c.190C>T	p.R64C	Het	0.00005	29.1	1	1 MHN	*
AMPD1	rs61752479	c.230C>T	p.P77L	Het	0.0884	27.8	11	4 MHSh /7 MHN	
AMPD1	rs61738827	c.311G>A	p.R104H	Het	0.0051	23.4	1	1 MHN	*
AMPD1	rs34526199	c.947A>T	p.K316I	Het	0.0282	32	4	4 MHN	
AMPD1	rs61752478	c.1017G>T	p.M340I	Het	0.0031	29.2	1	1 MHSh	*
ATP2A1	rs763211121	c.1613C>T	p.T538M	Het	0.00002	27.1	1	1 MHSh	*
ATP2A1	rs114675305	c.1619C>T	p.P540L	Het	0.0027	15.92	2	2 MHN	*
ATP2A1	rs74573581	c.1948G>A	p.D650N	Het	0.0015	21.7	1	1 MHSh	*
CLCN1	rs10282312	c.352T>G	p.W118G	Het	0.0139	18.83	5	4 MHN/ 1 MHSh	
CLCN1	rs111482384	c.461A>G	p.Q154R	Het	0.0031	0.53	2	1 MHN/ 1 MHSh	
CLCN1	rs118066140	c.899G>A	p.R300Q	Het	0.0046	32	4	1 MHSh/ 2 MHN/ 1 ?	*
CLCN1	rs41276054	c.1309G>A	p.A437T	Het	0.0111	0.002	1	1 MHN	
CLCN1	rs140205115	c.1842G>C	p.K614N	Het	0.0014	24.4	1	?	**
CLCN1	rs13438232	c.2180C>T	p.P727L	8 Hom/ 37 Het	0.3974	15.32	45	29 MHN/ 13 MHSh/ 2 MHShc/ 2 ?	
CPT2	rs2229291	c.1055T>G	p.F352C	Het	0.0218	24.4	1	1 MHN	
CPT2	rs1799821	c.1102G>A	p.V368I	17 Hom/ 31 Het	0.4841	0.002	48	31 MHN/ 14 MHSh/ 1 MHShc/ 2 ?	
CPT2	rs1799822	c.1939A>G	p.M647V	1 Hom/ 20 Het	0.162	23	20	13 MHN/ 5 MHSh/ 2 ?	
PYGM	rs116987552	c.148C>T	p.R50*	Het	0.0014	35	1	1 MHSh	*
PYGM	rs77656150	c.313G>T	p.A105S	Het	0.002	25.6	3	2 MHSh/ 1 MHN	*
PYGM	rs11231866	c.976C>G	p.R326G	Het	0.0207	17.16	1	1 MHSh	
PYGM	rs146919445	c.1015C>T	p.R339W	Het	0.00007	33	1	1 MHN	*
PYGM	rs139570786	c.1273A>G	p.I425V	Het	0.0029	12.81	1	1 MHN	
TRDN	rs9490809	c.383C>G	p.T128S	10 Hom/ 35 Het	0.492	0.316	45	30 MHN/ 11 MHSh/ 2 MHShc/ 2 ?	
TRDN	rs192289289	c.403G>A	p.E135K	Het	0.0073	24.3	2	1 MHSh/ 1 MHShc	*
TRDN	rs6902416	c.601C>G	p.L201V	45 Hom/ 7 Het	0.1741	0.705	52	34 MHN/ 15 MHSh/ 1 MHShc/ 2 ?	
TRDN	rs35766971	c.1016G>A	p.S339N	Het	0.0052	20.7	1	1 MHSh	*
TRDN	rs28494009	c.1211T>G	p.V404G	1 Hom/ 21 Het	0.2004	19.78	22	12 MHN/ 10 MHSh	
TRDN	rs17737379	c.1257C>A	p.D419E	1 Hom/ 12 Het	0.1374	9.356	13	3 MHN/ 8 MHSh/ 2 MHShc	
TRDN	rs2873479	c.1313T>G	p.I438S	Hom	0.924	7.345	12	7 MHN/ 2 MHSh/ 1 MHShc/ 2 ?	
TRDN	rs6569336	c.1408C>A	p.L470M	1 Hom/ 4 Het	0.0579	15.88	5	4 MHSh/ 1 MHN	

* Twelve rare (MAF ≤1%) and potentially pathogenic (C-score ≥15) variants were included in the Fluidigm genotyping screen.

** This variant was not included in the Fluidigm screen as the patient had not undergone heat tolerance testing or an IVCT.

Eighteen of the variants were identified more than once across the EHI cohort, four of which were heterozygous variants annotated as rare and potentially pathogenic (Table 2.19).

1. The first variant *ATP2A1* p.P540L was identified in 2 MHN EHI individuals (patient ID 26 and 30), neither of which harboured any rare variants in *RYR1* or *CACNA1S* genes.
2. *CLCN1* p.R300Q (MAF ExAC 0.0046, C-score 32) was identified in 4 EHI patients (1 MHSh, 2 MHN, 1 unknown). EHI patient 17 who was classified MHSh, also harboured rare variant *CACNA1S* p.S606N (MAF ExAC 0.0088) along with 2 common variants in the *RYR1* and *CACNA1S* genes. EHI patient 63, who was sequenced without IVCT carried this *CLCN1* variant along with a very rare *RYR1* variant (p.E879K), observed only once on the ExAC database. EHI patients 46 and 56, who were classified as MHN, did not carry any rare variants in *RYR1* or *CACNA1S*.
3. *PYGM* p.A105S (MAF ExAC 0.002, C-score 26.5) was identified in 3 EHI patients, two of which were classified MHSh and one MHN. EHI patient 14, who was classified MHSh, carried an additional rare variant, *CACNA1S* p.R683C (MAF ExAC 0.0031, C-score 34).
4. The fourth variant *TRDN* p.E135K was found in two EHI patients, who were both classified MH susceptible by IVCT (MHSh/ MHShc). EHI patient 5 also harboured *RYR1* p.R1622Q, a rare (MAF 0.0002) and predicted pathogenic (C-score 28.4) variant. EHI patient 3 carried *RYR1* p.R492H (MAF N/A, C-score 27.6) in addition to *TRDN* p.E135K.

Table 2.19: Rare and potentially deleterious variants detected more than once across the EHI cohort. Including additional rare *RYR1* and *CACNA1S* variants detected in the EHI patients who were classified MHShc/MHSh.

Gene	AA change	EHI	IVCT	*RYR1* or *CACNA1S* variants
ATP2A1	p.P540L	2	2 MHN	No variants
CLCN1	p.R300Q	4	1 MHSh/ 3 MHN/ 1?	*RYR1* p.E879K, *CACNA1S* p.S606N
PYGM	p.A105S	3	2 MHSh/ 1 MHN	*CACNA1S* p.R683C
TRDN	p.E135K	2	1 MHSh/ 1 MHShc	*RYR1* p.R1622Q, p.R492H

Five of the 31 specific variants identified in the EHI cohort have been shown to elicit a pathogenic effect implicating them in genetic disorders with an exercise intolerance phenotype (Table 2.20). Specifically, these included *AMPD1* deficiency, *CPTII*

deficiency and McArdle's disease, a glycogen storage disease type V caused by a *PYGM* deficiency. All the rare autosomal recessive conditions reported were caused by either homozygous recessive or compound heterozygous mutations; however, patients from the EHI cohort only carried a single copy of the pathogenic variants. A homozygous nonsense variant in *AMPD1* (p.Q45*) that has been shown to cause *AMPD1* deficiency (Morisaki *et al.*, 1992) and has always been found in on the same allele as *AMPD1* p.P77L, a combination which was observed in 11 of the EHI cohort.

Table 2.20: Reported disease association in specific variants identified in exercise intolerance linked genes.

Genetic variant	Variant disease association (HGMD)
AMPD1 c.133C>T p.Q45*	Adenosine monophosphate deaminase 1 deficiency (Morisaki *et al.*, 1992)
AMPD1 c.230C>T p.P77L	Always in *cis* with *AMPD1* c.133C>T p.Q45* (Morisaki *et al.*, 1992)
AMPD1 c.947A>T p.K316I	Adenosine monophosphate deaminase 1deficiency (Toyama *et al.*, 2004)
AMPD1 c.1017G>T p.M340I	Adenosine monophosphate deaminase 1 deficiency (Toyama *et al.*, 2004)
CPT2 c.1055T>G p.F352C	Carnitine palmitoyltransferase 2 deficiency (Isackson, Bennett and Vladutiu, 2006)
CPT2 c.1102G>A p.V368I	Found in combination with rare *CPT2* variants but not pathogenic alone (Yasuno *et al.*, 2008)
CPT2 c.1939A>G p.M647V	Found in combination with rare *CPT2* variants but not pathogenic alone (Yasuno *et al.*, 2008)
PYGM c.148C>T p.R50*	McArdle's disease (Tsujino, Shanske and DiMauro, 1993)

2.3.2.6 Fluidigm® SNP Type™ genotyping of variants in genes associated with an exercise intolerance phenotype

Fluidigm® SNP Type™ genotyping assays were designed for 12 rare (MAF ≤1%) and potentially deleterious (C-score ≥15) non-synonymous variants across 5 genes associated with an exercise intolerance phenotype (Table 2.21). Viable assays were produced for all variants, with 3 assays labelled as non-standard due to a high GC content (>65%). Again, this assay quality measure did not reflect the capacity for accurate genotype calls with all assays confirming positive EHI NGS results. Assay specificities were calculated, revealing 8 assays with 100% specificity, with the remaining 4 greater than 99.83% (Table 2.21).

Table 2.21: Specificity of Fluidigm SNP Type genotyping assays in variants identified in exercise intolerance linked genes.

Fluidigm assay	True negative	False positive	Specificity
AMPD1 c.190C>T p.R64C	1186	0	100%
AMPD1 c.311G>A p.R104H	1183	0	100%
AMPD1 c.1017G>T p.M340I	1178	0	100%
ATP2A1 c.1613C>T p.T538M	1186	2	99.83%
ATP2A1 c.1619C>T p.P540L	1182	1	99.92%
ATP2A1 c.1948G>A p.D650N	1185	0	100%
CLCN1 c.899G>A p.R300Q	1164	2	99.83%
PYGM c.148C>T p.R50*	1174	0	100%
PYGM c.313G>T p.A105S	1169	1	99.91%
PYGM c.1279C>T p.R427W	1186	0	100%
TRDN c.403G>A p.E135K	1157	0	100%
TRDN c.1016G>A p.S339N	1185	0	100%

Fluidigm® genotyping results for these genes have been presented in (Table 2.22) with Sanger sequencing and melt-curve confirmations presented in brackets for comparison. Four of the rare and potentially pathogenic variants screened were detected more than once across the EHI cohort and were also observed in the other populations according to expected genotype frequency (ExAC). Three extremely rare variants were only observed in the EHI cohort and absent from MHSh/hc, MHN and UK population samples. These included *AMPD1* p.R64C (MAF ExAC 0.00005), *ATP2A1* p.T538M (MAF ExAC 0.00002) and *PYGM* p.R427W (MAF ExAC 0.00007). Three variants were found in both EHI and MH populations, including *AMPD1* p.R104H, *ATP2A1* p.D650N and *TRDN* p.S339N. The remaining 6 variants screened were identified in EHI and MH populations in addition to MHN and/ or UK population samples.

Table 2.22: Fluidigm genotype screen results for variants identified in genes associated with an exercise intolerance phenotype. All variants were heterozygous and observed in independent families. Fluidigm results were confirmed using Sanger sequencing or melt-curve analysis (presented in brackets for comparison).

Gene	DNA change	AA change	EHI	MHSh/hc	MHN	UK POP
AMPD1	c.190C>T	p.R64C	1 (1)	–	–	–
AMPD1	c.311G>A	p.R104H	1 (1)	3 (3)	–	–
AMPD1	c.1017G>T	p.M340I	1 (1)	6 (6)	–	2 (2)
ATP2A1	c.1613C>T	p.T538M	1 (1)	2 (0)	–	–
ATP2A1	c.1619C>T	p.P540L	2 (2)	3 (2)	1 (1)	–
ATP2A1	c.1948G>A	p.D650N	1 (1)	1 (1)	–	–
CLCN1	c.899G>A	p.R300Q	4 (4)	7 (7)	3 (3)	11 (9)
PYGM	c.148C>T	p.R50*	1 (1)	3 (3)	–	9 (9)
PYGM	c.313G>T	p.A105S	4 (4)	6 (6)	7 (6)	2 (2)
PYGM	c.1279C>T	p.R427W	1 (1)	–	–	–
TRDN	c.403G>A	p.E135K	2 (2)	17 (17)	2 (2)	9 (9)
TRDN	c.1016G>A	p.S339N	1 (1)	1 (1)	–	–

2.3.2.7 Variants in genes associated with an exercise intolerance phenotype highlighted as very rare and potentially pathogenic

To further prioritise variants for follow up, those with a MAF ≤0.1% and a C-score ≥15 were highlighted in Table 2.23. Only three non-synonymous variants in three genes (*AMPD1*, *ATP2A1* and *PYGM*) had a population frequency lower than 0.1% and were identified in three EHI patients, respectively.

Table 2.23: Very rare (MAF ExAC ≤0.1%) and potentially deleterious (C-score ≥15) variants identified in genes previously associated with an exercise intolerance phenotype.

Gene	Variant ID	DNA change	AA change	MAF (ExAC)	C-score	EHI
AMPD1	rs139512772	c.190C>T	p.R64C	0.00005	29.1	1
ATP2A1	rs763211121	c.1613C>T	p.T540M	0.00002	27.1	1
PYGM	rs146919445	c.1015C>T	p.R339W	0.00007	33	1

2.3.2.8 Additional genes central to calcium homeostasis and metabolism

In the remaining 39 genes investigated 141 non-synonymous variants were detected across 30 genes. Of these, 71 were highlighted as rare (MAF ≤1%) with 47 also annotated as potentially damaging (C-score ≥15) (Table 2.24). The 47 variants were all heterozygous and identified within 16 genes (Table 2.24). Six of these variants were previously unreported on population databases and in the literature. Although *HSPB1*

p.T151S was not identified in the 60,706 unrelated individuals represented on the ExAC database, it was identified once in the 1000 Genomes Project comprising 2,504 unrelated individuals.

Five variants were observed twice across the EHI cohort, including *ACADVL* p.V207A, *HOMER* p.P142L, *HRC* p.R88C, *NEB* p.S5302C and *SLC8A3* p.R314G. The EHI patients who carried one of these five variants produced conflicting contracture responses by IVCT. None of the positive contracture responses could be explained by an additional rare variant in the *RYR1* or *CACNA1S* genes. Twenty-seven non-synonymous variants annotated as rare (MAF ExAC ≤1%) and pathogenic (C-score ≥15) from 13 genes were selected for the Fluidigm® SNP Type™ genotyping screen, highlighted by an asterisk in Table 2.24.

2.3.2.9 Fluidigm® SNP Type™ genotyping results for variants identified in additional genes related to calcium homeostasis and metabolism

Fluidigm® SNP Type™ genotyping assays were designed for 27 rare (MAF ≤1%) and potentially deleterious (C-score ≥15) non-synonymous variants across 13 genes related to calcium homeostasis and metabolism. Viable assays were produced for 24 variants, effectively detecting variants in positive control samples. The failed assay for variant *SYPL2* p.N213S was highlighted as non-standard with a 67% GC content during the design process. The other two variants not detected by Fluidigm® SNP Type™ genotyping (*ASPH* p.V84G and p.A85P) were identified in a single EHI individual (patient 31), located in close proximity. NGS paired-end reads showed these heterozygous variants in *cis* on both forward and reverse reads, therefore it is likely that the allele-specific primers failed to bind and amplify the variant allele. These variants were subsequently confirmed by Sanger sequencing. Two additional assays also had high GC contents (>65%), but both effectively distinguished between homozygous and heterozygous genotypes, confirming the genotype of the EHI positive control.

Table 2.24: Non-synonymous variants annotated as rare and potentially deleterious in additional genes involved in calcium homeostasis and metabolism. All variants were present in the heterozygous form.

Gene	dbSNP ID	DNA change	AA change	MAF (ExAC)	C-score	EHI	
ACADVL	rs113994167	c.620T>C	p.V207A	0.0014	26	2	*
ACADVL	rs753624994	c.777C>A	p.H259Q	0.00002	22.9	1	*
ACADVL	rs139425622	c.1339G>A	p.G447R	0.0004	26.4	1	
ASPH	rs527506012	*c.251T>G*	*p.V84G*	0.0009	21.1	1	*
ASPH	N/A	*c.253G>C*	*p.A85P*	N/A	21.1	1	*
ASPH	N/A	c.263A>C	p.K88T	N/A	20.9	1	*
ASPH	rs147012895	c.1189C>T	p.R397C	0.00045	22.4	1	*
CALR	N/A	c.733C>G	p.P245A	N/A	23	1	*
CASQ1	rs140253806	c.130G>A	p.D44N	0.002	29.3	1	*
CASQ1	rs770893881	c.557T>A	p.F186Y	0.000008	28.6	1	*
CHERP	rs763728092	c.1112C>T	p.P371L	0.0001	20.3	1	
HOMER1	rs200295734	c.425C>T	p.P142L	0.0003	22.9	2	*
HRC	rs200176524	c.1189C>T	p.R397*	0.0002	34	1	
HRC	rs148966785	c.262C>T	p.R88C	0.0041	20.2	2	
HSPA4	rs61749631	c.2086C>T	p.P696S	0.0071	27.4	1	
HSPB1	rs28937568	c.452C>G	p.T151S	N/A	22.7	1	*
NEB	rs201714437	c.19895A>G	p.K6620R	0.0003	22.5	1	
NEB	rs763365852	c.24020C>T	p.S8007L	0.0002	26.5	1	
NEB	rs62167164	c.15941C>G	p.S5302C	0.0091	25.1	2	
NEB	rs371568550	c.10073A>G	p.H3346R	0.0001	23.9	1	
NEB	rs184262608	c.6069G>A	p.M2023I	0.0065	17.95	1	
NEB	rs144180493	c.5555T>G	p.M1852R	0.0033	24.6	1	
NEB	rs201545521	c.4463T>C	p.M1488T	0.0004	23.8	1	
NEB	N/A	c.4442T>G	p.F1481C	N/A	26.3	1	
NEB	rs201141958	c.3623T>C	p.I1208T	0.0012	17.73	1	
NEB	rs187343008	c.3191A>G	p.Y1064C	0.0066	24.4	1	
NEB	rs143123053	c.2603T>C	p.L868P	0.0015	25.5	1	
NEB	N/A	c.2432A>T	p.D811V	N/A	24.6	1	
NEB	rs147305883	c.1856A>G	p.K619R	0.0011	23.9	1	
NEB	rs747225286	c.491C>T	p.S164L	0.00003	29.7	1	*
SCN4A	rs749841448	c.5233C>T	p.R1745C	0.00002	24.6	1	*
SCN4A	rs776355318	c.4303G>C	p.D1435H	0.00002	25	1	*
SCN4A	rs377277110	c.2995G>A	p.V999M	0.00007	25.5	1	
SCN4A	rs113462659	c.2188G>A	p.V730M	0.0006	30	1	*
SCN4A	rs768087254	c.1773C>A	p.N591K	0.000008	29.1	1	*
SCN4A	rs80338952	c.968C>T	p.T323M	0.0087	24.9	1	
SLC8A3	rs144289733	c.454G>A	p.V152M	0.0004	33	1	*
SLC8A3	rs376525495	c.1204C>T	p.P402S	0.000077	23.6	1	*
SLC8A3	rs141396102	c.1064G>T	p.R355L	0.0004	32	1	*
SLC8A3	rs34816272	c.940A>G	p.R314G	0.0034	17.69	2	*
SRL	rs374884498	c.1192C>T	p.R398C	0.00006	27.4	1	*
STIM1	rs146873551	c.1511C>T	p.T504M	0.0009	21.3	1	*
STIM1	rs35637264	c.1838C>A	p.S613Y	0.0008	27.4	1	*
SYPL2	rs199821906	c.194G>A	p.R65H	0.0003	23.2	1	*
SYPL2	rs62641754	c.638A>G	p.N213S	0.0059	25.7	1	*
TRPM6	N/A	c.3263T>G	p.M1088R	N/A	23.6	1	*
TRPM6	rs150874152	c.496G>A	p.G166R	0.0026	34	1	*

* Twenty-seven rare (MAF ≤1%) and potentially pathogenic (C-score ≥15) variants were included in the Fluidigm genotyping screen.

Fluidigm® SNP Type™ assays designed for the remaining 24 variants were good quality, all producing specificities greater than 99.66% (Table 2.25).

Table 2.25: Specificity of Fluidigm SNP Type genotyping assays in variants identified in the remaining 39 genes of the target panel.

Fluidigm assay	True negative	False positive	Specificity
ACADVL c.620T>C p.V207A	1183	0	100%
ACADVL c.777C>A p.H259Q	1184	0	100%
ASPH c.263A>C p.K88T	1186	0	100%
ASPH c.1189C>T p.R397C	1185	0	100%
CALR c.733C>G p.P245A	1186	4	99.66%
CASQ1 c.130G>A p.D44N	1183	0	100%
CASQ1 c.557T>A p.F186Y	1186	1	99.92%
HOMER1 c.425C>T p.P142L	1181	1	99.92%
HSPB1 c.452C>G p.T151S	1186	0	100%
NEB c.491C>T p.S164L	1186	2	99.83%
SCN4A c.5233C>T p.R1745C	1186	1	99.92%
SCN4A c.4303G>C p.D1435H	1185	0	100%
SCN4A c.2188G>A p.V730M	1183	0	100%
SCN4A c.1773C>A p.N591K	1186	2	99.83%
SLC8A3 c.454G>A p.V152M	1183	0	100%
SLC8A3 c.1204C>T p.P402S	1186	0	100%
SLC8A3 c.1064G>T p.R355L	1182	0	100%
SLC8A3 c.940A>G p.R314G	1135	1	99.91%
SRL c.1192C>T p.R398C	1186	3	99.75%
STIM1 c.1511C>T p.T504M	1185	0	100%
STIM1 c.1838C>A p.S613Y	1186	9	99.25%
SYPL2 c.194G>A p.R65H	1184	0	100%
TRPM6 c.3263T>G p.M1088R	1186	3	99.75%
TRPM6 c.496G>A p.G166R	1174	0	100%

Fluidigm® SNP Type™ genotyping results for 24 genetic variants in 13 additional genes involved in calcium homeostasis and metabolism have been presented in Table 2.26 with Sanger sequencing and melt-curve confirmations for comparison. The figures provided in the EHI column represent both NGS results for the 64 EHI patients and Fluidigm results for the EHI positive controls. The MHSh/hc, MHN and UK population columns represent Fluidigm genotype results for 658 MHSh/hc, 180 MHN and 285 UK population samples screened.

Table 2.26: Fluidigm genotype screen results for variants in additional genes central to calcium homeostasis and metabolism. Twenty-seven (MAF ≤1%) and potentially pathogenic (C-score ≥15) variants were selected for the genotyping screen. All variants were heterozygous and observed in independent families. Fluidigm results were confirmed using Sanger sequencing or melt-curve analysis (presented in brackets for comparison).

Gene	DNA change	AA change	EHI	MHSh/hc	MHN	UK POP
ACADVL	c.620T>C	p.V207A	2 (2)	2 (2)	−	−
ACADVL	c.777C>A	p.H259Q	1 (1)	2 (2)	−	−
ASPH	c.263A>C	p.K88T	1 (1)	−	−	−
ASPH	c.1189C>T	p.R397C	1 (1)	1 (1)	−	−
CALR	c.733C>G	p.P245A	1 (1)	1 (0)	−	3 (0)
CASQ1	c.130G>A	p.D44N	1 (1)	3 (3)	−	−
CASQ1	c.557T>A	p.F186Y	1 (1)	1 (0)	−	−
HOMER1	c.425C>T	p.P142L	2 (2)	2 (1)	1 (1)	2 (2)
HSPB1	c.452C>G	p.T151S	1 (1)	−	−	−
NEB	c.491C>T	p.S164L	1 (1)	2 (0)	−	−
SCN4A	c.5233C>T	p.R1745C	1 (1)	−	−	1 (0)
SCN4A	c.4303G>C	p.D1435H	1 (1)	1 (1)	−	−
SCN4A	c.2188G>A	p.V730M	1 (1)	2 (2)	−	1 (1)
SCN4A	c.1773C>A	p.N591K	1 (1)	2 (0)	−	−
SLC8A3	c.454G>A	p.V152M	1 (1)	3 (3)	−	−
SLC8A3	c.1204C>T	p.P402S	1 (1)	−	−	−
SLC8A3	c.1064G>T	p.R355L	1 (1)	2 (2)	1 (1)	1 (1)
SLC8A3	c.940A>G	p.R314G	2 (2)	31 (31)	10 (9)	10 (10)
SRL	c.1192C>T	p.R398C	1 (1)	3 (0)	−	−
STIM1	c.1511C>T	p.T504M	1 (1)	1 (1)	−	−
STIM1	c.1838C>A	p.S613Y	1 (1)	8 (0)	1 (0)	−
SYPL2	c.194G>A	p.R65H	1 (1)	−	1 (1)	1 (1)
TRPM6	c.3263T>G	p.M1088R	1 (1)	3 (0)	−	−
TRPM6	c.496G>A	p.G166R	1 (1)	8 (8)	1 (1)	3 (3)

Fluidigm® SNP Type™ assays failed for variants *ASPH* p.V84G, *ASPH* p.A85P and *SYPL2* c.638A>G p.N213S so they were excluded from table.

Five variants were only identified once in the EHI cohort and were not observed in the 1,123 samples screened comprising MHSh/hc, MHN and UK population individuals. These variants (*ASPH* p.K88T, *HSPB1* p.T151S, *SLC8A3* p.P402S, *SRL* p.R398C and *TRPM6* p.M1088R) were all extremely rare seen only a handful of times on ExAC and/ or 1000G databases, with *ASPH* p.K88T and *TRPM6* p.M1088R previously unreported. The novel *TRPM6* variant was observed in EHI patient 2, who displayed a positive contracture by IVCT to both caffeine and halothane (MHShc). Sequencing did not reveal any rare variants in *RYR1* or *CACNA1S*. The other six rare variants were identified in EHI patients displaying negative IVCT responses.

Interestingly ten of the variants presented in Table 2.26 were only observed in EHI and MHSh/hc patients and absent in MHN and UK population control samples. Three variants were identified in EHI, MHSh/hc and MHN samples and absent from the UK population samples. It is important to note that the 180 MHN samples comprised MHN probands and family members of MHSh/hc probands. The remaining six variants were identified in UK population samples in addition to EHI, MHSh/hc and/ or MHN samples.

2.3.2.10 A subset of very rare and potentially deleterious non-synonymous variants identified in genes related to calcium homeostasis and metabolism

Thirty-two variants relating to calcium homeostasis and metabolism were highlighted as particularly rare (MAF ExAC $\leq$0.1%) and therefore would be prioritised for functional characterisation (Table 2.27). Interestingly, five of these were identified in *SCN4A*, which encodes the $Na_v1.4$ channel, which initiates membrane depolarisation in EC-coupling. Three of the five variants (p.V730M, p.V999M and p.R1745C) were identified in EHI patients who demonstrated a positive IVCT phenotype. *SCN4A* p.V730M was the only rare variant identified in an IVCT positive EHI patients who did not harbour an *RYR1* variant, which could account for the abnormal contracture response.

Table 2.27: Variants identified in genes involved in calcium homeostasis and metabolism annotated as very rare (MAF ≤0.1%) and pathogenic (C-score ≥15).

Gene	Variant ID	DNA change	AA change	MAF (ExAC)	C-score	EHI
ACADVL	rs753624994	c.777C>A	p.H259Q	0.00002	22.9	1
ACADVL	rs139425622	c.1339G>A	p.G447R	0.0004	26.4	1
ASPH	rs527506012	*c.251T>G*	*p.V84G*	0.0009	21.1	1
ASPH	N/A	*c.253G>C*	*p.A85P*	N/A	21.1	1
ASPH	N/A	c.263A>C	p.K88T	N/A	20.9	1
ASPH	rs147012895	c.1189C>T	p.R397C	0.00045	22.4	1
CALR	N/A	c.733C>G	p.P245A	N/A	23	1
CASQ1	rs770893881	c.557T>A	p.F186Y	0.000008	28.6	1
CHERP	rs763728092	c.1112C>T	p.P371L	0.0001	20.3	1
HOMER1	rs200295734	c.425C>T	p.P142L	0.0003	22.9	2
HRC	rs200176524	c.1189C>T	p.R397*	0.0002	34	1
HSPB1	rs28937568	c.452C>G	p.T151S	N/A	22.7	1
NEB	rs747225286	c.491C>T	p.S164L	0.00003	29.7	1
NEB	N/A	c.2432A>T	p.D811V	N/A	24.6	1
NEB	N/A	c.4442T>G	p.F1481C	N/A	26.3	1
NEB	rs201545521	c.4463T>C	p.M1488T	0.0004	23.8	1
NEB	rs371568550	c.10073A>G	p.H3346R	0.0001	23.9	1
NEB	rs201714437	c.19895A>G	p.K6620R	0.0003	22.5	1
NEB	rs763365852	c.24020C>T	p.S8007L	0.0002	26.5	1
SCN4A	rs768087254	c.1773C>A	p.N591K	0.000008	29.1	1
SCN4A	rs113462659	c.2188G>A	p.V730M	0.0006	30	1
SCN4A	rs377277110	c.2995G>A	p.V999M	0.00007	25.5	1
SCN4A	rs776355318	c.4303G>C	p.D1435H	0.00002	25	1
SCN4A	rs749841448	c.5233C>T	p.R1745C	0.00002	24.6	1
SLC8A3	rs144289733	c.454G>A	p.V152M	0.0004	33	1
SLC8A3	rs141396102	c.1064G>T	p.R355L	0.0004	32	1
SLC8A3	rs376525495	c.1204C>T	p.P402S	0.000077	23.6	1
SRL	rs374884498	c.1192C>T	p.R398C	0.00006	27.4	1
STIM1	rs146873551	c.1511C>T	p.T504M	0.0009	21.3	1
STIM1	rs35637264	c.1838C>A	p.S613Y	0.0008	27.4	1
SYPL2	rs199821906	c.194G>A	p.R65H	0.0003	23.2	1
TRPM6	N/A	c.3263T>G	p.M1088R	N/A	23.6	1

2.3.2.11 Family studies

Eleven available family members from three unrelated EHI families had the coding regions of the 50 target genes sequenced to identify variants co-segregating with IVCT status within families. The EHI index case (patient 7) annotated in the family 1 pedigree as II-1 (Figure 2.15) had a rare (ExAC MAF 0.0018) and likely deleterious (C-score 26.1) heterozygous non-synonymous variant in the *RYR1* gene (p.R3539H). The same variant was found in just one of the MHSh brothers (II-2) and absent from the other MHSh brother (II-3) and MHN sister (II-4). Unfortunately, IVCT and genetic information was never obtained for either parent (I-1 and I-2).

RYR1 p.R3539H was also identified in six unrelated non-EHI MH susceptible individuals during routine screening of *RYR1* variants at the Leeds MH Unit. Four of these individuals were classified MHShc and two MHSh. Follow up of respective family members had been previously completed for one of the families by staff at the Leeds MH Unit, with *RYR1* p.R3539H co-segregating with MH susceptible classification. Four of the MH families were not screened for *RYR1* p.R3539H because a functionally characterised *RYR1* mutation had already been identified in these families. Family members of the final non-EHI MHShc individual had not been genetically characterised.

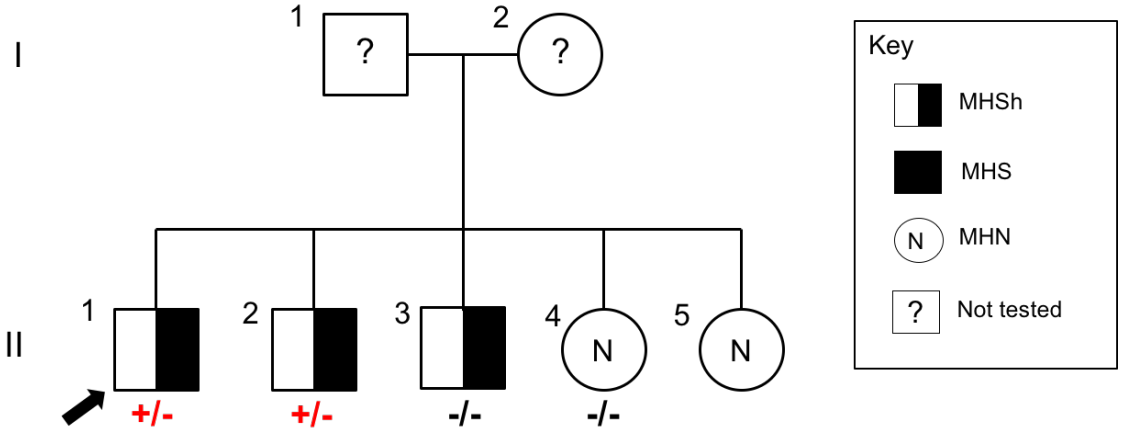

Figure 2.15: EHI family 1 pedigree representing variant *RYR1* p.R3539H. Genotypes of variant *RYR1* c.10616G>A p.R3539H have been displayed below the individual symbols.

EHI patient 15 from family 2 (Figure 2.16), III-4, revealed a relatively rare (ExAC MAF 0.0088) and potentially pathogenic (C-score 26.8) heterozygous non-synonymous variant in *CACNA1S* (p.S606N). The variant co-segregated with IVCT status in this family and was inherited from the paternal side. *CACNA1S* p.S606N was identified in the MHSh father (II-1) and sister (III-3) of the EHI index case, whereas his MHN sister (III-2) did not carry the variant. Interestingly, both parents displayed a positive contracture during the IVCT. The EHI index case did not share any rare variants in common with his mother (II-2) in the genes investigated. The EHI patient's mother and aunt did not have any rare (MAF ≤1%) variants in the genes investigated that could account for their positive IVCT responses.

The same *CACNA1S* variant was also detected in 3 additional unrelated EHI patients (10, 17 and 42), 24 non-EHI MHSh/hc individuals (of 548) and 3 non-EHI MHN

individuals (of 180) across the Leeds patient cohort. The variant was also detected in 7 out of 285 unrelated UK population samples purchased from ECACC via Sigma-Aldrich. An additional rare variant *ASPH* p.E159G (MAF ExAC 0.0081, C-score 14.17) was detected in the EHI proband, but was not detected in either parent suggesting that it had arisen *de novo* or was a false positive variant produced as an artifact by NGS.

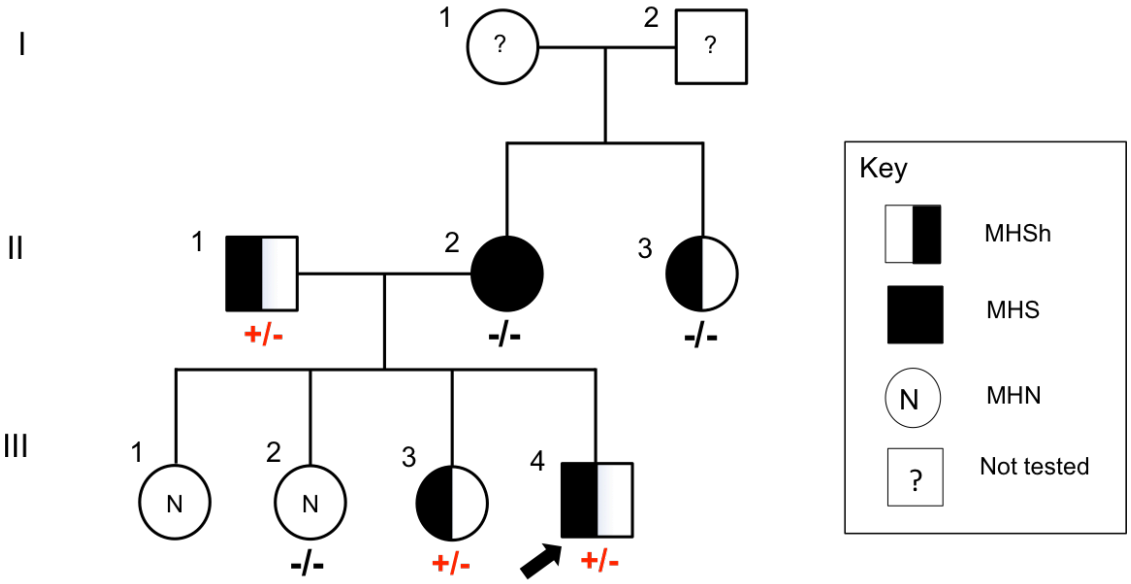

Figure 2.16: EHI family 2 pedigree representing variant *CACNA1S* p.S606N. Genotypes of variant *CACNA1S* c.1817C>T p.S606N have been displayed below the individual symbols.

The third EHI family (Figure 2.17) comprised 4 members including the index case (EHI patient 21), who was classified as MHSh along with both parents. Of the non-synonymous variants detected in the family only *SCN4A* p.V730M was annotated as rare and potentially deleterious of the genes investigated. This variant was present in the heterozygous form in both the MHSh EHI proband and his MHSh father but absent from his MHSh mother and MHN brother. The EHI patient also carried an additional rare variant in the *TRPM6* gene (p.M333I), but *in silico* predictions proved benign (C-score 0.001). He shared these rare variants with his MHSh father along with *TRPC1* p.A14T (MAF 0.013), which was also identified in his MHN brother. Of these variants only *SCN4A* p.V730M met the criteria for Fluidigm high throughput screening (MAF ≤1%, C-score ≥15) and was subsequently identified in three non-EHI individuals comprising 1 MHShc, 1 MHSh and 1 UK population sample.

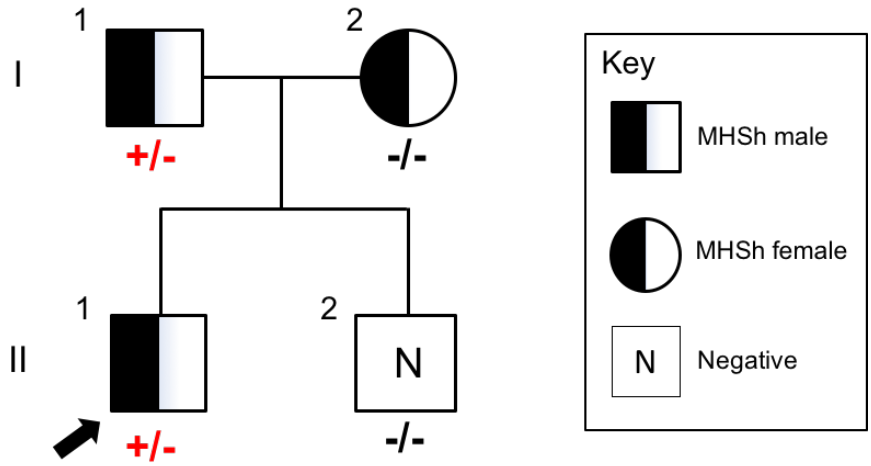

Figure 2.17: EHI family 3 pedigree representing variant *SCN4A* p.V730M. The EHI index has been indicated by an arrow. Genotypes of variant *SCN4A* c.2188G>A p.V730M have been displayed below the individual symbols.

2.3.2.12 Insertions and deletions identified across all genes

Nine insertions or deletions (INDELs) were detected in the coding region of 6 genes, with 54 of the EHI cohort possessing at least one INDEL (Table 2.28). Homozygous in-frame deletion *ORAI1* c.127_132delCCGCCA was detected at a higher frequency in the EHI cohort (25 observations) than expected based on its reported MAF 0.005 (ExAC); however, new genome release GRCh38 amended the annotation of the first 66 amino acids of *ORAI1* to fall into 5' untranslated region (UTR). A frame-shift insertion (*ASPH* c.252_253insTTCTGGGA) was identified in the same codon as c.251T>G p.V84G and upstream of p.A85P, identified in *cis* in the same EHI patient.

Table 2.28: Insertions and deletions identified in the coding regions of the 50 target genes. Eight INDELs were identified across the 50 target genes of the 64 EHI patients. The MAF represents INDEL frequencies from the ExAC database.

Gene	ID	Type	Ref allele	MAF	EHI
ASPH	rs553543086	Frameshift insertion	c.252_253insTTCTGGGA	0.0009	1
CHERP	rs762824932	Inframe deletion	c.1005_1007delGCA	0.09	1
HRC	rs778245363	Inframe insertion	c.784_785insATG	0.06	7
HRC	rs569932130	Inframe deletion	c.773_784delATGATGATGATG	0.01	1
HRC	rs66501117	Inframe deletion	c.784_786delATG	0.47	43
HRC	rs147238387	Inframe insertion	c.605_606insGGA	0.31	21
LPIN1	rs149564563	Inframe deletion	c.850_852delTCT	0.08	1
ORAI1	rs141919534	Inframe deletion	c.127_132delCCGCCA	0.005	25
SYPL2	rs201507882	Inframe insertion	c.723_724insCAGGGC	0.009	1

2.4 Discussion

The clinical episodes experienced by the EHI cohort were diverse as were their *ex vivo* muscle responses to caffeine and halothane during IVCTs. The majority of EHI referrals were unable to effectively thermoregulate. VO_2 max scores, core temperature and sweat production varied between each of the EHI patients and provided additional quantitative measures to explore. The varied level of clinical detail reported across the EHI cohort made it difficult to categorise EHI patients based on their clinical presentation alone.

A rise in serum CPK levels was a common feature of EHI and exertional rhabdomyolysis with counts more than 100,000 IU/L documented in severe cases, suggesting extensive muscle breakdown. It is important to note that normal CPK ranges are sex, age and ethnicity-dependent with baseline levels differing greatly between individuals (Neal *et al.*, 2009). Specifically, serum CPK concentrations are also notably higher in males and individuals of African American decent. Therefore, without reference values it is difficult to interpret the significance of high CPK levels seen in these EHI cases. There is no universally accepted threshold of serum CPK that signifies ER, with rises between 5-fold and 50-fold associated with the condition (Voermans, Snoeck and Jungbluth, 2016). CPK levels should therefore be considered on a patient-specific basis and 'normal' ranges referenced by diagnostic laboratories should be interpreted with caution. A number of factors in addition to heat and exercise can adversely affect CPK levels, including alcohol, drugs and viral infections (Voermans, Snoeck and Jungbluth, 2016). These all need to be considered as potential triggers when identifying the genetic contribution to exertional rhabdomyolysis. Dehydration was reported as a potential contributing factor in five of the documented EHI cases, but only one of these individuals presented with symptoms consistent with rhabdomyolysis.

The fitness capacities of EHI patients who went on to display an increased sensitivity to halothane/ caffeine were significantly lower than those who demonstrated normal IVCT responses. In this subset of EHI patients, a reduced fitness capacity (VO_2 max) may have been a contributing factor towards the development of EHI, a previously identified risk factor (F Wallace *et al.*, 2006). This group of EHI patients with abnormal IVCT results only contained 20 individuals, so may not reflect the actual distribution of VO_2 max scores of the EHI/ MH susceptible population. EHI patients who produced normal contracture responses had higher fitness levels on average, and therefore would be working at a higher absolute workload during the HTT. They did not however appear to increase their sweat rate to compensate for the assumed rise in heat production. It is

possible that the sweat glands sustained damage during the EHI episodes and that these patients had not fully recovered prior to their IVCT.

Assessing quantitative differences in IVCT contracture responses between EHI and MH individuals, aimed to provide further characterisation of the EHI phenotype in relation to MH. Twenty-two EHI patients displayed a positive contracture in response to halothane, with only four of these exhibiting abnormal reactions to both RyR1 agonists. A large proportion of the EHI cohort (41 out of 64) exhibited normal IVCT responses, indicating that the underlying pathophysiology of EHI is distinct to MH in an abundance of these individuals. The distribution of IVCT classifications across the EHI cohort highlights their lack of sensitivity to caffeine, with only 4 individuals out of 64 showing an abnormal response to caffeine. Although both caffeine and halothane are known to activate RyR1, their mechanistic action remains poorly understood (O'Brien *et al.*, 2002; Jiang *et al.*, 2008; Dias and Vogel, 2009). More recently, caffeine-specific binding sites have been identified within the C-terminal domain of RyR1, but activation of the channel relies on conformational changes so binding can also be indirectly modified (des Georges *et al.*, 2016). A study investigating the correlation between IVCT phenotypes and *RYR1* genotypes revealed that different *RYR1* variants determined the severity of IVCT responses, clinical MH reactions and CPK levels (Carpenter, Robinson, *et al.*, 2009). IVCT contracture responses differed in response to caffeine and halothane and in severity relative to 'weak' *RYR1* variant c.7300G>A, p.G2434R.

The viability of EHI muscle was significantly reduced relative to MH susceptible individuals, which is interesting considering no histopathological features were identified in these patients on examination. Increased sample numbers are required to determine whether this is a sampling artefact or whether the differences observed are status-specific. Despite the similar strength of contractures between EHI and MH susceptible individuals at 2% halothane, it is important to consider what defines a severe IVCT response. As with the clinical phenotype, it is difficult to determine whether the rate of onset, sensitivity to triggering agents or the strength of contracture is the most appropriate measure of severity. For example, EHI patient 11 developed slight contractures in response to both caffeine and halothane and therefore his IVCT response would be classified as weak. In contrast, EHI patient 21 produced a strong 1 g contracture on exposure to 2% halothane, but did not react to caffeine. Reacting to a lower dose of halothane or caffeine, represents an increased sensitivity to the agent regardless of the degree of response. Despite this, contractures at 2% halothane/ 2mM caffeine were presented to ensure consistency and clarity in data interpretation. Overall,

the varied IVCT and HTT responses seen among EHI patients, along with the spectrum of clinical features observed suggests that EHI may have a complex molecular aetiology.

The HaloPlex™ target enrichment system was chosen as a library preparation method to enrich the exons of fifty genes in the cohort of EHI patients and their relatives because it was in routine use at the UK MH Investigation Unit in Leeds. The HaloPlex™ target enrichment system incorporates Illumina® sequencing adapters making it compatible with all Illumina® sequencing platforms. Although this method is fast, cost effective and provides high target specificity (Samorodnitsky *et al.*, 2015), the use of restriction enzymes to digest the gDNA generates non-random fragments, resulting in a high PCR duplicate rate and an overall lack of coverage compared to other technologies. Moreover, if a variant exists within a restriction site, preferential amplification of the wild-type allele may occur. The 7 universal gaps identified in *RYR1* coverage were present in all samples, suggesting a technical issue with HaloPlex™ target enrichment rather than variations in sample quality. The HaloPlex™ method does not perform well with regions containing a high GC content (Samorodnitsky *et al.*, 2015), such as exon 91, which was routinely covered by Sanger sequencing to account for this. Achieving full coverage of the coding regions of *RYR1* and *CACNA1S* was prioritised due to their proven role in the pathophysiology of MH (Girard *et al.*, 2001; Yang *et al.*, 2006; Zullo *et al.*, 2009; Pirone *et al.*, 2010). Overall, HaloPlex™ target enrichment was chosen over comparable target capture methods such as SureSelect (Agilent Technologies) and Nextera (Illumina®) due to a reduced preparation time, maximising time for data analysis.

In addition to the limitation of HaloPlex™ coverage, variant detection is also reliant on SureCall software parameters to effectively detect all variants and to expose sequencing artefacts as false positives. Setting parameters to call only high-quality variants may potentially sacrifice the software's sensitivity to detect true variants with low read depth and low base-call quality.

The 50 target genes were chosen initially to investigate the cause of MH in patients who did not harbour genetic variants in *RYR1* and *CACNA1S* and therefore this target panel of genes may not necessarily represent the genetic contribution to EHI. In addition to the 64 EHI patients sequenced, 220 MH index cases and 29 of their family members have also been included in the targeted 50 gene NGS screen to date. The gene panel could be expanded to include a more exhaustive list of genes causing metabolic myopathies involving muscle dysfunction related to exercise intolerance. For example,

mutations in *PGAM2* and *LDHA* have been shown to cause phosphoglycerate mutase deficiency and lactate dehydrogenase deficiency, respectively (Kanno *et al.*, 1988; Tsujino, Shanske and DiMauro, 1993). Both disorders are characterised by exercise intolerance, cramps, and myoglobinuria. Other gene candidates could include *UCP3*, which encodes the muscle specific isoform of a mitochondrial uncoupling protein. This protein controls the regulation of body temperature and energy metabolism, with mutations increasing sensitivity, activation and heat production (Argyropoulos *et al.*, 1998; Trenker *et al.*, 2007).

Overall, due to the limited understanding of EHI and the suggested link between MH and EHI (Hopkins, 2007; Muldoon *et al.*, 2008; Thomas and Crowhurst, 2013), we adopted a target gene approach based on the routine genetic investigation of MH. This approach allowed us to explore the link between EHI and MH, while investigating the genetic basis of EHI susceptibility. A targeted gene approach was chosen as a cost-effective method, producing a workable dataset in genes central to calcium homeostasis and metabolism. Although both whole exome (WES) and whole genome sequencing (WGS) methods would provide comprehensive coverage of all genes, a targeted strategy was considered appropriate in the first instance.

Screening for non-synonymous variants was prioritised, particularly in genes encoding structural proteins such as *RYR1* and *CACNA1S*. Functionally characterised variants in these genes have been shown to alter channel sensitivity to triggering agents; halothane and caffeine by increasing activation by Ca^{2+} and decreasing inhibition by Mg^{2+} (Yang *et al.*, 2003, 2006). Family studies have assumed MH as an autosomal dominant condition, predominately caused by heterozygous variants in *RYR1*; however, due to the unknown mode of inheritance of EHI a more inclusive approach was adopted, considering different types of genetic variants across the genes including heterozygous, homozygous, non-synonymous, nonsense variants as well as INDELS. This study did not investigate the role of non-coding variants but rather focused on variants that had the potential to alter the structural and functional characteristic of the proteins.

Population frequencies of genetic variants identified in the EHI cohort were obtained using online databases, primarily ExAC. ExAC was favoured as the project included the largest number of unrelated individuals (60,706) and was most representative of our EHI population due to the inclusion of 33,370 European samples. In contrast, the 1000G project only included 94 British samples (out of 514 of European decent). Where appropriate, the ExAC variant frequencies have been discussed in terms of the specific population from which the patient originated. The EHI cohort in this study only included

64 individuals, and therefore may not provide a true representation of variant frequencies in the general population. This also needs to be considered when discussing Fluidigm® SNP Type™ genotype frequencies as sample sizes are relatively small.

The Fluidigm® SNP Type™ technology relies on two PCR steps; locus-specific pre-amplification (STA) and allele-specific amplification to genotype. This provides two opportunities for preferential amplification of the wild-type allele to occur resulting in false negatives. For all viable assays that could effectively genotype, none displayed a lack of sensitivity, with all variants confirmed in EHI positive control samples. It is not possible however to calculate true assay sensitivity as the majority of genotypes have not been confirmed by an additional technology, therefore false negatives were unknown. On the other hand, calculating assay specificity was possible as false positives were detected by confirming all positive variant genotypes using either Sanger sequencing or melt-curve analysis. Genotyping assays for variants identified across the 50 genes revealed impressive specificities (>99.25%), with all but one assay producing less than 5 false positives across the 1,123 non-EHI samples screened.

The assumption of a heritable element to EHI originates from the phenotypic link to MH and positive IVCT responses observed in EHI patients and their family members. *RYR1* and *CACNA1S* variants have also been shown to segregate with positive IVCT responses in these families. True co-segregation analyses of genetic variants with EHI phenotypes were not possible due to a lack of a diagnostic test available to family members of military personnel, specifically the HTT. The IVCT was adopted as a surrogate marker for EHI patients who displayed a positive contracture response and who had family members tested. Although no functionally characterised *RYR1* or *CACNA1S* variants were identified in any of the 64 EHI patients, the detection of 16 rare and potentially pathogenic variants in *RYR1* and *CACNA1S* suggests that these genes may play a role in a subset of cases. Genetic factors are also likely to contribute to EHI susceptibility in this cohort as the condition has been observed in otherwise young, fit and healthy military personnel, who have no known predisposing factors and have shown an inability to thermoregulate on more than one occasion.

Choosing an appropriate MAF cut-off proved difficult due to the unknown prevalence of EHI susceptibility in the general population. EHI is a notifiable disorder in UK military personnel; however, there is no centralised or consistent record of EHI in the civilian population. In addition to limited documentation of EHI cases, civilian EHI patients are poorly characterised. Variants with a MAF less than 1% were prioritised for the genotype

screen; however, variants found at a higher frequency cannot be disregarded at this stage. SNPs are defined as variants with a population frequency greater than 1% (Karki *et al.*, 2015). When considering a rare disorder with a major gene effect, only rare variants are considered, whereas a common variant could potentially modify the phenotype. Due to the limited understanding of the genetic susceptibility to EHI and the multifactorial nature of the condition, the penetrance of EHI is unknown. Variant alleles could also be present at a high proportion in the general population if many individuals remain asymptomatic. The selected C-score cut-off (≤15) was also arbitrary and included substitutions in the human genome predicted to elicit the most deleterious effect (top 5%). All 42 functionally characterised variants in *RYR1*, which demonstrated altered Ca^{2+} release of the RyR1 channel had C-scores higher than 15 (Schiemann and Stowell, 2016) and a MAF ≤0.1%. Pathogenicity annotations should be used as a guide with variants considered on a gene-by-gene and individual basis. Nevertheless, population frequencies and *in silico* pathogenicity predictors offer valuable insight, which allowed variants to be ranked to produce a manageable subset of variants for the genotyping screen.

None of the 42 functionally characterised MH mutations were identified in the EHI cohort or any of their family members; however, 24 EHI patients did carry an uncharacterised *RYR1* variant, with 18 different non-synonymous variants detected by NGS and Sanger sequencing. All 18 variants were located in the cytoplasmic domain of RyR1, with no variants detected across the transmembrane channel region (Figure 2.18). The entire cytoplasmic region of RyR1 has the structural capacity to allosterically regulate RyR1 via conformational changes transmitted to the channel domain (Yan *et al.*, 2015). The specific mechanisms of channel opening have not yet been fully elucidated as RyRs are the largest ion channels and RyR1 is yet to be fully resolved (Yan *et al.*, 2015). The structural characterisation of RyR1 to date has relied on single-particle electron cryomicroscopy, with a current overall resolution of 3.8 Å (Yan *et al.*, 2015). Partial crystallised RyR1 fragments of a higher resolution have also been reported, including a 2.2Å crystallised fragment covering the major phosphorylation site of RyR1, Ser2843 (Sharma *et al.*, 2012) and the N-terminal region spanning amino acids 1-599 at 2.5Å (Amador *et al.*, 2009).

The genetic variants identified in EHI patients were distributed across the cytoplasmic RyR1 protein domains, with eight variants clustering in the helical and central domains. The protein domains of RyR1 can be divided into 3 distinct zones; a central tower (channel, central and N-terminal domain) a crown-like structure surrounding the tower

(handle and helical domain) and the peripheral domains (P1, P2 and SPRY1-3) (Yan *et al.*, 2015). Four variants were detected in the central domain (Figure 2.18), which is the only domain to directly interact with the channel domain triggering opening/ closure of the channel via allosteric conformational changes in the cytoplasmic region (Yan *et al.*, 2015). Four non-polymorphic (≤1%) and potentially deleterious (C-score ≥15) variants were identified in the helical domain, which extensively interacts with the central tower and provides a scaffold for RyR1 modulators to bind to. *RYR1* p.S2776F is located in the RyR-P2 peripheral domain, which has been identified as a phosphorylation hotspot in all isoforms of the ryanodine receptor (RyR) (Yan *et al.*, 2015).

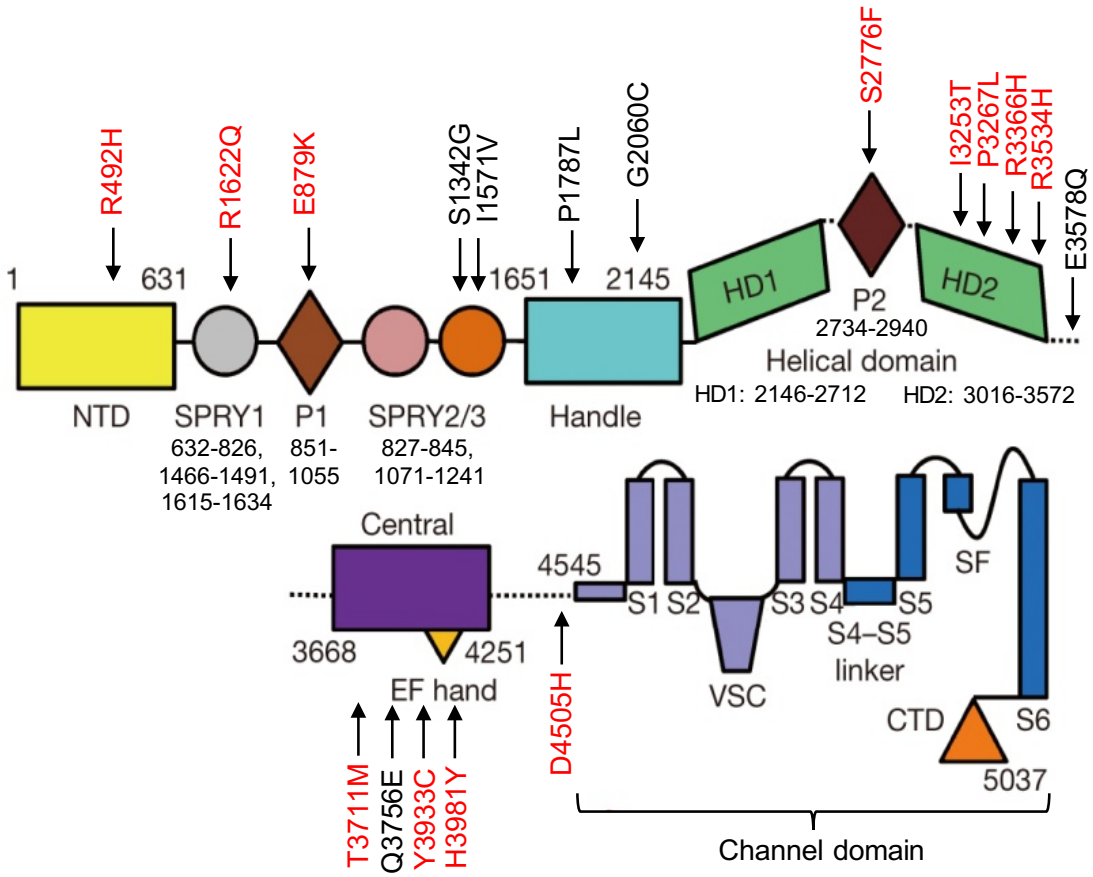

Figure 2.18: Distribution of non-synonymous *RYR1* variants across the protein domains of rabbit RyR1 identified in EHI patients. Rare (≤1%) and potentially deleterious (C-score ≥15) variants highlighted in red, whereas polymorphic, likely non-pathogenic variants are highlighted in black. Original schematic illustration of domain organization published by (Yan *et al.*, 2015).

The functionally characterised MH mutations to date have been identified in the N-terminal (12), helical (18) and channel (6) domains; however, the clustering of MH mutations is likely an artefact of 'hotspot' sequencing historically, with more than 200

reported uncharacterised variants distributed evenly across the gene (Robinson *et al.*, 2006).

RYR1 is highly conserved among different species. Eight of the twelve *RYR1* variants annotated as rare and potentially deleterious in this study were located at highly conserved amino acid residues. Five of these variants were also very rare and will be prioritised for functional characterisation. These included *RYR1* p.R492H, p.E879K, p.I3253T, p.P3267L and p.T3711M. For example, the novel variant, which substitutes the arginine residue for histidine at position 492 was conserved across a range of species (Figure 2.19). Variants identified in conserved positions are more likely to elicit a functional effect as natural selection has ensured the preservation of these residues over time (Choi *et al.*, 2012).

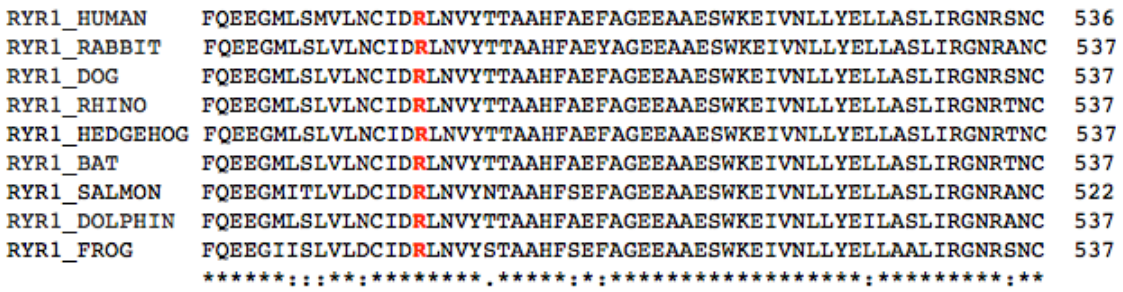

Figure 2.19: Multiple sequence alignment of *RYR1* highlights conservation across species. The arginine residue has been highlighted as the site of novel variant p.R492H. Multiple sequence alignment was performed using Protein-BLAST v.2.8.0 (NCBI) and Clustal O v.1.2.4 (EMBL-EBI).

RYR1 p.R492H, which was unreported on the ExAC database of 60,706 individuals, was located in the N-terminal domain (NTD) of RyR1, which contains 13 of the 42 functionally characterised MH mutations. A variant associated with ER (*RYR1* p.R401C) has also been reported in the N-terminal region of RyR1 in 3 unrelated families (Davis *et al.*, 2002). This variant was also unreported on the ExAC database. All three index cases were classified MHShc by IVCT, two of which were diagnosed with ER featuring high CPK, cramps and myalgia. The same variant was later shown to weaken the thermal stability of the NTD of RyR1, along with a number of other variants in this domain (Kimlicka *et al.*, 2013). The melting-temperature of the NTD of RyR1 was significantly reduced by >5˚C relative to wild-type RyR1-NTD. This could explain the temperature-sensitive phenotype observed in EHI individuals carrying *RYR1* variants as a slight rise in both core and muscle temperature is observed during exercise. This ER-associated variant (p.R401C) lies in close proximity to a rare functionally characterised MH mutation also associated with CCD (*RYR1* p.I403M) (Tong, McCarthy and MacLennan, 1999).

This variant also reduced the thermal stability of the RyR1-NTD, but to a lesser degree (~2˚C), which may explain why it has not been associated with a heat-sensitive phenotype (Kimlicka *et al.*, 2013). This mutation increased caffeine-induced Ca^{2+} release in homotetrameric RyR1 channels, but did not significantly alter resting cytoplasmic Ca^{2+} levels. This was unexpected due to its association with a myopathic phenotype (Tong, McCarthy and MacLennan, 1999).

RyR1 is a homotetramer comprising four identical subunits (Lanner *et al.*, 2010). Le Xu and colleagues suggested that in the presence of a heterozygous *RYR1* variant heterotetrameric proteins are formed expressing both variant and wild-type *RYR1* alleles (Xu *et al.*, 2008). Grievink and Stowell showed that allele-specific expression of wild-type *RYR1* was higher than the *RYR1* p.H4833Y mutant allele. Unfortunately, they did not demonstrate subunit architecture within individual RyR1 channels (Grievink and Stowell, 2010). Allele-specific expression of *RYR1* is likely to depend on variant-specific RNA stability, although if bi-allelic expression occurs, RyR1 subunits are likely to form heterotetramers containing both wild-type and variant alleles.

Neither of the 2 functionally characterised MH mutations in *CACNA1S* (p.R1086H and p.R174W) were identified in the EHI cohort or any of their family members. Fifty-four EHI patients did however carry at least one of the 10 uncharacterised *CACNA1S* variants identified in this study. As with RyR1, the complete structure of $Ca_v1.1$ has only been characterised using cryogenic electron microscopy (cryo-EM) to a current resolution of 3.6 Å (Wu *et al.*, 2016). The 10 non-synonymous variants identified across the *CACNA1S* gene were located in various transmembrane, extracellular, cytoplasmic and pore-forming domains. Each of these domains contained one variant that was annotated as non-polymorphic (MAF ≤1%) and potentially pathogenic (C-score ≥15).

CACNA1S p.S606N was the only variant located in the pore-forming domain. Although this variant was identified in 4 unrelated EHI patients, it was relatively common in the general population (ExAC MAF 0.88%) and enriched in the European non-Finnish population (ExAC MAF 1.22%). Despite the location of this variant in the pore-forming region and the high *in-silico* pathogenicity prediction score, the serine residue substituted for aspartic acid at this position was only conserved across certain mammalian species (Figure 2.20). This may negate its potential to cause a pathogenic phenotype. Therefore, the functional effect of this variant, if any, is likely to be mild rather than act as a major contributory locus of EHI.

```
CACNA1S_HUMAN      FEDTEVRRSNFDNFPQALISVFQVLTGEDWTSMMYNGIMAYGGPSYPGMLVCIYFIILFV  646
CACNA1S_RABBIT     FEDTEVRRSNFDNFPQALISVFQVLTGEDWNSVMYNGIMAYGGPSYPGVLVCIYFIILFV  646
CACNA1S_DOG        FEDTEVRRSNFDNFPQALISVFQVLTGEDWNSMMYSGIMAYGGPSYPGVLVCIYFIILFV  646
CACNA1S_RHINO      FEDTEVRRSNFDNFPQALISVFQVLTGEDWNSVMYNGIMAYGGPSYPGMFVCIYFIILFV  646
CACNA1S_SALMON     FPDQEIRRSNFDNFPQALISVFQVLTGEDWNSIMYNGIMAYGGPVFPGILVSIYFIILFT  656
CACNA1S_HEDGEHOG   FDEMQTRRSTFDNFPQSLLTVFQILTGEDWNSVMYDGIMAYGGPSFPGMLVCIYFIILFI  709
CACNA1S_BAT        FDEMQTRRSTFDNFPQSLLTVFQILTGEDWNSVMYDGIMAYGGPSFPGMLVCIYFIILFI  712
CACNA1S_DOLPHIN    FEDTVVRRSNFDNFPQALITVFQVLTAEDWNSVMYDGIMAYGGPTYPGVLVCIYFIILFV  646
CACNA1S_FROG       FEDTEIRRSTFDNFPQSLITVFQILTGEDWNTVMYNGIMAYGGPSSPGMFICIYFVILFV  642
                   * :    **.**.***:*::***:**.***.::**.****:***  **::::.***:***
```

Figure 2.20: Multiple sequence alignment of *CACNA1S*, highlighting conserved amino acid residues in mammalian species. The serine residue substituted in variant p.S606N has been highlighted. Multiple sequence alignment was performed using Protein-BLAST v.2.8.0 (NCBI) and Clustal O v.1.2.4 (EMBL-EBI).

All three other residues in *CACNA1S* revealing variants annotated as rare and potentially deleterious were conserved to a higher degree, with p.G258D and p.R498H conserved across all species investigated. *CACNA1S* p.R498H was reported to be very rare (MAF ExAC 0.0002) as well as highly conserved, so will be prioritised for functional characterisation. The other conserved variant (*CACNA1S* p.G258D) was mapped to the extracellular loops of the α1 subunit, which interacts with the α2δ subunit. The 4 variants identified in *CACNA2D1,* were located in the extracellular domain of the α2δ subunit, which functions to regulate Ca^{2+} current density and activation/ inactivation kinetics of $Ca_v1.1$. Specifically *CACNA2D1* p.N307I was visualised within a β-strand of the von Willebrand factor domain A (VWA), which is thought to interact with the extended extracellular loops of α1 subunit (*CACNA1S*) (Wu *et al.*, 2016). *CACNA2D1* p.S709N and p.D1045A were resolved in the α-helices and C-terminus of α2δ, respectively. *CACNA2D1* p.T50I, p.S709N and p.D1045A were all annotated as rare and pathogenic is this gene, with p.D1045A identified in 2 EHI patients. *CACNA2D1* p.T50I was the only variant identified in this gene annotated as very rare (unreported on ExAc), so will therefore be prioritised for follow-up studies.

Of the 22 EHI patients who demonstrated a positive IVCT response (MHShc or MHSh), 10 carried one or more variants in the *RYR1* gene. One of these (EHI patient 4), revealed five heterozygous *RYR1* variants, namely *RYR1* p.I1571V, p.G2050C, p.R3366H, p.3711M and Y3933C. Three of these variants were annotated as non-polymorphic and potentially deleterious, with p.R3366H, p.3711M identified as very rare on the ExAC database, MAFs 0.0009 and 0.000008, respectively. It remains unknown whether these variants are present in *cis* or in *trans*, but it is likely that at least one of the variants is responsible for the patient's clinical phenotype and IVCT response. Interestingly, a combination of these variants (p.I1571V, p.R3366H and Y3933C) were previously identified in *cis* in four unrelated MH families (Kraeva *et al.*, 2015). Kraeva and

colleagues revealed the presence of CCD mutation, *RYR1* p.V4849I, in *trans* with the variant triplet. This combination of *RYR1* variants in a compound heterozygous state was shown to confer susceptibility to both MH and CCD. This highlights that specific *RYR1* variants are able to elicit distinct pathogenic phenotypes.

RYR1 p.R3366H and Y3933C have also been reported together in a patient who experienced anaesthetic-induced cardiac arrest and rhabdomyolysis (Duarte *et al.*, 2011). The presence of additional *RYR1* variants cannot be excluded in this patient as only select regions of *RYR1* were sequenced. Additional features included fatigue and myalgia, with muscle histology revealing multi-minicores and a type I fibre predominance. EHI patient 4 from our UK cohort collapsed with EHI and developed rhabdomyolysis with CPK levels rising to 48,986 IU/L with no abnormal muscle histology reported.

The p.R3366H p.Y3933C p.I1571V mutant allele was also reported in combination with *RYR1* p.R391P in a limb-girdle muscular dystrophy patient with a cardiomyopathy (Savarese *et al.*, 2014). These findings suggest that combinations of *RYR1* variants may produce a spectrum of phenotypes ranging from mild hypermetabolic disorders through to severe dystrophic muscle diseases. One copy of the p.R3366H/ Y3933C/ p.I1571V mutant *RYR1* allele was associated with an abnormal response to both caffeine and halothane by IVCT (Kraeva *et al.*, 2015) It is therefore likely that the *RYR1* variants detected in EHI patient 4 are sufficient to cause a mild EHI/ MHShc phenotype, and that the myopathic conditions reported in the literature require the presence of an additional pathogenic *RYR1* variant.

Genetic variants in *RYR1* did not account for positive IVCT responses observed in 12 of the 22 EHI individuals. More specifically, of the 12 patients who demonstrated symptoms consistent with rhabdomyolysis, only 5 carried a *RYR1* variant. Despite *RYR1*-related rhabdomyolysis being widely reported in the literature (Sambuughin *et al.*, 2009; Dlamini *et al.*, 2013; Voermans, Snoeck and Jungbluth, 2016), within the IVCT positive ER group, seven patients did not carry any *RYR1* variants to account for their abnormal *in vitro* contracture responses. This is like MH, where *RYR1* variants only account for 76% of cases MH susceptible diagnosed by IVCT.

Both EHI patients 11 and 14, who presented with rhabdomyolysis and produced positive contractures by IVCT carried the same heterozygous variant, *RYR1* p.S1342G. This variant is common in the general population with a MAF of 0.0221 reported on the ExAC database, so is unlikely to have a major pathogenic effect. *RYR1* p.S1342G has

previously been associated with ER in 6 African American patients either alone or in combination with additional *RYR1* variants; however, this variant has since been identified as enriched in the African American population (MAF 0.2275 ExAc) (Sambuughin *et al.*, 2009; Capacchione *et al.*, 2010). These individuals experienced ER featuring myoglobinuria and/ or myalgia, one of whom went on to experience an MH reaction under anaesthesia (Capacchione *et al.*, 2010). *RYR1* p.S1342G has also been identified in Caucasian MH patients in combination with other *RYR1* variants (Levano *et al.*, 2009). The variant is observed at a lower frequency in the European non-Finnish population on the ExAC database, specifically 0.0005. The 2 ER patients from our EHI cohort carrying *RYR1* p.S1342G and the patient reported by Capacchione and colleagues all harboured the same common variant in *CACNA1S*, p.L1800S (MAF ExAC 0.15); however, the significance of this remains unclear.

EHI patients 11 and 14 experienced ER featuring muscle cramps, with patient 14 also presenting with EHI, loss of consciousness, acute renal failure and myocardial hypertrophy. EHI patient 14 carried an additional *RYR1* variant (p.H3981Y), which was annotated as rare (MAF 0.0012) and pathogenic (C-score 24.5), which could account for the severe clinical phenotype. Heterozygous inheritance of *RYR1* p.H3981Y has also been previously identified in patients with centronuclear myopathy, which causes muscle weakness and wasting (Wilmshurst *et al.*, 2010). *RYR1* p.S1342G was not included in the genotyping screen as in addition to a MAF ≥1%, the *in silico* pathogenicity C-score was lower than the cut-off of 15 (C-score 9.927).

One *RYR1* variant annotated as non-polymorphic and potentially pathogenic (p.D4505H, MAF 0.0061, C-score 23.4) was identified in EHI patient 59 who displayed evidence of rhabdomyolysis, with raised serum CPK and cramps and who was subsequently classified MHN by IVCT. Therefore, this *RYR1* variant does not increase sensitivity to halothane and caffeine under IVCT conditions. The variant may however increase RyR1 sensitivity to other agonists and environmental triggers such as heat. This EHI patient only demonstrated a mild intolerance to heat during the HTT and although he reached a maximum core temperature of 39.3°C, he felt comfortable throughout the test. It is possible that the IVCT lacks sensitivity to detect mild alterations to RyR1 channel sensitivity. *RYR1* p.D4505H was also identified in 7 unrelated non-EHI MHSh/hc samples and 1 UK population sample during the Fluidigm® genotyping screen as well as 3 MHShc samples from New Zealand (Kathryn Stowell, 2017, personal communication).

The same variant was also reported in the literature in combination with a second *RYR1* variant (p.R3983C) in a child who died of a non-anaesthetic induced hypermetabolic reaction after experiencing a similar reaction 2 years earlier (Groom *et al.*, 2011). She presented clinically with MH-like and EHI-like symptoms, including a raised core temperature (42.2°C), muscle rigidity and seizures and on both occasions revealed evidence of a recent viral infection. *In vitro* classification of these two *RYR1* variants supported the negative IVCT response shown by our EHI patient. Both variants were introduced into RyR1-null mouse myotubes and displayed only a modest caffeine-induced increase in Ca^{2+} sensitivity in *trans* compared to wild-type RyR1. Each variant alone caused no significant difference in caffeine-induced Ca^{2+} release relative to wild-type. When characterising *RYR1* variants identified in EHI patients it is important to consider the use of caffeine to activate RyR1 considering the marked lack of sensitivity of the EHI cohort to caffeine exposure during IVCTs.

RYR1 S2776F was identified in 7 independent MHShc/ MHSh individuals, one of whom was an EHI patient (ID 19). Interestingly, all but one of these patients carried an additional variant in the *RYR1* gene. Four of these MH patients carried the same additional *RYR1* variant (p.T2206M), which appeared in *cis* with p.S2776F within these families. *RYR1* p.T2206M is one of the 42 functionally characterised MH mutations and has been identified in 27 independent families across the UK MH population. The original method of characterisation was completed on *ex vivo* muscle, where *RYR1* was only screened for 'hot spots', not including p.S2776F (Wehner *et al.*, 2002). More recently however, the pathogenic effect of *RYR1* p.T2206M has been shown in HEK293 cells, with increased caffeine-induced Ca^{2+} release and higher resting cytoplasmic Ca^{2+} levels (Murayama *et al.*, 2016). One of the other IVCT positive patients carrying *RYR1* S2776F, also harboured an additional *RYR1* variant, p.E3104K. The EHI patient revealed an alternative second variant in *RYR1* (p.E3583Q), which was more common and was reported at an allele frequency of 1.49% in the ExAC population. One individual classified as MHN carried *RYR1* p.S2776F, although with genotype-phenotype discordance reported in over 25% of MH families, this variant may still prove pathogenic. Without functional investigation of *RYR1* p.S2776F it is not possible to determine whether or not this variant is contributing to the positive IVCT and clinical phenotypes in these patients. The location of *RYR1* p.S2776F in the 'phosphorylation hotspot' RyR-P2 peripheral domain supports the investigation of this variant as a potential mutation contributing to EHI susceptibility. A serine residue in the same domain (ser^{2843}) is phosphorylated by protein kinase A (PKA), which releases FKBP12 activating RyR1 (Reiken *et al.*, 2003). The prevalence of *RYR1* p.S2776F was higher in the European non-Finnish population on the ExAC database (0.00112), but was still only identified in

67 out of a total of 29,899 individuals screened of European descent. This variant remains a high priority candidate for functional characterisation.

The slow progress which has been made attempting to functionally characterise *RYR1* variants has stemmed from experimental limitations due to the size of RyR1 channels (5,032 amino acids, 563.5 kilodalton (kDa) mass) (MacLennan Zorzarto *et al.*, 1989). The resulting *in vitro* experiments using *ex vivo* muscle and *in vitro* myotubes have been limited by an inability to control for genetic background. Prior to the development of NGS technologies, samples were only screened for specific MH mutations meaning that the presence of more than one variant within *RYR1* was not ruled out prior to characterisation (Wehner *et al.*, 2002). Immortalized B lymphocytes have also been used to measure altered Ca^{2+} release after exposure to RyR1 agonists (Girard *et al.*, 2001; Zullo *et al.*, 2009), although proteins in the EC coupling complex are not expressed. This means that any variants altering the interactions between RyR1 and its modulators would not be detected by the Ca^{2+} release assay and therefore this approach only has the sensitivity to detect certain *RYR1* variants. To address the issue of genetic background, *RYR1* variants were transiently or stably transfected into HEK-293 cells to measure altered Ca^{2+}-release upon activation of RyR1 (Tong *et al.*, 1997; Monnier *et al.*, 2000; Brini *et al.*, 2005). To account for the absence of EC coupling machinery in these models, attempts were made to transduce a dyspedic murine cell line with rabbit RyR1 containing several MH-associated variants (Yang *et al.*, 2003). This approach proved difficult due to the large size of the cDNA constructs. The fundamental aim remained to develop an *in vitro* system using a homogenous population of human skeletal muscle cells, without relying on the expression of large *RYR1* cDNA constructs. The development of Clustered Regularly Interspaced Short Palindromic Repeats-CRISPR associated protein 9 (CRISPR-cas9) as a gene editing approach offers the potential to generate immortal myotubes with the same genetic background harbouring specific variants within the gene of interest (Doudna and Charpentier, 2014).

Of the 13 variants annotated as rare and pathogenic across five genes associated with an exercise intolerance phenotype (*AMPD1*, *ATP2A1*, *CLCN1*, *PYGM* and *TRDN*), four were detected more than once in the EHI cohort. *CLCN1* p.R300Q and *PYGM* p.A105S were found in both MHSh and MHN classified EHI patients, but only the EHI MHSh patients revealed an additional variant in *RYR1* or *CACNA1S.* This suggests that the additional variants in either *RYR1* or *CACNA1S* are responsible for their abnormal IVCT responses, although *CLCN1* p.R300Q and *PYGM* p.A105S may still contribute to the pathogenicity of EHI. Both *CLCN1* p.R300Q and *PYGM* p.A105S were detected in MHSh/hc, MHN and UK population samples on the Fluidigm® variant screen.

A heterozygous variant identified in the *ATP2A1* gene (p.P540L) was identified in 2 MHN EHI patients (26 and 30). *ATP2A1* encodes a SERCA pump, which transports Ca^{2+} into the SR lumen allowing muscle relaxation. To date, *ATP2A1* p.P540L has not been reported in association with Brody's myopathy. This variant was located in the cytoplasmic domain of the SERCA protein at a residue, which is highly conserved across mammalian species (Figure 2.21). This residue was not conserved in the frog family; however, Ca^{2+} uptake in amphibian muscle may differ to humans. Both patients harbouring *ATP2A1* p.P540L demonstrated normal contracture responses to caffeine and halothane during their IVCT, suggesting that any potential genetic variants contributing to EHI susceptibility do not alter RyR1 sensitivity to halothane or caffeine. Neither patient revealed any additional rare variants in *RYR1* or *CACNA1S* genes and therefore a gain-of-function *ATP2A1* variant may alter RyR1 Ca^{2+} release indirectly by increasing Ca^{2+} uptake into the SR. Conversely, *ATP2A1* p.P540L could cause a loss-of-function effect, elevating cytosolic Ca^{2+} levels by limiting SR Ca^{2+} uptake. Considering neither patient experienced cramps or muscle stiffness but presented with strong acute clinical reactions, a gain-of-function effect is more likely. *ATP2A1* p.P540L was also identified in 2 non-EHI MHShc samples and 1 non-EHI MHN sample on the Fluidigm® variant screen.

```
ATP2A1_HUMAN      KEFTLEFSRDRKSMSVYCSPAKSSRAAVGNKMFVKGAPEGVIDRCNYVRVGTTRVPLTGP  540
ATP2A1_RABBIT     KEFTLEFSRDRKSMSVYCSPAKSSRAAVGNKMFVKGAPEGVIDRCNYVRVGTTRVPMTGP  540
ATP2A1_DOG        KEFTLEFSRDRKSMSVYCSPAKS-RAAVGNKMFVKGAPEGVIDRCNYVRVGTTRVPMTGP  539
ATP2A1_RHINO      KEFTLEFSRDRKSMSVYCSPAKS-RAAVGNKMFVKGAPEGVLERCNYVRVGTTRLPMTGP  539
ATP2A1_HEDGEHOG   KEFTLEFSRDRKSMSVYCSPAKSSRAAVGNKMFIKGAPEGVIDRCNYLRVGTTRVPMTGP  540
ATP2A1_BAT        KEFTLEFSRDRKSMSVYCSPAKS-RAAVGNKMFVKGAPEGVIDRCTYVRVGTTRVPMTGP  539
ATP2A1_SALMON     KEFTLEFSRDRKSMSVFCSPAKSSKAAVGNKMFVKGAPEGVIERCAYVRVGTTRVPLSEP  540
ATP2A1_DOLPHIN    KEFTLEFSRDRKSMSVYCSPAKS-RAAVGNKMFVKGAPEGVIDRCNYVRVGTTRVPMTGP  539
ATP2A1_FROG       KEFTMEFSRDRKSMSVYCTPAKASRAAVGNKMFVKGAPEGVIDRCNYVRVGTTRVPLTSA  540
                  ****:***********:*:***: :********:*******::** *:******:*::
```

Figure 2.21: Multiple sequence alignment of *ATP2A1,* highlighting a proline residue, which is altered in variant p.P540L. The proline residue substituted in variant p.P540L has been highlighted. Multiple sequence alignment was performed using Protein-BLAST v.2.8.0 (NCBI) and Clustal O v.1.2.4 (EMBL-EBI).

Both EHI patients 3 and 5, who harboured *TRDN* p.E135K, also carried a different but rare and predicted pathogenic variant in *RYR1*, which could account for their differential responses to caffeine by IVCT (MHShc/ MHSh). Despite this, *TRDN* p.E135K may still elicit a pathogenic effect in these individuals. Without family studies and functional characterisation of these variants, it is not possible to determine the contribution of each variant to EHI susceptibility. In addition to the 2 EHI patients identified with *TRDN* p.E135K, this heterozygous variant was also identified in 17 non-EHI MHSh/hc, 2 MHN and 9 UK population samples across the Fluidigm® genotyping screen. With a reported MAF of 0.0073 on the ExAC database and an expected heterozygous genotype

frequency of 0.015, the variant was observed at a slightly higher frequency than expected in EHI, MHSh/hc and UK population samples, although this variant is relatively common in the general population. In particular, it was identified in 117 European non-Finnish ExAC individuals out of a total of 4,402 who were screened (0.0134). This variant is therefore unlikely to elicit a dominant pathogenic phenotype. *TRDN* p.E135K, like pathogenic variant *TRDN* p.T59G is located in the luminal region of triadin. This variant has the potential to contribute to and modify the clinical phenotypes observed in the 2 EHI patients; however, this study lacks the power to investigate the modifying effect of genetic variants. All variants identified in *TRDN* across the EHI cohort were located within the luminal domain of triadin.

The luminal domain of triadin interacts directly with RyR1, calsequestrin and junctin forming a multi-protein complex, which regulates Ca^{2+} release from the SR (Guo and Campbell, 1995; Glover *et al.*, 2001). The triadin binding site on RyR1 has been localised to the intraluminal loop of RyR1, specifically residues Asp4878, Asp4907 and Glu4908, whereas the RyR1 binding site on triadin has been localised to the luminal domain (amino acids 200-232) (Lee *et al.*, 2004). Triadin has been shown to regulate the interaction between RyR1 and FKBP12, a complex which reduces the open probability of RyR1 (Shen *et al.*, 2007; Eltit *et al.*, 2013). A disruption of the RyR1/ FKBP12 interaction in triadin-null mice results in higher resting myplasmic Ca^{2+} levels (Eltit *et al.*, 2013). Therefore loss-of function or knock-out mutations would be expected to increase the basal activity of RyR1 causing disorders with myopathic features. Ventricular tachycardia, catecholaminergic polymorphic 5, with or without muscle weakness (CPVT5) is an autosomal recessive disorder resulting from intracellular retention and degradation of triadin. A homozygous mutation in p.T59R causes exercise and stress-induced CPVT5, characterised by tachycardia, recurrent syncope, muscle weakness and cardiac arrest (Roux-Buisson *et al.*, 2012).

Interestingly, six common *TRDN* variants were identified in the EHI cohort, two of which were present in a high proportion of EHI individuals. All variants found were present in the two isoforms of triadin expressed in human skeletal muscle, Trisk 51 and 95. *TRDN* p.L201V was identified in 52 out of 64 patients, despite having an MAF in the general population of 0.17 (ExAC). Of these, 45 EHI patients harboured this variant in the homozygous form. The presence of homozygous *TRDN* variants in the EHI cohort is consistent with other autosomal recessive myopathic conditions associated with this gene. The variant allele was observed at a significantly higher proportion in the EHI cohort compared with the ExAC population (chi-squared, 2-tailed, p=<0.0001). Interestingly, this variant is located within the RyR1 binding domain, so could alter RyR1

regulation (Lee *et al.*, 2004). A second common *TRDN* variant, p.T128S was identified in 45 EHI patients and although this variant had a MAF 0.49 (ExAC), 39 of the individuals harboured both p.L201V and p.T128S. It therefore possible that these patients are compound heterozygotes, which highlights the potential of combinations of common variants contributing to EHI susceptibility.

Five specific variants identified in this cohort of EHI patients have been previously associated with autosomal recessive disorders featuring an exercise intolerance phenotype. Two of these were nonsense variants, *PYGM* p.R50* and *AMPD1* p.Q45*. *PYGM* p.R50* was annotated as rare and deleterious and was only present in MHSh EHI patient 6, who collapsed from EHI with loss of consciousness. This patient did not carry any rare *RYR1* or *CACNA1S* variants to account for his positive contracture by IVCT. In the homozygous form this variant causes McArdle's disease, a rare condition characterised by the absence of myophosphorylase, an enzyme required to convert glycogen to glucose-1-phosphate in human skeletal muscle (Tsujino, Shanske and DiMauro, 1993). To date, 147 mutations have been reported in association with this glycogen storage disease. Of these, *PYGM* p.R50* is most frequently associated with the condition (Nogales-Gadea *et al.*, 2015). The variant either causes mRNA nonsense mediated decay or produces a truncated protein. Heterozygous nonsense mutations would likely cause a reduction in the level of functional enzyme produced. *PYGM* p.R50* was also identified in 3 MHSh samples on the Fluidigm® genotyping screen, although 9 UK population samples also carried the variant. It is possible that preferential *PYGM* allele amplification occurs in order to compensate for the mutant allele, thus restoring myophosphorylase levels.

The second nonsense variant (*AMPD1* p.Q45*) has been shown to cause the loss of adenosine monophosphate deaminase production in the homozygous form, which is required for the conversion of adenosine monophosphate (AMP) to inosine monophosphate (IMP). This process is vital for energy production in skeletal muscle cells and a deficiency causes muscle weakness and myalgia after exercise (Morisaki *et al.*, 1992). The *AMPD1* p.Q45* variant allele is common in the general population (MAF ExAC 0.0871), with a predicted heterozygous genotype frequency of 0.16. Eleven EHI patients carried this variant in the heterozygous form, which was always found in *cis* with *AMPD1* p.P77L. These variants were also observed in *cis* in the *AMPD1* deficiency population reported by (Morisaki *et al.*, 1992). Despite this, the p.P77L allele would never be expressed due to its location downstream of the p.Q45* stop codon. AMP deaminase (AMPD) deficiency is the most common skeletal muscle metabolic disorder, with a prevalence of 2% in the Caucasian population (Gross *et al.*, 2002). It has been

suggested that a deficiency in this enzyme associated with the p.Q45* mutant allele increases circulating levels of adenosine, offering protection against heart disease (Loh *et al.*, 1999; Anderson *et al.*, 2000). Adenosine has been shown to reduce the rate of ATP production, reduce neutrophil superoxide production and inhibit inflammatory cells and platelet localisation to the endothelium, which all contribute to the molecules protective capacity (Mangoni and Barrère-Lemaire, 2004). This cardioprotective effect could explain the high frequency of mutant alleles in the general population.

Two additional *AMPD1* variants identified in the EHI cohort are associated with autosomal recessive *AMPD1* deficiency, specifically *AMPD1* p.K316I and *AMPD1* p.M340I (Toyama *et al.*, 2004). These variants were detected in 4 MHN patients and 1 MHSh patient, respectively. The MHSh EHI patient carrying *AMPD1* p.M340I also carries the pathogenic *AMPD1* p.Q45* and p.P77L haplotype. It is not known whether p.M340I is in *cis* or in *trans* with p.Q45* + p.P77L. *AMPD1* p.M340I has always been reported in combination with p.Q45* + p.P77L in the literature (Toyama *et al.*, 2004). It has been suggested that *AMPD1* p.M340I acts to lower the catalytic activity of AMPD and reduce the affinity to adenosine monophspate, although this has not been functionally proven (Toyama *et al.*, 2004). EHI patient 20, who harboured these variants did not reveal any rare variants in *RYR1* or *CACNA1S* and was the only female in the EHI cohort. Although her clinical reaction was mild she failed 3 HTTs and displayed a positive contracture in response to halothane. Of the 4 MHN patients from the EHI who revealed *AMPD1* p.K316I, only 1 was found to carry the p.Q45* + p.P77L haplotype. Their clinical reactions varied, while none of the 4 had any rare variants in *RYR1* or *CACNA1S*. *AMPD1* p.M340I was included in the Fluidigm® variant screen and was detected in 6 MHSh/hc samples but was also present in 2 UK population samples. Interestingly, the 3 of the 6 patients MH susceptible patients were classified MHShc by IVCT and also harboured a familial *RYR1* variant. The evident range of diagnostic phenotypes could represent the underlying genetic complexity, with *a* combination of variants eliciting a modifying effect.

Two common variants, *CPT2* p.V368I and p.M647V were found at a high frequency in our EHI cohort, 75% and 25%, respectively. All 20 observations of p.M647V were seen in combination with p.V368I. These variants have always been found in combination with rare *CPT2* variants in cases of CPTII deficiency, but are not thought to be pathogenic alone (Yasuno *et al.*, 2008). Evidence suggests that *CPT2* p.V368I alone does not affect enzymatic activity of CPTII, instead it is thought to modify the effect of rare pathogenic variant *CPT2* p.R631C (Yasuno *et al.*, 2008). EHI patient 48, who was classified MHN, harboured a heterozygous *CPT2* variant (p.F352C), which has been

shown to cause CPT2 deficiency in the homozygous form (Isackson, Bennett and Vladutiu, 2006). This patient also harboured the common p.V368I variant and presented clinically with severe rhabdomyolysis (CK 10,000 IU/ L) resulting in renal failure in addition to EHI with collapse, loss of consciousness and seizures. A number of *CPT2* mutations including p.V368I and p.F352C have been shown to accelerate the temperature-induced inactivation of CPTII at 40°C, demonstrating a significantly lower enzyme activity compared to wild type (Yao *et al.*, 2015). It is therefore possible that exercise could alter the activity of CPTII mitochondrial enzymes in patients harbouring one or more *CPT2* variants. It is unknown whether a heterozygous *CPT2* variant is sufficient to trigger an EHI phenotype alone or whether the genetic contribution to the disorder in these patients is more complex.

The *ASPH* gene is alternatively spliced producing three distinct proteins: aspartyl beta-hydroxylase, junctin and junctate, with all three isoforms expressed in human skeletal muscle (Jones *et al.*, 1995; Feriotto *et al.*, 2005; Hong, Kwon and Kim, 2007). Junctin is expressed from a promoter known as MEF-2, which is specific to excitable tissues (Hong, Kwon and Kim, 2007). Junctin is a transmembrane protein which directly interacts with RyR1, triadin and calsequestrin, a complex which regulates calcium release from the SR (Zhang *et al.*, 1997). Three of the four very rare and potentially deleterious *ASPH* variants identified in the EHI cohort were located within the junctin transcript (NM_032467, NP_115856), specifically p.V84G, p.A85P and p.K88T. These variants were only detected once in the EHI cohort and were absent from the 1,123 MHSh/hc, MHN and UK population control samples. Interestingly, EHI patient 31 harboured both *ASPH* p.V84G and p.K85P in *cis* along with a frame-shift insertion (*ASPH* c. c.252_253insTTCTGGGA). Due to the location of the frame-shift insertion in the same codon as *ASPH* p.V84G, the junctin transcript is expected to be out-of-frame from residue 84, unless a new down-stream initiation codon is present, which would create a shorter transcript. Regardless, these variants are likely to significantly alter the function of the mutant junctin protein. The patient was a fit and healthy individual (VO_2 max 61 $mL.min^{-1}.kg^{-1}$) who collapsed during a military exercise and was unconscious for 30mins, recording a rectal temperature of 42°C. EHI patient 46, who carried *ASPH* p.K88T experienced a similar EHI episode, with loss of consciousness during a military exercise. All genetic variants identified in *ASPH* were located in the SR luminal tail of junctin, which interacts with the RyR1 EC coupling complex (Jones *et al.*, 1995).

Both junctin knock-out mice and the ablation of junctin in cardiomyocytes have demonstrated increased Ca^{2+} release from the SR (Yuan *et al.*, 2007; Boncompagni *et al.*, 2012), suggesting that loss-of-function mutations in *ASPH* could enhance RyR2 Ca^{2+}

release reaching a pathological threshold during exertion. Due to the extensive alternative splicing of ASPH, p.V84G, p.A85P and p.K88T are only expressed in the junctin isoforms of the gene. The fourth *ASPH* variant, p.R397C is located within the C-terminal Aspartyl ß-hydroxylase catalytic domain only expressed in the longest isoform, known as ASPH. This isoform is expressed in a wide variety of tissues, functioning as a post-translational modification hydroxylase, but the specific function in skeletal muscle remains unclear (Gronke *et al.*, 1990; Hong, Kwon and Kim, 2007).

Two variants were detected in the *TRMP6* gene, which encodes an Mg^{2+} channel essential for Mg^{2+} homeostasis (Schlingmann *et al.*, 2007). Mg^{2+} negatively regulates RyR1 in human skeletal muscle by competing with Ca^{2+} binding to both the activation and inhibition sites of RyR1 channels (Steele and Duke, 2007). Loss-of-function mutations in *TRPM6* cause autosomal recessive hypomagnesemia and hypocalcaemia, a neonatal condition characterised by muscle spasms and seizures (Walder *et al.*, 2002). Two heterozygous *TRMP6* variants (p.G166R and p.M1088R) were identified in 2 different EHI patients, both of which were annotated as rare and pathogenic. EHI patient 59, who carried *TRPM6* p.G166R, demonstrated a negative IVCT response and presented with faintness and cramps and collapse with a 40°C core temperature during a 10 mile military march. This variant was observed in 12 unrelated samples across the 1,123 MHSh/hc, MHN and UK population control samples. In contrast, EHI patient 2, who carried novel variant *TRPM6* p.M1088R, demonstrated a positive contracture in response to both caffeine and halothane. They also presented with faintness and collapse but also experienced loss of consciousness and a core temperature measuring 41°C. *TRPM6* p.M1088R was not detected across the 1,123 screened MHS, MHN and UK population samples and was not reported on the ExAC database. It is unknown whether the pathogenic phenotype associated with homozygous *TRPM6* variants is detectable in the heterozygous state, although it is possible that a slight reduction in SR Mg^{2+} levels could disrupt RyR1 regulation sufficiently to trigger EHI.

Heterozygous mutations in the *HSPB1* gene cause distal hereditary motor neuropathy type 2B (Evgrafov *et al.*, 2004). This autosomal dominant condition is characterised by muscle weakness and progressive muscular atrophy due to a disruption of neuronal cell function (Irobi *et al.*, 2004). *HSPB1* encodes a 27 kDa heat shock protein, which contains a highly conserved Hsp20–α-crystallin domain. EHI patient 60 harboured a variant within the same domain, *HSPB1* p.T151S. Interestingly, an alternative allele has been previously reported in association with distal hereditary motor neuropathy type 2B, specifically *HSPB1* p.T151I (Evgrafov *et al.*, 2004). The EHI patient in this study did not

display evidence of atrophy however felt very weak during the 3 reported EHI episodes. It is important to note that the onset of this motor neuropathy is usually aged 15-25 and the EHI patient was 21 years old when EHI occurred and may be displaying the first signs of the condition. *HSPB1* p.T151S is extremely rare and was not reported in the ExAC database and was not detected in the 1,123 MHSh/hc, MHN or UK population samples screened by Fluidigm® genotyping.

Three variants were identified in the *ACADVL* gene (p.V207A, p.H259Q, p.G447R), which encodes the mitochondrial enzyme, VLCAD. This enzyme is required for fatty acid metabolism (Oliveira *et al.*, 2013). Interestingly, 3 of the 4 EHI patients harbouring heterozygous *ACADVL* variants displayed evidence of rhabdomyolysis, cramps and high CPK levels (10,000- 11,000 IU/L). Two of the variants (p.V207A, p.H259Q) were included in the Fluidigm® variant screen and were only identified in the MHSh/hc sample population and absent from the MHN and UK population samples. Non-synonymous variants, which may allow residual enzyme activity were associated with the milder form, whereas the severe neonatal form was caused by a complete absence of functional enzyme (Andresen *et al.*, 1999). Homozygous variant *ACADV*L p.V207A has been previously associated with VLCAD deficiency in a number of unrelated families, with functional characterisation demonstrating a reduction of enzyme activity relative to the controls (Andresen *et al.*, 1996, 1999). Both EHI patients 7 and 17, who harboured this variant in the heterozygous form displayed evidence of rhabdomyolysis with high CPK levels (11,000 and 27,000 IU/L, respectively), with patient 17 experiencing prolonged fatigue for months after the initial EHI episode. Both patients produced positive contractures in response to halothane during their IVCT, although they each carried a non-polymorphic heterozygous *RYR1* variant (p.R3539H and p.E3583Q), which could potentially account for their abnormal IVCT reaction.

Two variants were identified in the *CASQ1* gene, p.D44N and p.F186Y. *CASQ1* encodes calsequestrin (CASQ1), an SR Ca^{2+} binding protein, which forms part of the RyR1 multi-protein complex regulating Ca^{2+} release from the SR (Protasi, Paolini and Dainese, 2009; Tomasi *et al.*, 2012). Interestingly, *CASQ1* p.D44N has been shown to cause an autosomal dominant condition known as tubular aggregate myopathy, which is characterised by muscle weakness, cramps, myalgia and the presence of CASQ1 aggregates in skeletal muscle (Barone *et al.*, 2017). EHI patient 26, who harboured this variant collapsed and complained of myalgia and dizziness. *CASQ1* p.D44N was also identified in three MH susceptible patients from the UK MH cohort. Unlike EHI patient 26, these individuals demonstrated abnormal contracture responses by IVCT. All three

MH susceptible individuals harboured a familial *RYR1* variant, in contrast to the MHN EHI patient, who did not carry any variants in *RYR1* or *CACNA1S* annotated as rare or potentially deleterious. It is therefore possible that *CASQ1* p.D44N alone triggers an EHI phenotype and in combination with an *RYR1* variant modifies the MH phenotype. Dizziness was also a prominent feature during the EHI episode of patient 44 who carried *CASQ1* p.F186Y, and although this variant has not been previously implicated in a disease, the variant is extremely rare and was only reported once on the ExAC database. Neither of the variants were identified in MHN or UK population samples in the Fluidigm® variant screen. Mutant and defective CASQ1 proteins could alter RyR1 regulation, resulting in elevated Ca^{2+} release from the SR, which would explain the clinical features of EHI in this patient. Other heterozygous mutations in *CASQ1*, specifically p.D244G and p.M87T, have been shown to cause vacuolar myopathy with CASQ1 aggregates, characterised by muscle fatigue, cramps and serum high CPK levels (Rossi *et al.*, 2014; Di Blasi *et al.*, 2015). The p.D244G variant elicits a stronger effect due to its location within a high-affinity Ca^{2+} binding site (Sanchez *et al.*, 2012). Interestingly, CASQ1-null mice demonstrate lethal heat and anaesthetic-induced hypermetabolic reactions (Dainese *et al.*, 2009).

Six rare and potentially deleterious variants were identified in the *SCN4A* gene, which encodes the α-subunit of a voltage-sensitive Na^+ channel type 4 ($Na_v1.4$). $Na_v1.4$ is responsible for generation of action potentials in human skeletal muscle, a vital step in the initiation of EC coupling. Mutations distributed across this gene have been associated with a number of rare autosomal dominant Na^+ channelopathies, which all delay the inactivation of the channel resulting in Na^+ influx and K^+ efflux from muscle cells, causing periodic myotonia and/ or paralysis (Matthews *et al.*, 2009; Yoshinaga *et al.*, 2012; Ørstavik *et al.*, 2015). This could delay the recovery of membrane potential and therefore delay the re-activation of $Ca_v1.1$. Increased Na^+ influx could trigger the Na^+/Ca^{2+} exchanger (NCX) to restore the membrane potential by expelling Na^+ from the cell in exchange for Ca^{2+} influx.

The 6 *SCN4A* variants detected in the EHI cohort (p.T323M, p.N591K, p.V730M, p.V999M. p.D1435H and p.R1745C) have not been previously reported in association with a channelopathy. Despite this, studies on rat $Na_v1.4$ demonstrated that aspartate residue 1435 (1428 $rNa_v1.4$) is located within an inactivation site of the channel and binds to Scorpion α-toxin Lqh-3, which slows down channel inactivation (Leipold *et al.*, 2004). Mutation of the aspartate residue to glutamate abolishes the interaction with the α-toxin, highlighting the sites importance in the inactivation of $Na_v1.4$ (Leipold *et al.*, 2004). The substitution of a negatively charged aspartate with a positively charged

histidine within this inactivation site is likely to modify the channels kinetics, thus altering Ca^{2+} homeostasis in human skeletal muscle.

The remaining variants were located in a number of regions across $Na_v1.4$, including cytoplasmic, transmembrane and extracellular loop domains. The EHI patients carrying these variants displayed a range of responses, both clinically and during their IVCTs. *SCN4A* p.N591K and p.R1745C were very rare and not detected across the 1,123 samples included on the Fluidigm® variant screen and *SCN4A* p.D1435H was observed in 1 MHSh sample. All variants identified in this gene except p.T323M were annotated as very rare (MAF ExAC ≤0.1%) making this an interesting gene to explore further through the functional characterisation of these $Na_v1.4$ variants.

Four variants annotated as non-polymorphic and pathogenic were uncovered in the *SLC8A3* gene, which encodes a Na^+/Ca^{2+} exchanger, vital for maintaining Ca^{2+} homeostasis across the sarcolemmal membrane. No diseases of skeletal muscle have been associated with the gene to date: however, disruption of Na^+/Ca^{2+} exchanger kinetics could result in high levels of intracellular Ca^{2+}, which would explain the EHI phenotype. Two of the variants, *SLC8A3* p. R355L and p.R314G, were identified in MHSh/hc, MHN and UK population samples across the Fluidigm® variant screen, whereas *SLC8A3* p.V152M was only identified in 1 MHShc sample and 2 MHSh samples. The fourth variant, *SLC8A3* p.P402S was not observed in any of the 1,123 samples screened. *SLC8A3* p.V152M was located in the helical domain of the protein, with the remaining 3 variants located in the cytoplasmic region.

Two heterozygous non-synonymous variants were detected in *STIM1*, which encodes a Ca^{2+} sensing protein located in the SR membrane. STIM1 interacts with ORAI1, a Ca^{2+} release activated Ca^{2+} (CRAC) channel, which triggers extracellular Ca^{2+} influx when SR Ca^{2+} stores are depleted. Gain-of-function mutations in *STIM1* cause tubular aggregate myopathy, a rare condition characterised by myalgia, cramping, weakness and exercise-induced muscle fatigue (Böhm *et al.*, 2013; Hedberg *et al.*, 2014; Endo *et al.*, 2015). Tubular aggregate myopathy has been reported as a both autosomal dominant and recessive condition (Jain *et al.*, 2008); however, neither of the heterozygous variants identified in the EHI patients have been implicated to date. Both variants were annotated as very rare according to the ExAC database. Both EHI patients harbouring either *STIM1* p.T504M or p.S613Y, displayed positive contractures by IVCT but they also both carried an *RYR1* variant annotated as rare and pathogenic. *STIM1* p.T504M was only detected in 1 MHShc sample on the Fluidigm® variant screen. This

STIM1 variant in combination with an *RYR1* variant could lower the threshold for both RyR1 Ca^{2+} release and extracellular Ca^{2+} entry (SOCE) during exercise, triggering a hypermetabolic phenotype.

To date, only eleven family members of 3 unrelated EHI patients have been referred to the Leeds MH Investigation Unit. The lack of relatives of EHI patients limits the follow-up of potentially pathogenic variants through co-segregation studies. Only family members of patients who display positive contractures by IVCT are offered an IVCT and only a limited number of these opt to undergo a muscle biopsy to receive an IVCT diagnosis. This has restricted the potential of EHI family studies and interpretation of variants identified in the EHI cohort. EHI co-segregation studies are also reliant on the use of IVCT data as a surrogate phenotype due to the lack of a gold-standard diagnostic test for EHI susceptibility. Interestingly, for 2 of the EHI families tested, both parents demonstrated a positive IVCT response. This was unexpected as EHI susceptibility is thought to be relatively rare. A positive contracture response in both parents suggests that the underlying muscle defect predisposing individuals to EHI, may be more common than previously thought. This also presents the possibility that in some cases EHI arises from a combination of genetic risk factors inherited from both parents. IVCT positive EHI patients are likely to represent a subtype of EHI, that is phenotypically and genetically distinct from EHI in IVCT negative patients.

The rare and potentially pathogenic *RYR1* variant identified in EHI family 1 (p.R3539H) did not fully segregate with IVCT classification, with an IVCT positive sibling not carrying the variant. This discordant sibling did not reveal any other variants in the coding region of *RYR1* or *CACANA1S* during a routine diagnostic genetic screen performed by the Leeds Genetics Laboratory NHS service. It is therefore likely that the genetic predisposition to EHI is more complex in this family, with either the presence of an alternative variant or multiple variants contributing to the IVCT phenotype. Unfortunately, both genetic and phenotypic data are missing for both parents in this family, so it is not possible to determine the inheritance pattern of variants with only one generation characterised. Although the variant co-segregated with MH susceptible classification in one of the families from the UK MH cohort, four of the families harboured an alternative familial *RYR1* variant. Historically, family members have only been screened for the familial variant, therefore *RYR1* p.R3539H genotypes were not available for family members of these four MH susceptible individuals. This highlights an issue with the routine genetic investigation of MH, which has led to missing genetic data. Genotypic and phenotypic data are also often missing in MH families because if the first parent tested is classified MH susceptible then the second parent is not investigated as MH is

a rare condition. The presence of more than one *RYR1* variant within several MH families suggests genetic complexity, which may explain phenotypic variation.

Both EHI family 2 and 3 are consistent with an autosomal dominant mode of inheritance with a rare and potentially deleterious heterozygous variants co-segregating with positive IVCT phenotypes. Both parents in these families displayed abnormal responses to halothane during an IVCT, but rare and potentially pathogenic variants were not detected in the 50 candidate genes in either mother of either EHI family. The non-synonymous variant identified in third family was located in the *SCN4A* gene, which encodes a Na^+ channel in skeletal muscle. Interestingly, non-synonymous mutations in this *SCN4A* cause several related autosomal dominant conditions, which alter the channel kinetics of $Na_v1.4$ (Matthews *et al.*, 2009; Corrochano *et al.*, 2014). *SCN4A* p.V730M was identified in 1 MHShc, 1 MHSh and 1 UK population sample in addition to the 1 MHSh EHI patient. This EHI patient did not harbour any variants in *RYR1* or *CACNA1S*, which could account for the abnormal contracture response. This gene represents an interesting candidate for EHI susceptibility due to its central role in regulating Ca^{2+} release in human skeletal muscle.

Investigation of the genetic contribution to EHI susceptibility has not only been limited by a lack of genetically and phenotypically characterised family members but also by the practical limitations of functionally characterising genetic variants. The functional characterisation of variants causing MH has largely focussed on *RYR1* as the major gene contributing to MH in 75.8% of cases. As discussed, the size of the gene and protein has complicated attempts to clone, manipulate and fully elucidate the structure of this Ca^{2+} channel. The development of CRISPR-cas9 gene editing in combination with immortalised myoblast cell lines created by the Leeds MH Investigation Unit will overcome previous limitations and advance understanding of MH genetics. The disadvantage of previous functional studies utilising primary myoblasts and B lymphocytes is the presence of different genetic backgrounds between patient samples. Other studies which have used HEK-293 cells have required RyR1 to be cloned and transfected into the cell line, which has been problematic due to the size of RyR1, and also lacks the other regulatory proteins of the RyR1 complex. With over 200 genetic variants reported to date, functional characterisation needs to be time efficient and cost effective to fully explain the genetic heterogeneity of MH susceptibility. The functional investigation of genetic variants associated with EHI susceptibility will be dependent on the genes implicated, but studies are likely to advance fundamental understanding of skeletal muscle biology.

With 24 patients in the EHI cohort carrying one or more uncharacterised *RYR1* variants and 22 displaying positive contractures during an IVCT, there is significant crossover with the phenotypic and genetic diagnosis of MH. Interpretation of these data are limited by a poor understanding of the mechanistic action of caffeine and halothane, the indirect effect of variants in other genes on RyR1 sensitivity to agonists and the effect of heat on RyR1. This is of particular importance as only 4 EHI patients were sensitive to the effects of caffeine, but it is not clear why this is the case. Caffeine has been shown to have specific binding sites within the interfaces of the C-terminal domain of RyR1 and other channels (des Georges *et al.*, 2016). Variants conferring susceptibility to EHI may not alter RyR1's sensitivity to caffeine. With 41 EHI patients responding normally to both caffeine and halothane it is clear that the IVCT is not an appropriate phenotypic surrogate for EHI susceptibility and that family segregation studies using IVCT data should be interpreted with caution. As none of the EHI cohort have experienced a hyper-metabolic episode on exposure to inhalational anaesthetics it is not known whether they are genetically predisposed to MH and EHI or EHI alone.

The variants identified in this study suggest that EHI is a genetically and clinically heterogeneous condition. Due to the diverse phenotypic features of EHI it is possible that a combination of variants within each individual contribute to the development of this potentially fatal condition. This is supported by the presence of several rare and potentially deleterious variants within EHI patients in genes relating to calcium homeostasis and energy metabolism. Eleven heterozygous non-synonymous variants annotated as rare and pathogenic were identified more than once across the EHI cohort, again suggesting that the genetics of EHI is complex and is not a single gene disorder. This study also highlighted ten genes with more than one rare and potentially deleterious variant, five of which encoded structural proteins involved in Ca^{2+} homeostasis in human skeletal muscle. These included Ca^{2+} channels (RyR1, $Ca_v1.1$ and SERCA1), a Na^+ channel ($Na_v1.4$) and a Na^+/Ca^{2+} exchanger (NXC3). A mutation in any of these ion channels expressed in skeletal muscle has the potential to dysregulate EC coupling and trigger EHI. This could be directly related to increased muscle contraction, increased core temperature or a combination of both. In contrast, several genes of the genes identified encoded enzymes required for energy metabolism, such as VLCAD, AMPD1 and PYGM. A deleterious mutation could alter circulating levels of these proteins or their enzymatic activity, resulting in exercise intolerance and in some cases EHI. Ultimately, the functional characterisation of the genetic variants identified in this cohort will confirm their role in EHI susceptibility.

3 Metabolic and transcriptional response of RyR1 mutant and wild-type mice to acute heat stress

3.1 Introduction

A clinical case study of a child who experienced MH under anaesthesia followed by a fatal EHI reaction was retrospectively associated with a familial *RYR1* mutation, p.R163C (Tobin *et al.*, 2001). A viable heterozygous RyR1 R163C knock-in mouse model was subsequently created, with homozygous mice displaying a lethal embryonic phenotype (Yang *et al.*, 2006). Heterozygous RyR1 R163C mice display fatal hypermetabolic episodes on exposure to both anaesthetics and heat, specifically 1.25-1.75% halothane and a 15-minute exposure to 42˚C ambient temperature (T_a) (Yang *et al.*, 2006). Clinical features include a rise in rectal temperature, respiratory rate, metabolic acidosis and death followed by hyper acute rigor mortis. Mutant RyR1 R163C myotubes cultured from *ex vivo* muscle demonstrate significantly elevated resting myoplasmic Ca^{2+} levels compared with wild-type myotubes, reduced RyR1 inhibition by Mg^{2+} and increased Ca^{2+} transient amplitudes (Yang *et al.*, 2006; Feng *et al.*, 2011). Mutant RyR1 R163C channels loaded onto artificial bilayers also demonstrate increased myoplasmic Ca^{2+} at rest, along with increased open probability (Feng *et al.*, 2011). The increased basal Ca^{2+} levels observed in the skeletal muscle of mutant mice has been shown to trigger mitochondrial dysfunction (Giulivi *et al.*, 2011). Features include accumulation of Ca^{2+} in the mitochondrial matrix, increased ROS production and mitochondrial uncoupling resulting in reduced oxidative phosphorylation and glycolysis capacity. The RyR1 R163C mutation has been shown to induce conformational changes in RyR1, which delay the inactivation of the voltage-sensor in $Ca_v1.1$, therefore increasing RyR1 Ca2+ release from the SR (Estève *et al.*, 2010).

Heat and exercise have both been shown to upregulate Ca^{2+} cycling and energy metabolism. Exercise increases metabolic rate and is further accentuated in warm climates (McLellan, Jacobs and Bain, 1993; Krustrup *et al.*, 2003). Deficiencies of Ca^{2+} related and energy metabolism genes expressed in skeletal muscle have previously been associated with conditions characterised by an exercise intolerance phenotype (Pusch, 2002; Roux-Buisson *et al.*, 2012; Guglielmi *et al.*, 2013; Ørstavik *et al.*, 2015). Therefore, the expression of genes related to both Ca^{2+} and energy metabolism may be altered in the heat stress response. Over-expression of both junctin (*ASPH*) and calsequestrin (*CASQ1*) increase sarcoplasmic reticulum (SR) Ca^{2+} storage capacity and the interaction between RyR1 and $Ca_v1.1$, increasing RyR1 Ca^{2+} release (Zhang *et al.*,

2001; Divet *et al.*, 2007; Tomasi *et al.*, 2012). This highlights the importance of maintaining balanced expression of these regulatory proteins. Metabolic deficiencies of glycogen phosphorylase (*PYGM*), adenosine monophosphate deaminase (*AMPD1*) and glycogen synthase (*GYS1*) limit energy availability in skeletal muscle triggering an exercise intolerance phenotype featuring muscle weakness and pain (Nogales-Gadea *et al.*, 2008; Wang *et al.*, 2008; Cameron *et al.*, 2009). The expression of these enzymes could therefore be dysregulated during the heat stress response.

Hyperthermia has been shown to activate an anti-inflammatory cytokine response distinct from the classic innate response in the skeletal muscle of wild-type mice (Welc *et al.*, 2012, 2013). Specfically, mice were subject to acute heat stress (T_a 39.5˚C) until their core temperature (T_c) rose to 42˚C, after which they recovered at room temperature. The heat stress response in soleus muscle was characterised by a rapid rise in levels of interleukin-6 (IL-6), interleukin-10 (IL-10), toll-like receptor 4 (TLR-4) and transient suppression of tumour necrosis factor-α (TNF-α), followed by a second response after 24-hours recovery. In addition, c-Jun and c-Fos, which form the transcription factor AP-1, were both upregulated. AP-1 has been shown to regulate several cellular processes in response to oxidative stress in skeletal muscle (Zhou, Johnson and Rando, 2001). Heat shock protein 70 (*Hspa1a*) was also transiently elevated in skeletal muscle. Interestingly, heat stroke has been shown to elicit a protective hypothermic response during the initial recovery period in wild-type mice, followed by mild hyperthermia in the subsequent 24-hours (Leon, DuBose and Mason, 2004; Leon *et al.*, 2010). In contrast, high levels of pro-inflammatory cytokines (TNF-α, IL-6) and chemokines (IL-8) were detected in a patient who had presented with exertional heat stroke, rhabdomyolysis and multi-organ failure (Broessner *et al.*, 2005).

In addition to heat, exercise has been shown to trigger the release of IL-6 from human skeletal muscle. IL-6 acts as an anti-inflammatory myokine when it binds to membrane-bound IL-6 receptors (rather than soluble IL-6 receptors) in the absence of TNF-α (Scheller *et al.*, 2011; Muñoz-Cánoves *et al.*, 2013). This exercise-induced IL-6 response has been attributed to increased Ca^{2+} release via activated RyR1 channels and glycogen depletion (Keller *et al.*, 2001; Treves *et al.*, 2011). Human myotubes harbouring functionally characterised *RYR1* variants have been shown to release significantly higher levels of IL-6 compared to wild-type myotubes, particularly *RYR1* variants associated with CCD, such as p.I4898T and p.R4893W (Ducreux *et al.*, 2004). Chronically elevated levels of IL-6 in skeletal muscle are thought to promote muscle atrophy, a prominent feature of CCD. In contrast, IL-6 can stimulate muscle growth after acute exposure post-exercise (Haddad *et al.*, 2005).

Both heat and exercise-induced stress have been shown to activate a heat stress protein (HSP) response to protect against cellular damage and restore homeostasis (Kregel and Moseley, 1996; McMillan *et al.*, 1998). HSPs are a diverse group of molecular chaperones maintaining protein and cytoskeletal stability under conditions of cellular stress, offering a protective response fundamental to thermotolerance and cellular survival (Haslbeck *et al.*, 2005). Although the mechanisms which activate HSPs are yet to be fully elucidated, oxidative stress is thought to act as a potent stimulator of HSPs in skeletal muscle (Khassaf *et al.*, 2001; Dimauro, Mercatelli and Caporossi, 2016). Regulatory elements located within the promoters of HSP genes are bound by redox-sensitive transcription factors, such as c-Jun (Fittipaldi *et al.*, 2015). Consistent with these data, both HSP70 and c-Jun were shown to be upregulated in mouse skeletal muscle post-acute heat stress (Welc *et al.*, 2013). Other exercise-induced HSPs include HSP27 (*HSPB3*), HSP60 (*HSPD1*), and HSP90 (*HSP90AA1*), all of which are regulated by the master transcription factor, heat shock factor 1 (HSF1) (Inouye *et al.*, 2007; Morton *et al.*, 2009; Périard *et al.*, 2012; Welc *et al.*, 2013). TLR-4 is thought to be critical to long-term survival after exposure to environmental heat stress and can be directly activated by HSPs and was also shown to be upregulated in response to heat stroke in wild-type mice (Dehbi *et al.*, 2012; Welc *et al.*, 2013).

This chapter aims to explore the transcriptional response to acute heat stress in RyR1 R163C mutant and wild-type mice to advance current understanding of the mechanisms underlying heat illness. Based on the literature, the expression of a panel of candidate genes will be quantified to help refine the whole-transcriptome experimental design. The objective is to identify the appropriate time points and muscle type for RNA-seq. The candidate genes chosen include five genes relating to Ca^{2+} homeostasis and energy metabolism, five immune-response genes and five genes encoding exercise-induced heat shock proteins (Table 3.1). Three genes reported to be stably expressed in mouse skeletal muscle were chosen as internal reference genes (Thomas *et al.*, 2014). This study will then explore global gene expression profiles characteristic of the heat stress response, to identify differentially expressed genes between wild-type and heterozygous RyR1 R163C mutant mice over a 24-hour recovery period.

Table 3.1: Candidate genes selected for TaqMan® real-time PCR.

Gene	Function	Reference
ASPH (Aspartate beta-hydroxylase)	Regulates Ca^{2+} release from the SR forms complexes with Casq1 and RyR1.	(Zhang *et al.*, 2001; Divet *et al.*, 2007)
CASQ1 (Calsequestrin 1)	Ca^{2+}-binding protein acting as an internal calcium store in muscles.	(Tomasi *et al.*, 2012; Rossi *et al.*, 2014)
PYGM (Phosphorylse, glycogen, muscle)	Breaks down glycogen into glucose-1-phosphate.	(Nogales-Gadea *et al.*, 2008)
AMPD1 (Adenosine Monophosphate Deaminase 1)	Catalizes conversion of AMP to IMP in skeletal muscle.	(Norman, Sabina and Jansson, 2001; Wang *et al.*, 2008)
GYS1 (Glycogen synthase 1)	Converts glucose to glycogen for storage.	(McCue *et al.*, 2008)
IL6 (Interleukin 6)	Anti-inflammatory myokine in response to heat stress.	(Welc *et al.*, 2012, 2013)
IL8 (Interleukin 8)	Exercise-induced anti-inflammatory myokine.	(Lu *et al.*, 2004; Broessner *et al.*, 2005)
IL10 (Interleukin 10)	Heat-induced cytokine.	(Welc *et al.*, 2013)
IL15 (Interleukin 15)	Exercised-induced myokine.	(Ducreux *et al.*, 2004)
TLR4 (Toll-like receptor 4)	Up-regulation of TLR-4 in response to heat stroke.	(Welc *et al.*, 2013)
HSPA1A (HSP70)	Exercised-induced heat shock protein.	(Morton *et al.*, 2006; Welc *et al.*, 2013)
HSPD1 (HSP60)	Exercised-induced heat shock protein.	(Morton *et al.*, 2006; Welc *et al.*, 2013)
HSPB3 (HSP27)	Exercised-induced heat shock protein.	(Thompson *et al.*, 2003; Périard *et al.*, 2012)
HSP90AA1 (HSP90)	Exercised-induced heat shock protein.	(Goto *et al.*, 2003; Morton *et al.*, 2009)
HSF1 (Heat shock factor 1)	Promotes expression of HSPs and regulates IL-6 via IL-6 promoter.	(Inouye *et al.*, 2007)
Aldoa (aldolase A)	Reference gene in mouse skeletal muscle.	(Thomas *et al.*, 2014)
Rpl27 (ribosomal protein 27)	Reference gene in mouse skeletal muscle.	(Thomas *et al.*, 2014)
Rer1 (retention in endoplasmic reticulum 1)	Reference gene in mouse skeletal muscle.	(Thomas *et al.*, 2014)

3.2 Materials and methods

3.2.1 *In vivo* experimental design

The *in vivo* acute heat stress metabolic study was completed at the Mouse Metabolic Phenotyping Center (MMPC) at the University of California, Davis. The study was completed in collaboration with Professor Paul Allen and Professor Jon Ramsey at UC, Davis. Eighteen RyR1$^{R163C/wt}$ mutant and eighteen RyR1$^{wt/wt}$ wild-type N4.C57BL/6//129Sv mice were exposed to incremental changes in temperature within Oxymax- Comprehensive Lab Animal Monitoring System (CLAMS) indirect calorimetry chambers (Columbus Instruments) (Table 3.2). Four RyR1$^{R163C/wt}$ and four RyR1$^{wt/wt}$ additional mice were selected for use as untreated baseline controls. All mice used in this study were male, 4-6 months old and selected from the same colony.

Table 3.2: RyR1 mutant and wild-type mice included in the *in vivo* acute heat stress response study. Mice were either heterozygous for the p.R163C allele (R163C/wt) or wild-type (wt/wt).

Genotype	Untreated	0 hrs recovery	1 hr recovery	24 hrs recovery
RyR1$^{R163C/wt}$	4	6	6	5
RyR1$^{wt/wt}$	4	6	6	7
Total	8	12	12	12

RyR1 mutant and wild-type mice were placed into individual Oxymax/ Comprehensive Lab Animal Monitoring System (CLAMS) cages 24-hours prior to experimentation at room temperature to adjust to their environment prior to the test. Pairs of mice in individual cages were placed in an Oxymax-CLAMS open-circuit calorimetry chamber, which measures energy expenditure, while monitoring body mass, activity levels, feeding and drinking. The rate of energy expenditure is expressed as heat (kcal/hr) and is calculated using oxygen consumption (VO_2) and carbon dioxide production (VCO_2) values:

$$Respiratory\ exchange\ ratio\ (RER) = \frac{VCO_2}{VO_2}$$

$$Calorific\ value\ (CV) = 3.815 + 1.232 * RER$$

$$Heat = CV * VO_2$$

Eighteen pairs of RyR1 mutant/ wild-type mice were acclimatised for 1 hour at 30°C, while basal metabolic rates (BMR) were determined. The chamber temperature was ramped to 33°C for ~30 minutes and increased to 34°C until the BMR of RyR1 mutant mice rapidly increased, corresponding to distinct behavioural patterns. Due to the heat-sensitive phenotype of RyR1$^{R163C/wt}$ mutant mice, the duration of heat exposure for each genotype pair was dependent on the metabolic and behavioural responses of the mutant mouse. Specifically, their VO_2 traces (recorded in 6-minute intervals) were monitored for spikes, which deviated from VO_2 observed in the wild-type mice. Their behaviour was also monitored for signs of heat stress, including disorientation, arching of the back and rearing up to the corner of the cage. This aimed to ensure that all mutant mice were sufficiently heat stressed before recovery at room temperature, while avoiding any of the mice developing an irreversible hyper-metabolic episode.

Six pairs of mice were killed immediately (0 hours), six pairs after 1-hour recovery (1 hour) and six pairs after a 24-hour recovery (24 hours) at room temperature. Four pairs of untreated mice were killed after being housed at room temperature (baseline). Mice were killed by CO_2 asphyxiation to avoid pooling of blood caused by cervical dislocation, thus allowing blood collection in sufficient volumes.

Soleus and extensor digitorum longus (EDL) muscles were dissected from each leg and preserved in cryogenic vials containing 1 mL RNA*later*® Stabilisation Solution (Invitrogen™). Preserved muscles were stored at 4°C overnight and transferred to -80°C for long-term storage prior to expression studies. Whole gastrocnemius and quadriceps muscles were dissected from each leg, snap frozen and stored in LN_2 in case of future protein work. Blood samples were also collected and stored for any future studies. Approximately 2.5 mL of whole blood was collected in EDTA tubes via cardiac puncture. White blood cells (WBCs) were then isolated by centrifugation at 1,500 x *g* for 15 minutes, after which the buffy coat containing the WBCs was transferred to a cryogenic vial containing 200 µl RNA*later*® and stored at -80°C. The plasma fraction was snap frozen and stored in LN_2. Preserved samples were transferred to Leeds in a LN_2 dry shipper and stored either at -80°C or in LN_2 tanks.

3.2.2 RNA extraction

RNA*later*® preserved muscle tissues (soleus or EDL) were placed in 1 mL TRIzol® Reagent (Invitrogen™), homogenised and left to lyse for 5 minutes at room temperature. 200 µl chloroform was added and mixed thoroughly to produce a homogenous solution.

Samples were centrifuged at 13,000 rpm (15,700 x *g*) for 10 minutes at 4°C to separate samples into an aqueous and organic phase. The aqueous phase containing RNA was transferred to a 1.5 mL tube and isopropanol was added at a 1:1 ratio and stored overnight at -80°C to precipitate the RNA. Samples were thawed and spun for 30 minutes at 13,000 rpm (15,700 x *g*) at 4°C to pellet the RNA. Isopropanol was removed and the pellet was washed twice in 500 µl 75% cold ethanol, spun for 10 minutes at 13,000 rpm (15,700 x *g*) at 4°C. The supernatant was removed and the RNA pellet was air dried and resuspended in 100 µl RNase free water (Ambion®).

3.2.3 RNA purification and quantification

RNA was purified and concentrated with the RNeasy® Micro Kit (Qiagen) according to the manufacturer's instructions. Briefly, RNA samples were diluted with lysis buffer and ethanol and added to RNeasy® MinElute™ spin columns. RNA molecules longer than 200 nucleotides are selectively bound to the silica-gel membranes of the MinElute™ columns. Contaminants were removed with wash buffers and ethanol prior to elution in RNA-free water. Purified RNA samples were quantified and quality checked using Agilent's RNA ScreenTape assay and 2200 TapeStation instrument (Agilent technologies, Santa Clara, CA, USA) according to the manufacturer's instructions. RNA integrity numbers (RIN) equivalent to Agilent's Bioanalyzer 2100 system (RIN^e) were calculated by the TapeStation software as a measure of RNA quality.

3.2.4 Reverse transcription

Reverse transcription was performed to synthesise single-stranded complimentary DNA (cDNA) for downstream applications. The High Capacity cDNA Reverse Transcription Kit (Applied Biosystems™, Foster City, CA) was used according to manufacturer's instructions. In brief, 200 ng total RNA was added to a reaction containing 1X RT buffer, 1X dNTP mix, 1X RT random primers, 2.5 U/µl MultiScribe™ Reverse Transcriptase, 1.0 U/µl RNase Inhibitor and nuclease-free water. Tubes containing the 20 µl cDNA reverse transcription reactions were placed into a thermal cycler for 10 minutes at 25˚C, 120 minutes at 37˚C and 5 minutes at 85˚C. The synthesised cDNA products were diluted 1:10 with nuclease-free water and stored at -20˚C.

3.2.5 TaqMan® gene expression analysis

Messenger RNA (mRNA) expression levels of fifteen candidate genes were investigated by real-time PCR using TaqMan® gene expression assays (Applied Biosystems®, Foster City, CA). Pre-designed TaqMan assays were purchased for each mouse gene including: *Asph* (Mm01211480_m1), *Casq1* (Mm00486725_m1), *Pygm* (Mm00478582_m1), *Ampd1* (Mm01308676_m1), *Gys1* (Mm00472712_m1), *Il6* (Mm00446190_m1), *Il8* (Mm04208136_m1), *Il10* (Mm00439614_m1), *Il15* (Mm00434210_m1), *Tlr4* (Mm00445273_m1), *Hspa1a* (Mm01159846_s1), *Hspd1* (Mm00849835_g1), *Hspb3* (Mm00517345_s1), *Hsp90aa1* (Mm00658568_gH), *Hsf1* (Mm01201402_m1), *Aldoa* (Mm00833172_g1), *Rpl27* (Mm01245874_g1) and *Rer1* (Mm00471276_m1). TaqMan® chemistry uses transcript specific probes to detect and quantify target gene expression. TaqMan® assays incorporate unlabelled primers and a sequence-specific fluorescently labelled probe, which is cleaved by *Taq* DNA polymerase releasing VIC™ or FAM™ dye molecules proportional to the amount of product synthesised (Figure 3.1).

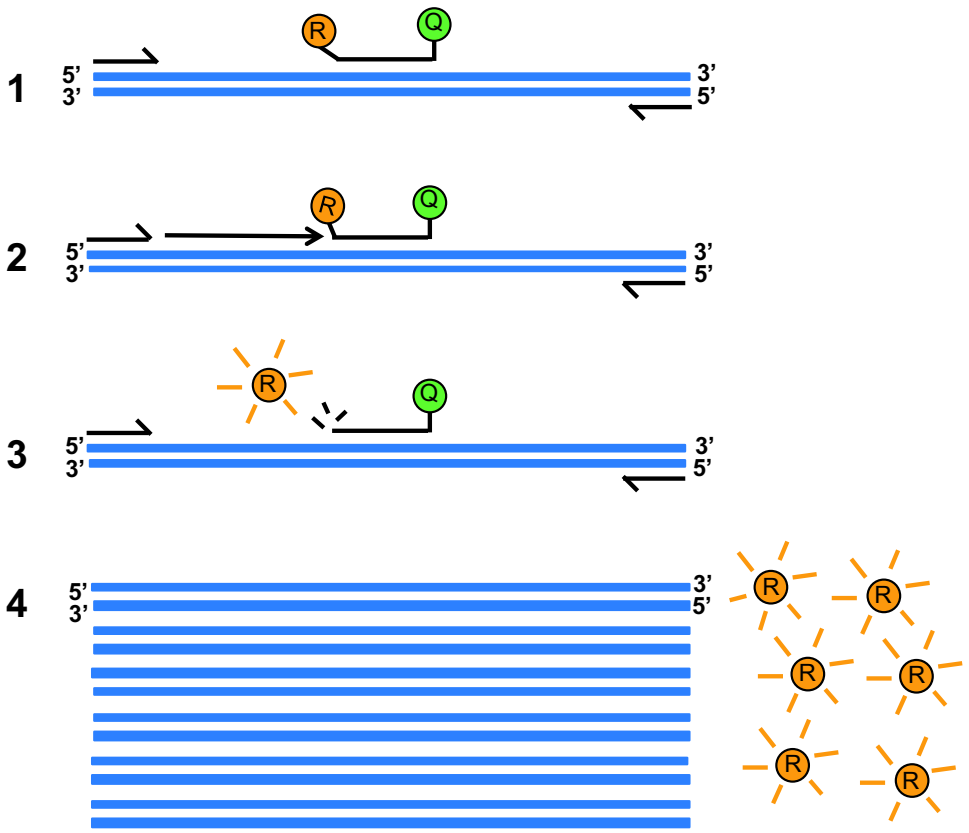

Figure 3.1: Schematic representing TaqMan real-time PCR chemistry. Fluorescently-labelled probes bind to the target transcript and emit a fluorescent signal in real-time as the DNA template is amplified by PCR. Adapted and redrawn (*Thermo Fisher Scientific*, 2017).

Three reference genes, *Aldoa*, *Rer1* and *Rpl27*, which are stably expressed in mouse skeletal muscle were chosen to normalise for varying quantities of input cDNA (Thomas *et al.*, 2014). Soleus and EDL muscles from the left and right leg of each mouse were investigated by TaqMan® real-time PCR, totalling 176 samples. Reactions for each of the 15 candidate genes and 3 reference genes were performed in triplicate.

TaqMan® real-time PCR reactions contained 1X TaqMan® Gene Expression Assay, 1X TaqMan® Gene Expression Master Mix, 2 ng cDNA template and RNase-free water. Each reaction was performed in triplicate. TaqMan® real-time PCR reactions were performed using the Applied Biosystems 7900HT Real-Time PCR instrument, with reactions held at 50˚C for 2 minutes, 95˚C for 10 minutes followed by 40 cycles of 95˚C for 15 seconds and 60˚C for 1 minute. Cycle threshold (C_T) values were exported from the software to allow relative quantification of genes using geNorm through Microsoft® Excel (Vandesompele *et al.*, 2002). The geNorm algorithm calculates a normalisation factor for each sample based on the geometric mean of the most stable reference gene values.

Relative gene expression values were imported into RStudio 1.0.136, an open source statistical package (RStudio, 2016). The relative expression values for each candidate gene were compared between $RyR1^{R163C/wt}$ mutant and $RyR1^{wt/wt}$ wild-type muscle over the recovery time points. Due to the identification of the wild-type baseline group as outliers, final analyses were performed excluding the baseline groups.

A linear model was fitted to each gene of interest and muscle type. Genotype, recovery time point, mouse leg and the genotype time point interaction were defined as factors within the models. The Analysis of Variance (ANOVA) method was used to test for differences between the group means, with *p* values corrected for multiple testing with the Benjamini-Hochberg (BH) procedure (Benjamini and Hochberg, 1995), reducing the false discovery rate (FDR). A post-hoc Tukey's honest significant difference (HSD) test was performed for genes revealing significantly differential expression between genotypes. The Tukey HSD test allows multiple pair-wise comparisons, which are internally corrected for multiple testing issues, identifying specific levels within the groups where the means significantly differ.

3.2.6 TruSeq® Stranded mRNA library preparation

A subset of twenty-four RNA samples (twelve pairs) extracted from RyR1$^{R163C/wt}$ mutant and RyR1$^{wt/wt}$ wild-type soleus muscle were selected for global gene expression profiling by RNA-seq. The mice chosen for the RNA-seq study responded similarly to acute stress, with comparable heat exposure times. In contrast, the twelve excluded mice were outliers and either became heat stressed quickly prior to exposure to 34°C or took longer to respond to the acute heat stress. Libraries were created by staff at the on-site NGS facility using the TruSeq Stranded mRNA library preparation kit (Illumina®), according to the manufacturer's instructions (Figure 3.2).

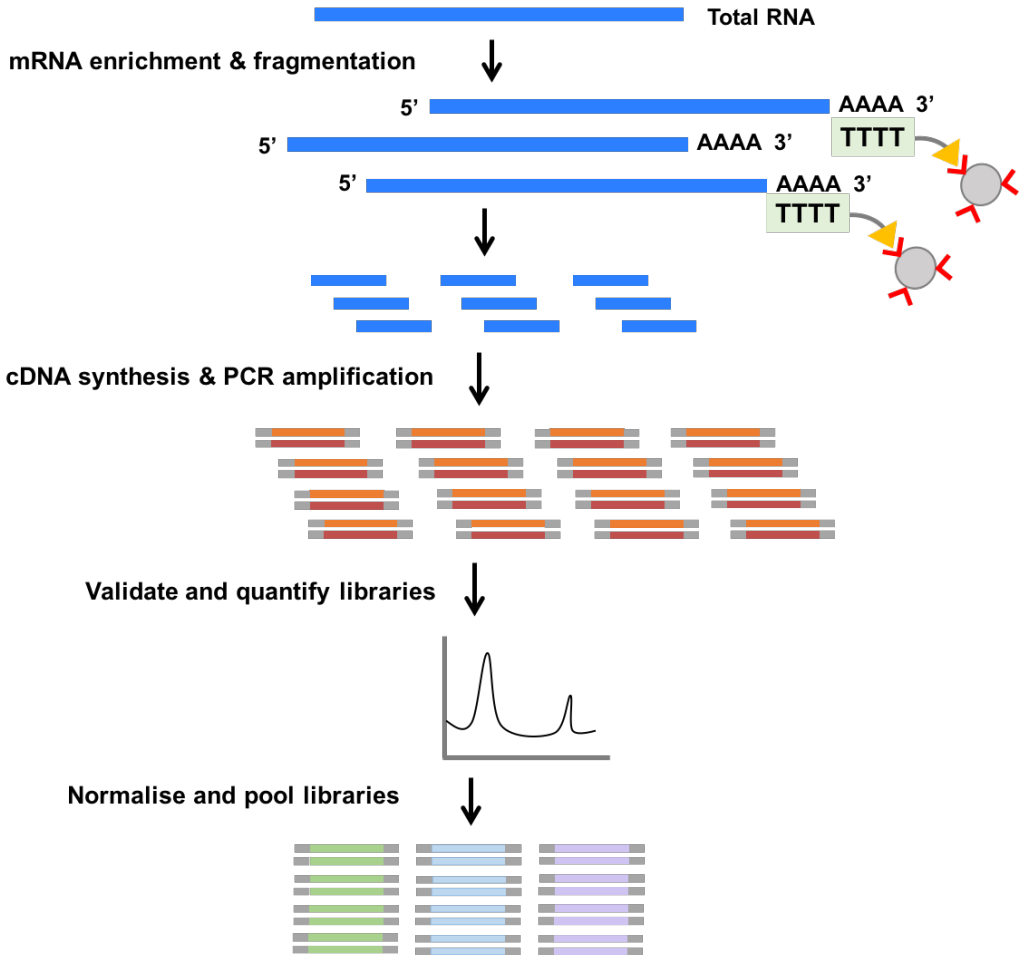

Figure 3.2: Schematic illustration of Illumina® TruSeq® mRNA library preparation workflow. Based on graphic produced by (*Applied Biological Materials (abm) Inc.*, 2017), adapted and redrawn.

Briefly, mRNA samples were purified using oligo-dT magnetic beads and heat fragmented and primed for cDNA synthesis. First strand cDNA was synthesised followed

by second strand cDNA, with 3' ends adenylated and 5' end repaired. Sequencing adapters were ligated to the adenylated 3' ends of the double stranded cDNA and libraries were amplified by PCR. Libraries were quantified and quality checked using Agilent's High Sensitivity RNA ScreenTape assay and 2200 TapeStation instrument (Agilent technologies, Santa Clara, CA, USA) according to the manufacturer's instructions.

3.2.7 Illumina® HiSeq® NGS

The mRNA enriched cDNA libraries were sequenced by the NGS facility using Illumina's HiSeq® 3000 platform, according to the manufacturer's instructions. Equimolar concentrations of each library were pooled and run across two lanes of the Illumina® HiSeq® 3000 sequencer to produce 150-bp paired-end reads. The platform adopts the same clonal bridge amplification and SBS technology as the MiSeq® platform described in chapter 2, section 2.2.4. Reads were de-multiplexed using the unique indexes, generating a forward and reverse FASTQ file for each sample.

3.2.8 Differential gene expression analysis

A schematic overview of the RNA-seq analysis pipeline has been presented in Figure 3.3, with details provided in appendix B. Sequence data were pre-processed using the Medical Advanced Research Computer 1 (MARC1), a high-performance computer cluster at the University of Leeds. Each FASTQ file was quality checked using the FastQC tool (Version 0.11.3), which provides information including sequence quality and adapter contamination (Andrews, 2010). Technical replicates across HiSeq lanes were merged into one FASTQ file and trimmed to remove poor quality base calls (<20) and adapter contamination using cutadapt (Martin, 2011). Trimmed reads were re-checked using FastQC to confirm that all adapter sequences had been removed and that the remaining reads were all good quality. Reads were pseudo-aligned to the mouse reference genome (GRCm38-ensembl 85) using Kallisto, to quantify transcript abundances (Bray *et al.*, 2016). Transcript-level abundance estimates were summarised to gene-level and imported into RStudio 1.0.136 using tximport (version 1.3.0) (Soneson C, 2016). Rstudio is an open source statistical package and was used to implement differential gene expression analyses using the DESeq2 package, according to manufacturer's instructions (version 1.15.2) (Love, Huber and Anders, 2014; RStudio, 2016).

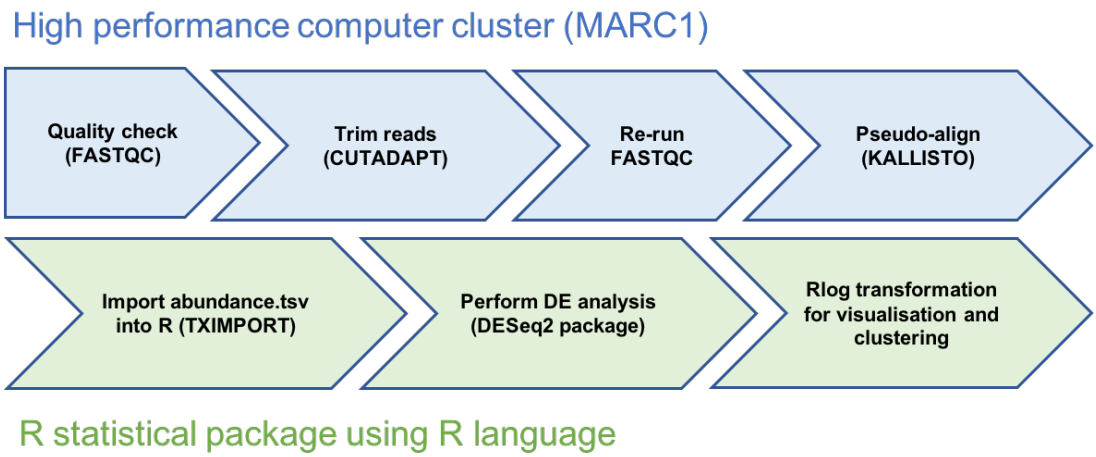

Figure 3.3: RNA-seq analysis pipeline.

The DESEq function within the DESEQ2 package incorporates a multi-step process into one user-friendly function to implement differential expression analysis. In brief, a generalised model (GLM) was fitted to each gene assuming a negative binomial distribution in order to test the impact of heat stress and genotype on gene expression. Abundances of cDNA fragments were scaled by a normalisation factor, accounting for library size and average transcript length. Dispersion estimates were calculated using maximum likelihoods allowing log2 fold-changes to be weighted relative to gene-wise variation and the mean-dispersion relationship (Figure 3.4). Statistical significance of the final log2 fold-change estimates were evaluated using the Wald test, with p-values adjusted for multiple testing using BH correction to control for the FDR error (Benjamini and Hochberg, 1995; Narum, 2006).

Two factors were defined within the model, specifically genotype and time point. Two levels were specified within genotype; mutant and wild-type. Three levels were specified within time point; baseline, 1-hour recovery and 24-hours recovery. Each of the size groups comprised four RyR1 mutant and four wild-type mice. The original multi-factor design formula included three terms: genotype, time point and the interaction between the two factors. The design formula was later altered to exclude the baseline group and investigate pair-wise comparisons between the two genotypes, both 1 hour and 24 hours' recovery post heat exposure. Specific pair-wise comparisons were drawn, differentially expressed genes were ranked by adjusted p-value and then exported into Microsoft® Excel.

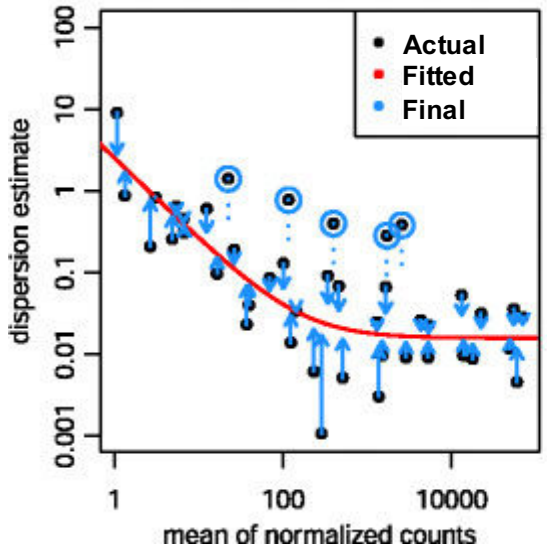

Figure 3.4: The relationship between average expression strength and gene-wise dispersion. Dispersion estimates (black) are shrunk towards the fitted estimates (red line) to weight log2 fold-changes relative to variation to limit false-positive calls. Image adapted from DESeq2 methods paper (Love, Huber and Anders, 2014).

Count data were also transformed to the log2 scale with the regularized log (rlog) transformation, which corrects for library size while removing the dependence of the variance on the mean counts across a gene (Love, Huber and Anders, 2014). The rlog transformation is performed separately to differential expression analysis and is necessary for visualisation of count data and clustering to identify sample outliers. A principal component analysis (PCA) was performed clustering samples in 2-dimensional space based on global gene expression profiles. PCA plots were customised using the ggplot function to allow easy interpretation of the analysis. Graphs representing gene counts across the 24 samples were produced for select genes using the ggplot2 package in Rstudio. All plots of normalised counts were produced using the ggplot function to allow customisation of each figure to aid interpretation.

3.3 Results

3.3.1 Metabolic responses of RyR1 mutant and RyR1 wild-type mice to acute heat stress

All thirty-six treated mice were exposed to ramps in environmental temperature within the indirect calorimetry chambers, although exposure times varied between the mouse pairs (Table 3.3). Due to the heat-sensitive phenotype of the heterozygous RyR1 R163C mice, mice were closely monitored for signs of heat stress (metabolic and behavioural), which would likely develop into a fatal hypermetabolic reaction. As such, two RyR1 R163C mice, HET10 and HET18 were particularly sensitive so were removed from the chambers at 33ºC and allowed to recover at room temperature with their respective wild-type pair. The remaining thirty-two mice were exposed to chamber temperatures of

30ºC, 33ºC and 34ºC. The majority of mice took an hour to acclimatise to an ambient temperature of 30ºC. Twenty-four mice with comparable heat exposures were chosen for the RNA-seq study, to reduce intra-group biological variability.

Table 3.3: Exposure times of mice to varying temperatures within the indirect calorimetry chambers. Duration at each temperature was dependent on the metabolic responses of each pair of mice.

Animal pairs	30ºC (hh:mm)	33ºC (hh:mm)	34ºC (hh:mm)	Recovery	
WT1 & HET1	01:18	00:30	01:11	0 hours	
WT2 & HET2	01:12	00:42	00:55	0 hours	
WT3 & HET3	01:22	00:33	00:27	0 hours	*
WT4 & HET4	01:07	00:40	00:18	0 hours	*
WT5 & HET5	01:22	00:29	00:38	0 hours	*
WT6 & HET6	01:23	00:35	00:37	0 hours	*
WT7 & HET7	01:06	00:45	00:20	1 hour	*
WT8 & HET8	01:04	00:39	00:34	1 hour	
WT9 & HET9	00:58	00:37	00:24	1 hour	*
WT10 & HET10	01:00	00:17	—	1 hour	
WT11 & HET11	00:59	00:24	00:24	1 hour	*
WT12 & HET12	01:31	00:38	00:14	1 hour	*
WT13 & HET13	01:16	00:28	00:33	24 hours	*
WT14 & WT14b	00:54	00:30	00:23	24 hours	
WT15 & HET15	00:54	00:34	00:19	24 hours	*
WT16 & HET16	01:06	00:32	00:45	24 hours	*
WT17 & HET17	01:48	00:29	00:12	24 hours	*
WT18 & HET18	01:12	00:30	—	24 hours	
Average:	**01:12**	**00:32**	**00:31**		

*Twenty-four mice were selected for the RNA-seq study.

The RyR1 R163C mutant mice revealed significantly higher energy expenditures (heat kcal/hr) than RyR1 wild-type mice at 30ºC (p <0.05) (Figure 3.5). There were no significance differences observed between RyR1 mutant and wild-type mice at 33ºC and 34ºC. Average energy expenditure decreased as ambient temperature increased with a rise in metabolic rate in RyR1 R163C mutant mice at 34ºC prior to transfer to room temperature.

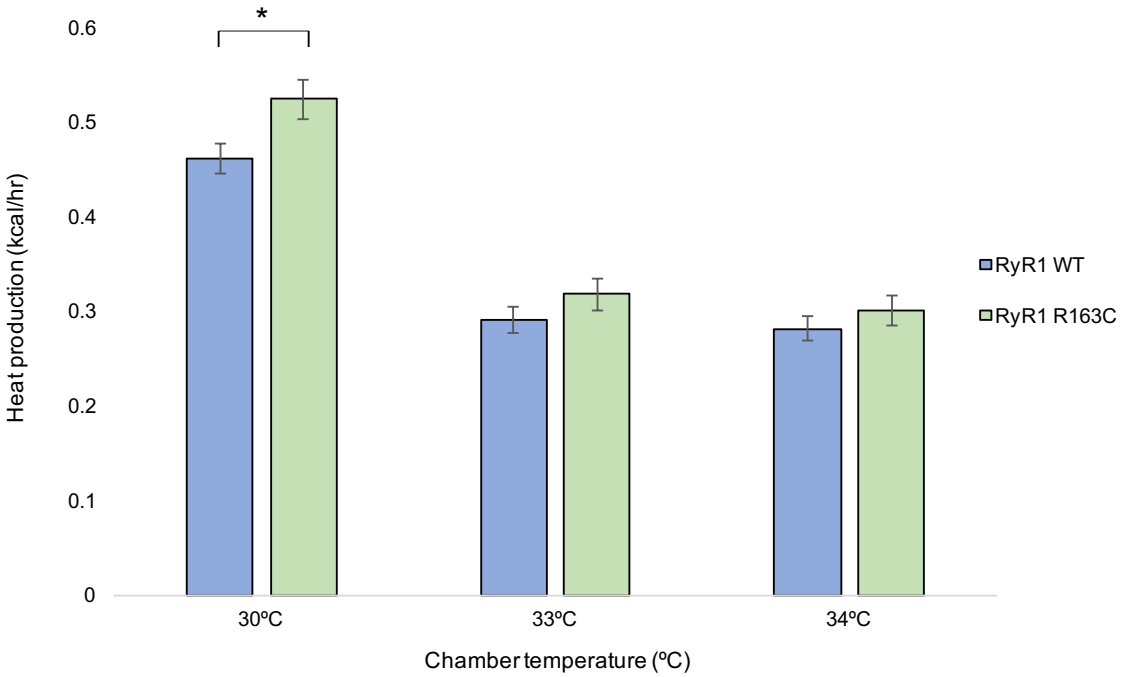

Figure 3.5: Mouse metabolic heat production during acute heat stress.
Error bars represents standard errors of the mean. Significant differences between genotypes highlighted (*p* values <0.05 *).

Figure 3.6 represents a pair of RyR1 wild-type and R163C mice that were tested in parallel and illustrates the steady reduction of energy expenditure as the mice acclimatise to an ambient temperature of 30ºC, which is within their thermoneutral zone (Ganeshan and Chawla, 2017; Gordon, 2017). As the chamber temperature is ramped to 33ºC both mice display a rise in metabolic rate, with the RyR1 R163C mouse appearing more sensitive and responding more quickly to the temperature change. The energy expenditure of both genotypes groups steadily declined and plateaued, with neither responding immediately to an increase of ambient temperature to 34ºC. After 24 minutes at 34ºC the RyR1 R163C mouse demonstrated a rise in metabolic rate and was removed from the chamber along with the paired wild-type mouse.

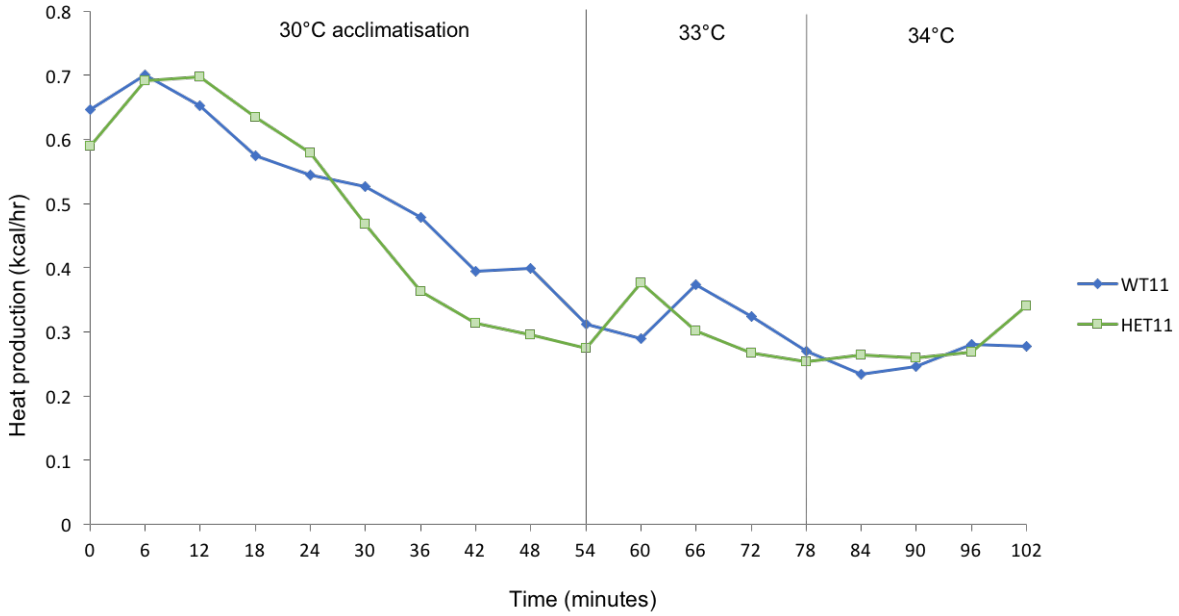

Figure 3.6: Metabolic heat production of a pair of RyR1 mutant and wild-type mice exposed to acute heat stress.

Traces of heat production (kcal/hr) representing the metabolic rates of each RyR1 wild-type and R163C mutant mouse have been presented in Figure 3.7. The overall pattern of energy expenditure is similar between the genotypes with a decline observed in metabolic rate as the chamber temperature increased. The average metabolic rate of the RyR1 wild-type group declined at a steadier rate once placed in the thermoneutral zone (30ºC) than the RyR1 R163C group of mice. The energy expenditure of certain mice was less stable and fluctuated throughout the period of heat exposure. All RyR1 heterozygous mice showed a rise in energy expenditure and/ or a change in behaviour consistent with heat stress before removal from the heat chambers. All mice recovered once transferred back to room temperature with no RyR1 R163C mice developing irreversible hyper-metabolic reactions.

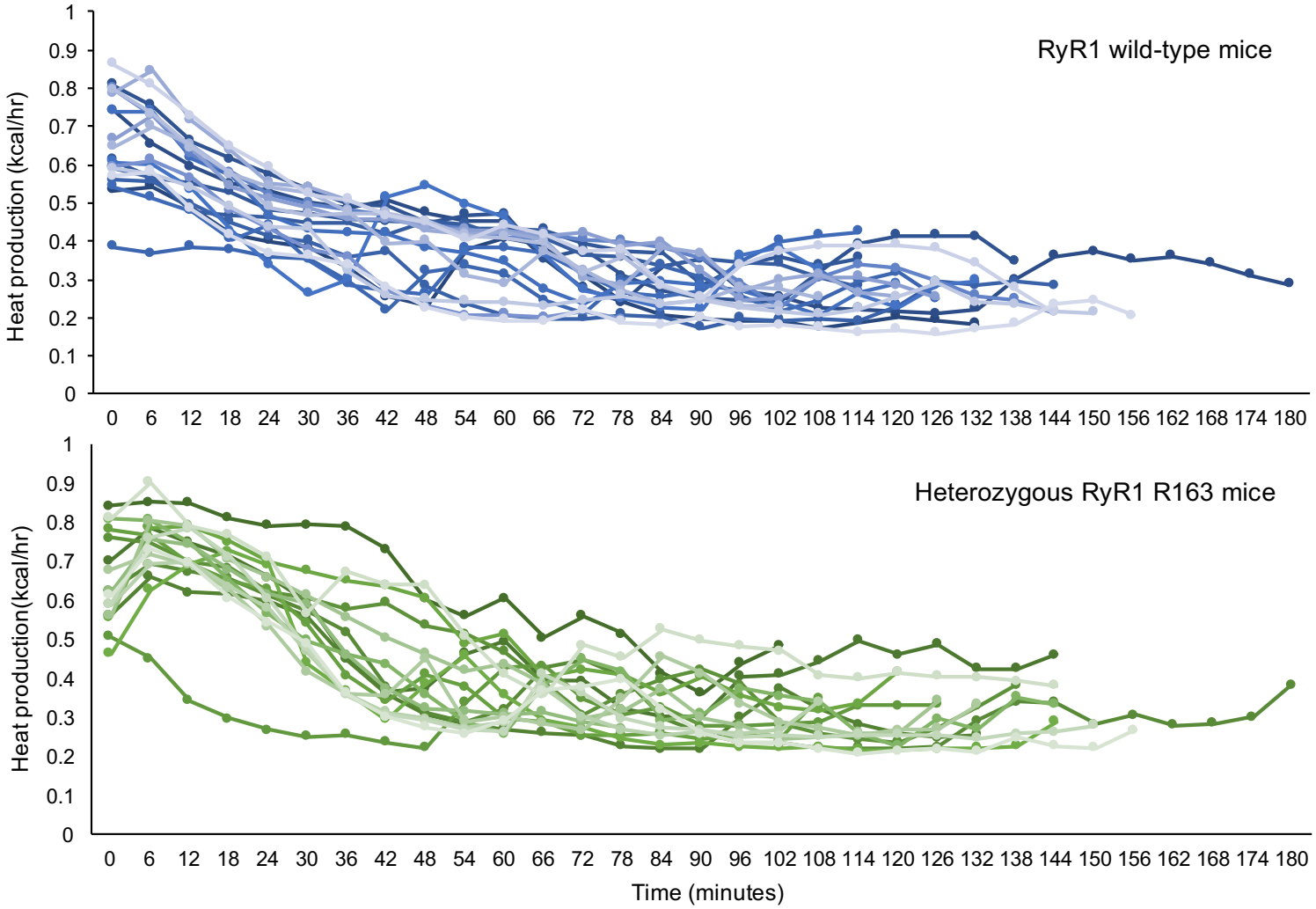

Figure 3.7: Metabolic heat production of RyR1 wild-type and mutant mice during acute heat stress. Mice were acclimatised for ~1 hour at 30°C, then exposed to 33°C for ~30 minutes then 34°C for ~30 minutes.

The respiratory exchange ratio (RER), which is the rate of CO_2 production relative to O_2 consumption, allows an estimation of the respiratory quotient (RQ). The RQ value indicates whether fats or carbohydrates are being utilised for energy metabolism. An RER of ~0.7, suggests that fat is being metabolised as the primary fuel, whereas 100% carbohydrate metabolism would produce an RER of ~1. No significant differences were observed in the average RER between RyR1 mutant and wild-type mice (Figure 3.8). The decrease in RER as the chamber temperature increases, demonstrates an increased proportion of fat metabolism as the mice become less active in the chambers and their metabolic rates decline.

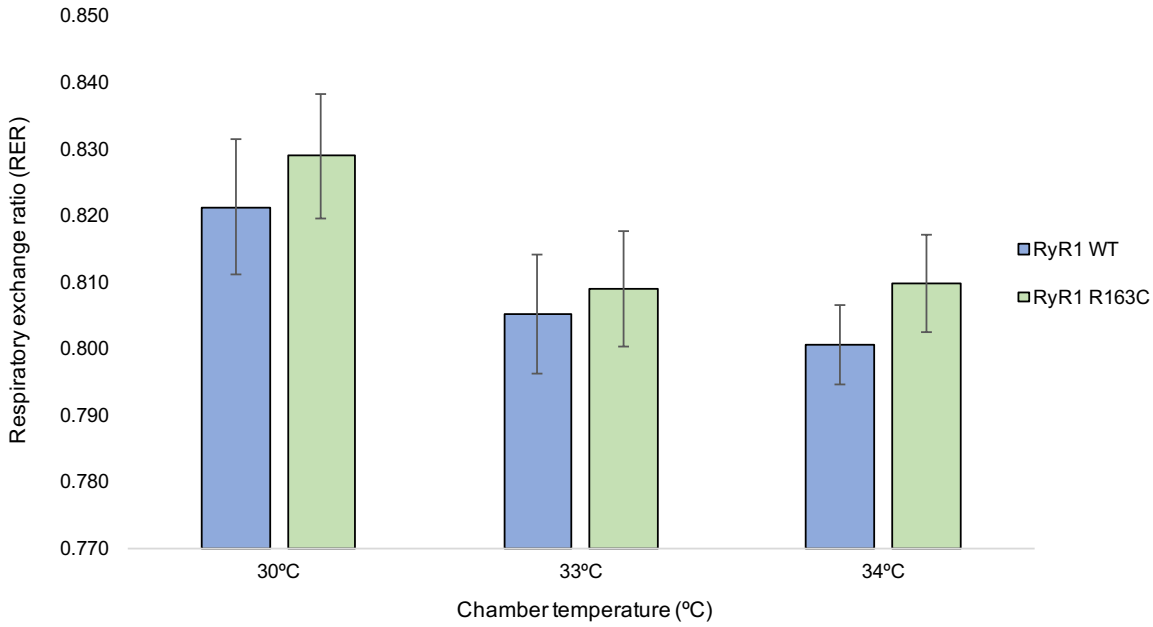

Figure 3.8: Average respiratory exchange ratio (RER) during acute heat exposure. Error bars represents standard errors of the mean. Significant differences between genotypes highlighted (*p* values <0.05 *).

3.3.2 The effect of acute heat stress on candidate gene expression between RyR1 mutant and wild-type mice

Expression levels of fifteen genes were quantified by TaqMan® real-time PCR in EDL and soleus muscle. The baseline group has been presented for illustrative purposes but was removed from all statistical analyses due to the untreated wild-type mice being identified as outliers in the subsequent RNA-seq study. Two genes, interleukin 10 (Il10) and chemokine ligand-15 (Cxcl15), were not detected in any of the samples tested. The remaining thirteen genes were expressed across all samples. Gene expression assays

were performed separately for EDL and soleus muscle extracted from the left and right legs of each animal to measure technical variation resulting from dissection times and sample preparation. No significant differences in gene expression were observed between the left and right legs of the mice (*p* values <0.05).

When considering expression differences at the genotype level across all recovery time points using the ANOVA method, four genes revealed significant differences (Table 3.4). These included *Hspa1a* (EDL), *Hsp90aa1* (EDL and soleus), *Il15* (soleus) and *Hsf1* (soleus), with only *Hsp90aa1* (EDL) and *Hsf1* (soleus) maintaining significance after FDR-correction using the BH procedure (Benjamini and Hochberg, 1995).

Table 3.4: Statistical comparison of gene expression between genotypes using Analysis of Variance (ANOVA) method. Adjusted *p* values have been corrected for multiple testing using the Benjamini-Hochberg procedure.

Gene	Muscle	*p* value	*p* adj.	Gene	Muscle	*p* value	*p* adj.
Asph	EDL	0.4658	0.7124	*Asph*	Soleus	0.4813	0.7124
Casq1	EDL	0.3834	0.7124	*Casq1*	Soleus	0.3127	0.7124
Pygm	EDL	0.2475	0.6934	*Pygm*	Soleus	0.5365	0.7342
Ampd1	EDL	0.2667	0.6934	*Ampd1*	Soleus	0.4646	0.7124
Gys1	EDL	0.6719	0.8319	*Gys1*	Soleus	0.2337	0.6934
Il6	EDL	0.9958	0.9958	*Il6*	Soleus	0.9879	0.9958
Il15	EDL	0.915	0.9913	*Il15*	Soleus	**0.0341***	0.2176
Tlr4	EDL	0.3494	0.7124	*Tlr4*	Soleus	0.4932	0.7124
Hspa1a	EDL	**0.0030****	0.0259	*Hspa1a*	Soleus	0.1363	0.5906
Hspd1	EDL	0.159	0.5906	*Hspd1*	Soleus	0.9132	0.9913
Hspb3	EDL	0.6524	0.8319	*Hspb3*	Soleus	0.3845	0.7124
Hsp90aa1	EDL	**0.0007*****	**0.0186***	*Hsp90aa1*	Soleus	**0.0418***	0.2176
Hsf1	EDL	0.741	0.8757	*Hsf1*	Soleus	**0.0024****	**0.0259***

Significance codes: '***' 0.001, '**' 0.01, '*' 0.05

Post-hoc tests enabling multiple comparison of means was performed using Tukey's HSD and uncovered the specific time points at which significant differences were evident (Table 3.5). These included, differential expression in EDL muscle of *Hspa1a* immediately post-acute heat stress and *Hsp90aa1* after 1-hour recovery at room temperature.

Table 3.5: Tukey's honest significant difference (HSD) test was performed on genes revealing a significant difference between mouse genotypes using the ANOVA method. All *p* values have been corrected for multiple testing.

Tukey's post-hoc test (adjusted *p* value, 95% confidence level)				
Gene	**Muscle**	**WT:0hrs - R163C:0hrs**	**WT:1hr - R163C:1hr**	**WT:24hrs - R163C:24hrs**
Il15	Soleus	0.9902	0.7535	0.8230
Hspa1a	EDL	**0.0297***	0.0940	1.0000
Hsp90aa1	EDL	0.7144	**<0.001*****	0.9998
Hsp90aa1	Soleus	0.2903	0.8693	0.9990
Hsf1	Soleus	0.0739	0.6041	0.6865

Five of the candidate genes were chosen from the HaloPlex 50 gene panel, two related to calcium homeostasis (*Asph*, *Casq1*) and three involved in metabolism (*Pygm*, *Ampd1*, *Gys1*) (Figure 3.9). Differential gene expression was not detected between genotypes in any of these genes, although the patterns of expression did differ between predominately slow-twitch soleus and fast-twitch EDL muscle types. There was an increase of all five genes in EDL muscle 1-hour post heat exposure, particularly in the RyR1 R163C group. The mutant EDL group also showed a marked increase in variability at the 1-hour recovery time point relative to all other groups. In contrast, intra-group variability was highest 24-hours post heat exposure in the soleus muscle type across both genotypes, again where expression was at its highest.

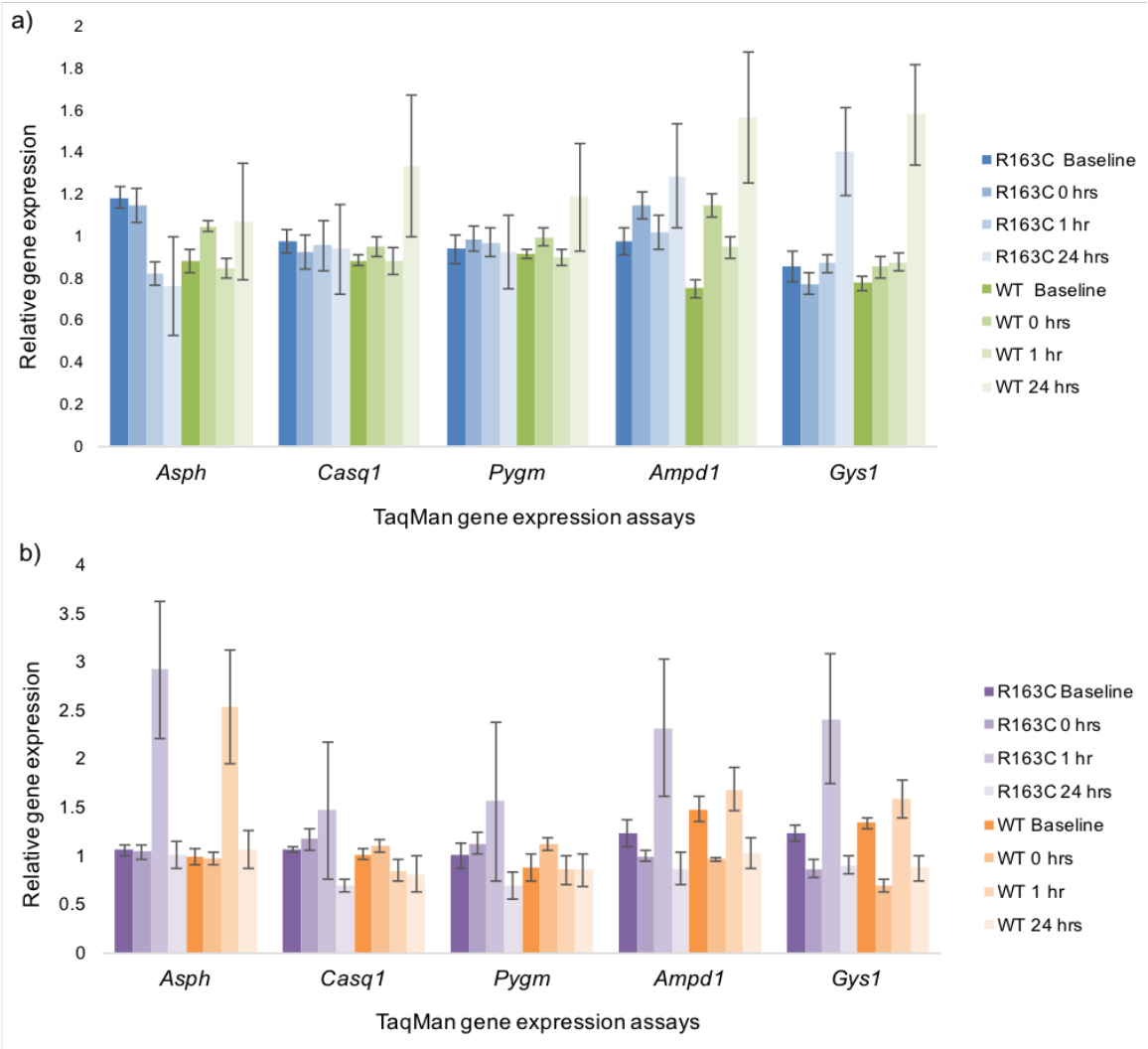

Figure 3.9: Expression of calcium-related and metabolic genes in RyR1 R163C mutant and wild-type soleus and EDL muscle. a) Relative expression of genes in mouse soleus muscle b) Relative expression of genes in mouse EDL muscle. Error bars represents the standard error of the mean.

Three immune response genes were expressed in all groups across both muscle types, specifically interleukins *Il6* and *Il15* and *Tlr4* (Figure 3.10). Similar expression patterns of these genes were observed in EDL muscle to that seen for the calcium-related and metabolic genes, with increased expression 1-hour post heat stress and a return to baseline levels by 24 hours. Relative expression of these genes was similar between the mutant and wild-type mice at each time point, with increased variability again at the 1-hour time point. Similar expression patterns between the two genotypes were also evident in mouse soleus muscle, with no significant differences between mutant and wild-type mice detected in *Il6*, *Il15* or *Tlr4. Il6* expression decreased post-heat exposure and continued to decrease over the recovery period. *Il15* expression also decreased after acute heat stress, but had returned to baseline levels after 24-hours recovery.

Finally, *Tlr4* expression remained relatively stable across the time points and appeared unaffected by heat exposure.

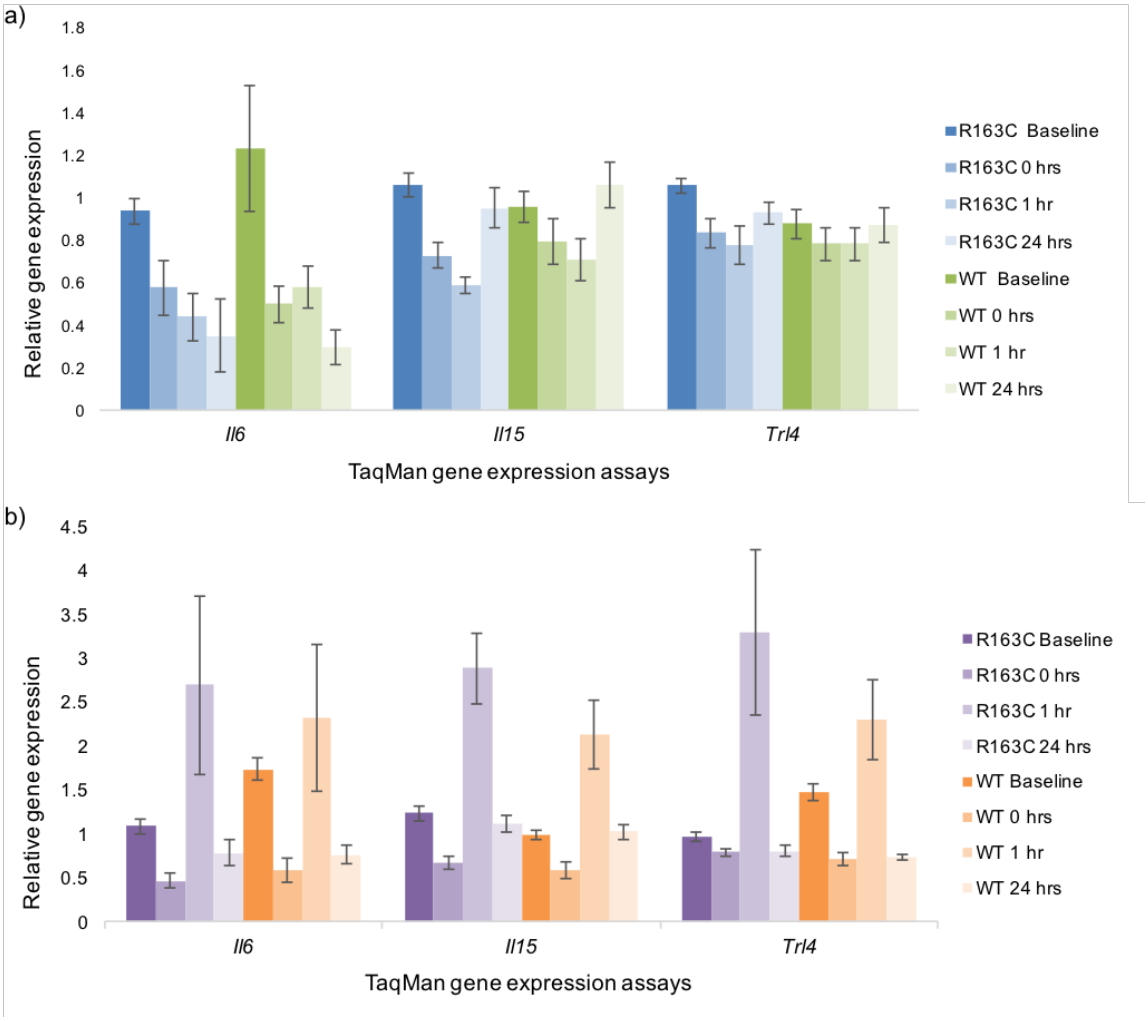

Figure 3.10: Expression of immune response genes in RyR1 R163C mutant and wild-type soleus and EDL muscle. a) Relative expression of genes in mouse soleus muscle b) Relative expression of genes in mouse EDL muscle. Error bars represents the standard error of the mean.

Five genes encoding heat-shock proteins were expressed in both soleus and EDL muscle types in both RyR1 mutant and wild-type mice (Figure 3.11). Expression in EDL muscle was again highest 1-hour post heat exposure; however, there was more intra-group variability in gene expression at this time point. *Hspa1a,* which encodes heat shock protein 70 (Hsp70) was expressed at a lower level is both EDL and soleus relative to the other four genes. Expression of *Hspa1a* was significantly higher in RyR1 mutant mice immediately post-acute heat stress compared to their RyR1 wild-type counterparts, specifically 3.9-fold, producing an adjusted *p* value of 0.028 (Table 3.5). Expression of *Hsp90aa1*, which encodes heat shock protein 90 (Hsp90) was also significantly higher

in RyR1 mutant mice 1-hour post heat exposure at 1.6-fold (adjusted *p* value 0.00001) (Table 3.5). The expression of the five genes remained more constant across the time points in soleus than in EDL muscle, with expression fluctuating in EDL muscle across the recovery time points.

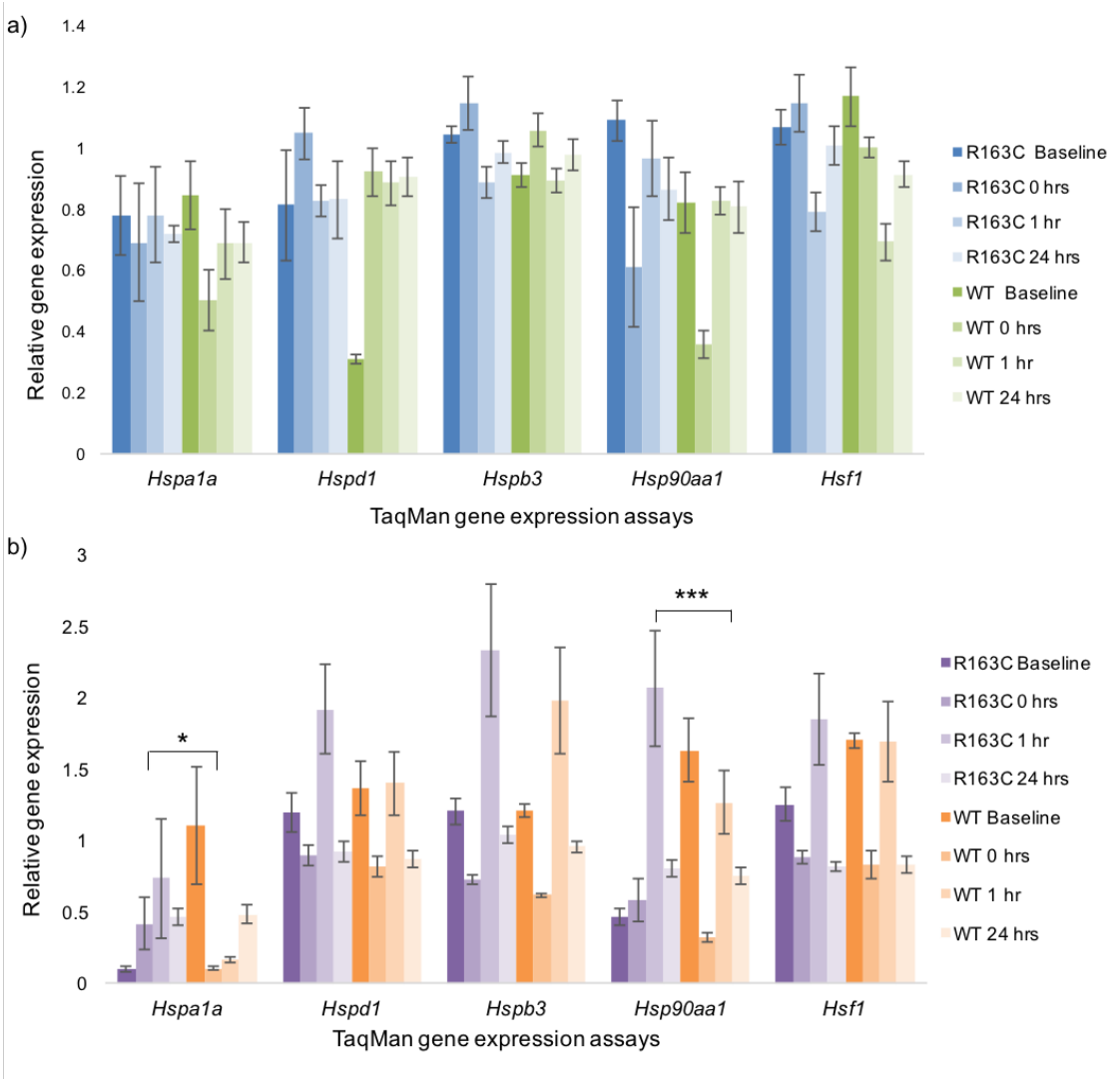

Figure 3.11: Expression of heat shock genes in RyR2 R163C mutant and wild-type soleus and EDL muscle. Relative expression of genes in mouse soleus muscle b) Relative expression of genes in mouse EDL muscle. Error bars represents the standard error of the mean. All *p* values have been adjusted for multiple testing, * <0.05, ** < 0.01, *** <0.001.

3.3.3 Global gene expression profiles of RyR1 mutant and wild-type mouse soleus in response to acute heat stress

All 24 mouse soleus RNA samples produced good quality libraries for RNA-seq, producing an average of 33.4 million 150 bp paired-end reads per sample (SD ± 8.7

million) (Table 3.6). FastQC revealed that a high level of quality was maintained across the 150 bases of each read, highlighted in Figure 3.12 by the per base quality report of heterozygous RyR1 R163C mouse 11. On average 90% sequenced reads (± 1%) were successfully pseudo-aligned and quantified by Kallisto using 98,492 annotated transcripts from the mouse genome (GRCm85) as a reference (Table 3.6). Quantified transcripts were summarised to gene-level by Tximport to allow gene-wise differential expression analysis to be performed.

Table 3.6: Kallisto pseudo-alignment genome mapping efficiency.

Sample ID	Processed reads	Pseudo-aligned reads	Reads mapped (%)
HET12	21,695,666	18,689,646	86.14
HET11	23,830,359	21,391,748	89.77
HET17	35,260,549	31,816,576	90.23
HET16	30,015,694	27,000,244	89.95
HET9	32,440,357	29,203,574	90.02
HET15	26,934,349	24,246,375	90.02
HET13	37,280,345	33,645,525	90.25
HET7	34,939,978	31,805,558	91.03
HETC1	43,100,405	38,750,110	89.91
HETC2	54,269,325	48,949,848	90.20
HETC3	34,624,617	31,314,198	90.44
HETC4	37,936,444	34,011,894	89.65
WT12	22,204,083	20,025,636	90.19
WT11	28,528,455	25,485,195	89.33
WT17	32,738,092	29,344,325	89.63
WT16	26,695,122	23,877,609	89.45
WT9	26,549,965	23,728,048	89.37
WT15	30,031,793	26,543,529	88.38
WT13	31,467,414	28,440,949	90.38
WT7	26,427,447	23,876,883	90.35
WTC1	28,213,733	25,381,907	89.96
WTC2	49,492,618	44,328,422	89.57
WTC3	50,019,487	44,644,827	89.25
WTC4	37,475,146	34,036,962	90.83

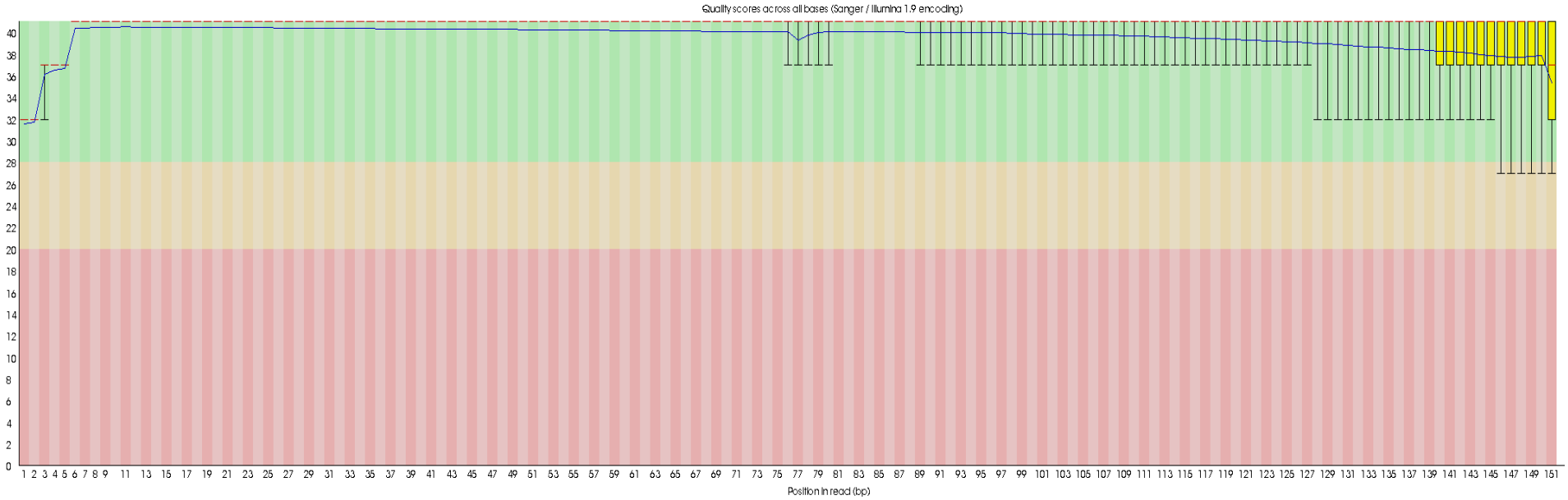

Figure 3.12: FastQC: average quality per base across an individual RNA-seq library. Schematic representation of a high-quality RNA-seq library created from the soleus muscle of heterozygous RyR1 R163C mouse 11.

Average expression strength (counts) was plotted against variation (dispersion) and highlighted the mean-dispersion relationship, showing an increased level of variation for weakly expressed genes (Figure 3.13). The estimates of gene-wise variation across the data were shrunk towards the fitted estimates and were used to weight log2 fold-changes to avoid underestimating variation and remove the dependence of fold-change on the expression strength of a gene.

A PCA analysis was used as a diagnostic to identify subgroups or outliers by visualising the genetic distance between the global gene expression profiles of each mouse (Figure 3.14). The samples formed distinct clusters according to their treatment rather than their genotyping suggesting that the RyR1 mutant and wild-type mice respond similarly to acute heat stress at a global level. The baseline wild-type samples formed a distinct group spatially isolated from all other samples highlighting the group as an outlier. To reduce the gene-wise dispersion estimates and increase the statistical power, the baseline groups were removed prior to differential expression analysis.

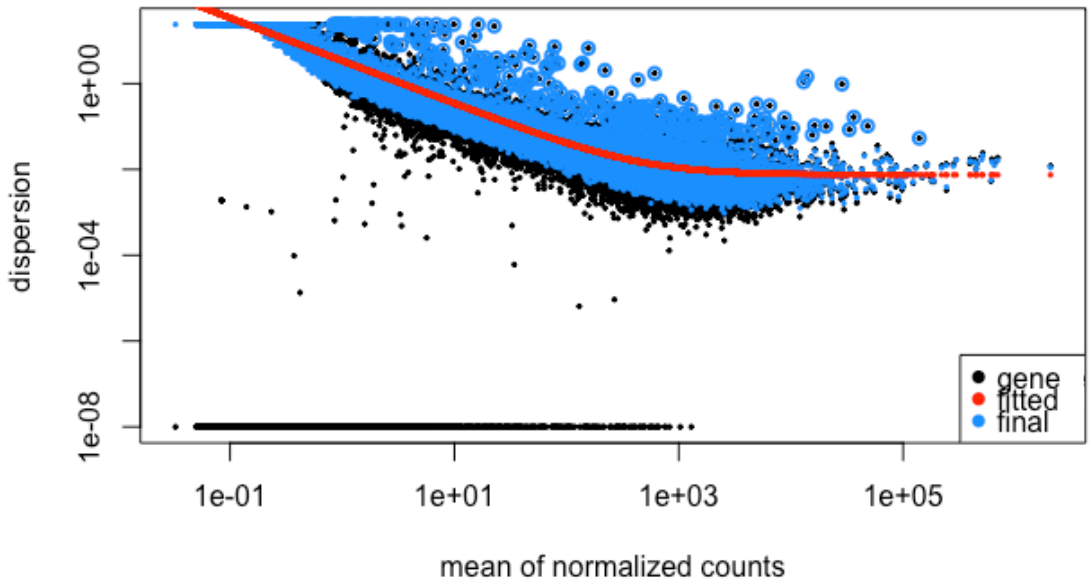

Figure 3.13: Plot of gene-wise dispersion estimates against mean of normalised counts across all twenty-four mouse soleus samples. Schematic representation of the mean-dispersion relationship and the final dispersion estimates (blue) shrunk towards the fitted estimates (red) for each gene. Log2 fold-changes are weighted relative to the final gene-wise dispersion estimates.

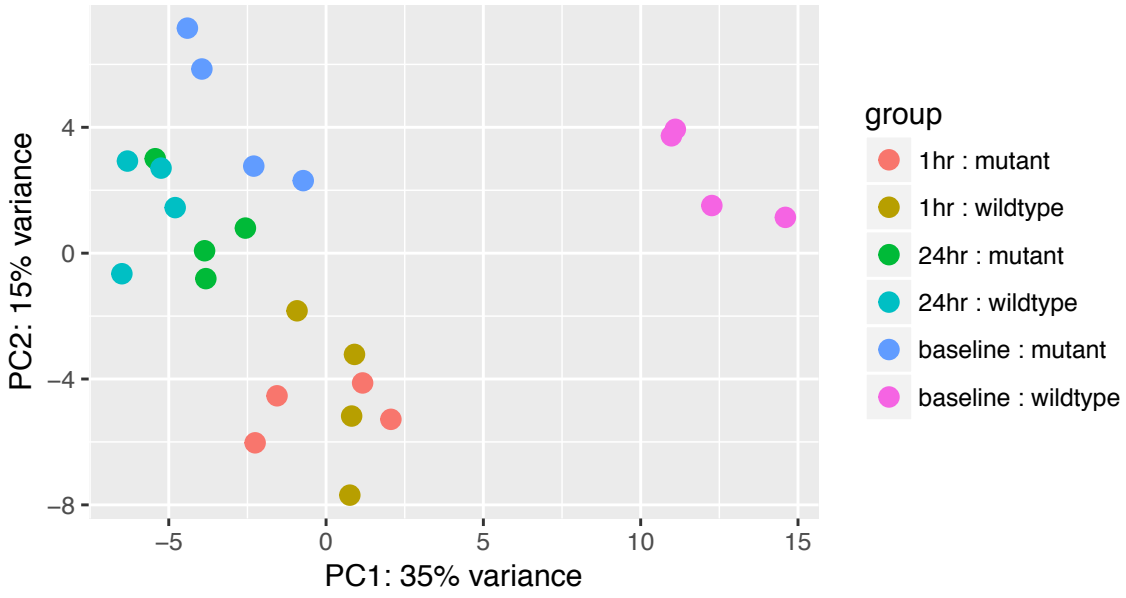

Figure 3.14: Principal component analysis representing global gene expression profiles of RyR1 mutant and wild-type mice exposed to acute heat stress. The PCA plot is a visual representation of the spread of data at the level of the transcriptome. Distance between data points along the X axis represents greater variation in gene expression data than spread along the Y axis.

Plotting the global log2 fold-change between RyR1 R163C mutant and wild-type mice both 1-hour (Figure 3.15) and 24-hours (Figure 3.16) post-acute heat stress reveals the similarity between the two genotypes at the whole-transcriptome level. No genes had shrunken log2 fold-changes greater than ± 1 (2-fold differences) at either time point highlighting the overall similarity in response to acute-heat stress between RyR1 mutant and wild-type mice.

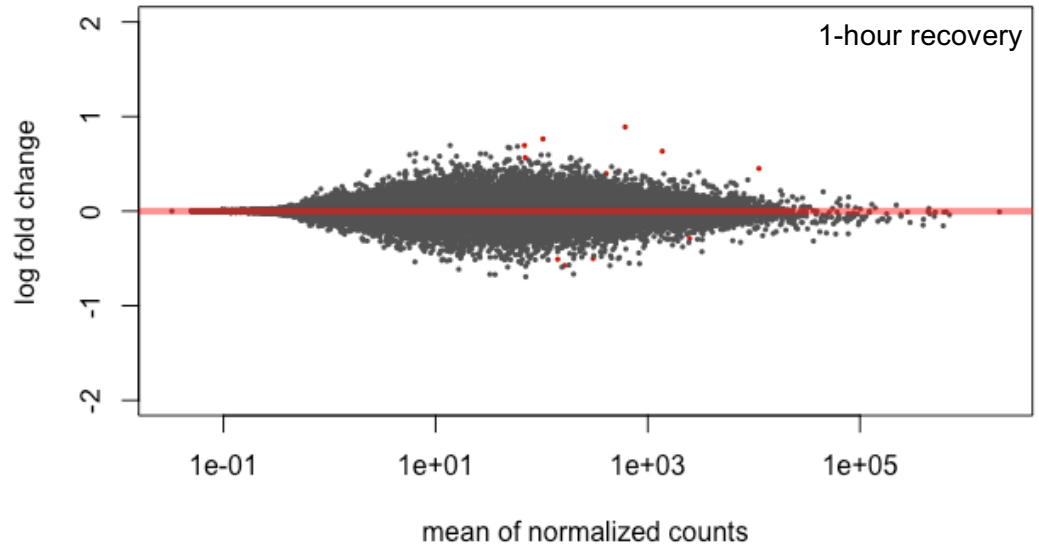

Figure 3.15: Global log2 fold-change between RyR1 mutant and wild-type mouse soleus 1-hour post-acute heat stress over mean of normalised counts. Data points representing genes are coloured red if adjusted *p* value <0.1.

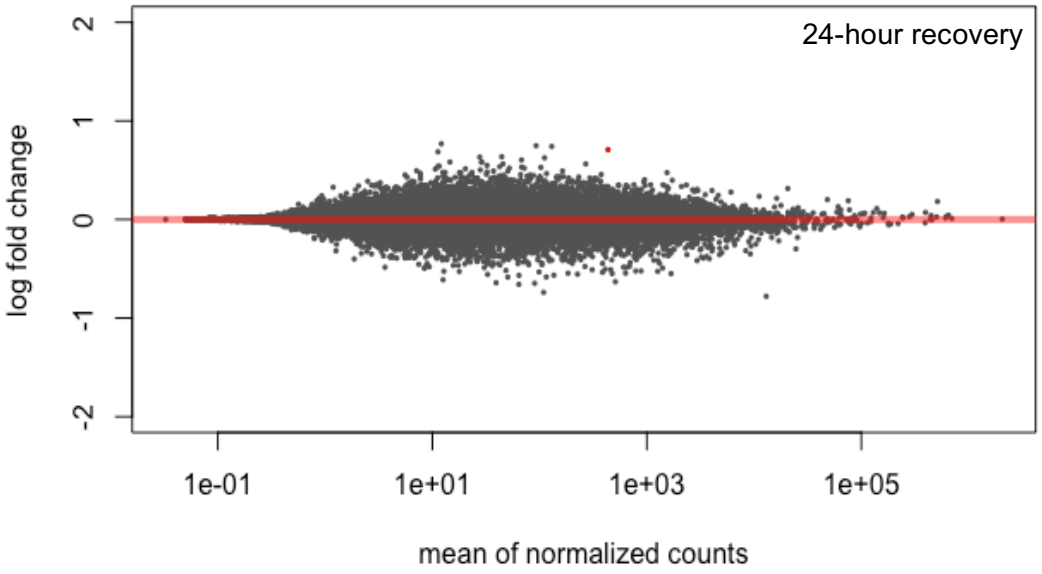

Figure 3.16: Global log2 fold-change between RyR1 mutant and wild-type mouse soleus 24-hours post-acute heat stress over mean of normalised counts. Data points representing genes are coloured red if adjusted *p* value <0.1.

Shrunken log2 fold-changes were ranked by FDR-adjusted *p* value revealing nine differentially expressed genes between RyR1 mutant and wild-type mouse soleus 1-hour post-acute heat stress (FDR-adjusted *p* value <0.05) (Table 3.7). Shrunken log2 fold-changes were modest, with a maximum significant difference of -0.746 fold between the genotypes observed in *Cyp2f2.*

Table 3.7: Genes differentially expressed between RyR1 R163C mutant and wild-type mouse soleus 1-hour and 24-hours post-acute heat stress. Log2 fold-changes represent shrunken values produced in the DESeq2 analysis. Negative values reflect lower expression in mutant compared to wild-type soleus muscle.

Recovery	Gene	Log2 fold-change	Standard error	*p* value	*p* adjusted
1 hour	*Cyp2f2*	-0.746	0.129	7.60E-09	0.000096
1 hour	*Zfp618*	-0.463	0.095	9.94E-07	0.004202
1 hour	*Lgals4*	-0.737	0.149	8.10E-07	0.004202
1 hour	*Atp1b4*	0.534	0.118	5.62E-06	0.017819
1 hour	*Fancg*	-0.608	0.142	1.81E-05	0.038289
1 hour	*I7Rn6*	0.275	0.064	1.73E-05	0.038289
1 hour	*Hsp90aa1*	0.420	0.101	3.48E-05	0.048980
1 hour	*Arhgef2*	0.354	0.085	3.22E-05	0.048980
1 hour	*Tceal7*	0.474	0.113	2.88E-05	0.048980
24 hours	*Hdac9*	-0.682	0.110	5.07E-10	0.000007
24 hours	*S1pr1*	0.361	0.077	2.61E-06	0.018090

Plotting normalised counts of *Cyp2f2*, a monooxygenase, showed lower expression in mutant mice compared to wild-type across all time points, with no changes detected in response to heat stress (Figure 3.17). In contrast, *Atp1b4,* a transcriptional co-regulator during muscle development *is* expressed at a higher level in RyR1 mutant soleus relative to wild-type, increasing post-heat exposure (Figure 3.17). Two heat shock-related genes *I7Rn6* and *Hsp90aa1* are also expressed at higher levels in RyR1 mutant soleus relative to wild-type, but the pattern of expression across the time points differs (Figure 3.17). *I7Rn6* expression remained stable in the mutant groups post-heat exposure and decreased in the wild-type group, while expression of *Hsp90aa1* increased 1-hour post heat exposure in the mutant group and decreased in the wild-type group.

Relative expression of Hsp90aa1 quantified by TaqMan® real-time PCR mirrored the expression patterns observed by RNA-seq for both the 1-hour and 24-hour time point, although the two methods conflicted at baseline measurements (Figure 3.11). Specifically, *Hsp90aa1* expression was highest in the untreated mutant group when quantified by TaqMan® real-time PCR, but when quantified by RNA-seq had the lowest average count.

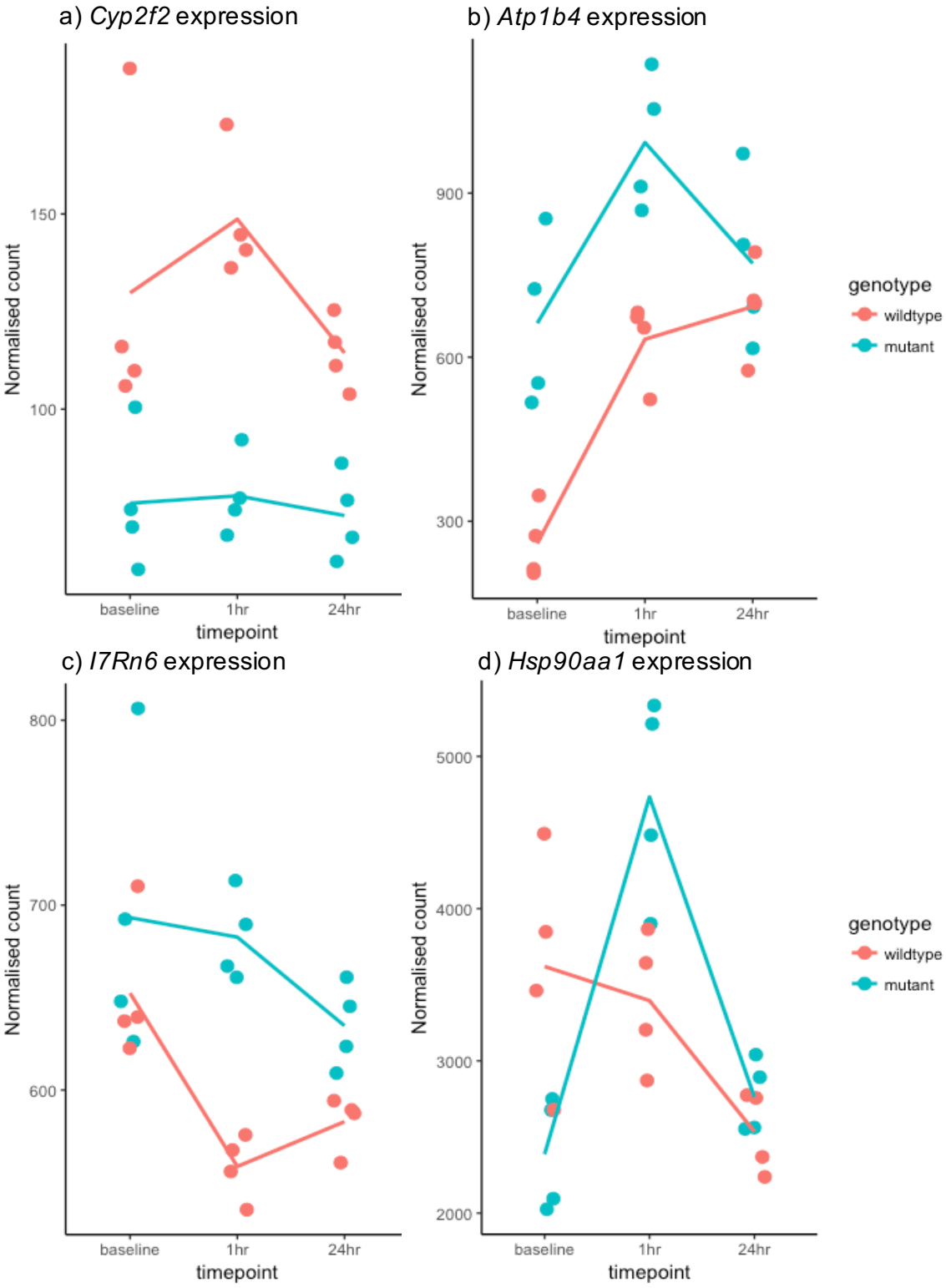

Figure 3.17: Expression plots of *Cyp2f2*, *Atp1b4*, *I7Rn6* and *Hsp90aa1* in RyR1 R163C mutant and wild-type mouse soleus 1-hour post-acute heat stress. Significant differences were observed after 1-hour recovery at room temperature (FDR adjusted *p* value <0.05).

Using an FDR-corrected *p* value threshold of 0.05, two genes were differentially expressed 24-hours post-acute heat stress, *Hdac9* and *S1pr1* (Table 3.7). Expression of *Hdac9*, a histone deacetylase, was lower in the RyR1 mutant mouse group than in the wild-type group (Figure 3.18). In contrast, expression of *S1pr1*, G-protein coupled receptor, was slightly higher in the RyR1 mutant soleus muscle but appeared to be unaffected by heat exposure (Figure 3.18).

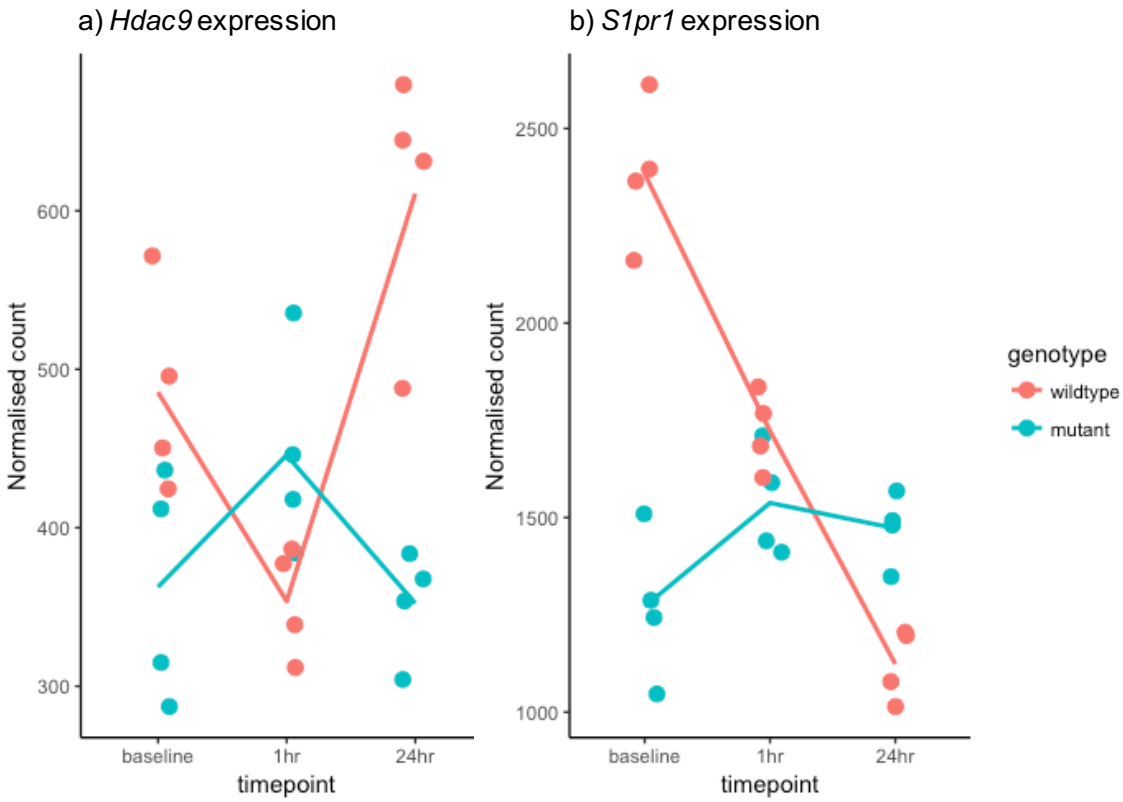

Figure 3.18: Plot of *Hdac9* and *S1pr1* expression in RyR1 R163C mutant and wild-type mouse soleus 24-hours post-acute heat stress. Significant differences were observed after 24-hour recovery at room temperature (FDR adjusted *p* value <0.05).

3.4 Discussion

The heat stress response remains poorly understood, with limited research investigating the pathophysiology of this potentially fatal condition. The development of a heat-sensitive knock-in mouse model, which harbours a functionally characterised RyR1 mutation associated with EHI in humans, created an opportunity to explore the muscle-specific response to acute heat stress at the transcriptome level. Investigating global gene expression profiles provides an effective method to elucidate the pathological mechanisms contributing to heat illness, without an *a priori* hypothesis.

Gene expression studies are inherently sensitive to technical and biological variation influenced by several factors, such as age, sex and sample preparation (Roth *et al.*, 2002). It is therefore important to control variables where possible to limit variation and reduce experimental noise, thereby increasing statistical power to detect differential expression. Mice were age and sex-matched and selected from the same colony, the majority of which were littermates. This aimed to ensure a homogenous population of mice, only differing by RyR1 genotype. Due to practical limitations, the eight mice selected as untreated controls were not transferred to the MMPC facility, but were all housed at room temperature with free access to food and water. It is important to consider that for genotypes which impact on energy expenditure, the animal's body mass may in turn be affected. To account for this, O_2 consumption and CO_2 production rates were normalised to the body mass (kg) of each mouse, although this adjustment does not account for differences in composition (ratio of lean mass to fat). Previous studies have demonstrated how tissue-specific metabolic rates can be identical between two mice with different compositions and consequently whole body normalised metabolic rates would appear different (Speakman, 2013).

Unfortunately, due to the heat-sensitive phenotype of mice carrying a heterozygous RyR1 R163C mutation, heat exposure times had to be varied between the pairs of mice. Previous studies investigating the phenotypic heat stress response of this knock-in mouse model reported that the onset of hypermetabolic reactions triggered by ambient temperatures 42°C heat were sudden and invariably fatal (Yang *et al.*, 2006). All heterozygous RyR1 R163C mice experienced fatal hypermetabolic episodes within an average of 11.5 minutes (± 1.8 minutes), with an average increase in core temperature of 7.5°C (Yang *et al.*, 2006). Therefore, mice in this study were allowed to acclimatise to the chamber environment at 30˚C, with the length of exposure to 33˚C and 34˚C tailored to the specific metabolic and behavioural responses of each mutant mouse. This ensured that no hypermetabolic reactions were triggered within the period of acute heat stress, allowing all mice to recover and be included in the gene expression analysis. As such, it is possible that mutant mice were not sufficiently heat stressed to cause differential expression between the genotype groups. Pairing each mutant mouse to a RyR1 wild-type mouse from the same colony provided the study with matched controls. Due to the limited understanding and characterisation of the heat stress response in this RyR1 R163C knock-in mouse model, this study attempted to address fundamental questions about the heat phenotype in these mutant mice.

Energy expenditure is the sum of basal metabolic rate, activity, thermogenesis and the thermic effect of food, so therefore may vary between mice with identical genetic

backgrounds. When performing *in vivo* studies that measure metabolic responses to heat, it is important to consider the individual metabolic rates of each animal to ensure that all mutant mice are experiencing acute heat stress to a similar degree. To reduce potential variation within the groups, 24 mice with similar exposure times to 30, 33˚C and 34˚C were selected for RNA-seq. The chosen chamber temperatures were considerably lower than in previous heat stress studies, due to the increased heat sensitivity of RyR1 R163C mutant mice (Yang *et al.*, 2006; King *et al.*, 2015). An intermediary temperature rise from 30˚C to 33˚C was incorporated into the experimental design to avoid shocking the mutant mice, potentially triggering a hypermetabolic reaction.

The thermoneutral zone in mice is higher than in humans, with mice favouring warmer environmental climates (Gordon, 2017). The thermoneutral zone of an endotherm can be defined as the range of ambient temperatures at which heat production and heat loss are in equilibrium (Kingma *et al.*, 2014). The chosen acclimatisation temperature of 30˚C falls within the thermoneutral zone of mice and allowed the basal metabolic rate (BMR) of the mice to be measured as they settled within the chambers. The O_2 consumption of each mouse began to plateau prior to any ramps in temperature. Heat production was indirectly inferred from gas exchange measurements (CO_2 production and O_2 consumption), and is a widely-accepted method to measure *in vivo* energy metabolism (Speakman, 2013). Indirect calorimetry chambers offer a more accurate measure of metabolic activity than direct measurement of heat production because heat can be stored by animals, introducing error into the system (Speakman, 2013).

The recovery time points were selected based on previous *in vivo* studies that investigated changes in cytokine expression 1-hour and 24-hours hours post-acute heat stress (Welc *et al.*, 2012, 2013). These recovery times proved sufficient in detecting significant changes in cytokine expression in wild-type mice. The same recovery periods may not necessarily be appropriate for the RyR1 mutant mice so recovery periods spanning 0-hours to 24-hours recovery were chosen and aimed to capture potentially fluctuating gene expression profiles. The heat-induced hypermetabolic reactions observed previously in the RyR1 R163C heterozygous mice developed rapidly, so it is therefore possible that differential expression does not occur prior to the onset of the heat illness episode.

RyR1 mutant mice displayed significantly higher energy expenditure at 30˚C relative to RyR1 wild-type mice. Previous studies have demonstrated higher resting Ca^{2+} in myotubes from heterozygous RyR1 R163C mice (Yang *et al.*, 2006), which could explain

the observed increase in basal metabolic rate. An elevated BMR in the mutant mice could alter their composition, increasing the proportion of lean muscle mass relative to fat, further increasing their overall BMR. In addition, the RyR1 R163C mutation has been shown to elicit basal mitochondrial uncoupling and dysfunction in heterozygous knock-in mice, characterised by increased matrix Ca^{2+}, increased reactive oxygen species (ROS) production and reduced glycolysis, fatty acid oxidation and oxidative phosphorylation, which was not compensated by anaerobic glycolysis (Giulivi *et al.*, 2011). Chronic uncoupling and disruption of mitochondrial function could account for the increased heat production observed in R163C mutant mice at baseline.

Estimating metabolic rate by measuring whole-body oxygen consumption can prove inaccurate if mitochondrial efficiency is affected (Salin *et al.*, 2015). Mitochondrial uncoupling dissipates the proton gradient required to drive ATP production during oxidative phosphorylation (OXPHOS), therefore altering the balance between O_2 consumption and ATP production. With RyR1 R163C knock-in mice demonstrating reduced mitochondrial efficiency, oxygen consumption would likely increase to compensate (Giulivi *et al.*, 2011). Energy expenditure rates, which are computed based on O_2 consumption, would therefore prove inaccurate, overestimating ATP production. Regardless whether or not O_2 consumption and CO_2 production accurately represent the underlying metabolic rate in RyR1 R163C mice, the whole-body calorimetry chambers still offer an effective method to detect differences in O_2 consumption between the mutant and wild-type mice. The rate of energy expenditure is expressed as heat production; however, mitochondrial uncoupling via mitochondrial uncoupling proteins (UCP) 1, 2 and 3, increase the ratio of heat production relative to ATP production. Therefore, the metabolic data reported by Oxymax may underestimate the heat production of RyR1 R163C mice.

Cold temperatures trigger mitochondrial uncoupling in brown adipose tissue through activation of mitochondrial uncoupling protein 1 (UCP1), which in turn drives thermogenesis (Cannon and Nedergaard, 2004). Mice have higher levels of brown fat than adult humans, therefore mitochondrial uncoupling plays a fundamental role in mouse thermogenesis. Interestingly, the relative activity and function of UCP1 is similar in humans, although the differences in thermogenesis between humans and mice due to proportion of brown fat must be considered in a study of this kind (Porter 2016). Particularly as heterozygous R163C mice appear to display a more severe heat-sensitive phenotype than humans harbouring the same mutation. The muscle-specific isoform UCP3 is less important for thermogenesis than UCP1, but uncoupling via UCP3 in skeletal muscle protects against oxidative stress by generating a proton-leak across

the inner mitochondrial membrane, thereby reducing ROS production (Nabben *et al.*, 2008).

Recent studies have suggested that mice are able to alter their core temperature to adapt to environmental stresses, while their energy expenditure remains constant (Gordon, 2017). Therefore, without measuring the core temperature of mice it is not possible to fully interpret the degree of heat stress, as mice may be lowering their core temperature to compensate. It should not be assumed that mice maintain a stable core temperature within the same range and to the same degree as human subjects, who have a lower tolerance to fluctuations in core temperature. Unfortunately, measuring core temperature of the mice in this study was not possible due to the set-up of the CLAMS Oxymax system.

As expected, the average heat production of all mice steadily declined as the chamber temperature increased, with low activity levels maintained for nearly all mice. Immediately prior to removal from the chambers, the heat production of RyR1 mutant mice rose, suggesting that the thermal homeostasis of these mice had been compromised. Their activity levels also increased in parallel, which conflicts with normal behaviour of mice exposed to hot environmental temperatures, suggesting the mice were heat stressed and were trying to move a cooler climate. During the previous characterisation of the RyR1 R163C mutant mouse model, the same spontaneous increase in activity was observed in response to heat (Yang *et al.*, 2006). In the current study, the mutant mice appeared more sensitive to rises in chamber temperature, responding more quickly than their wild-type counterparts. If these mice exhibit higher metabolic rates at baseline, perhaps they are primed to respond, reaching the threshold of the thermoneutral zone more quickly than RyR1 wild-type mice.

The average RER between RyR1 mutant and wild-type mice steadily decreased as the chamber temperature increased, with no significant differences detected between the genotypes. Average RER values at 34˚C were maintained at ~0.8, suggesting an increased preference for but not reliance on fatty acid oxidation in warmer climates. This suggests that mutant mice were able to elicit a normal metabolic response to heat prior to the first signs of heat stress at 34˚C, as the RER values were relatively stable and similar to wild-type mice. A previous study investigating metabolic responses of heat-stressed wild-type mice (core temperatures >42˚C), revealed that mice displayed a protective hypothermic response following heatstroke, associated with core temperatures <33˚C, reduced O_2 consumption, and an average RER ~0.71 (Leon *et al.*, 2010). The metabolic rates of the mice in this study were not monitored during their

recovery period; however, previous characterisation of RyR1 R163C mice did not reveal a hypothermic response prior to their fatal hypermetabolic reactions (Yang *et al.*, 2006).

Predominantly slow-twitch soleus muscle was chosen for the whole-transcriptome analysis as it has been shown to share the greatest molecular similarity to human skeletal muscles, with similar transcriptomes and mitochondrial coupling regulation (Kho *et al.*, 2006; Jacobs *et al.*, 2013). The average fibre type composition of mouse soleus is comparable to human *vastus lateralis* and *medialis* muscles, comprising ~50% type I, slow-twitch oxidative fibres and ~50 type II, fast-twitch fibres (Gouzi *et al.*, 2013; Kammoun *et al.*, 2014). Fibre type proportions are age and sex-dependent, with slow-twitch fibres more predominant in women and further increasing with age (Gouzi *et al.*, 2013). In contrast, EDL is a fast-twitch muscle comprising type II fibres and was used for comparison to explore the differences in the heat stress response between fast glycolytic and slow-twitch oxidative skeletal muscle (Burkholder *et al.*, 1994). Predominately fast-twitch quadriceps and gastrocnemius muscles were also collected, snap-frozen and stored in LN_2, to provide additional material in order to perform any future protein work required.

TaqMan® was chosen as a real-time PCR method to quantify expression of candidate genes rather than assays incorporating SYBR® green chemistry. TaqMan® gene expression assays provide increased target specificity owing to the use of target-specific fluorescent probes, thereby reducing false positives. Quantification of genes relative to stably expressed references genes acts as an internal control for variation in input cDNA quantities and has become standard practice for real-PCR gene quantification methods (Schmittgen and Livak, 2008). The geNorm algorithm was chosen as a normalisation method as it ranks the expression stability of the reference genes based on pair-wise variation and calculates a normalisation factor using the geometric mean of the 2 most stably expressed genes (Vandesompele *et al.*, 2002). This is particularly important as commonly used reference genes, such as *GAPDH*, have been shown to vary considerably between samples and across treatment conditions (Dheda *et al.*, 2004; Barber *et al.*, 2005; Mane *et al.*, 2008). The three reference genes chosen for this study, *Aldoa*, *Rer1* and *Rpl27*, had been previously validated for use in skeletal muscle from the C57BL/6j mouse strain (Thomas *et al.*, 2014). The C57BL/6j strain was the same genetic background used to create the RyR1 R163C knock-in mice, so these reference genes represent ideal candidates for normalisation of real-time PCR data in this study. The geNorm algorithm assumes 100% amplification efficiency when calculating relative expression values, nevertheless, these assumptions should be met as TaqMan® assays are advertised to produce amplification efficiencies close to 100%.

Many of the candidate genes for TaqMan® real-time PCR were differentially expressed in response to acute heat stress, but responded similarly between the two genotypes. Overall, the expression patterns of genes involved in Ca^{2+} homeostasis and metabolism were similar between the mutant and wild-type mice; however, differences in expression were detected between the predominately slow-twitch and fast-twitch EDL muscle types. Two genes encoding enzymes required for energy production in skeletal muscle, *Ampd1* and *Gys1*, were differentially expressed between predominantly slow-twitch soleus and fast-twitch EDL muscle. This highlights the contrasting energy requirements of each muscle type. Expression of *Ampd1* and *Gys1* increased 1-hour post-acute heat stress in EDL muscle, suggesting an increased energy demand post-heat exposure. The response in soleus muscle was delayed, with an increase in both *Ampd1* and *Gys1* expression detected 24-hours post-heat exposure. Glycogen utilisation is higher in fast-twitch muscle than slow-twitch, as indicated by the elevated glycogen synthase 1 (GYS1) levels observed in mouse EDL muscle (Cussó *et al.*, 2003). AMP deaminase 1 (AMPD1) is also expressed at high levels in type II fast-twitch fibres, due to its role in energy metabolism, converting AMP to IMP, which allosterically regulates ATP synthesis (Sahlin, Gorski and Edstrom, 1990; Kuppevelt *et al.*, 1994). *Asph* expression was also elevated after 1-hour recovery at room temperature in EDL muscle in both mutant and wild-type mice. It should be noted that the *Asph* TaqMan® assay would not have been able to detect the muscle-specific isoform of the *Asph* gene, which forms junctin. This assay binds to and amplifies across the boundary of exon 7-8 in the full-length *Asph* transcript, which is absent in the truncated junctin isoform. Junctin forms a complex with RyR1 regulating Ca^{2+} release; however, the function of aspartate beta-hydroxylase in skeletal muscle remains poorly understood.

The three immune-response genes, *Il6*, *Il15* and *Tlr4*, were differentially expressed across the recovery time points, with remarkably similar expression patterns demonstrated between the RyR1 mutant and wild-type mice. In EDL muscle, all three genes were upregulated after 1-hour recovery and had returned to baseline levels by 24-hours post heat exposure. This suggests a heat-induced activation of an acute-phase immune response, specific to glycolytic EDL muscle. Previous studies detected a transient rise in cytokines in wild-type mouse soleus 1-hour post 39.5˚C heat stress, but this study only observed an immune response in EDL muscle (Welc *et al.*, 2012, 2013). EDL muscle appears more sensitive to changes in heat than soleus, responding more rapidly to changes in environmental temperature. Detection of an immune response in mouse soleus, reported by Welc *et al.*, 2012 and 2013 was evident after exposure to higher ambient temperatures, which would likely trigger a stronger response detectable

in slow-twitch muscle fibres. Exercise has also been shown to upregulate muscle-specific *Il6* expression, where it is released as a myokine, stimulating an anti-inflammatory response in the absence of TNF-α (Muñoz-Cánoves *et al.*, 2013). Significantly higher levels of interleukin-6 are released from human myotubes harbouring *RYR1* mutations associated with CCD, where chronic elevation of Il6 is thought to promote muscle atrophy (Ducreux *et al.*, 2004; Treves *et al.*, 2011). In contrast, RyR1 R163C mice appear to display a normal immune response to heat prior to developing hypermetabolic episodes when compared their wild-type littermates. Expression of *Il10* was not detected in any of the samples, conflicting with a previous study which revealed upregulation of IL10 in response to heat stroke in wild-type mice (Welc *et al.*, 2013).

Expression of *Hspa1a* and *Hsp90aa1* were significantly higher in RyR1 mutant EDL muscle, although this difference was not observed in soleus samples. Exercise-induced heat shock proteins elicit diverse protective effects to restore cellular homeostasis and protect against ROS and heat damage by (Morton *et al.*, 2009; Dimauro, Mercatelli and Caporossi, 2016). Unfortunately, the overall similar expression profiles observed between the two genotypes suggests that the mutant mice were not under significantly greater heat stress than wild-type mice prior to their removal from the calorimetry chamber.

Adopting a candidate gene approach helped guide the selection of two appropriate recovery time points for whole-transcriptome analysis. Both the 1-hour and 24-hour groups revealed the greatest response to heat in the genes investigated so were chosen for RNA-seq. RNA-seq, as the name suggests, applies NGS methods to transcriptomics, and has transformed the capabilities of global gene expression studies (Wang, Gerstein and Snyder, 2009). As the cost of NGS technologies continue to fall, RNA-seq has become an affordable high-throughput method, which has overcome many of the limitations arising from traditional microarray approaches (Marioni *et al.*, 2008). RNA-seq is a count-based method and offers a higher degree of sensitivity than fluorescence-based microarrays by limiting background signal (Mortazavi *et al.*, 2008). By design, microarrays rely on probe sets to quantify expression and therefore only have the potential to identify known transcripts, whereas RNA-seq reads can be either mapped to a reference genome or assembled *de novo.* Microarrays also have a lower detection range than RNA-seq, with weak expression masked by background noise and the saturation of fluorescent signals limiting the detection of strongly expressed genes (Wang, Gerstein and Snyder, 2009). RNA-seq has the power to detect novel transcripts and alternative splice-variants, although differential expression analysis in this study

was performed at the gene-level (Hartley and Mullikin, 2016). Sequencing of mRNA libraries using Illumina® NGS platforms has proven reproducible, with low levels of technical variation identified between replicates distributed across lanes (Marioni *et al.*, 2008).

A sufficient read depth was obtained for the 24 samples from 2 lanes of the Illumina® HiSeq® 3000 sequencer, with an average of 33.4 million reads produced per sample. All libraries were pooled together and split across two lanes of a flow-cell to avoid a lane effect contributing to inter-group variation, although variation between lanes is thought to be low (Marioni *et al.*, 2008). All samples were run on the same flow-cell to prevent any sequencing batch effects, which could potentially mask true differences between the genotypes. 150 bp paired-end reads were chosen to increase the accuracy and sensitivity of alignment and quantification. The raw FASTQ files contained 137 GB of sequence data, presenting data storage as a limitation to be considered in addition to the trade-off between coverage and cost. RNA-seq studies present a number of bioinformatics challenges, requiring access to high-performance computer clusters to be able to process the large volume of sequence data.

Kallisto was chosen to pseudo-align sequenced reads to the mouse reference genome and estimate transcript abundances, offering a significantly faster approach requiring a fraction of the RAM necessary for traditional alignment tools, such as STAR and Bowtie/ Tophat (Bray *et al.*, 2016). Kallisto does not compromise on accuracy or sensitivity successfully pseudo-aligning and quantifying ~90% of reads across the 24 samples in this study. Kallisto was also a suitable alignment method for this study as it was designed to focus on looking for differential expression in known transcripts. Transcript abundance estimates were summarised to gene-level using the R package, Tximport because performing differential expression analysis at the gene-level has been shown to reduce technical biases, increasing accuracy and statistical power (Soneson C, 2016). Tximport corrects for potential differences in gene length across samples due to differential isoform usage, which would influence the absolute read count. Transcript abundance estimates have shown higher levels of variability than gene-level estimates due to unidentifiable transcripts caused by uneven coverage across genes (Soneson C, 2016). Read depth is also reduced when partitioning reads across expressed transcripts ultimately reducing the power to detect differential expression. Current transcript-level quantification tools do not correct for amplification bias, which would create errors in quantification estimates, further highlighting the advantage of gene-level analyses.
There is currently no consensus regarding an optimal pipeline for the analysis of transcriptomic data and each method has its limitations. The DESeq2 package was

chosen to perform differential expression analysis as it performed well when compared to alternative methods, offering a conservative and easy to use tool with good FDR error control (Soneson and Delorenzi, 2013). Selecting a conservative method comes at the cost of power to detect small expression differences in weakly expressed genes, although the differentially expressed gene lists produced are robust. DESeq2 assumes a negative distribution when fitting a GLM to each gene, which is more appropriate for count data, rather than applying methods, which assume normal distribution (Anders and Huber, 2010; Love, Huber and Anders, 2014). The Empirical Bayes shrinkage approach used to estimate gene-wise dispersion and weight log fold-changes (LFCs) takes into account the heteroscedasticity of RNA-seq count data, ranking genes based on estimation of effect sizes. A similar weighting strategy is taken by the voom-limma approach, although this is performed on log-transformed counts normalised for library size (Law *et al.*, 2014). By penalising LFC estimates for genes with high levels of variation, false discovery rates are reduced and gene lists become more biologically relevant. The incorporation of GLMs into the DESeq2 tool allows complex experimental designs to be defined, not limiting studies to simple pair-wise comparisons like in the Cufflinks package (Trapnell *et al.*, 2012).

The Benjamini-Hochburg (BH) procedure was used to correct for multiple testing during differential expression analysis of RNA-seq data, controlling the FDR (Benjamini and Hochberg, 1995). There are several alternative correction methods, such as the conservative Bonferroni procedure, which controls the family-wise discovery rate, but when considering whole-transcriptome studies Bonferroni has less statistical power. Adjusting *p* values with the BH method has become standard practice for RNA-seq analyses and has been incorporated into the DESeq2 package as the default correction method (Storey and Tibshirani, 2003; Love, Huber and Anders, 2014). Statistical power is further increased by removing genes with mean normalised counts below a filtering threshold prior to statistical testing and FDR correction.

A principal component analysis revealed that the transcriptional profiles of untreated wild-type mice were distinct from the remaining groups. This highlighted the group as an outlier, posing subsequent analytical difficulties, with no reliable baseline measurement for the wild-type genotype. The RyR1 wild-type mice selected for the untreated baseline group were ~1 month older than the other mice, which may account for their differential global gene expression profiles. Other factors, such as stress levels and cage temperature could also set the RyR1 wild-type mice apart from the other mice included in the study. The distinct grouping of untreated wild-type samples on the PCA plot could also represent authentic differences arising from differences in metabolism

between untreated wild-type and RyR1 mutant mice. The RyR1 mutant mice at baseline may exhibit signs of metabolic stress, which are similar to the heat exposure responses observed in all other mice in the study. Untreated wild-type mice may therefore be the only group with transcriptomes truly representative of a baseline state in the C57BL/6 mouse strain. An additional study investigating baseline expression differences between supplementary RyR1 wild-type and R162C mutant mice would be required to determine the origin of this biological variation.

Global gene expression profiles were similar between the two genotypes at both 1-hour and 24-hours post-acute heat stress, suggesting that at a whole-genome level all treated mice respond similarly to heat. These data are consistent with the candidate gene expression responses investigated by TaqMan® real-time PCR, which showed similar responses between RyR1 wild-type and mutant mice. Again, more genes were differentially expressed 1-hour post-acute heat stress than after 24-hours recovery at room temperature. Interestingly, *Hsp90aa1* was one of nine genes highlighted as differentially expressed between the genotypes 1-hour post-heat exposure and was detected at higher levels in the mutant mice. This gene was also included in the candidate gene approach, with the same pattern observed in both soleus and EDL muscle. *Cyp2f2* gene expression was lower in mutant mice after 1-hour recovery and encodes a monooxygenase (cytochrome P450, family 2, subfamily F, member 2), which functions to metabolise potentially toxic compounds (Li *et al.*, 2011). The differential regulation of this gene has not previously been associated with a heat stress phenotype. *Atp1b4* expression was significantly higher in the mutant mice at the 1-hour time point. This gene encodes a member of the Na/K-ATPase family, which function as ion pumps in skeletal muscle; however, the *Atp1b4* isoform is thought to have lost its function at a β-subunit and now acts as a transcriptional co-regulator during muscle development (Pestov *et al.*, 2007). *Hdac9* expression was significantly lower in the mutant mice after 24-hours recovery at room temperature and is thought to inhibit skeletal muscle myogenesis, therefore suggests an increase in muscle regeneration in the RyR1 R163C mouse soleus.

An important limitation to consider is that the experimental design did not address the exertional element of heat illness but rather investigated the passive effects of heat stress. The pathophysiology of EHI is thought to differ from classic heat illness, with a wild-type EHI mouse model demonstrating accelerated heat injury, with additional features such as multiple-organ injury and significant muscle damage featuring rhabdomyolysis (King *et al.*, 2015) The C57Bl/6 mice in the study by King and colleagues reached core temperatures of up to 42.5°C and exercised until they became

unconscious. A study directly comparing passive and exertional heat stress demonstrated that exercise-induced hyperthermia develops more quickly and to a higher degree than passive hyperthermia (Hubbard *et al.*, 1977). The active group of rats exhibited a higher mortality rate at lower thermal loads than the inactive group. The core temperature cooling rate of survivors was also slower in EHI rats. Applying an exertional experimental design to the heat sensitive heterozygous RyR1 R163C mice would risk the development of fatal hypermetabolic episodes prior to the recovery period.

When using mouse models, it is important to consider the fundamental differences between humans and mice when inferring the biological significance of data. As discussed, brown fat thermogenesis may modify the heat stress response in mice and may not relate directly to the human heat stress response. Mice have markedly higher levels of brown adipose tissue than humans, which is central to their thermoregulation capacity, although the significance of this mechanism in response to heat stress is unknown. It is also important to remember that the thermoneutral zone is higher in mice than humans, so temperatures triggering heat stress in mice cannot be directly related to humans.

The previously assumed correlation between mRNA and protein levels has been disputed in recent years, highlighting the need to confirm findings from gene expression studies by quantifying protein levels for genes of interest (Koussounadis *et al.*, 2015). Although individual proteins can be quantified with various methods, such as western-blots, enzyme-linked immunosorbent assays (ELISAs), mass spectrometry and more recently TaqMan® Protein Assays, high throughput technologies have also been developed to screen whole proteomes, including DEEP SEQ mass spectroscopy (Zhou 2013).

This study aimed to uncover underlying differences in the response to heat in RyR1 R163C mutant and wild-type mice by measuring changes in gene expression over a 24-hour recovery period. Both mouse genotypes responded similarly to heat at the transcriptional-level, suggesting that heat stress response in RyR1 mutant mice is similar prior to the development of a hypermetabolic reaction. RyR1 R163C mutant mice revealed higher metabolic rates than wild-type mice at thermoneutral temperatures. If these mice are subject to basal metabolic stress, they may have adapted to tolerate mild heat stress and therefore their gene expression profiles would not differ from wild-type mice. With only four mice per group it is also possible that there was not significant power to detect different expression between the genotypes. Thus, an optimised

experimental design would be to increase the sample size and refine the temperature exposure times to ensure that sufficient heat stress levels were reached prior to recovery. Using a heat-sensitive mouse model harbouring a variant that has been associated with exertional heat illness in humans offers great potential to investigate this poorly understood condition. Study parameters need to be further refined, with a detailed investigation of the heat response in these mice over a range of temperatures. Knock-in mouse models offer a powerful tool to investigate the pathophysiology of exertional heat illness, particularly as so little is known at both the phenotypic and genotypic level.

4 Global gene expression profiles in response to acute heat stress in patients with malignant hyperthermia and exertional heat illness

4.1 Introduction

A lack of understanding of the link between EHI and MH susceptibility stems from the limited access to well characterised EHI patients and the poor documentation and follow-up of civilian EHI cases. This has restricted research to clinical case studies and retrospective genetic investigations of known MH mutations (Tobin *et al.*, 2001; Fiszer *et al.*, 2015). In addition, little is known about the exercise capacity and heat tolerance of MH susceptible individuals due to the absence of a publicly available diagnostic test for EHI susceptibility to determine thermoregulatory capacity. Of the EHI patients who were characterised by IVCT for an underlying muscle defect, 35% demonstrated an abnormal contracture response to RyR1 agonists, caffeine and halothane (Chapter 2.2.1, Table 2.1).

Previous studies have made attempts to characterise the exercise tolerance and thermoregulatory capacity of MH susceptible patients. These studies compared core temperature and metabolite levels in MH susceptible patients with those of fitness matched controls (Campbell *et al.*, 1983; Green *et al.*, 1987). During progressively intensive exercise, body temperature recorded in the ear canal, was higher in the MH susceptible patients, in contrast to measurements taken at the thumb, which showed a delayed rise in temperature in the same patients. This was attributed to a delay in the onset of vasodilatation in these individuals. Serum free fatty acids, cortisol and blood lactate were all higher in the MH susceptible patients, highlighting an underlying metabolic disturbance in these individuals during intense exercise (Campbell *et al.*, 1983). Interestingly, the same differences were not observed during mild exercise (Campbell *et al.*, 1983; Green *et al.*, 1987). These studies were performed at room temperature and therefore these subjects were not challenged with environmental heat stress.

Exercise capacity and muscle energy metabolism has also been measured in military personnel recovering from EHI episodes, featuring hyperthermia (≥40°C), neurological impairment and rhabdomyolysis (Vanuxem *et al.*, 2001). The EHI group revealed lower VO_2 max scores and lower maximal workloads than healthy controls during maximal

exercise on a cycloergometer, more than 5 months after they presented with EHI. They also demonstrated a limited thermoregulatory capacity, with higher body temperature post-exercise than the healthy controls. Plasma free fatty acids, glycerol and blood lactate levels were also significantly higher in the EHI patients during and after exercise, suggesting increased lipolysis and impairment of the OXPHOS pathway.

The INM's heat tolerance test measures an individual's capacity to thermoregulate when subjected to exertional heat stress and is performed following a standardised protocol at the heat illness clinic (HIC), INM (Roiz de Sa and House, 2015). In brief, each subject completes a VO_2 max test, to calculate maximal oxygen consumption as a measure of aerobic fitness so that the HTT parameters can be adjusted relative to fitness capacity. Both the VO_2 max test and HTT are performed within a heat-controlled chamber set to 34°C (dry bulb temperature) with 40% relative humidity, producing a wet bulb globe temperature (WBGT) index of 27°C. Volunteers exercise at 60% of their VO_2 max on a treadmill while carrying a 14kg Bergen and full military kit for the first 30 minutes. Their Bergen and jackets are removed as they continue to walk for a further 15 minutes. After 45 minutes, their t-shirts are removed and they continue until a plateau in rectal temperature is observed or 90 minutes has passed. If rectal temperatures reach 39.5°C, they are removed from the chamber and actively cooled. The HTT is routinely used to characterise the thermoregulatory capacity of military personnel who have experienced a clinical EHI episode and has proved effective at identifying those with an underlying muscle defect.

The exact sensitivity and specificity of the HTT has not been calculated due to the absence of a validated diagnostic test for EHI susceptibility, although there have been concerns regarding the sensitivity of the HTT at the INM's HIC. There have been examples of EHI military personnel who effectively thermoregulate during assessment and later develop a second case of EHI and go on to demonstrate an abnormal skeletal muscle contracture by IVCT (Roiz de Sa, personal communication 2013). There is only one other HTT protocol of its kind, developed by the Israeli Defence Forces (IDF) (Moran *et al.*, 2004). British and Israeli protocols have been tailored to emulate the environmental conditions and exercise intensities at which EHI commonly occurs in the specific military population. This study developed in collaboration with the INM and in agreement with the MoD hypothesised that MH susceptible individuals produce more metabolic heat during exercise due to elevated basal cytosolic Ca^{2+} levels and therefore will be at increased risk of developing EHI.

Humans activate a number of physiological mechanisms to effectively thermoregulate, including vasodilation, sweating and adjusting metabolic heat production (Sawka, Wenger and Pandolf, 2010). During exercise, heat production dramatically increases due to the inefficient thermodynamics of muscle contraction, with a large proportion of mechanical energy lost as heat (Krustrup *et al.*, 2003). Heat gain triggers heat dissipation mechanisms, with elevated environmental temperatures reducing the rate of heat loss (Sawka *et al.*, 2011). If thermal equilibrium is not established and heat storage continues to exceed heat dissipation, exertional heat illness and ultimately exertional heat stroke will arise. A number of intrinsic and extrinsic factors are thought to contribute to the final clinical phenotype (Moore *et al.*, 2016). Despite the complex nature of EHI some aerobically fit individuals fail to thermoregulate on numerous occasions, suggesting the existence of an underling metabolic defect or heat dissipation deficiency. A predisposing susceptibility to EHI is particularly likely when only one case is observed out of hundreds or thousands participating in an endurance activity.

It is widely accepted that EHI, which advances to EHS triggers a systematic inflammatory response, which can lead to multi-organ failure and death in extreme cases (Bouchama and Knochel, 2002; Sawka *et al.*, 2011). Molecular studies on human EHI patients however are limited, with the few existing studies finding it difficult to dissociate the EHI immune response from the normal effects of exercise and heats stress (DuBose *et al.*, 2003; Sonna *et al.*, 2004). Elevated release of pro-inflammatory cytokines have been detected in EHI patients relative to exertional controls (Lu *et al.*, 2004). In contrast, IL-6 has been labelled as an exercise-induced anti-inflammatory myokine and is secreted at significantly higher levels in human myotubes harbouring *RYR1* mutations, suggesting a direct link to Ca^{2+} homeostasis (Ducreux *et al.*, 2004; Nielsen and Pedersen, 2007). As discussed in chapter 3.1, a skeletal muscle cytokine response, including IL-6, was also detected in a mouse model of environmental heat stroke (Welc *et al.*, 2013).

This study will utilise the standardised heat tolerance test developed by the INM, to determine whether a cohort of MH susceptible patients can effectively thermoregulate alongside a group of EHI and control military personnel. This research also aims to explore global gene expression profiles extracted from a cohort of MHS, EHI and control volunteers. A snapshot of peripheral blood RNA will be captured pre-HTT, 2-hours post and 24-hours post-HTT and aims to uncover the status-specific responses to exertional heat stress in addition to baseline differential expression between the groups. Ethical approval by the Ministry of Defence Research Ethics Committee (MODREC) offers a unique opportunity to explore the heat tolerance capacity of civilian MH patients carrying

a familial *RYR1* variant and will allow the investigation of the transcriptional exertional heat stress response in individuals with two related hypermetabolic conditions, MH and EHI.

4.2 Materials and methods

4.2.1 Experimental design

The human HTT study was completed at the heat illness clinic, located at the INM. The study was developed in collaboration with Dr Daniel Roiz De Sa and Carol House and approved by MODREC, approved protocol number: 647/MODREC/15. Patients were recruited into groups based on their clinical phenotype and included 6 members of the armed forces who had presented with EHI, 6 healthy military personnel and 6 MHShc patients referred from the Leeds MH cohort who were age, sex and fitness-matched to the military volunteers. The EHI recruits demonstrated a range of phenotypes, including collapse, loss of consciousness and hyperthermia. Individuals recruited into the MH susceptible group were either MH index cases or family members but had all displayed a positive contracture by IVCT and carried a genetic variant in the *RYR1* gene. An additional EHI volunteer was recruited at a later stage due to technical issues obtaining core temperature and sweat measurements from a member of the original EHI cohort. All subjects were male, aged 18-40 years old, with a good base level of fitness.

All 19 volunteers underwent the INM's heat tolerance test, according to the HIC's standardised protocol (Roiz de Sa and House, 2015), carried out by exercise physiologists in survival and thermal medicine including Carol House and overseen by Dr Dan Roiz de Sa at the INM. Measurements of heart rate, core (rectal and intestinal) and skin temperature, heat flow data, blood flow data, and sweat capsule data were recorded at 1 minute intervals throughout the test. All HTT data were provided by Carol House. Blood samples for global gene expression analysis were collected into PAXgene® Blood RNA tubes (PreAnalytiX® GmbH) at three time points (baseline, 2-hours and 24-hours) and stored at -20°C in the HIC facility prior to transfer to the Leeds MH Investigation Unit to be processed.

4.2.2 Statistical analyses and visualisation of HTT output

Age, relative sweat rates and VO_2 max data were tested for normality using the Shapiro-Wilk test built into the IBM® SPSS® Statistics package (version 24). Non-normal data were log-transformed and re-tested for normality prior to statistical analysis. Log-transformed age and relative sweat values were compared between EHI, MH and control groups using the one-way ANOVA test within the SPSS® software, whereas VO_2 max scores were compared using the non-parametric Independent-Samples Kruskal-Wallis test. Physiological data were visualised using the 'ggplot2' package in the Rstudio software.

4.2.3 RNA extraction and quantification

RNA was extracted from the fifty-seven whole blood samples using PAXgene® Blood RNA kits (PreAnalytiX® GmbH) according to the manufacturer's instructions. Briefly, samples were centrifuged at 3,000 x *g* for 10 minutes at room temperature to pellet the contents of the PAXgene® tubes. The pellets containing the RNA fraction were resuspended with a lysis buffer, proteins were digested with proteinase K and samples were filtered through PAXgene® Shredder spin columns by centrifugation. The flow-through fractions were mixed with ethanol and RNA was selectively bound to the silica membranes within the PAXgene® RNA spin columns. The bound RNA was washed and purified, residual DNA was digested with DNase 1 and RNA was eluted and store at -80°C.

Purified RNA samples were quantified and quality checked using Agilent's RNA ScreenTape assay and 2200 TapeStation instrument (Agilent technologies, Santa Clara, CA, USA) according to the manufacturer's instructions. RNA integrity numbers (RIN) equivalent to Agilent's Bioanalyzer 2100 system (RIN^e) were calculated by the TapeStation software as a measure of RNA quality.

4.2.4 TruSeq® Stranded mRNA library preparation

All fifty-seven purified RNA samples extracted from whole blood were included in the whole-transcriptome analysis by RNA-seq. Libraries were created by staff at the on-site NGS facility using the TruSeq Stranded mRNA library preparation kit (Illumina®), according to the manufacturer's instructions as described in Chapter 3, section 3.2.6.

Libraries were then quantified and quality checked using Agilent's High Sensitivity RNA ScreenTape assay and 2200 TapeStation instrument (Agilent technologies, Santa Clara, CA, USA) according to the manufacturer's instructions.

4.2.5 Illumina® HiSeq® NGS

Equimolar concentrations of each mRNA enriched cDNA library were pooled and sequenced across seven lanes of Illumina's HiSeq® 3000 platform, according to the manufacturer's instructions, as described in chapter 3, section 3.2.7. The 150 bp paired-end reads were de-multiplexed to produce a forward and reverse FASTQ file for each sample. Sequencing was performed by the Leeds University NGS facility, located at St. James's University Hospital, Leeds.

4.2.6 Differential gene expression analysis

Sequence data were processed using the MARC1 high-performance computer cluster remotely and imported into Rstudio 1.0.136 to perform differential gene expression analysis using the DESeq2 package (v.1.15.2), as described previously in Chapter 3.2.8 and summarised in Figure 3.3. Firstly, baseline differences in gene expression between the MH and EHI status groups relative to controls were identified by performing specific pairwise comparisons. Two distinct questions were then asked of the dataset by firstly using an interaction term to identify genes that responded differently to exertional heat stress between the status groups (Figure 4.1a) and secondly by identifying genes that represented a threshold response model whereby they were differentially expressed between status groups and across the recovery time points (Figure 4.1b). Finally, the general heat stress response regardless of phenotype was investigated by identifying differentially expressed genes at both recovery time points relative to baseline expression.

Samples were also re-grouped into 'heat tolerant' and 'heat intolerant' phenotype groups based on their ability to thermoregulate during the HTT. The same analyses were performed on these data, although with only four volunteers failing to thermoregulate during the HTT, the results have not been presented in this thesis.

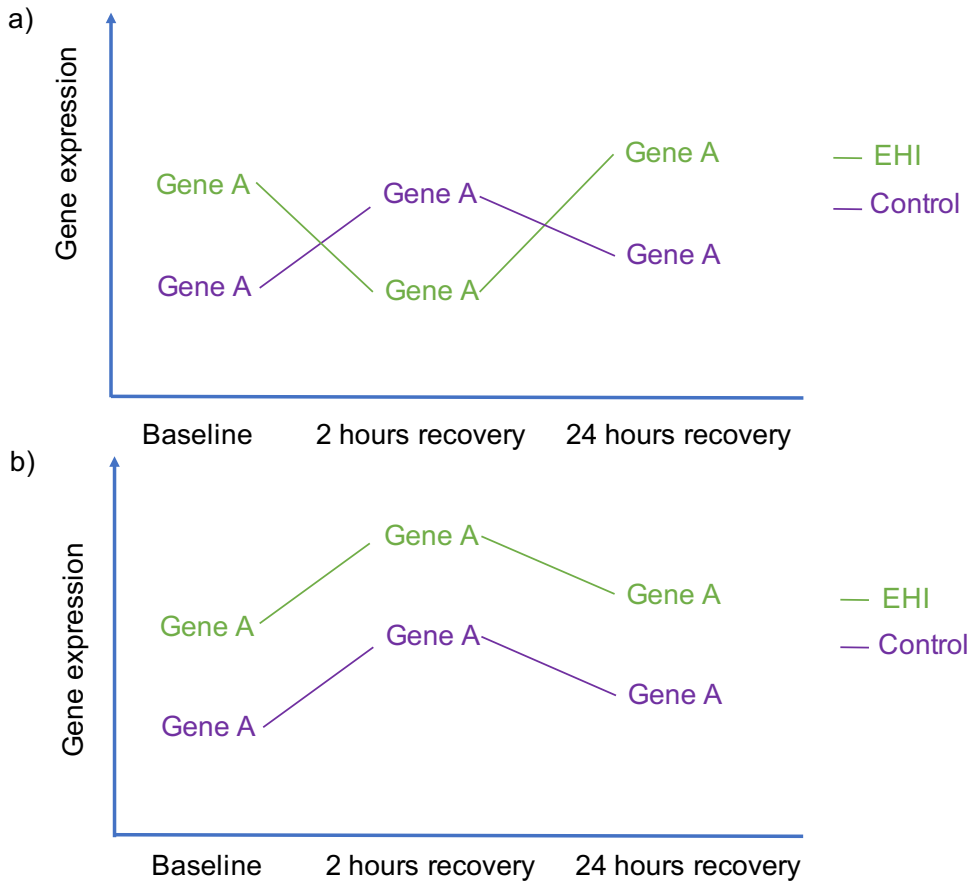

Figure 4.1: Alternate transcriptional response patterns identified using DESeq2 generalized linear models. a) Status-specific response model using the interaction term, status:timepoint b) Threshold response model.

1. Differentially expressed genes at baseline

A GLM was designed by defining the nine specific groups within the analysis and specifying 'group' as the factor in the design formula. The nine groups included control_baseline, control_2hrs, control_24hrs, EHI_baseline, EHI_2hrs, EHI_24hrs, MHS_baseline, MHS_2hrs and MHS_24hrs. The pair-wise group comparisons allowed the detection of differentially expressed genes at baseline. Gene lists were ranked by FDR-adjusted *p*-values and exported from DESEq2 into Microsoft Excel spread sheets.

2. Status-specific responses to heat stress

An alternative model was designed to investigate the status-specific response to heat stress. Two factors were defined prior to fitting a GLM to each gene, specifically status and time point. Status included three distinct phenotype categories; EHI, MH and control, while three different time points were included in the analysis; baseline, 2-post HTT and 24-hours post-HTT. The multi-factor design formula included three terms; status, time point and the interaction between the two. The interaction term allowed

comparisons between the status groups across the two recovery time points and therefore determined genes characteristic of a status-specific response to exertional heat stress. Extracting the interaction term from the model produced four lists of differentially expressed genes (log2 fold-changes) ranked by FDR-adjusted *p* values including:

Status group comparison	Time course
MH vs control	Baseline to 2 hours
EHI vs control	Baseline to 2 hours
MH vs control	Baseline to 24 hours
EHI vs control	Baseline to 24 hours

3. Threshold model of heat stress

To determine genes that represented treatment-specific responses that may elicit a pathogenic effect at a critical threshold level a combination of the first two models were used to produced gene lists. Specifically, genes that were differentially expressed in response to the HTT and also differentially expressed between the status groups at 2-hours and 24-hours post-HTT were highlighted as candidate genes fitting a threshold response model. Genes representing a threshold response model may follow the same expression pattern but still differ between the status groups at each time point due to inherent baseline differences in expression.

4. General heat stress response

Finally, to investigate the general heat stress response, the 'timepoint' term was extracted from the model to identify genes differentially expressed from baseline to 2-hours and baseline to 24-hours. Gene lists were ranked by FDR-adjusted *p* values.

4.2.7 Functional annotation of differentially expressed genes

All differentially expressed gene lists (FDR adj. *p* value <0.05) were annotated with functional information obtained from two bioinformatics resources, the Database for Annotation, Visualization and Integrated Disovery (DAVID) and Go Ontology's Protein ANalysis THrough Evolutionary Relationships (PANTHER) classification system (Dennis *et al.*, 2003; Huang, Sherman and Lempicki, 2008). Both databases allow genes lists to be uploaded and classified according to molecular function, biological processes and pathways. A more comprehensive pathway analysis was completed using

GeneGo's MetaCore™ package provided by Thompson Reuters (version 6.32). MetaCore™ is an integrated software package that allows functional analysis of high throughput data, producing pathway maps to aid interpretation of gene lists. Gene lists were uploaded and processed by performing an enrichment analysis in pathway maps to determine which pathways were most significant in these data. Pathway schematics were exported from the software as .pdf files.

4.2.8 Gene expression signatures predictive of MH susceptibility in human blood post-acute heat stress

A penalised regression model incorporating Least Absolute Shrinkage and Selection Operator (LASSO) penalties was fitted to each gene to determine whether there was a gene expression signature predictive of MH susceptibility. Specifically, a generalised linear model was fitted to gene expression data from blood samples of MH and control individuals at baseline. The estimated regression coefficients were shrunk towards zero using LASSO penalties to prevent overfitting (Tibshirani, 1996). For the subset of genes identified as predictive of MH susceptibility, a risk score was calculated using their shrunken regression coefficients. Predictive modelling was implemented using the 'penalized' package in Rstudio 1.0.136 (Goeman, 2010) on rlog transformed expression data, which had been normalised for differences in library size and transcript length. Expression data were used as input in Rstudio and had been extracted from DESEq2 and saved as a matrix.

Prior to fitting a penalised regression model, the lambda 1 (L1) tuning parameter was optimised using the optL1 function within the 'penalized' package. The L1 value controls the strength of the penalty and is specified when performing penalised estimation using the 'penalized' function. The L1 parameter was estimated based on the dataset of interest, in this case, a matrix of expression data. A small lambda 2 (L2) value was also specified (1e-10) to bypass an error in the optL1 and penalized functions due to the high-dimensionality of the data. The penalised regression model with L1 and L2 tuning parameters specified was fitted to these expression data.

The genes with non-zero coefficients were used to create a formula to calculate an MH susceptibility risk score for each sample, which included the sum of expression values weighted by the regression coefficients for all predictive genes. The risk score should effectively distinguish between MH susceptible and control individuals. The 'eval'

function was used to specify the formula and calculate risk scores using the expression strength of all predictive genes. Risk scores were plotted in Rstudio to determine a range of scores that distinguish the heat-stress response in MH susceptible individuals from controls.

4.2.9 Sample size calculation for RNA-seq

A sample size calculation was performed for future work, which aimed to expand sample numbers in each status group to provide clearly defined phenotypes prior to gene expression analyses. The 'ssizeRNA' package in R was used to calculate a basic estimation of sample size required to reach a power of 0.8. The calculation produces a simplified estimation, making the assumption that all genes share the same average read count, equal dispersion and fold change across each group. The number of genes to be tested was set to 20,000, the proportion of non-differentially expressed genes as 0.8, the average read count for each gene as 50, dispersion as 0.1, fold-change as 2, the FDR level as 0.05 and the desired power as 0.8. This produced an estimated sample size of 9 for each group and time point required to reach a power of 0.86. Power versus sample size was plotted for visual interpretation.

4.3 Results

4.3.1 Heat tolerance test phenotypes

Eighteen male volunteers were initially recruited to undergo heat tolerance testing at the INM, including six MH susceptible individuals characterised IVCT, six military personnel who had experienced an EHI episode and six fit and healthy control volunteers. An additional individual was recruited into the EHI group as there was a technical issue recording core temperature in one of the original recruits. The subjects recruited were aged 21-40, with no significant difference observed between the cohorts of EHI, MH and control volunteers (One-way ANOVA of log-transformed values, *p* value 0.15). One control recruit however, was 40 years old and 5 years older than all other subjects (Figure 4.2).

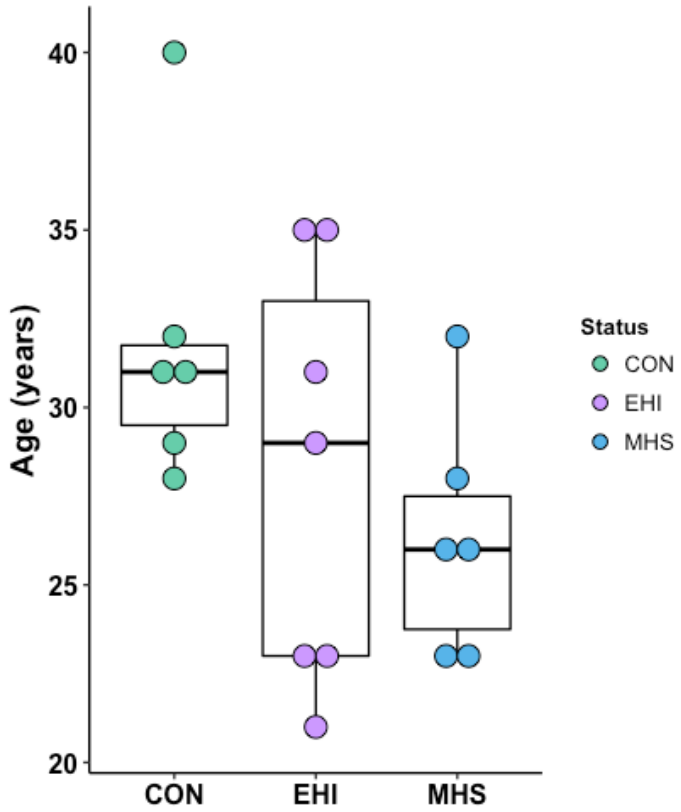

Figure 4.2: Age distribution of volunteers recruited into the INM HTT study across control, EHI and MH phenotype groups. Boxplots represent the median, interquartile ranges (IQRs) and 1.5X the IQR (whiskers).

Of the nineteen volunteers who were tested, four demonstrated an inability to thermoregulate with no plateau observed in rectal temperature prior to reaching a rectal temperature of 39.5°C (Figure 4.3). Two of these individuals were from the EHI group, one was from the MH group and one from the control group. The control volunteer who appeared heat intolerant reached a core temperature of 39.5°C, although the rate of rise was slowing towards a plateau as the test was completed, visible in Figure 4.3. The remaining fifteen individuals could effectively thermoregulate and achieve a plateau in core temperature. All four individuals who failed to thermoregulate during the HTT and who were subsequently classified heat intolerant (HI) had reached a core temperature of 39°C by 50 minutes, and from that point onwards remained higher than the remaining recruits who displayed a normal thermoregulatory response (Figure 4.3). Of the heat intolerant volunteers, two reached a rectal temperature of 39.5°C 50 minutes into the test, whereas the other two HI recruits took 75 minutes to reach the 39.5°C threshold.

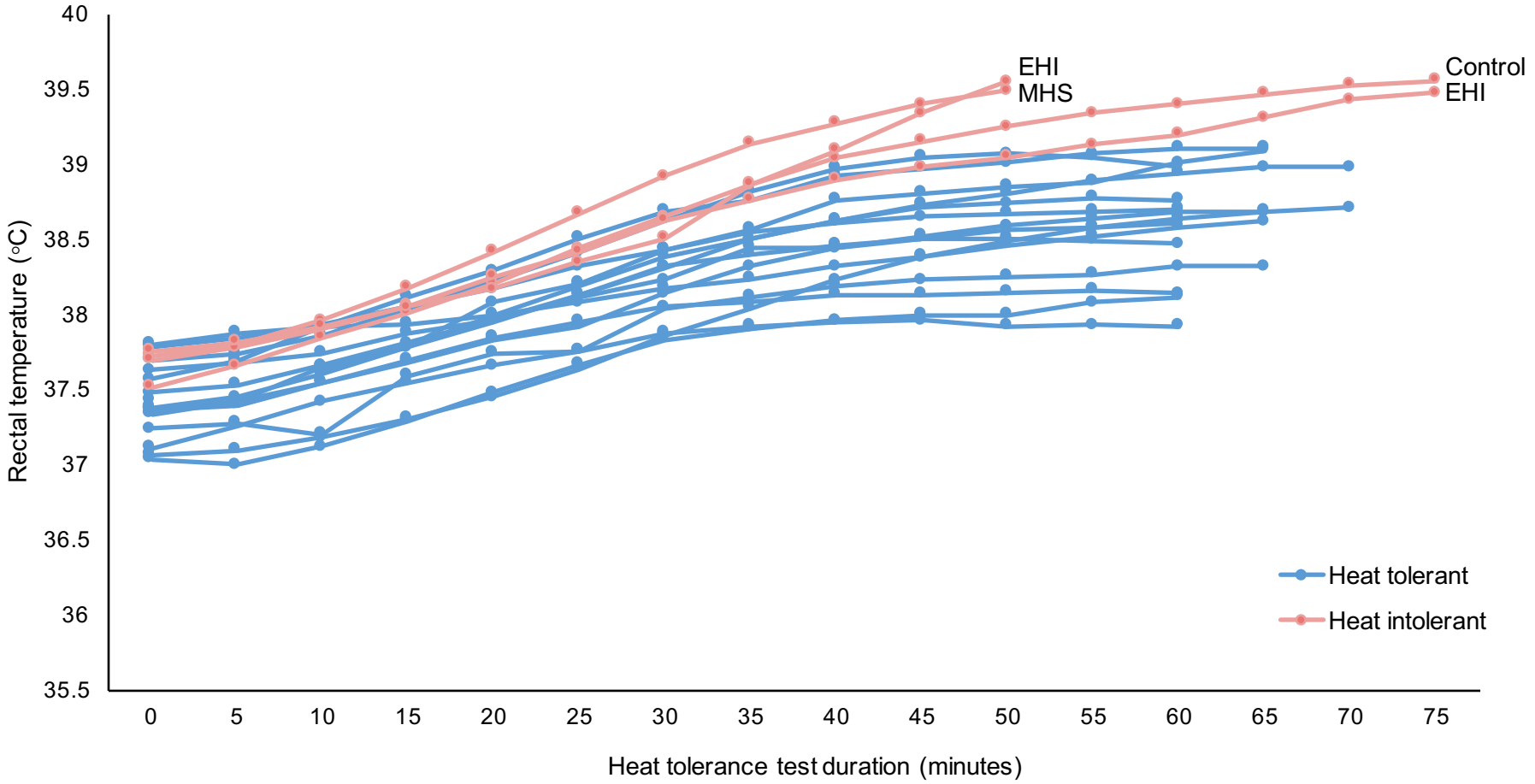

Figure 4.3: Rectal temperatures of volunteers who passed and failed the INM's heat tolerance test during the exertional heat stress study.

All volunteers demonstrated good fitness levels with relative maximal oxygen consumption rates (VO_2 max) ranging from 42.3 to 67.7 $mL.min^{-1}.kg^{-1}$. There were no significant differences between VO_2 max scores of EHI, MH and control individuals (Independent-Samples Kruskal-Wallis Test *p* value 0.465) (Figure 4.4). The MH group showed the greatest variation in fitness capacity, although four of the six MH susceptible civilians recruited into the study demonstrated very high VO_2 max scores.

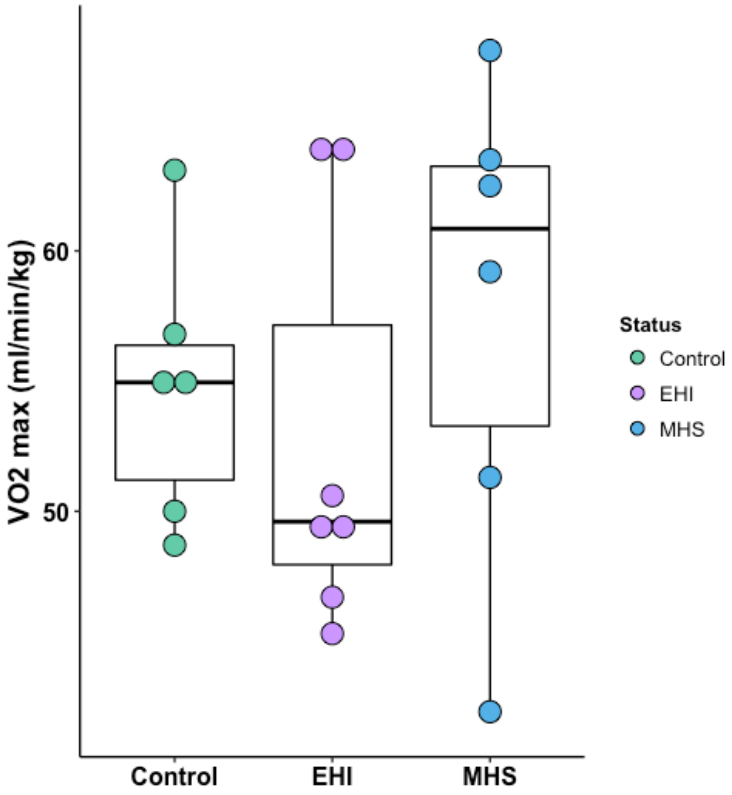

Figure 4.4: Comparison of relative maximal oxygen consumption rates between EHI, MH and control volunteers. Boxplots represent the median, interquartile ranges (IQRs) and 1.5X the IQR (whiskers).

Plotting the sweat rate of individuals during their HTTs against their VO_2 max capacity revealed a positive correlation between the two variables (Pearson's 2-tailed correlation *p* value 0.046) (Figure 4.5). Low sweat rates correlated with low VO_2 max scores in contrast to high sweat rates corresponding to high VO_2 max scores. It is important to remember that exercise intensity during the HTT was adjusted relative to the patient's fitness capacity and therefore recruits with higher maximal oxygen capacities sustained higher absolute workloads.

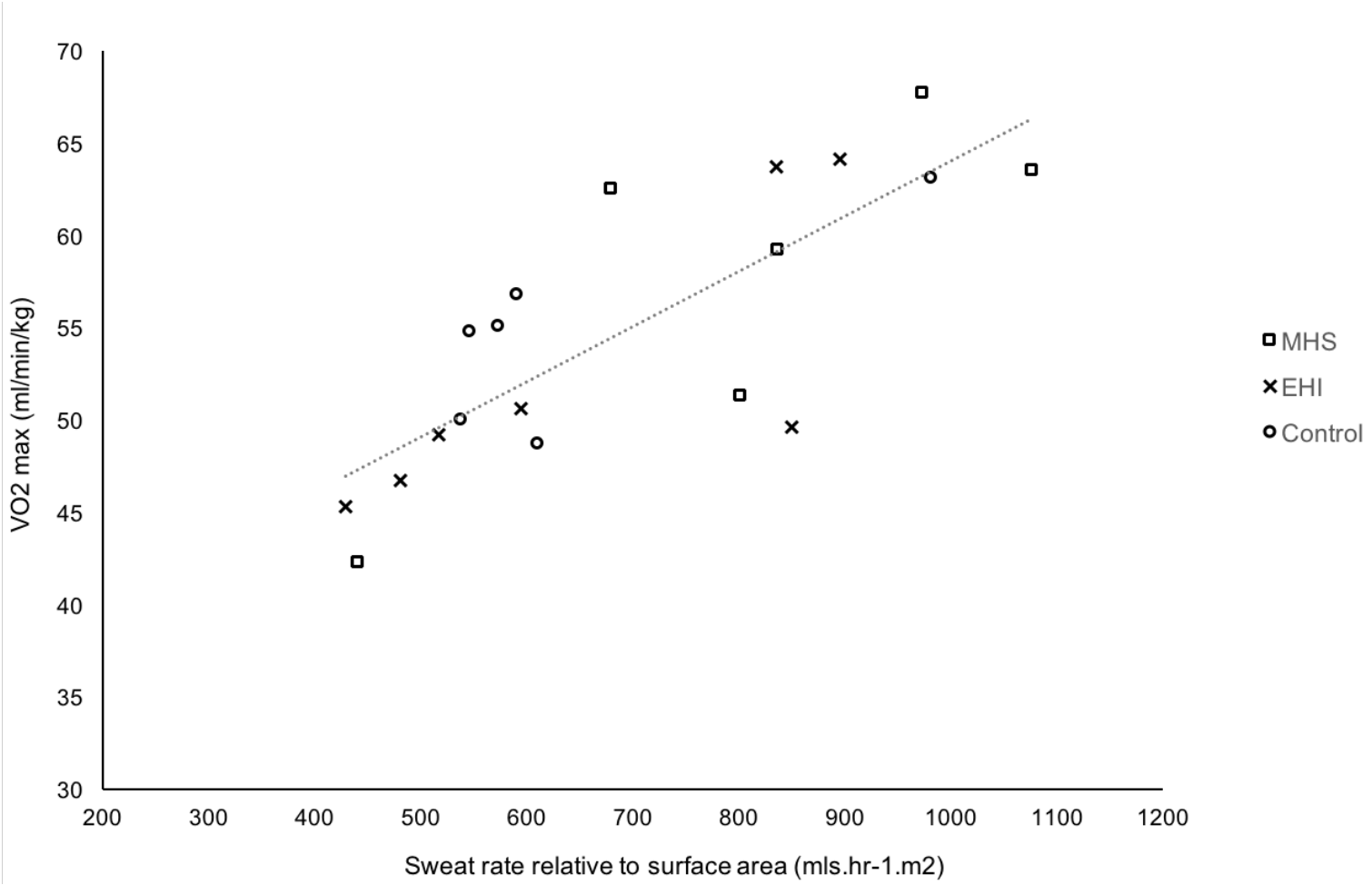

Figure 4.5: Individual sweat rates plotted against VO_2 max scores.

To account for differences in physical workload, which would affect heat production and subsequently sweat production, sweat rates were normalised relative to VO_2 max scores and presented beside average sweat rates for comparison (Figure 4.6). Average sweat rates relative to fitness levels were compared between EHI, MH and control groups and revealed no significant differences in sweat production (One-way ANOVA on log-transformed values *p* value 0.34). All four individuals who failed the HTT demonstrated adequate sweat rates relative to the heat tolerant volunteers.

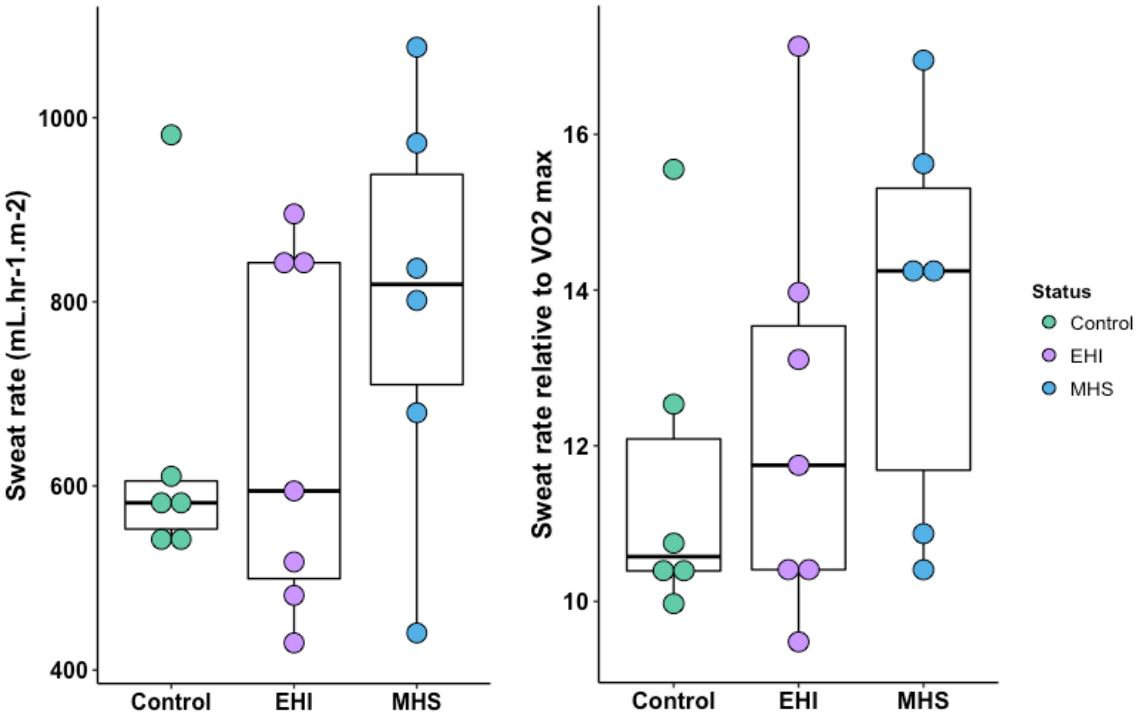

Figure 4.6: Individual sweat rates during heat tolerance testing. a) Relative sweat rates, b) Relative sweat rates adjusted for VO_2 max fitness. Boxplots represent the median, interquartile ranges (IQRs) and 1.5X the IQR (whiskers).

4.3.2 Global gene expression profiles of EHI, MH and control volunteers in response to exertional heat stress

4.3.2.1 Quality metrics and DESeq2 model parameters

All fifty-seven samples generated good quality libraries for sequencing producing an average of 48.2 million reads per sample (SD ± 4.5 million) (Table 4.1). On average 88.6% sequenced reads (SD ± 2.5%) were successfully pseudo-aligned and quantified by Kallisto against the 178,146 annotated transcripts from the human reference genome (GRCh38) (Table 4.1). Each volunteer had three blood samples taken pre-HTT (P), immediatetly post-HTT (M) and 24-hours post-HTT (F).

Table 4.1: Kallisto pseudo-alignment mapping efficiency.

Sample ID	Processed reads	Pseudo-aligned reads	Reads mapped (%)
CON1_F	52,872,091	46,350,582	87.7
CON1_M	45,375,837	40,696,713	89.7
CON1_P	39,665,068	36,253,319	91.4
CON2_F	56,847,952	49,670,472	87.4
CON2_M	53,135,213	48,049,892	90.4
CON2_P	51,042,730	46,056,332	90.2
CON3_F	47,126,809	41,975,811	89.1
CON3_M	52,416,707	45,633,566	87.1
CON3_P	51,274,438	45,531,688	88.8
CON4_F	48,399,007	43,356,989	89.6
CON4_M	50,197,033	42,579,065	84.8
CON4_P	41,908,370	38,190,408	91.1
CON5_F	46,484,353	40,937,276	88.1
CON5_M	49,171,069	41,519,831	84.4
CON5_P	50,587,379	44,639,812	88.2
CON6_F	32,906,159	30,218,629	91.8
CON6_M	47,433,970	43,098,523	90.9
CON6_P	50,125,272	46,160,269	92.1
EH1_F	49,628,465	40,636,568	81.9
EH1_M	47,235,107	41,605,874	88.1
EH1_P	42,747,595	39,191,417	91.7
EH2_F	51,495,050	44,068,312	85.6
EH2_M	47,832,409	41,038,450	85.8
EH2_P	45,783,093	38,471,647	84.0
EH3_F	49,172,959	41,912,032	85.2
EH3_M	40,259,751	36,037,864	89.5
EH3_P	48,645,796	43,217,781	88.8
EH4_F	53,645,309	49,800,942	92.8
EH4_M	56,112,986	50,663,173	90.3
EH4_P	53,352,902	49,069,084	92.0
EH5_F	58,606,461	51,236,551	87.4
EH5_M	55,465,114	49,894,427	90.0
EH5_P	53,474,752	48,904,279	91.5
EH6_F	48,705,185	43,284,671	88.9
EH6_M	44,196,603	40,026,274	90.6
EH6_P	48,219,589	44,840,312	93.0
EH7_F	48,541,067	43,231,525	89.1
EH7_M	47,128,285	41,856,415	88.8
EH7_P	44,051,727	39,980,809	90.8
MH1_F	47,155,294	42,107,087	89.3
MH1_M	46,514,550	41,368,156	88.9
MH1_P	45,817,466	40,927,018	89.3
MH2_F	49,621,535	40,895,517	82.4
MH2_M	47,793,704	41,630,148	87.1
MH2_P	45,897,503	40,821,701	88.9
MH3_F	54,398,090	47,769,642	87.8
MH3_M	50,733,939	43,661,261	86.1
MH3_P	47,260,553	42,281,628	89.5
MH4_F	41,851,592	35,578,214	85.0
MH4_M	43,884,790	38,299,021	87.3
MH4_P	47,093,230	40,567,596	86.1
MH5_F	47,640,582	42,078,039	88.3
MH5_M	48,852,747	43,244,641	88.5
MH5_P	45,204,769	40,752,298	90.2
MH6_F	45,331,261	41,188,123	90.9
MH6_M	44,732,572	40,231,169	89.9
MH6_P	48,623,446	42,880,727	88.2

FastQC revealed high quality scores maintained across the 150 bases of each read for all RNA-seq libraries, visually represented with an example FastQC report in Figure 4.7

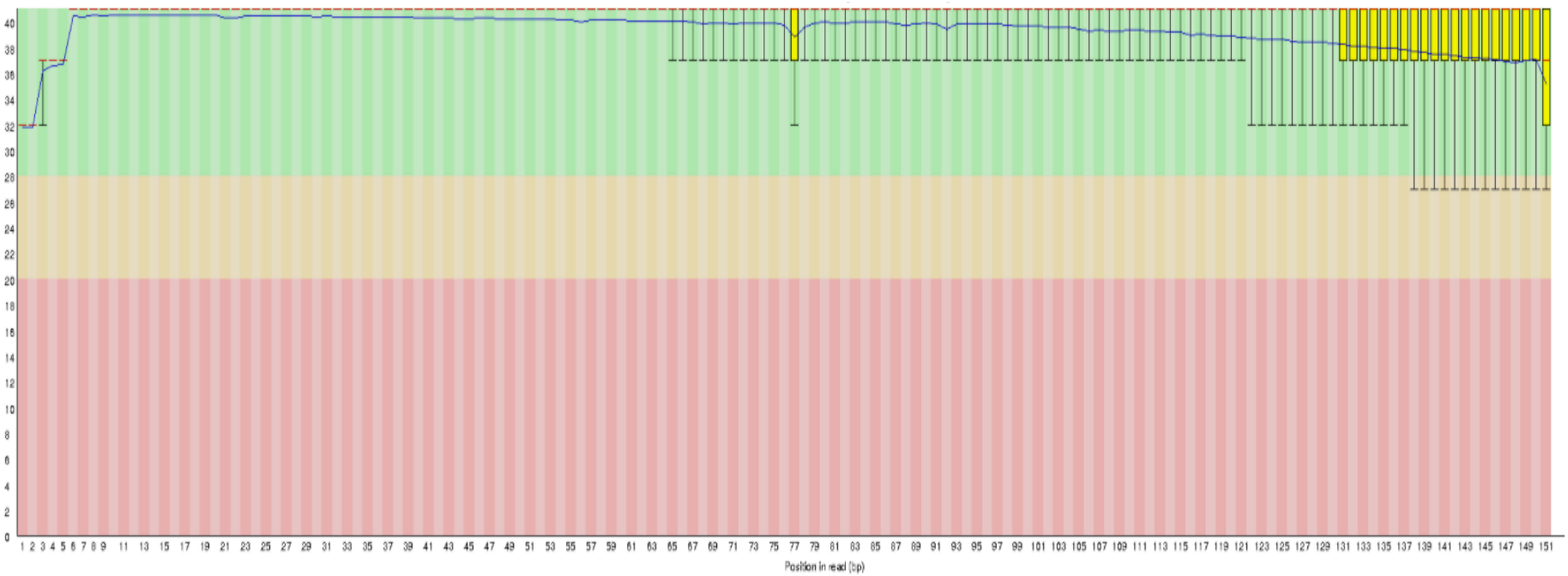

Figure 4.7: FastQC: average quality per base across RNA-seq library. Schematic representation of a high-quality RNA-seq library created from a human blood sample.

Prior to differential expression analysis global gene-level variation was plotted against mean counts to investigate the relationship between expression strength and dispersion (Figure 4.8). This highlights increased levels of variation for weakly expressed genes, requiring log2 fold-changes to be down-weighted relative to dispersion.

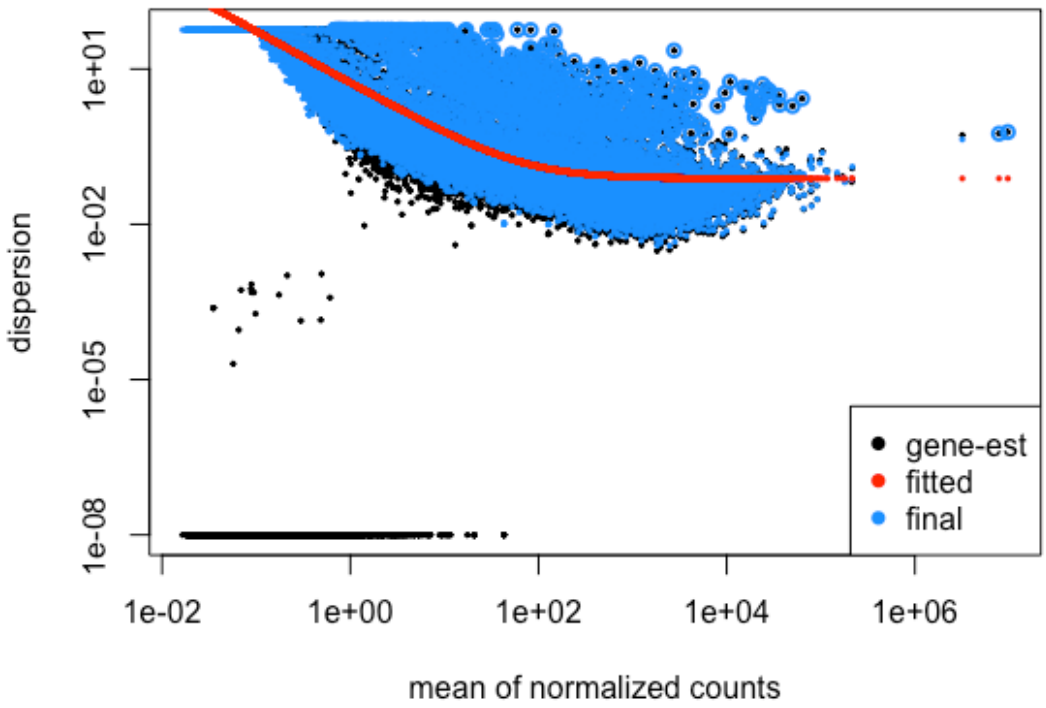

Figure 4.8: Plot of gene-wise dispersion estimates against the mean of normalised counts across all fifty-seven human blood samples. Schematic representation of the mean-dispersion relationship (black) and the final dispersion estimates (blue), shrunk towards the fitted estimates (red) for each gene. Log2 fold-changes were weighted relative to the final gene-wise dispersion estimates.

A PCA plot was created as a diagnostic to identify sample outliers by plotting variance in global gene expression profiles in 2-dimensional space. A PCA plot revealed the EHI group (shown in green) to have the most similar transcriptional profiles to one another, whereas the control samples (shown in red) showed the highest intra-group variability (Figure 4.9). The control volunteer who reached a core temperature of 39.5°C during the HTT revealed gene expression profiles across the three time points, which were distinct from the remaining samples (clustered on the far left of the PCA plot) (Figure 4.9). At a whole-transcriptome level the samples did not cluster according to treatment, suggesting that the status effect was greater than the treatment effect. The subsequent differential gene expression analysis aimed to reveal status-specific responses to exertional heat stress in addition to baseline differences between the groups.

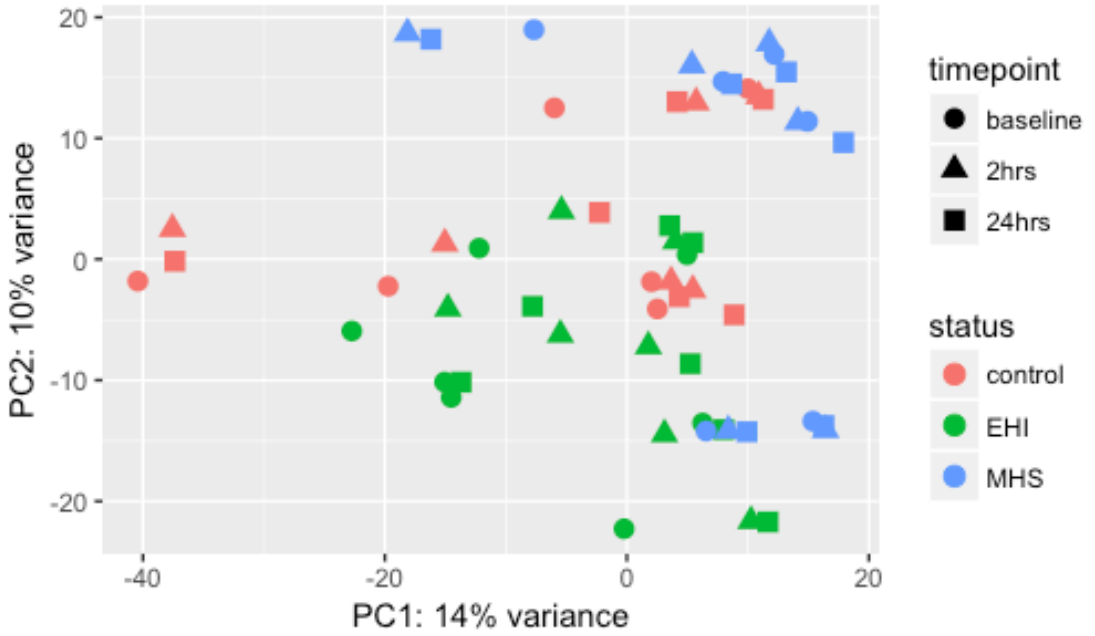

Figure 4.9: Principal component analysis representing global gene expression profiles of human blood samples pre- and post-acute heat stress. The PCA plot is a visual representation of the spread of data at the transcriptome level. Distance between data points along the X axis represents greater variation between the samples than the spread along the Y axis.

The DESEq2 package was used to generate negative binomial GLM's for each gene to determine statistically significant differentially expression using the Wald test. A number of specific comparisons were made to address three distinct biological questions, including which genes demonstrate baseline differences in expression, which gene represent a status-specific heat stress response and finally which genes show a treatment-specific response that may elicit a pathogenic effect at a critical threshold level. The differentially expressed gene lists produced by each comparison were based on log2 fold-changes and ranked by FDR-corrected *p* value.

4.3.2.2 Basal gene expression profiles in MHS, EHI and control volunteers (1)

At baseline, pair-wise comparisons were made between EHI, MH and control group means to identify fundamental differences between the expression profiles of each group (Figure 4.10). Comparing MH to control samples at baseline revealed 1,475 genes that were differentially expressed (FDR *p* value <0.05). Fewer genes were highlighted when comparing EHI to control samples (FDR *p* value <0.05), with 118 genes differentially expressed between the two groups. Fifty-nine of these genes

overlapped with the MH and control comparison group, highlighting a gene expression signature representative of both MH and EHI patient groups at baseline.

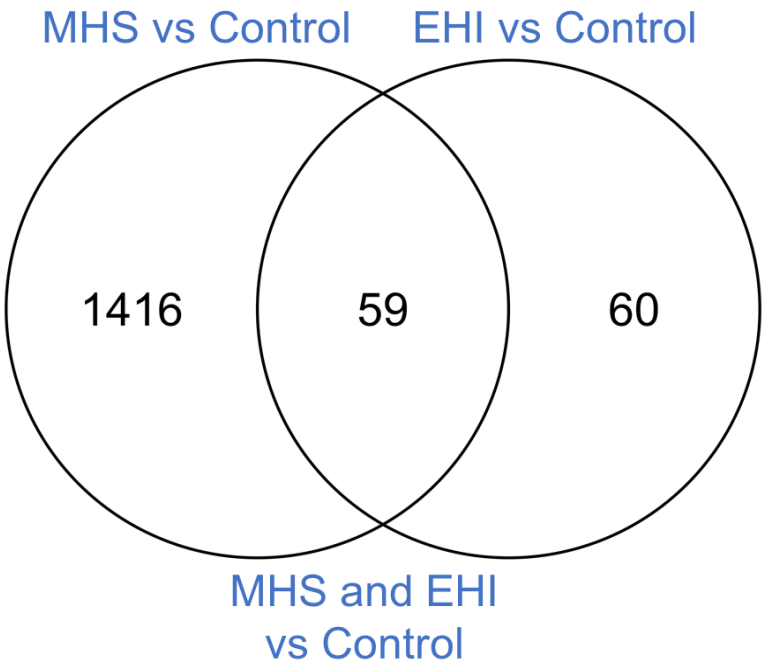

Figure 4.10: Venn diagram representing overlapping genes differentially expressed at baseline between the two disease groups relative to healthy control volunteers. Includes genes with an FDR-corrected *p* value <0.05.

Each gene list was functionally annotated and clustered using both DAVID Bioinformatics Resource 6.8 and PANTHER™ version 12.0. Of the 1,475 genes that were differentially expressed between MH and control volunteers at baseline 1,432 were annotated on DAVID v.68. Functional classification and enrichment revealed that 142 of these genes were related to mitochondrial function, with 29 of them specifically encoding proteins central to oxidative phosphorylation (OXPHOS) in the inner mitochondrial membrane. In contrast, only five genes differentially expressed between EHI and control volunteers were functionally related to mitochondria, none of which were involved in the OXPHOS process. Four genes involved in mitochondrial function were differentially expressed in both MH and EHI individuals relative to controls (Table 4.2). These included pyruvate dehyrogenase phosphatase catalytic subunit 1 (*PDP1*), acyl-CoA synthetase long-chain family member 4 (*ACSL4*), fumarate hydratase (*FH*) and mitochondrial ribosomal protein S9 (*MRPS9*). Expression of both *ACSL4* and *PDP1* were higher in MH and EHI individuals relative to controls. *PDP1* encodes the catalytic subunit of pyruvate dehydrogenase phosphatase, which positively regulates pyruvate dehydrogenase increasing the conversion of pyruvate to acetyl-coA (Reed, 1974).

PDP1 expression was ~2-fold higher in MH and EHI volunteers at baseline when compared to healthy controls (Table 4.2). Interestingly, *ACSL4* mRNA was also elevated nearly 2-fold in both MH and EHI patients and encodes long chain acyl-CoA synthetase, which converts free long chain fatty acids into fatty acyl-CoA (Fujino *et al.*, 2001). Acyl-CoA then undergoes β-oxidation to form acetyl-coA, which feeds into the Citric Acid Cycle. In contrast, both *FH* and *MRPS9* were expressed at slightly lower levels in MH and EHI groups relative to controls (Table 4.2). The *FH* gene encodes fumarate hydratase, which catalyses the conversion of fumarate to malate in the Citric Acid Cycle (Pollard *et al.*, 2005), while *MRPS9* is a nuclear gene, which encodes *a* mitochondrial ribosomal protein, which translates RNA transcribed from mitochondrial DNA (mtDNA) (Cavdar Koc *et al.*, 2001).

Table 4.2: Genes relating to mitochondrial function differentially expressed at baseline in both MH and EHI groups relative to controls.

Comparison	Gene	Log2 FC	Standard error	*p* value	*p* adjusted
EHI vs Control	*ACSL4*	0.88	0.24	0.00030	0.04
MH vs Control	*ACSL4*	0.97	0.25	0.00009	0.01
MH vs Control	*FH*	-0.28	0.10	0.00461	0.05
EHI vs Control	*FH*	-0.37	0.10	0.00012	0.03
MH vs Control	*MRPS9*	-0.39	0.12	0.00170	0.03
EHI vs Control	*MRPS9*	-0.44	0.12	0.00022	0.04
MH vs Control	*PDP1*	0.99	0.29	0.00053	0.02
EHI vs Control	*PDP1*	1.08	0.28	0.00022	0.04

Log2 fold-changes have been shrunken based on the fitted model. *P* values were adjusted using the FDR-correction method.

Of the differentially expressed genes identified between MH and control groups at baseline, 29 were related to the OXPHOS metabolic pathway (Table 4.3). All 29 genes were expressed at consistently lower levels in MH patients relative to healthy controls. The genes encoded proteins from complexes I, III, IV and V of the oxidative phosphorylation pathway, including NADH dehydrogenase subunits, ubiquinol-cytochrome c reductases, cyctochrome c1, cytochrome c oxidase subunits and mitochondrial ATP synthases. NADH dehydrogenase forms complex I of the electron transport chain (ETC) and catalyses the transfer of electrons from NADH to coenzyme Q10. Cytochome c1 and ubiquinol-cytochrome c reductases form part of complex III, which transfers electrons from the Rieske protein onto cytochrome c. Cytochrome c oxidase forms complex IV, the final enzyme of the ETC, which transfers electrons from cytochrome c onto oxygen molecules to produce water. Finally, mitochondrial ATP

synthases form complex V, which utilise energy from the proton electrochemical gradient to synthesise ATP from ADP, thus completing OXPHOS.

Table 4.3: Oxidative phosphorylation genes differentially expressed between MH and control volunteers at baseline.

Gene	Log2 FC	Standard error	*p* value	*p* adjusted
ATP5B	-0.38	0.13	0.0038	0.04
ATP5G2	-0.46	0.14	0.0013	0.03
ATP5G3	-0.32	0.11	0.0036	0.04
ATP5H	-0.52	0.16	0.0009	0.02
ATP5J2	-0.54	0.19	0.0038	0.04
ATP6V0E1	-0.56	0.16	0.0006	0.02
NDUFS7	-0.53	0.17	0.0019	0.03
NDUFS8	-0.58	0.17	0.0006	0.02
NDUFA1	-0.65	0.19	0.0005	0.02
NDUFA10	-0.34	0.10	0.0012	0.03
NDUFA12	-0.70	0.16	0.0000	0.003
NDUFA13	-0.62	0.18	0.0004	0.02
NDUFA3	-0.55	0.15	0.0003	0.01
NDUFA8	-0.40	0.11	0.0002	0.01
NDUFA9	-0.32	0.11	0.0040	0.04
NDUFAB1	-0.45	0.14	0.0009	0.02
NDUFB10	-0.42	0.14	0.0026	0.04
NDUFB7	-0.58	0.17	0.0008	0.02
NDUFB8	-0.48	0.14	0.0006	0.02
NDUFB9	-0.36	0.12	0.0030	0.04
NDUFC2	-0.56	0.14	0.0001	0.01
NDUFS6	-0.45	0.16	0.0049	0.05
COX5B	-0.66	0.16	0.0001	0.01
COX6A1	-0.58	0.18	0.0014	0.03
COX6B1	-0.62	0.18	0.0004	0.02
CYC1	-0.49	0.15	0.0007	0.02
UQCRH	-0.63	0.20	0.0017	0.03
UQCRFS1	-0.29	0.10	0.0034	0.04
UQCR10	-0.53	0.16	0.0008	0.02

Log2 fold-changes have been shrunken based on the fitted model. *P* values were adjusted using FDR-correction.

Twenty-three of the OXPHOS genes were clustered into a pathway map produced by MetaCore™ (Figure 4.11). All genes which were down-regulated in the MH patients relative to healthy controls are highlighted in red. Many distinct subunits and isoforms are evident in this pathway, highlighting the complexity of the multi-protein complexes forming the OXPHOS pathway located in the inner mitochondrial membrane.

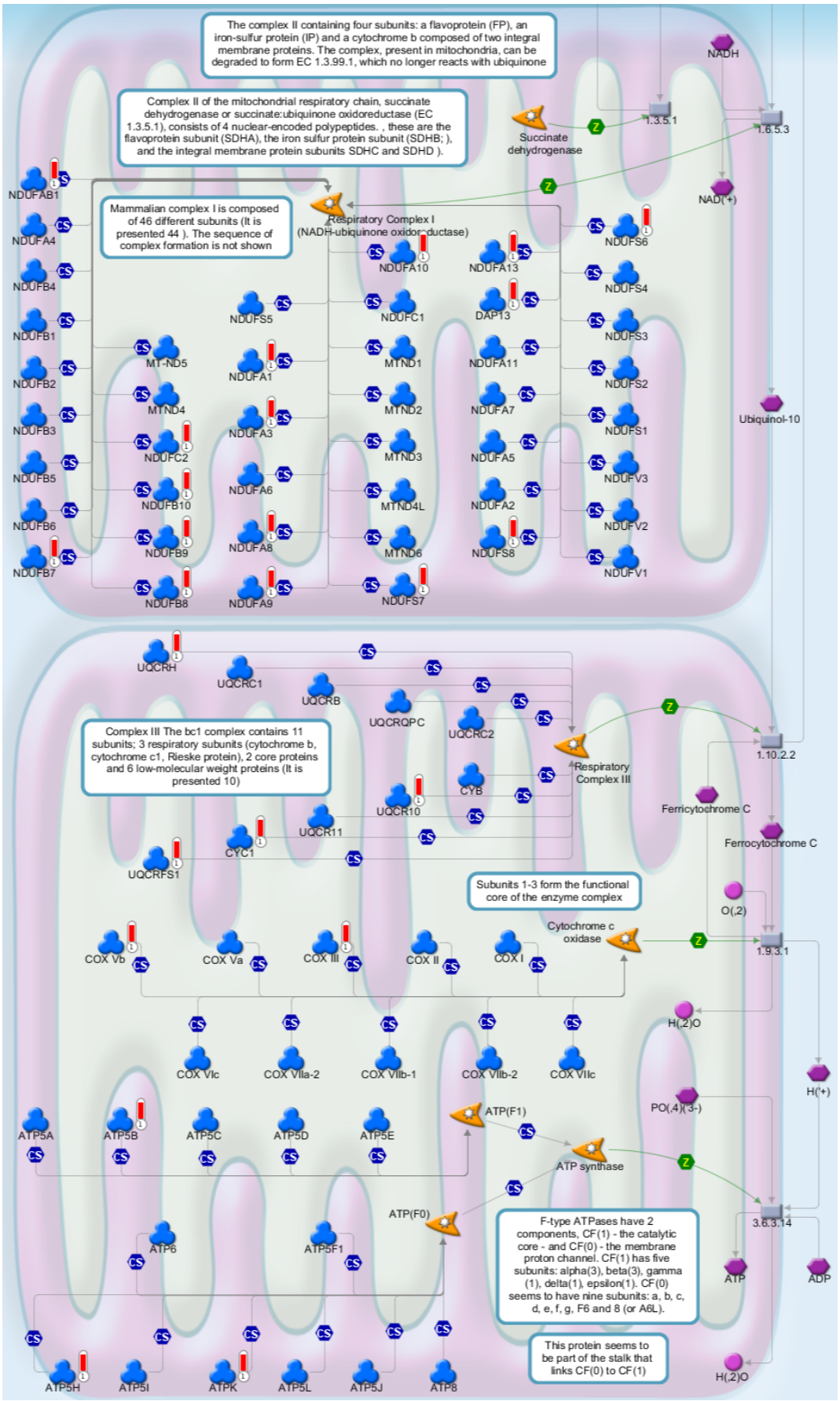

Figure 4.11: Oxidative phosphorylation pathway highlighting genes differentially expressed in MH volunteers' relative to healthy controls. All genes down-regulated in MH samples have been highlighted in red. Pathway map produced using GeneGo's MetaCore™ (Thomson Reuters).

4.3.2.3 Gene expression signature predictive model

To determine if there was a gene expression signature, which was predictive of MH susceptibility in human peripheral blood, a penalised regression model was fitted to the matrix of expression data from MH and control samples at baseline. Only two genes produced non-zero shrunken regression coefficients and were used to calculate susceptibility risk as a proof of principle. These included *HLA-C* (coefficient 0.001) and *AC114801.3* (coefficient 0.664) and could differentiate between MH and control samples at baseline in this dataset. *HLA-C* had a positive regression coefficient and is therefore a positive predictor of MH susceptibility, whereby expression is elevated in MH samples relative to controls. In contrast, *AC114801.3* had a negative regression coefficient, therefore represents a negative predictor of MH susceptibility, with lower expression in MH patients relative to healthy controls.

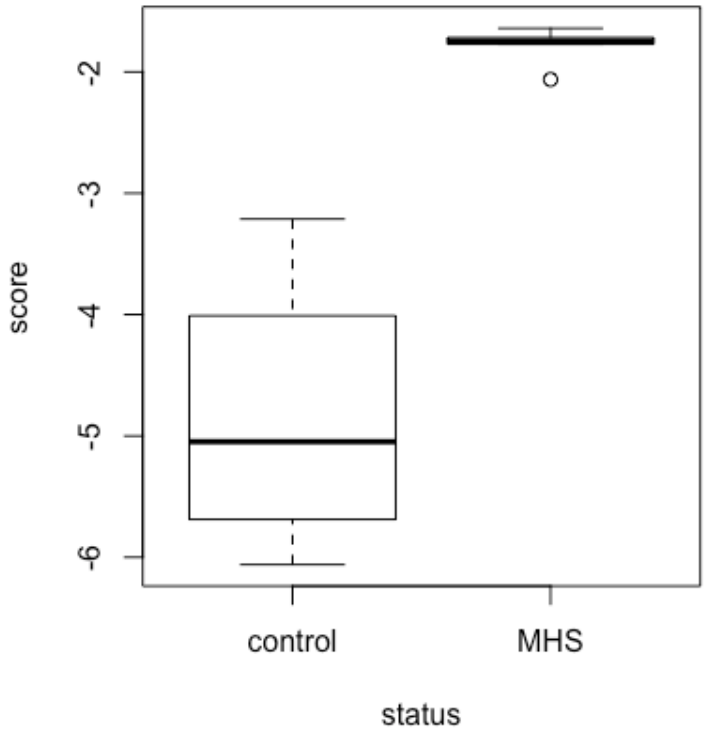

Figure 4.12: Plot of MH susceptibility risk scores calculated using expression values and penalised regression coefficients.

A penalised regression model was also fitted to the baseline EHI and control expression data to determine if there was a gene expression signature that was predictive of EHI susceptibility in human peripheral blood. No genes were identified in this model with all regression coefficients shrunk to zero.

4.3.2.4 Status-specific response to exertional heat stress (2)

To determine whether gene expression profiles could reveal an underlying status-specific response to exertional heat stress the interaction term 'status:timepoint' was included in the GLM design formula. For each status-specific comparison shrunken log2 fold-changes were ranked by FDR-adjusted *p* value. Both MH and EHI expression profiles were compared to controls to detect differential responses from baseline to 2 hours and baseline to 24 hours. Filtering for genes with FDR-adjusted *p* values <0.05 revealed 14 different genes representing a differential response to exertional heat stress (Table 4.4).

HSPA1A, which encodes heat shock protein 70, demonstrated a differential response between MH and control patients at 24-hours relative to baseline expression (Figure 4.13). *HSPA1A* was not expressed in MH patients in response to the HTT, whereas expression was detected in both other groups. Although *HSPA1A* appeared to be differentially expressed in EHI individuals relative to both the MH and groups, it was not revealed to be statistically significant, likely due to the high intra-group variation.

Table 4.4: Genes that display a status-specific response to exertional heat stress.

Time course	Contrast	Gene	Log2 FC	Standard error	*p* value	*p* adjusted
Baseline to 2 hours	EHI vs Control	*RP5-850E9.3*	-24.48	4.93	6.78E-07	0.0139251
		RP11-1305N21.3	-6.1	1.24	9.55E-07	0.0139251
		IGHV5-51	-30	6.29	1.83E-06	0.01775718
		SPDYE2B	2.53	0.56	5.28E-06	0.03848104
Baseline to 2 hours	MH vs Control	*KIR2DL3*	-30	4.16	5.68E-13	0.00000002
		TTN	25.28	4.14	1.01E-09	0.0000147
		CTD-2545G14.7	26.95	5.68	2.06E-06	0.01998518
Baseline to 24 hours	EHI vs Control	*HLA-DQA2*	-23.66	3.5	1.43E-11	0.00000042
		CTD-2545G14.7	-29.98	5.47	4.15E-08	0.00060513
		KIR2DL3	19.98	4.02	6.84E-07	0.00664724
		CTC-432M15.3	-18.55	3.85	1.41E-06	0.01027817
		KIR2DL1	30	6.35	2.33E-06	0.01355963
		IGHV1-18	21.69	4.78	5.78E-06	0.02808938
		MBOAT7	20.81	4.81	1.55E-05	0.03758172
Baseline to 24 hours	MH vs Control	*HSPA1A*	-20.16	3.18	2.19E-10	0.00000526
		HLA-L	-29.61	4.9	1.55E-09	0.0000186
		CTD-2545G14.7	27.59	5.68	1.17E-06	0.00704046
		KIR2DL3	20.45	4.16	8.95E-07	0.00704046
		CTC-432M15.3	-17.74	3.98	8.54E-06	0.04106888

The status:timepoint interaction term was extracted from DESeq2 to identify differentially expressed genes between the status groups in response to the heat tolerance test. Log2 fold-changes have been shrunken based on the fitted model. *P* values were adjusted using FDR-correction

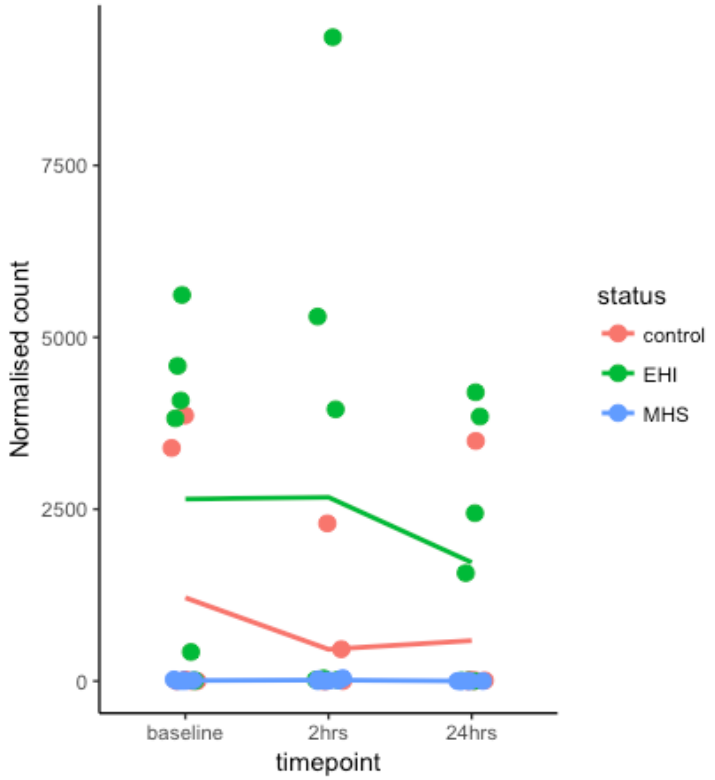

Figure 4.13: Status-specific expression of *HSPA1A* in response to the heat-tolerance test between MH and control groups. Based on shrunken log2 fold-changes and FDR-corrected *p* values <0.05. The plot was created and a loess trend line was fitted using ggplot2.

4.3.2.5 Differential gene expression in response to exertional heat stress representing a threshold model (3)

To identify genes that were differentially expressed between the status groups while also demonstrating a treatment effect, pairwise comparisons were made at 2-hours and 24-hours post HTT and matched to genes identified using the 'time point' model term. This approach aimed to uncover genes representing a threshold model of pathogenesis, whereby expression of the gene may elicit a pathogenic effect once a critical threshold is reached. Only one gene was identified using this strategy, *PTPRN2*, which was differentially expressed between EHI and control volunteers both at baseline and 2-hours post HTT (FDR-corrected *p* value <0.05). *PTPRN2* encodes a protein tyrosine phosphatase receptor, which is thought to regulate insulin secretion (van den Maagdenberg *et al.*, 1998).

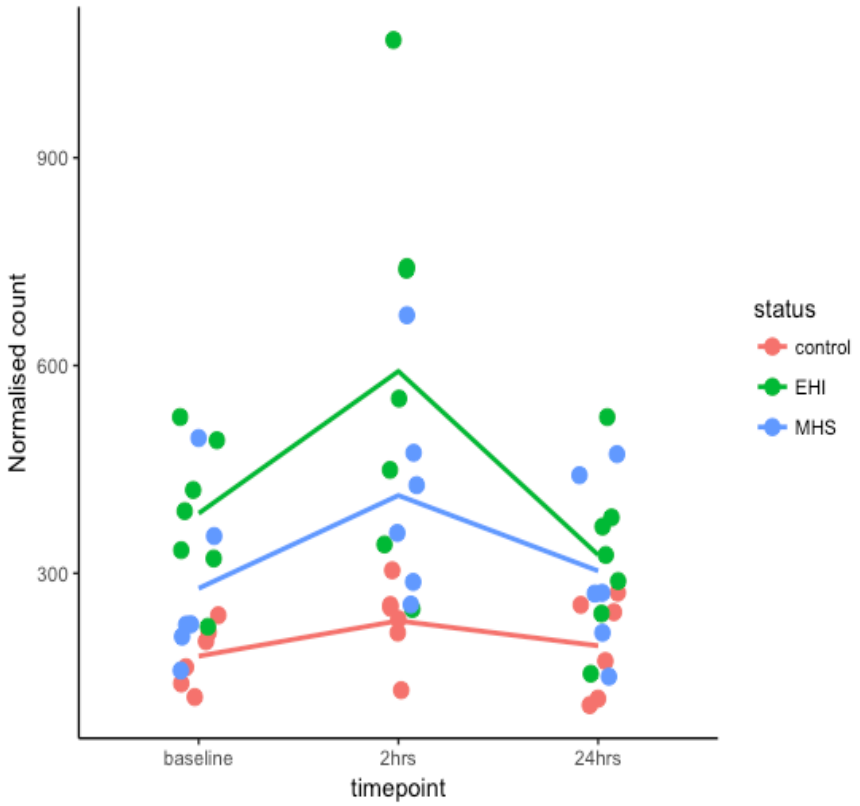

Figure 4.14: Expression of *PTPRN2* pre- and post-HTT representing a threshold response to exertional heat stress. Significantly differential expression was detected between EHI and control groups at baseline and 2-hours post-HTT (FDR-corrected *p* value <0.05). The plot was created and a loess trend line was fitted using ggplot2.

4.3.2.6 Genes characteristic of the human heat stress response (4)

To determine which genes were differentially expressed in response to exertional heat stress regardless of phenotype status, the 'timepoint' model term was extracted from the DESeq2 GLM. Shrunken log2 fold-changes comparing 2-hour post HTT to baseline and 24-hours to baseline were ranked by FDR-adjusted *p* value highlighting differentially expressed genes (p <0.05). This highlighted 5,312 genes which were up- or down-regulated following 2-hours recovery at room temperature following the HTT. After 24-hours recovery 7,550 genes were differentially expressed relative to baseline expression levels. A total of 2,620 genes were highlighted in both lists and therefore were differentially expressed at both recovery time points in response to exertional heat stress. Functional annotation and clustering of the 2,620 genes in common using DAVID Bioinformatics Resource 6.8 and PANTHER™ version 12.0 revealed 1001 genes related to metabolic processes, 265 of which were related to mitochondrial function. Seventy-nine genes were highlighted as immune response genes, including a complex pattern of both up- and down-regulated genes (Appendix C). For example, CD4, CD6, CD7 and CD46 were all down-regulated in response to exertional heat stress after both

2-hours and 24-hours recovery at room temperature. In contrast, TLR1, TLR4, TLR6 and TLR8 were all up-regulated at both recovery time points relative to pre-HTT levels.

4.4 Discussion

The pathophysiological mechanisms contributing to EHI remain unclear and research investigating the relationship to MH, a phenotypically similar condition, has proven insufficient. Of the EHI patients referred to the Leeds MH Investigation Unit for an IVCT and genetic screening to diagnose an underlying muscle defect, 35% demonstrated an abnormal contracture response to RyR1 agonists, caffeine and halothane. Of these, 45% carried a rare and potentially pathogenic variant in *RYR1*. This study offered a unique opportunity to test the exertional heat capacity of MH patients that carry an *RYR1* variant and advance understanding of the molecular basis of EHI. MODREC approval was granted in July 2015 allowing six volunteers to be recruited into each group. These numbers were based upon power calculations comparing rates of rise of rectal temperature in EHI military personnel that pass and fail the HTT. With only two EHI volunteers and one MH volunteer failing to thermoregulate during this study, the downstream analysis was problematic and lacked power, due to the poorly defined phenotypic groups.

Transcriptional profiles are markedly sensitive to environmental stresses (Whitney *et al.*, 2003; Radich *et al.*, 2004), and therefore the disparate HTT responses within each group would introduce biological variation and limit the power to detect a clear expression signature that is characteristic of the heat stress response. In contrast, by regrouping samples based on their HTT response there may be inherent variation in gene expression due to their clinical EHI and MH phenotypes. With only four individuals demonstrating ‘heat intolerant’ phenotypes based on the HTT, differential gene expression analyses based on re-grouped samples also lacked power and would not address the original aims of this study. Therefore, phenotypic and genotypic data from this study were presented according to the MHS, EHI and control phenotype groups into which they were recruited. The technical limitations of RNA-seq, both practical and analytical, have been discussed in detail in chapter 3.4. A sufficient read depth was obtained for the 57 samples from 7 lanes of the Illumina® HiSeq® 3000 sequencer, with an average of 48.2 million reads produced per sample. Samples from each status group and recovery time point were randomly split across the lanes of a flow-cell to avoid technical variation affecting downstream analyses, although lane-effects are thought to be modest (Marioni *et al.*, 2008). As with the previous RNA-seq study all samples were

run on the same flow-cell to prevent any sequencing batch effects, which could potentially obscure subtle differences in expression between the status groups.

Biological variation was limited where possible by recruiting age, sex and fitness matched volunteers, factors which have been shown to strongly influence gene expression (Roth *et al.*, 2002; Whitney *et al.*, 2003; Tang *et al.*, 2004). This was an important consideration when recruiting civilians so to match the fitness of military personnel. The civilian MH group demonstrated the highest median VO_2 max fitness capacity of the three groups, with the lowest median VO_2 max was observed in the EHI group. Low fitness levels may have contributed to the development of EHI in some of the military personnel in this study, particularly in those who were subsequently able to thermoregulate effectively during the HTT (Nichols, 2014). As the HTT is performed relative to maximal aerobic capacity, these individuals may have been working at a lower intensity during the HTT than during the EHI-triggering activity, whereby thermal equilibrium was not achieved. The complex nature of EHI means that a combination predisposing factors and environmental conditions could have contributed to the development of EHI.

When exercising in the thermoneutral zone (19-24°C), trained individuals working at the same relative intensity as untrained individuals will be exercising at a higher absolute workload and will generate more metabolic heat (Nadel *et al.*, 1974). Aerobically fit and heat acclimatised individuals adapt by lowering their threshold for vasodilation and sweating, increasing heat loss to compensate (Nadel *et al.*, 1974; Cheung and McLellan, 1998). Therefore, at a fixed workload, such as during a military exercise, individuals with low VO_2 max capacities will be working at a higher percentage of their VO_2 max and will be unable to dissipate heat as effectively, increasing the risk of heat injury. In contrast, when working at a relative intensity in high environmental temperatures the adaptive advantage of aerobic fitness is lost when heat production exceeds that of heat loss capacity (Mora-Rodriguez, 2012). Thermal equilibrium is achieved by offsetting metabolic heat production with heat dissipation and EHI occurs if these two processes become unbalanced. The four recruits in this study classified as heat intolerant were aged between 21 and 40 years old and demonstrated a range of VO_2 max capacities from 46.7 to 62.5 $mL.min^{-1}.kg^{-1}$, suggesting that neither age not fitness accounted for the abnormal thermoregulatory response in these individuals. Overall, six of the nineteen volunteers demonstrated average fitness levels relative to their age, with the remaining thirteen recording above average VO_2 max scores (Astrand, 1960; Bradshaw *et al.*, 2005).

As expected, the relative sweat rates recorded during the HTT were higher in the fitter individuals subjected to higher absolute workloads. It was therefore appropriate to normalise sweat rates relative to VO_2 max scores to enable comparison of heat loss capacity between the individuals. All four of the heat intolerant subjects produced sweat rates within normal ranges relative to their fitness (a proxy for workload), but were unable to increase their sweat production to compensate for the metabolic heat gain evidenced by their elevated core temperature. The relative sweat rates of the heat intolerant individuals although normal were in the lower range of those measured across the nineteen subjects. The median sweat rate calculated for MH volunteers was higher than EHI and control groups both before and after normalisation with VO_2 max scores. Enhanced sweat capacity in some patients with MH may represent a protective adaptation in response to a baseline metabolic defect. It would be interesting to model heat dissipation in MH individuals to determine whether reduced sweat rates would significantly limit their thermoregulatory capability. Reduced sodium concentrations in sweat have also been widely demonstrated as an adaptive advantage gained from aerobic fitness and heat acclimatisation (Baker, 2017); however, sweat sodium content was not measured in this study.

The large number of intrinsic and extrinsic factors that can contribute to EHI make diagnosing a predisposition to this condition difficult, as risk of EHI may depend on the interaction of several factors to trigger an episode. Several military personnel have been known to fail the HTT on one occasion and subsequently pass the test at a later date, questioning the reliability of the test to accurately identify high risk individuals, specifically those with a potential genetic predisposition to EHI (Schermann *et al.*, 2017). The control subject with no clinical history of EHI or MH, who failed to reach thermal equilibrium during the HTT was fit and healthy at the time of the test, with no known predisposing factors. The baseline, 2-hour post and 24-post transcriptional profiles generated from this heat intolerant volunteer revealed the greatest variation, with clear separation from all other samples on the PCA plot. Interestingly, this individual was the oldest recruit to the study, which may account for the distinct expression profiles highlighting him as an outlier (Whitney *et al.*, 2003). Following the Ministry of Defence Joint Service Protocol on heat illness, only military personnel with a history of EHI are referred to the INM for a HTT and therefore little is known about the distribution of heat stress responses in the general population (Ministry of Defence, 2017).

Despite the variable responses observed by HTT, a PCA plot visualising global gene expression profile variation between the samples showed that the status-effect was stronger than the time point effect. Limited transcriptomic data exploring the heat stress

response, particularly in humans, made the selection of recovery time points difficult. The 2-hour and 24-hour recovery periods were complimentary to the mouse acute heat stress study and to the time points chosen in previous *in vivo* mouse studies (Welc *et al.*, 2012, 2013). These recovery times were sufficient to detect differential expression profiles in wild-type mouse skeletal muscle. Limited access to human tissue samples has driven the use of blood to investigate the molecular basis of human disease states (Tang *et al.*, 2004; Sonna, Sawka and Lilly, 2007). These studies have proved successful at identifying gene expression profiles in human blood samples that represent the disease condition. More specifically, Sonna and colleagues performed a DNA microarray analysis on peripheral blood mononuclear cells (PBMC) and were able to detect differentially expressed genes characteristic of the stress response, including HSPs and immune response genes (Sonna *et al.*, 2004). Peripheral blood expression profiles have also been able distinguish between different metabolic disorders (Grayson, Wang and Aune, 2011). Whitney and colleagues explored the variation in gene expression profiles in peripheral blood samples owing to differences in the quantities of each cell subtype (Whitney *et al.*, 2003). Appropriate normalisation of gene expression data has to be considered in relation to the specific aims of the study and in this instance, the detection of both status-specific and treatment-specific responses were of interest. Presenting data which have been standardised against blood cell fractions, could mask responses related to both innate and adaptive immunity.

Basal gene expression profiles generated from peripheral blood samples were able to distinguish EHI and MH samples from age, sex and fitness matched controls. DESEq2 analysis revealed 1,432 genes, which were differentially expressed between MH and control volunteers. This list was enriched for genes related to mitochondrial function, particularly those involved in the OXPHOS pathway. These genes were consistently down-regulated in MH individuals and encoded key enzymes of complexes I, III, IV and V (Figure 4.15). Interestingly, complex I, III and IV activity was compromised in RyR1 R163C mutant mice due to high basal concentrations of mitochondrial matrix Ca^{2+} (Giulivi *et al.*, 2011). Increased uptake of Ca^{2+} into the mitochondrial matrix due to chronic exposure of the organelles to elevated Ca^{2+} is thought to dissipate the ETC electrochemical gradient, thereby reducing ATP production via complex V, causing mild mitochondrial uncoupling (Graier, Trenker and Malli, 2008). OXPHOS-specific ATP production was also significantly lower in human *RYR1* positive MH patients after short periods of exercise (Thompson *et al.*, 2017). All MH patients included in this study also carried a familial *RYR1* variant and had been classified by IVCT, the gold-standard diagnostic test. It is therefore possible that they exhibit a similar basal RyR1 Ca^{2+} leak, increasing Ca^{2+} mitochondrial uptake and accumulation. The down-regulation of

OXPHOS genes was MHS-specific, suggesting that it could be directly related to Ca^{2+} dysregulation via RyR1. Although 35% of EHI patients who fail the HTT show an abnormal IVCT contracture response, the military personnel recruited into this study had not been genetically screened or characterised by IVCT. Therefore, the role of OXPHOS regulation in EHI pathogenesis remains elusive. Recent work in the UK MH Investigation Unit has shown that MH muscles consume significantly more O_2 per mg of tissue than MHN patients, which has been attributed to increased numbers of mitochondria to compensate for reduced OXPHOS capacity (Chang et al., unpublished). This adaptive response may be specific to skeletal muscle. These data also suggest that mitochondria of MH susceptible individuals are less efficient than those of MHN individuals, specifically due to a complex II deficiency. The down-regulation of genes encoding complexes I, III and IV in the blood of MH patients in this study, could represent an adaptive response to re-balance the flow of electrons across all five OXPHOS complexes.

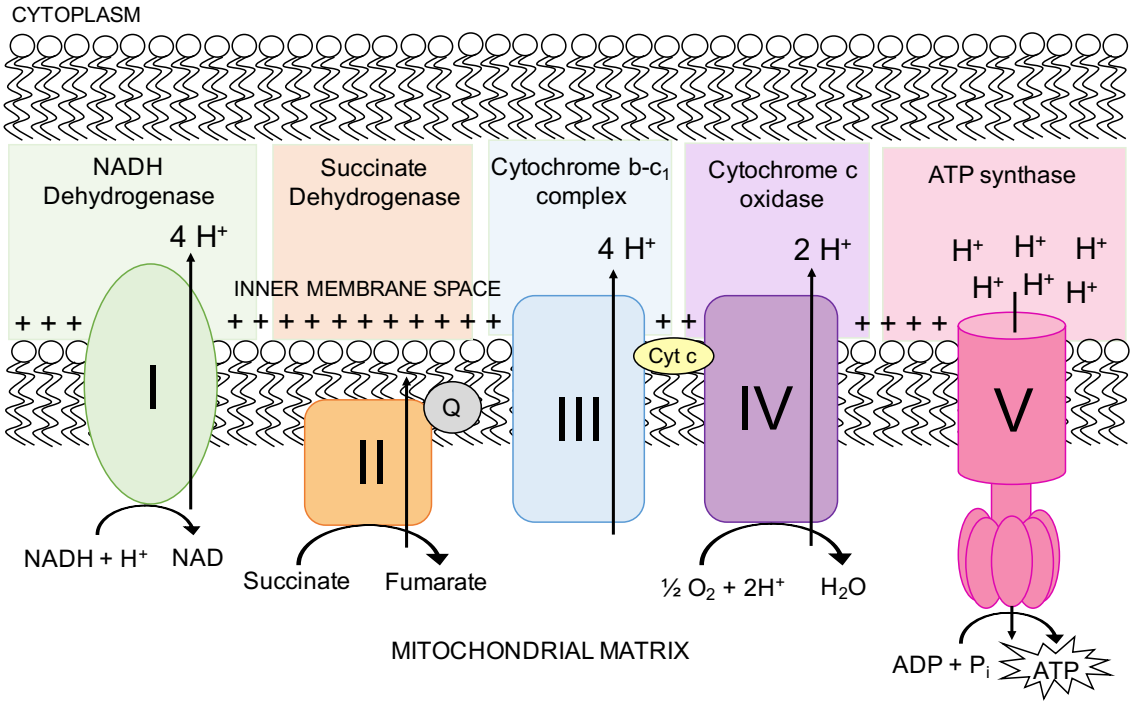

Figure 4.15: Schematic representation of the oxidative phosphorylation pathway. The electron transport chain produces an electrochemical gradient across the inner mitochondrial membrane, which drives ATP synthase and ATP production.

Fewer genes were differentially expressed between EHI and control individuals, although both groups comprised military personnel, who on average demonstrated similar HTT responses. The absence of a group with a clearly defined EHI phenotype will have introduced variation and reduced the power to detect a transcriptional signature

characteristic of the exertional heat stress response. Of the 118 genes differentially expressed at baseline between EHI and control subjects, five were related to aerobic metabolism, four of which were also differentially expressed in the MH group. Three of these genes encoded proteins functioning in pathways upstream of OXPHOS, including enzymes involved in fatty acid metabolism, the pyruvate oxidation link reaction and the citric acid cycle (Figure 4.16). Two genes involved in the synthesis of acetyl-CoA from pyruvate and fatty acids were both upregulated in EHI and MH patients relative to controls; however, expression of fumarate hydratase, a downstream citric acid cycle enzyme, was lower in EHI and MH samples (Figure 4.16). Physiological concentrations of mitochondrial Ca^{2+} directly activate several dehydrogenases involved in the Citric Acid Cycle, including pyruvate dehydrogenase, while stimulating OXPHOS activity (McCormack and Denton, 1979; Balaban, 2002). In contrast, high mitochondrial matrix Ca^{2+} levels have an inhibitory effect on cellular ATP production via complex V, also increasing ROS production (Grijalba, Vercesi and Schreier, 1999; Jekabsone *et al.*, 2003).

The status-specific gene expression signatures detected at baseline were insufficient to predict MH or EHI susceptibility in human peripheral blood using a LASSO penalised regression model. This may be due to high levels of biological variation within each group and small samples sizes effectively masking the small fold-changes evident between the status groups. The shrinkage parameters used in the LASSO approach are intentionally stringent to increase the robustness of gene set selection to effectively predict outcomes or classify disease groups (Tibshirani, 1996, 2011). The only annotated gene, which was identified as predictive of MH susceptibility was *HLA-C*, a human leukocyte antigen of the major histocompatibility complex (MHC) class I. More than 200 genes make up the MHC gene family, which encode diverse and highly variable peptide presentation molecules. *HLA* expression has been shown to be highly dependent on individual haplotypes, resulting in significant inter-person variations (Bettens, Brunet and Tiercy, 2014). It is therefore unlikely that the status-specific differences are observed in this cohort are related to MH pathogenesis, but rather have arisen by chance.

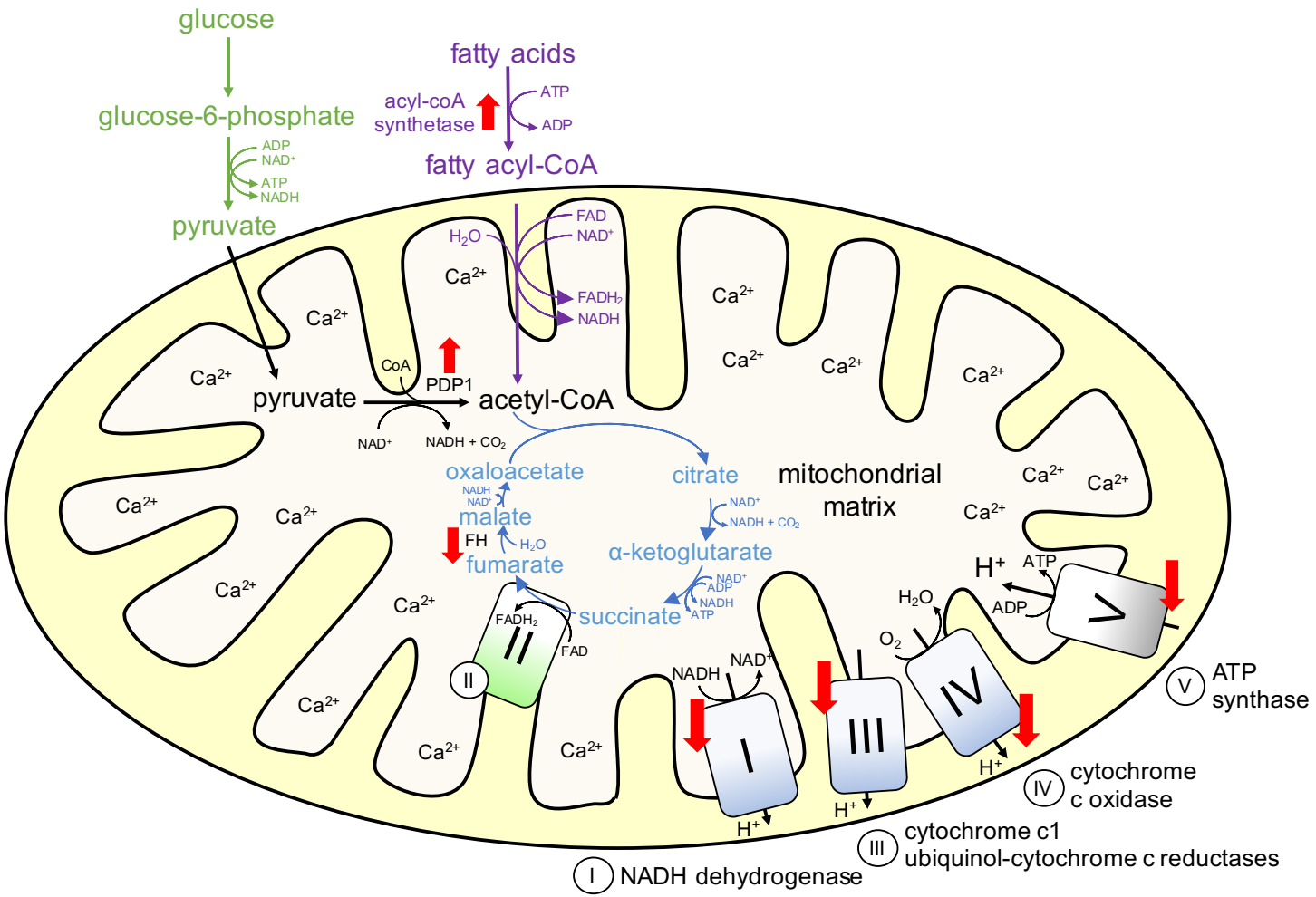

Figure 4.16: Schematic representation of aerobic respiration, highlighting dysregulated genes in MH and EHI patients. Genes up- or down-regulated in EHI and/ or MH individuals highlighted with red arrows. Figure adapted and redrawn (King, Selak and Gottlieb, 2006).

Of the genes which demonstrated a status-specific response to the HTT, only *HSPA1A* has been previously linked to the exertional heat stress response, eliciting a protective effect (Périard *et al.*, 2012). Overexpression of *HSPA1A* (HSP72) in rat skeletal muscle increased mitochondrial content and activity, increasing oxidative capacity (Henstridge *et al.*, 2014). *HSPA1A* was not expressed in MH samples in contrast to EHI patients who expressed the gene at far higher levels (~ 5000 counts), indicating low heat stress levels or low HSP activation in the MH individuals. The expression of this gene remained high in EHI patients across the time points, seemingly unaffected by the HTT. *HSPA1A* expression was also elevated in R163C mice immediately post 34°C heat exposure (see chapter 3.3.2). HSPs are very sensitive to activation by exertional heat stress, particularly the master regulator heat shock factor 1 (HSF1), which is upregulated in even mild cases of hyperthermia (Tulapurkar *et al.*, 2009).

Only one gene was consistent with a threshold model of pathogenicity, namely *PTPRN2.* The expression of this gene was significantly higher in EHI patients, relative to controls, both at baseline and in response to acute heat stress. *PTPRN2* was detected at a slightly higher level in MH patients, although not significantly so. Little is known about the function of this transmembrane protein, although it is thought to be involved in the regulation of insulin secretion. Interestingly, an insulin-resistance phenotype has been reported in heat and anaesthetic-sensitive heterozygous mice harbouring the *RYR1* p.R163C mutation (Giulivi *et al.*, 2011). It was suggested insulin-resistance developed as an adaptive response to Ca^{2+}-induced metabolic abnormalities, including impaired fatty acid oxidation, glycolysis and oxidative phosphorylation. Basal bioenergetics abnormalities have also been detected in insulin-resistant muscle from patients with type 2 diabetes, including reduced expression of mitochondrial proteins (Hwang *et al.*, 2010).

In this cohort of individuals 10,242 genes represented a generic signature of exertional heat stress. These genes were differentially expressed across the 24-hour recovery period following exertional heat stress, relative to baseline levels. The genes demonstrating a treatment-specific response at both recovery time points regardless of status were enriched for both metabolic and immune response genes, which are characteristic of the heat stress response (Starkie *et al.*, 2005; Rogers *et al.*, 2016).

Overall, the small samples sizes (n=6) in addition to the mixed HTT phenotypes observed within each group limited the power to detect status-specific expression signatures representative of the exertional heat stress response. Future work will therefore increase the individuals recruited into each group and only include heat intolerant military personnel (diagnosed by HTT) into the EHI group. A sample size

calculation based on an RNA-seq experimental design estimated that a sample size of 10 was required to reach a power of 0.9 (Figure 4.17). Ideally, sample size would be calculated using real RNA-seq data to simulate power using real dispersion estimates and average read count. By increasing samples numbers, it would become plausible to model RNA-seq data according to HTT classification, specifically comparing heat intolerant and heat tolerant global gene expression profiles to further investigate the exertional heat stress response.

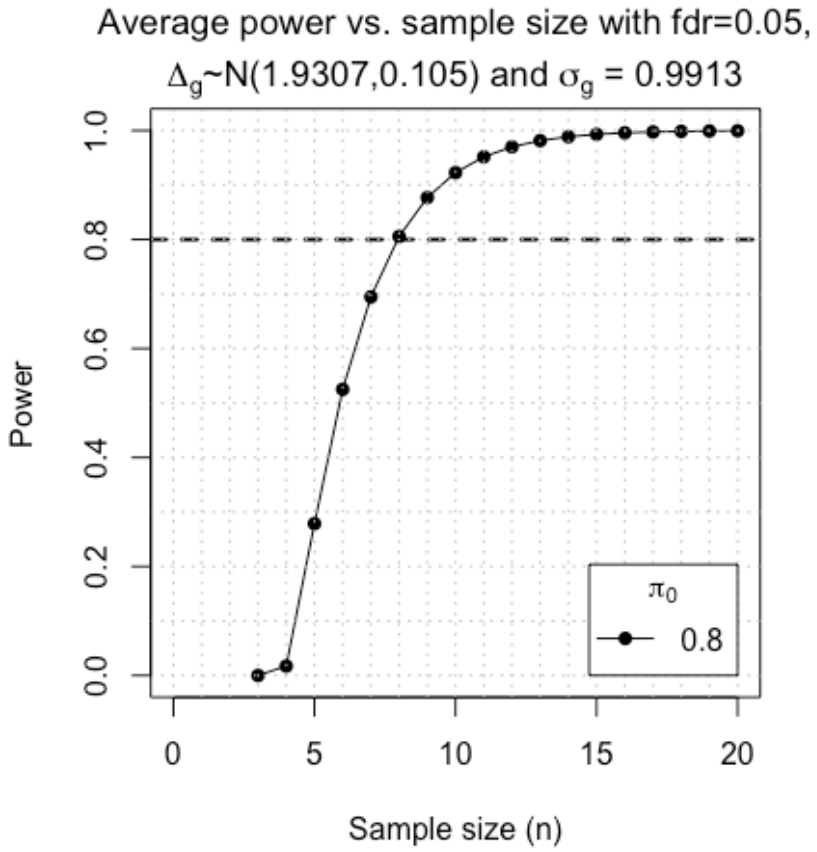

Figure 4.17: Sample size calculation using an RNA-seq experimental design. Sample size was calculated assuming 20,000 genes, dispersion 0.1, fold-change threshold 2, FDR level 0.05 and the proportion on non-DE genes 0.8.

Due to the limitations of whole-transcriptome approaches to accurately quantify expression levels of genes and with the presence of mapping errors, it is important to confirm interesting results with qPCR. That said, a number of studies have shown high correlation between RNA-seq data and qPCR follow-up (Wilhelm *et al.*, 2008). The differentially expressed gene lists identified in this study were not refined enough to warrant qPCR confirmation; however, future work will confirm genes of interest using TaqMan qPCR. Discrepancies between RNA and protein expression have been widely

reported, highlighting the need to confirm the presence of differential expression at the protein-level (Abreu *et al.*, 2009; Koussounadis *et al.*, 2015).

Overall, RNA-seq offers a valuable tool to explore gene expression at a whole-transcriptome level, helping to refine research questions, while avoiding hypothesis-driven experimental designs. The development and modification of large-scale bioinformatics tools in parallel with sensitive and affordable library preparation and sequencing technologies will continue to increase the power and interpretability of RNA-seq studies. In conclusion, these data are consistent with previous literature highlighting MH as a metabolic disorder associated with Ca^{2+} dysregulation, resulting in mitochondrial dysfunction. OXPHOS genes were consistently down-regulated in MH individuals, suggesting a subclinical reduction in oxidative capacity at rest. The study subjects showed variable HTT responses and therefore the molecular basis of the exertional heat stress response remains elusive.

5 General discussion

This thesis has provided the first high throughput investigation into the genetic risk factors contributing to EHI and has identified new genes and variants to guide future research in this field. This research also attempted to further characterise the acute heat stress response, by exploring the global gene expression profiles in *RYR1* mutant mice associated with EHI and MH. Finally, this thesis explored the transcriptional response to exertional heat stress in both EHI and MH individuals, while assessing their heat tolerance capabilities. The primary aim of this work was to make the first steps in identifying the genetic basis of EHI, in order to develop current understanding of EHI pathophysiology, with the intention to better diagnose, treat and prevent cases of EHI.

5.1 Is EHI an *RYR1*-related condition?

Uncharacterised *RYR1* variants were enriched amongst EHI individuals who demonstrated *ex vivo* muscle contractures in response to halothane. As with the MH population, *RYR1* variants were overrepresented in the EHI cohort, potentially explaining the genetic contribution in 45% of the IVCT positive EHI cases. Despite the association with *RYR1*, most of the *RYR1* variants identified in EHI individuals had not been previously associated with MH in the literature. Phenotypic data also highlighted differences between the conditions, with EHI patients demonstrating a lack of sensitivity to caffeine during an IVCT, unlike ~93% of UK MH patients who reacted to caffeine. As caffeine is thought to have an alternative site of action in RyR1 to halothane, specific *RYR1* variants are likely to elicit differential responses to RyR1 agonists (des Georges *et al.*, 2016). This research is consistent with the genotype-phenotype correlation presented by Carpenter and colleagues, whereby individual *RYR1* variants determined the severity of the IVCT phenotype (Carpenter, Robinson, *et al.*, 2009).

Phenotypic variation may also arise due to the presence of variants combinations, both within *RYR1* and other related genes (Robinson *et al.*, 2003). Four IVCT positive EHI patients harboured more than one *RYR1* variant, although only one of these individuals carried multiple rare and likely pathogenic *RYR1* variants. This EHI patient was one of only four who demonstrated abnormal contractures in response to both caffeine and halothane. Combinations of *RYR1* variants could also explain the differences between EHI and MH. For example, *RYR1* p.S2776F alone may trigger a heat-sensitive phenotype but the presence of a second *RYR1* variant may introduce a heightened

sensitivity to anaesthetics in MH patients. Combinations of rare *RYR1* variants have been previously associated with complex phenotypes, such as a *RYR1* compound heterozygosity conferring susceptibility to MH and a core myopathy phenotype (Kraeva *et al.*, 2015).

5.2 Does skeletal muscle Ca^{2+} dysregulation play a role in EHI?

The genotypic and phenotypic characterisation of EHI patients, highlighted the likely heterogeneity of this complex condition. The targeted NGS approach adopted in this study effectively identified sixty-eight rare and potentially deleterious variants in genes related to Ca^{2+} homeostasis and skeletal muscle function, with the potential to confer susceptibility to EHI. Of the twenty-two EHI patients who demonstrated dysregulated RyR1 Ca^{2+} release during an IVCT, twelve did not carry an *RYR1* variant. Highlighting rare and potentially pathogenic variants in the IVCT positive but *RYR1* negative patients revealed variants in five genes encoding channels related to Ca2+ homeostasis and EC coupling ($Ca_v1.1$, SERCA1, $Na_v1.4$, NCX and TRPM6) and one RyR1 regulatory protein (triadin).

Interestingly, variants were enriched in three of these genes, with four or more rare and potentially deleterious variants identified in *CACNA1S*, *SCN4A* and *SLC8A3* across the EHI cohort. Dysregulated RyR1 Ca^{2+} release has previously been implicated in heat and anaesthetic-induced hypermetabolic reactions in various *RYR1* and *CACNA1S* mutant mouse models and *in vitro* myotubes (Chelu *et al.*, 2006; Yang *et al.*, 2006, 2007). In addition, $Na_v1.4$ (*SCN4A*) and NCX (*SLC8A3*) are tightly regulated and have been co-localised to the skeletal muscle sarcolemmal membrane (Gershome *et al.*, 2010). Mutations in these channels could trigger Ca^{2+} influx via the Na^+/Ca^{2+} exchanger (NCX) either directly or indirectly due to excessive Na^+ influx via $Na_v1.4$. Enhanced Ca^{2+} entry via the Ca^{2+}/ Na^+ exchanger (*SLC8A3*) and SOCE channels has been identified in MH skeletal muscle (Duke *et al.*, 2010; Altamirano *et al.*, 2014). Mutations in $Na_v1.4$ could also cause delayed inactivation of $Ca_v1.1$, resulting in elevated RyR1 Ca^{2+} release (Petitprez *et al.*, 2008).

Both Ca^{2+} and Na^+ channels have demonstrated thermo-sensitivity, which can be exaggerated in the presence of mutations in the channels. An autosomal dominant mutation in *SCN4A* (p.P1158S) was identified in a family presenting with heat-induced myotonia (Sugiura *et al.*, 2000). This mutation causes delayed inactivation of $Na_v1.4$ channels, which stimulates voltage-dependent activation of $Ca_v1.1$ and Ca^{2+} entry via

the NCX preventing muscle relaxation (Altamirano *et al.*, 2014). Delayed inactivation of $Na_v1.4$ can also prevent reactivation of the channel, which is required to initiate EC coupling. The SR luminal Ca^{2+} sensor STIM1 can also be activated in a temperature-dependent manner, in the absence of depleted Ca^{2+} stores (Xiao *et al.*, 2011). This stimulation of STIM1 on exposure to elevated temperatures activates extracellular Ca^{2+} entry via SOCE channels, Orai1 and TRPC (Yarotskyy and Dirksen, 2012). Mutations in these genes could therefore increase the temperature sensitivity for activation and lower tolerance to exercise-induced rises in core-temperature.

Ca^{2+} related genes expressed in skeletal muscle have previously been associated with conditions characterised by an exercise intolerance phenotype, which further supports the role of Ca^{2+} regulation in EHI (Pusch, 2002; Roux-Buisson *et al.*, 2012; Guglielmi *et al.*, 2013; Ørstavik *et al.*, 2015). For example, variants in *ATP2A1* (SERCA1) have been associated with Brody's myopathy, featuring muscle cramps and stiffness and *TRDN* variants have been implicated in ventricular tachycardia, featuring muscle weakness (Vattemi *et al.*, 2010; Roux-Buisson *et al.*, 2012). Variants in both of these genes have been identified more than once across the EHI cohort in EHI patients who have tested IVCT positive and *RYR1* variant negative.

5.3 Is EHI a manifestation of reduced mitochondrial efficiency?

Mitochondrial Ca^{2+} uptake via the mitochondrial Ca^{2+} uniporter (MCU) directly regulates energy production (McCormack, Halestrap and Denton, 1990). Ca^{2+} dysregulation in MH and other muscle disorders has been frequently associated with mitochondrial dysfunction (McCormack and Denton, 1993; Peng and Jou, 2010). The EHI patients who produced positive contractures by IVCT demonstrated significantly lower fitness levels than those classified MHN: however, MH susceptible volunteers who underwent a HTT at the INM had increased aerobic capacity compared to the EHI volunteers. When directly comparing fitness levels between EHI and MHS subjects recruited into the heat stress study it is important to remember that the volunteers represent a self-selected group and therefore may not reflect the true fitness distribution of the EHI and MH populations. Although a reduced aerobic capacity is a risk factor for developing EHI, the HTT is performed relative to fitness and therefore the EHI cohort referred to the Leeds MH Unit were unable to effectively thermoregulate regardless of aerobic capacity.

The symptoms of metabolic acidosis and hyperthermia observed in both EHI and MH have indicated that mitochondrial dysfunction plays a role in the development of these

conditions (Giulivi *et al.*, 2011). Reduced oxidative capacity has since been identified in RyR1 mutant mice at baseline and *RYR1* mutation positive MH patients during exercise (Giulivi *et al.*, 2011; Thompson *et al.*, 2017). Previous literature has also shown that elevated mitochondrial Ca^{2+} concentrations can trigger mild mitochondrial uncoupling, which reduces ATP production (Graier, Trenker and Malli, 2008). Mitochondrial uncoupling proteins dissipate the electrochemical gradient required for ATP synthase (complex V) activity and in turn increase metabolic heat production. Recent work in our research group has detected elevated O_2 consumption in the mitochondria of *RYR1* positive MH patients, which appears to represent a rise in the number of mitochondria to compensate for reduced OXPHOS capacity (Chang *et al.*, no date). The imbalance between O_2 consumption and ATP turnover in the OXPHOS pathway, drives ROS production and oxidative stress (Graier, Trenker and Malli, 2008).

This thesis identified reduced expression of key OXPHOS genes in the blood of MH patients with known familial *RYR1* variants. This down-regulation of aerobic metabolism could represent a protective systemic response to chronic Ca^{2+} induced oxidative stress caused by an RyR1 Ca^{2+} leak in skeletal muscle. This response was not seen in the baseline expression of *RYR1* R163C mouse soleus nor mitochondria isolated from human MH muscle, so may reflect a tissue-specific adaptation of OXPHOS.

5.4 Is EHI associated with oxidative stress and mitochondrial damage?

Heat can directly induce the production of ROS via complex I, which further increases ROS production via the other complexes causing oxidative damage in skeletal muscle (Mujahid *et al.*, 2006; Hirst, King and Pryde, 2008; Li *et al.*, 2017). Heat also increases intracellular Ca^{2+} levels, which elevates mitochondrial Ca^{2+} uptake and in turn drives ROS production via the OXPHOS pathway (Brookes *et al.*, 2004; Görlach *et al.*, 2015). Therefore, defects in Ca^{2+} homeostasis could indirectly elevate ROS levels within skeletal muscle. Mutations altering energy metabolism could also generate ROS and cause a metabolic shift to anaerobic glycolytic pathways, resulting in lactic acidosis. This in turn could trigger a fibre type transition to type II fast-twitch fibre predominance. In mice harbouring certain MH mutations, a chronic basal RyR1 Ca^{2+} leak stimulates RNS production. This causes the post-translational modification of RyR1, known as S-nitrosylation, which increases its temperature sensitivity for activation (Durham *et al.*, 2008).

Muscle contraction during exercise has also been show to trigger the production of ROS and RNS and therefore can contribute to the oxidative stress observed in skeletal muscle (Powers and Jackson, 2008). Low levels of ROS/ RNS are actually required for normal muscle contraction; however, high levels cause muscle weakness and premature fatigue (Barclay and Hansel, 1991; Kobzik *et al.*, 1994). Increased expression of heat shock proteins have been detected in response to ROS/ RNS to protect against the effects of heat and exercise stress (Madamanchi *et al.*, 2001; Dimauro, Mercatelli and Caporossi, 2016). This thesis demonstrated elevated HSPs in both the blood of MH susceptible patients and in the muscle of RyR1 R163C mutant mice, consistent with a response to oxidative stress.

Mitochondrial dysfunction, oxidative stress and increased Ca^{2+} are thought to elicit an insulin resistance phenotype (Draznin, 1988; Kim, Wei and Sowers, 2008). In healthy patients, muscle contraction during exercise stimulates glucose uptake into skeletal muscle however in the disease state ROS/ RNS can limit glucose uptake and utilisation (Chambers *et al.*, 2009; Merry and McConell, 2009). Heterozygous RyR1 R163C mice adapt to chronically elevated Ca^{2+} by switching their bioenergetic state in a similar way to patients with type 2 diabetes (Giulivi *et al.*, 2011). Specifically, the adaptive response included reduced glucose uptake and fast-twitch fibre predominance in skeletal muscle. Elevated insulin levels have also been detected in the blood of MH susceptible patients (Campbell, Ellis and Evans, 1981). In this study, the baseline expression of *PTPRN2*, which is thought to regulate insulin secretion, was higher in the blood of both EHI and MHS patients' relative to controls. *PTPRN2* was also elevated in heat intolerant volunteers at baseline, once they had been regrouped by their ability reach thermal equilibrium during the HTT.

5.5 Do EHI patients suffer from a mild metabolic myopathy?

In contrast to a metabolic defect caused by chronically elevated mitochondrial Ca^{2+}, it is also possible that genetic mutations directly related to energy metabolism could cause a similar clinical phenotype. Particularly as genes involved in metabolic pathways have been previously associated with an exercise intolerance phenotype, including cramps, rhabdomyolysis and fatigue (Corti *et al.*, 2008; Wang *et al.*, 2008; Nogales-Gadea *et al.*, 2015). Fourteen variants uncovered in this study were identified in *AMPD1*, *CPT2* and *PYGM*, which encode metabolic enzymes, previously implicated in a metabolic myopathy. In addition, elevated expression of two enzymes required for acetyl-coA

synthesis were detected in the blood of MHS and EHI patients, specifically acyl-coA synthetase and pyruvate dehydrogenase phosphatase.

Exercise increases metabolic rate and is further accentuated in warm climates (McLellan, Jacobs and Bain, 1993; Krustrup *et al.*, 2003). Specifically, the increase in core temperature under these conditions was shown to increase glycogenolysis and lactate accumulation; however, heat has not yet been directly linked to rises in glycolytic enzymes (Febbraio, 2001). Interestingly, glycogen myophosphorylase encoded by *PYGM*, has been shown to be positively regulated by the transient rise of Ca^{2+} during muscle contraction (Brostrom, Hunkeler and Krebs, 1971; Ren and Hultman, 1990). Exercise under conditions of heat stress could prove pathogenic in individuals harbouring a genetic defect in a gene related to metabolic function, due to a lower heat tolerance. Patients with a subclinical muscle defect or mild metabolic myopathy may have a lower exercise tolerance at a metabolic level due to either reduced substrate availability or mitochondrial efficiency.

5.6 Is EHI a multifactorial condition?

The NGS study presented in this thesis, which investigates the genetic susceptibility of EHI, assumes a major gene effect, although modifier loci may in fact contribute to the diverse EHI phenotype. The heritability of EHI remains unknown; however, the genetic basis of EHI may be more complex than previously appreciated. For example, multiple common *TRDN* variants were enriched in the EHI cohort to a significantly higher degree than expected based on the reported population allele frequency. Due to the vital function of triadin in regulating RyR1 Ca^{2+} release, it is possible that in combination they could alter the regulation of RyR1. Two common *CPT2* variants were also detected in the EHI cohort, which could elicit a minor contributory effect in combination with an additional variant. This could explain the exercise intolerance and EHI episodes observed in these patients. *CPT2* encodes carnitine palmitoyltransferase 2, which is an enzyme required for fatty acid metabolism. A combination of rare variants from a common pathway could also explain the final clinical phenotype. Many of the patients in the EHI cohort harboured several rare and potentially deleterious variants, which could have an additive effect, triggering EHI in a threshold model. The small sample size and limited access to EHI family members restricted the ability to fully interpret the genetic variants identified in this study. EHI patients are continually referred to the Leeds MH Unit and as the genetically characterised cohort is expanded, the power to detect rare variants, which may modify the EHI phenotype will be increased. In contrast, a genome-

wide association study (GWAS) would allow the detection of common variants associated with EHI.

5.7 Proposed pathophysiology of EHI

The data presented in this thesis imply that various genetic causes of EHI are likely, resulting in a range of clinical and diagnostic phenotypes. A range of genes related to a common pathway could contribute to EHI susceptibility. The EHI patients revealed varied responses to both RyR1 triggering agents and environmental heat stress and can effectively be subdivided into IVCT positive or negative EHI cases and then further classified as *RYR1* positive or negative. Mutations in genes relating to muscle Ca^{2+} homeostasis could cause a temperature-sensitive rise in cytoplasmic Ca^{2+}, which would increase the metabolic demand due to muscle contraction and activation of ATP-dependent Ca^{2+} pumps. Myofilament activation is an inefficient process, with 85% of energy lost as heat and therefore serves as a substantial source of heat production. Increased cytoplasmic Ca^{2+} would lead to high mitochondrial Ca^{2+} levels and subsequent mitochondrial dysfunction. An increased metabolic rate would further increase heat production, which along with Ca^{2+} would drive ROS/ RNS production, supress antioxidant levels and reduce ATP production. Oxidative stress is known to cause widespread cellular damage to membrane lipids, nucleic acids and a wide range of proteins. ROS can also indirectly stimulate pro-inflammatory signalling pathways. RNS-dependent S-nitrosylation of RyR1 increases its temperature sensitivity for activation, which further stimulates Ca^{2+} release during exercise. Ca^{2+}-dependent phospholipases can cause the break down muscle cells causing rhabdomyolysis. A decrease in OXPHOS enzymes and an increase in glycolytic enzymes could increase the proportion of anaerobic fast-twitch muscle fibres and increase lactic acid production, ultimately causing lactic acidosis. Mutations in genes encoding metabolic enzymes could directly trigger mitochondrial dysfunction during exercise, eliciting the same downstream effects.

5.8 Direct impact of this research

The Leeds Genetics Laboratory currently provides NHS diagnostic testing for a wide range of inherited conditions. The service works closely with the Leeds MH Unit offering diagnostic screening of *RYR1*, *CACNA1S* and *STAC3* for MH referrals. The genetic laboratory plans to expand its current gene panel to include the twenty-four genes

identified in this study and to begin offering genetic screening to non-military EHI patients.

The ongoing collaboration between the Leeds MH Unit and the INM has been established for over 20 years and ultimately aims to develop a genetic test to screen UK military recruits, which will identify individuals at high risk of EHI. This would reduce impact on medical resources within the armed forces and limit fatal cases occurring on remote deployments with restricted access to medical aid.

Finally, the INM plans to reassess the parameters of the standardised HTT to increase the tests sensitivity using the physiological data obtained during the human heat tolerance study presented in chapter 4. They also plan to develop their own research studies to further investigate the heat tolerance response and the relationship to MH susceptible individuals.

5.9 Future directions

The UK MH Investigation Unit is currently adopting various approaches to functionally characterise *RYR1* variants, including immortalising primary human muscle cells harbouring specific *RYR1* variants to measure Ca^{2+} release relative to wild-type cells. The CRISPR-Cas9 technique is also being used to introduce variants such as p.S2776F into cell lines to measure differential Ca^{2+} release relative to wild-type RyR1. The functional characterisation of variants is required to fully interpret these genetic data and to implicate non-synonymous variants in the pathogenesis of EHI. For example, whole-cell patch-clamp electrophysiology will be used to functionally characterise *SCN4A* variants by investigating the properties of voltage-activated $Na_v1.4$ channels in myotubes from EHI patients. This specifically enables the measurement of the voltage required for channel activation, rate of channel inactivation and speed of recovery from inactivation. These electrophysiology experiments aim to quantify the potential pathogenic effects of each variant in this gene and elucidate the precise mechanism of action contributing to the EHI phenotype. They also have the capacity to determine the temperature sensitivity of wild-type and mutant Na^+ channels, addressing the impact of an exercise-induced rise in core temperature. To characterise the functional effect of heterozygous variants identified in genes encoding metabolic enzymes, for example myophosphorylase and carnitine palmitoyltransferase II, it is possible to assess the enzymatic activity and also quantify the proteins. These assays have been developed

for homozygous deficiencies, therefore it will be necessary to validate their sensitivity prior to the characterisation of heterozygous samples.

In cases where more than one rare and potentially deleterious variant has been identified within one gene, it important to determine whether they have been inherited in *cis* or in *trans* as some variants may have been inherited in the compound heterozygous form. The location of the variants on each allele will be confirmed using a combination of PCR, TA subcloning and Sanger sequencing.

The UK MH Investigation Unit is currently transitioning to a whole-exome sequencing approach, starting with the fourteen EHI patients with no rare and potentially pathogenic variants detected across the 50-gene panel. This broader strategy would increase the scope for variant detection and offer the potential to identify alternative mechanisms underlying EHI. As data analysis methods are refined, costs continue to fall and data storage issues are addressed, we will adopt whole-genome sequencing technologies. This would enable the exploration of non-coding regulatory regions, which may uncover modifier loci.

To determine whether genetic variants in *cis*-acting or *trans*-acting regulatory elements are influencing the expression of genes identified in the human heat stress study, it is possible to sequence expression quantitative trait loci (eQTL) in association with differentially expressed genes identified in the RNA-seq dataset. If the sequence variants identified within eQTLs segregate with the EHI or heat intolerant phenotype, then they are likely to directly contribute to the disease status. It is also possible to identify eQTLs specific to skeletal muscle tissue using databases such as the Genotype-Tissue Expression (GTEx) portal (Lonsdale *et al.*, 2013). The MoD research ethics committee has approved the continued recruitment of EHI military personnel into the human heat tolerance study, to increase numbers of heat intolerant individuals for differential gene expression analyses. This will increase the power to detect the heat stress response specific to EHI individuals and will subsequently support eQTL studies.

We also plan to investigate mitochondrial OXPHOS capacity in EHI samples using the Oroboros high-resolution respirometer, to compliment the current analyses using MH susceptible muscle tissue. This will make it possible to quantify the efficiency of each complex of the ETC by the step-wise addition of specific substrates required for the activity of each complex.

Overall, this thesis provides a foundation of research to guide future investigations into the genetic risk factors contributing to EHI. It also highlights the likely role of Ca^{2+} dysregulation and energy metabolism in the pathophysiology of this complex disorder.

6 References

1000GenomesProject. (2012). An integrated map of genetic variation from 1,092 human genomes. Nature, 491(7422),56–65.

Abreu, R. de S., Penalva, L. O., Marcotte, E. M., & Vogel, C. (2009). Global signatures of protein and mRNA expression levels. Molecular BioSystems, 5(12), 1512–1526.

Adeokun, A. M., West, S. P., Ellis, F. R., Halsall, P. J., Hopkins, P. M., Foroughmand, A. M., … Curran, J. L. (1997). The G1021A substitution in the RYR1 gene does not cosegregate with malignant hyperthermia susceptibility in a British pedigree. American Journal of Human Genetics, 60(4), 833–841.

Adzhubei, I. A., Schmidt, S., Peshkin, L., Ramensky, V. E., Gerasimova, A., Bork, P., … Sunyaev, S. R. (2010). A method and server for predicting damaging missense mutations. Nature Methods, 7(4), 248–249.

Altamirano, F., Eltit, J. M., Robin, G., Linares, N., Ding, X., Pessah, I. N., … Lopez, J. R. (2014). Ca2+ influx via the Na+/Ca2+ exchanger is enhanced in malignant hyperthermia skeletal muscle. Journal of Biological Chemistry, 289(27), 19180-19190.

Amador, F. J., Liu, S., Ishiyama, N., Plevin, M. J., Wilson, A., MacLennan, D. H., & Ikura, M. (2009). Crystal structure of type I ryanodine receptor amino-terminal β-trefoil domain reveals a disease-associated mutation “hot spot” loop. Proceedings of the National Academy of Sciences, 106(27), 11040–11044.

Anders, S., & Huber, W. (2010). Differential expression analysis for sequence count data. Genome Biology, 11,R106.

Anderson, J. L., Habashi, J., Carlquist, J. F., Muhlestein, J. B., Horne, B. D., Bair, T. L., … Hart, N. (2000). A common variant of the AMPD1 gene predicts improved cardiovascular survival in patients with coronary artery disease. Journal of the American College of Cardiology, 36(4), 1248–1252.

Andresen, B. S., Bross, P., Vianey-Saban, C., Divry, P., Zabot, M.-T., Roe, C. R., … Gregersen, N. (1996). Cloning and Characterization of Human Very-Long-Chain Acyl-CoA Dehydrogenase cDNA, Chromosomal Assignment of the Gene and Identification in Four Patients of Nine Different Mutations Within the VLCAD Gene. Human Molecular Genetics, 5(4), 461–472.

Andresen, B. S., Olpin, S., Poorthuis, B. J. H. M., Scholte, H. R., Vianey-Saban, C., Wanders, R., … Gregersen, N. (1999). Clear Correlation of Genotype with Disease Phenotype in Very–Long-Chain Acyl-CoA Dehydrogenase Deficiency. The American Journal of Human Genetics, 64(2), 479–494.

Andrews, S. (2010). FastQC: a quality control tool for high throughput sequence data.

Anzalone, M. L., Green, V. S., Buja, M., Sanchez, L. A., Harrykissoon, R. I., & Eichner, E. R. (2010). Sickle Cell Trait and Fatal Rhabdomyolysis in Football Training: A Case Study. Medicine & Science in Sports & Exercise, 42(1).

Applied Biological Materials (abm) Inc. (2017). Retrieved from https://www.abmgood.com/marketing/knowledge_base/next_generation_sequencing_experimental_design.php.

Aracena, P., Sánchez, G., Donoso, P., Hamilton, S. L., & Hidalgo, C. (2003). S-Glutathionylation Decreases Mg2+ Inhibition and S-Nitrosylation Enhances Ca2+ Activation of RyR1 Channels. Journal of Biological Chemistry, 278(44), 42927–42935.

Argyropoulos, G., Brown, A. M., Willi, S. M., Zhu, J., He, Y., Reitman, M., … Garvey, W. T. (1998). Effects of mutations in the human uncoupling protein 3 gene on the respiratory quotient and fat oxidation in severe obesity and type 2 diabetes. Journal of Clinical Investigation, 102(7), 1345–1351.

Armed Forces Health Surveillance Centre. (2015). Medical surveillance month report (Vol. 22).

Aruoma, O. I. (1998). Free radicals, oxidative stress, and antioxidants in human health and disease. Journal of the American Oil Chemists' Society, 75(2), 199–212.

Astrand, I. (1960). Aerobic work capacity in men and women with special reference to age. Acta Physiologica Scandinavica. Supplementum, 49(169), 1.

Avila, G., O'Brien, J. J., & Dirksen, R. T. (2001). Excitation–contraction uncoupling by a human central core disease mutation in the ryanodine receptor. Proceedings of the National Academy of Sciences, 98(7), 4215–4220.

Bailey, A. G., & Bloch, E. C. (1987). Malignant Hyperthermia in a Three-Month-Old American Indian Infant. Anesthesia & Analgesia, 66(10).

Baker, L. B. (2017). Sweating Rate and Sweat Sodium Concentration in Athletes: A Review of Methodology and Intra/Inter-individual Variability. Sports Medicine, 47(Suppl 1), 111–128.

Balaban, R. S. (2002). Cardiac Energy Metabolism Homeostasis: Role of Cytosolic Calcium. Journal of Molecular and Cellular Cardiology, 34(10), 1259–1271.

Bannister, R. A., Pessah, I. N., & Beam, K. G. (2009). The Skeletal L-type Ca2+ Current Is a Major Contributor to Excitation-coupled Ca2+ entry. The Journal of General Physiology, 133(1), 79-91.

Barber, R. D., Harmer, D. W., Coleman, R. A., & Clark, B. J. (2005). GAPDH as a housekeeping gene: analysis of GAPDH mRNA expression in a panel of 72 human tissues. Physiological Genomics, 21(3), 389-395.

Barclay, J., & Hansel, M. (1991). Free radicals may contribute to oxidative muscle fatigue. Canadian journal of physiology and pharmacology, 69, 279-284.

Barone, V., Del Re, V., Gamberucci, A., Polverino, V., Galli, L., Rossi, D., … Sorrentino, V. (2017). Identification and characterization of three novel mutations in the CASQ1 gene in four patients with tubular aggregate myopathy. Human Mutation, 38(12), 1761–1773.

BBC NEWS. (2015a). SAS deaths: The savage beauty of the Brecon Beacons. Retrieved from http://www.bbc.co.uk/news/uk-wales-33506589.

BBC NEWS. (2015b). SAS selection deaths: Coroner delivers neglect conclusion. Retrieved from http://www.bbc.co.uk/news/uk-wales-33512416.

BBC NEWS. (2016). Gavin Williams death: Army "failed to prevent beasting." Retrieved from http://www.bbc.co.uk/news/uk-wales-south-east-wales-35260947.

BBC NEWS. (2017). Brecon Beacons soldier training deaths: Two charged. BBC NEWS.

Beard, N. A., Sakowska, M. M., Dulhunty, A. F., & Laver, D. R. (2002). Calsequestrin is an inhibitor of skeletal muscle ryanodine receptor calcium release channels. Biophysical Journal, 82(1 Pt 1), 310–320.

Bellinger, A. M., Reiken, S., Dura, M., Murphy, P. W., Deng, S. X., Landry, D. W., … Marks, A. R. (2008). Remodeling of ryanodine receptor complex causes “leaky” channels: a molecular mechanism for decreased exercise capacity. Proceedings of the National Academy of Sciences of the United States of America, 105(6), 2198–2202.

Bendahan, D., Kozak-Ribbens, G., Confort-Gouny, S., Ghattas, B., Figarella-Branger, D., Aubert, M., & Cozzone, P. J. (2001). A Noninvasive Investigation of Muscle Energetics Supports Similarities Between Exertional Heat Stroke and Malignant Hyperthermia. Anesthesia & Analgesia, 93(3), 683-689.

Bendahan, D., Kozak-Ribbens, G., M. D., Rodet, L., Confort-Gouny, S. P., & Cozzone P. J., P. (1998). ^{31}Phosphorus Magnetic Resonance Spectroscopy Characterization of Muscular Metabolic Anomalies in Patients with Malignant Hyperthermia Application to Diagnosis. Anesthesiology, 88(1), 96–107.

Benjamini, Y., & Hochberg, Y. (1995). Controlling the false discovery rate: a practical and powerful approach to multiple testing. Journal of the Royal Statistical Society Series B (Statistical Methodology), 57(1), 289-300.

Bentley, D. R., Balasubramanian, S., Swerdlow, H. P., Smith, G. P., Milton, J., Brown, C. G., … Smith, A. J. (2008). Accurate Whole Human Genome Sequencing using Reversible Terminator Chemistry. Nature, 456(7218), 53–59.

Berardo, A., DiMauro, S., & Hirano, M. (2010). A Diagnostic Algorithm for Metabolic Myopathies. Current Neurology and Neuroscience Reports, 10(2), 118–126.

Berchtold, M. W., Brinkmeier, H., & Müntener, M. (2000). Calcium Ion in Skeletal Muscle: Its Crucial Role for Muscle Function, Plasticity, and Disease. Physiological Reviews, 80(3), 1215-1265.

Bettens, F., Brunet, L., & Tiercy, J.-M. (2014). High-allelic variability in HLA-C mRNA expression: association with HLA-extended haplotypes. Genes & Immunity, 15(3), 176–181.

Bilbey, D. L., & Prabhakaran, V. M. (1996). Muscle cramps and magnesium deficiency: case reports. Canadian Family Physician, 42, 1348–1351.

Binkley, H. M., Beckett, J., Casa, D. J., Kleiner, D. M., & Plummer, P. E. (2002). National Athletic Trainers’ Association Position Statement: Exertional Heat Illnesses. Journal of Athletic Training, 37(3), 329–343.

Böhm, J., Chevessier, F., De Paula, A. M., Koch, C., Attarian, S., Feger, C., … Laporte, J. (2013). Constitutive Activation of the Calcium Sensor STIM1 Causes Tubular-Aggregate Myopathy. The American Journal of Human Genetics, 92(2), 271–278.

Boncompagni, S., Rossi, A. E., Micaroni, M., Hamilton, S. L., Dirksen, R. T., Franzini-Armstrong, C., & Protasi, F. (2009). Characterization and temporal development of cores in a mouse model of malignant hyperthermia. Proceedings of the National Academy of Sciences, 106(51), 21996–22001.

Boncompagni, S., Thomas, M., Lopez, J. R., Allen, P. D., Yuan, Q., Kranias, E. G., … Perez, C. F. (2012). Triadin/Junctin Double Null Mouse Reveals a Differential Role for Triadin and Junctin in Anchoring CASQ to the jSR and Regulating Ca2+ Homeostasis. PLOS ONE, 7(7), e39962.

Bonnefont, J.-P., Djouadi, F., Prip-Buus, C., Gobin, S., Munnich, A., & Bastin, J. (2004). Carnitine palmitoyltransferases 1 and 2: biochemical, molecular and medical aspects. Molecular Aspects of Medicine, 25(5), 495–520.

Bouchama, A., & Knochel, J. P. (2002). Heat Stroke. New England Journal of Medicine, 346(25), 1978–1988.

Boveris, A., Oshino, N., & Chance, B. (1972). The cellular production of hydrogen peroxide. Biochemical Journal, 128(3), 617–630.

Bradshaw, D. I., George, J. D., Hyde, A., LaMonte, M. J., Vehrs, P. R., Hager, R. L., & Yanowitz, F. G. (2005). An Accurate VO2max Nonexercise Regression Model for 18–65-Year-Old Adults. Research Quarterly for Exercise and Sport, 76(4), 426–432.

Bray, N. L., Pimentel, H., Melsted, P., & Pachter, L. (2016). Near-optimal probabilistic RNA-seq quantification. Nature Biotechnology, 34(5), 525–527.

Brini, M., Manni, S., Pierobon, N., Du, G. G., Sharma, P., MacLennan, D. H., & Carafoli, E. (2005). Ca2+ Signaling in HEK-293 and Skeletal Muscle Cells Expressing Recombinant Ryanodine Receptors Harboring Malignant Hyperthermia and Central Core Disease Mutations. Journal of Biological Chemistry, 280(15), 15380–15389.

Broessner, G., Beer, R., Franz, G., Lackner, P., Engelhardt, K., Brenneis, C., … Schmutzhard, E. (2005). Case report: severe heat stroke with multiple organ dysfunction – a novel intravascular treatment approach. Critical Care, 9(5), R498.

Broman, M., Gehrig, A., Islander, G., Bodelsson, M., Ranklev-Twetman, E., Rüffert, H., & Müller, C. R. (2009). Mutation screening of the RYR1-cDNA from peripheral B-lymphocytes in 15 Swedish malignant hyperthermia index cases. BJA: British Journal of Anaesthesia, 102(5), 642–649.

Brookes, P. S., Yoon, Y., Robotham, J. L., Anders, M. W., & Sheu, S.-S. (2004). Calcium, ATP, and ROS: a mitochondrial love-hate triangle. American Journal of Physiology - Cell Physiology, 287(4), C817 LP-C833.

Brostrom, C. O., Hunkeler, F. L., & Krebs, E. G. (1971). The Regulation of Skeletal Muscle Phosphorylase Kinase by Ca2+. Journal of Biological Chemistry, 246(7), 1961–1967.

Brown, R. L., Pollock, A. N., Couchman, K. G., Hodges, M., Hutchinson, D. O., Waaka, R., … Stowell, K. M. (2000). A novel ryanodine receptor mutation and genotype–phenotype correlation in a large malignant hyperthermia New Zealand Maori pedigree. Human Molecular Genetics, 9(10), 1515–1524.

Brunelle, J. K., Bell, E. L., Quesada, N. M., Vercauteren, K., Tiranti, V., Zeviani, M., … Chandel, N. S. (2005). Oxygen sensing requires mitochondrial ROS but not oxidative phosphorylation. Cell Metabolism, 1(6), 409–414.

Burkholder, T. J., Fingado, B., Baron, S., & Lieber, R. L. (1994). Relationship between muscle fiber types and sizes and muscle architectural properties in the mouse hindlimb. Journal of Morphology, 221(2), 177–190.

Calderón, J. C., Bolaños, P., & Caputo, C. (2014). The excitation–contraction coupling mechanism in skeletal muscle. Biophysical Reviews, 6(1), 133–160.

Cameron, J. M., Levandovskiy, V., MacKay, N., Utgikar, R., Ackerley, C., Chiasson, D., … Robinson, B. H. (2009). Identification of a novel mutation in GYS1 (muscle-specific glycogen synthase) resulting in sudden cardiac death, that is diagnosable from skin fibroblasts. Molecular Genetics and Metabolism, 98(4), 378–382.

Campbell, I. T., Ellis, F. R., & Evans, R. T. (1981). Metabolic rate and blood hormone and metabolite levels of individuals susceptible to malignant hyperpyrexia at rest and in response to food and mild exercise. Anesthesiology, 55(1), 46–52.

Campbell, I. T., Ellis, F. R., Evans, R. T., & Mortimer, M. G. (1983). Studies of Body Temperatures, Blood Lactate, Cortisol and Free Fatty Acid Levels During Exercise in Human Subjects Susceptible to Malignant Hyperpyrexia. Acta Anaesthesiologica Scandinavica, 27(5), 349–355.

Cannon, B., & Nedergaard, J. (2004). Brown Adipose Tissue: Function and Physiological Significance. Physiological Reviews, 84(1), 277-359.

Cannon, S. C. (2017). Mind the magnesium, in dantrolene suppression of malignant hyperthermia. Proceedings of the National Academy of Sciences, 114(18), 4576–4578.

Capacchione, J. F., & Muldoon, S. M. (2009). The Relationship Between Exertional Heat Illness, Exertional Rhabdomyolysis, and Malignant Hyperthermia. Anesthesia & Analgesia, 109(4), 1065–1069.

Capacchione, Sambuughin, Bina, Mulligan, Lawson, & Muldoon. (2010). Exertional Rhabdomyolysis and Malignant Hyperthermia in a Patient with Ryanodine Receptor Type 1 Gene, L-type Calcium Channel α-1 Subunit Gene, and Calsequestrin-1 Gene Polymorphisms. Anesthesiology, 112(1), 239–244.

Carl, S. L., Felix, K., Caswell, A. H., Brandt, N. R., Brunschwig, J.-P., Meissner, G., & Ferguson, D. G. (1995). Immunolocalization of triadin, DHP receptors, and ryanodine receptors in adult and developing skeletal muscle of rats. Muscle & Nerve, 18(11), 1232–1243.

Carpenter, D., Ringrose, C., Leo, V., Morris, A., Robinson, R. L., Halsall, J. P., … Shaw, M.-A. (2009). The role of CACNA1S in predisposition to malignant hyperthermia. BMC Medical Genetics, 10(1), 104.

Carpenter, D., Robinson, R. L., Quinnell, R. J., Ringrose, C., Hogg, M., Casson, F., … Hopkins, P. M. (2009). Genetic variation in RYR1 and malignant hyperthermia phenotypes. British Journal of Anaesthesia, 103(4), 538–548.

Cavdar Koc, E., Burkhart, W., Blackburn, K., Moseley, A., & Spremulli, L. L. (2001). The Small Subunit of the Mammalian Mitochondrial Ribosome: IDENTIFICATION OF THE FULL COMPLEMENT OF RIBOSOMAL PROTEINS PRESENT. Journal of Biological Chemistry, 276(22), 19363–19374.

Chambers, M. A., Moylan, J. S., Smith, J. D., Goodyear, L. J., & Reid, M. B. (2009). Stretch-stimulated glucose uptake in skeletal muscle is mediated by reactive oxygen species and p38 MAP-kinase. The Journal of Physiology, 587(13), 3363–3373.

Chance, B., Sies, H., & Boveris, A. (1979). Hydroperoxide metabolism in mammalian organs. Physiological Reviews, 59(3), 527-605.

Chang, L., Nicoll Baines, K., Allen, P. D., Hopkins, P. M., Shaw, M.-A., & Boyle, J. (no date). ABSTRACT: Oxygen metabolism in Malignant Hyperthermia susceptible skeletal muscle and the effects of in vitro halothane exposure. British Journal of Anaesthesia.

Chaussain, M., Camus, F., Defoligny, C., Eymard, B., & Fardeau, M. (1992). Exercise intolerance in patients with McArdle's disease or mitochondrial myopathies. The European Journal of Medicine, 1(8), 457-463.

Chelu, M. G., Goonasekera, S. A., Durham, W. J., Tang, W., Lueck, J. D., Riehl, J., … Hamilton, S. L. (2006). Heat- and anesthesia-induced malignant hyperthermia in an RyR1 knock-in mouse. The FASEB Journal, 20(2), 329–330.

Cherednichenko, G., Hurne, A. M., Fessenden, J. D., Lee, E. H., Allen, P. D., Beam, K. G., & Pessah, I. N. (2004). Conformational activation of Ca2+ entry by depolarization of skeletal myotubes. Proceedings of the National Academy of Sciences of the United States of America, 101(44), 15793–15798.

Cherednichenko, G., Ward, C. W., Feng, W., Cabrales, E., Michaelson, L., Samso, M., … Pessah, I. N. (2008). Enhanced Excitation-Coupled Calcium Entry in Myotubes Expressing Malignant Hyperthermia Mutation R163C Is Attenuated by Dantrolene. Molecular Pharmacology, 73(4), 1203-1212.

Cheung, S. S., & McLellan, T. M. (1998). Heat acclimation, aerobic fitness, and hydration effects on tolerance during uncompensable heat stress. Journal of Applied Physiology, 84(5), 1731-1739.

Choi, R. H., Koenig, X., & Launikonis, B. S. (2017). Dantrolene requires Mg2+ to arrest malignant hyperthermia. Proceedings of the National Academy of Sciences, 114(18), 4811–4815.

Choi, Y., Sims, G. E., Murphy, S., Miller, J. R., & Chan, A. P. (2012). Predicting the Functional Effect of Amino Acid Substitutions and Indels. PLOS ONE, 7(10), e46688.

Cleeter, M. W. J., Cooper, J. M., Darley-Usmar, V. M., Moncada, S., & Schapira, A. H. V. (1994). Reversible inhibition of cytochrome c oxidase, the terminal enzyme of the mitochondrial respiratory chain, by nitric oxide. Federation of European Biochemical Societies Letters, 345(1), 50–54.

Cook, N. L., Viola, H. M., Sharov, V. S., Hool, L. C., Schöneich, C., & Davies, M. J. (2012). Myeloperoxidase-derived oxidants inhibit sarco/endoplasmic reticulum Ca(2+)-ATPase activity, and perturb Ca(2+) homeostasis in human coronary artery endothelial cells. Free Radical Biology & Medicine, 52(5), 951–961.

Cooper, E. R., Ferrara, M. S., Casa, D. J., Powell, J. W., Broglio, S. P., Resch, J. E., & Courson, R. W. (2016). Exertional Heat Illness in American Football Players: When Is the Risk Greatest? Journal of Athletic Training, 51(8), 593–600.

Cooper, L. L., Li, W., Lu, Y., Centracchio, J., Terentyeva, R., Koren, G., & Terentyev, D. (2013). Redox modification of ryanodine receptors by mitochondria-derived reactive oxygen species contributes to aberrant Ca2+ handling in ageing rabbit hearts. The Journal of Physiology, 591(23), 5895–5911.

Corrochano, S., Männikkö, R., Joyce, P. I., McGoldrick, P., Wettstein, J., Lassi, G., … Acevedo-Arozena, A. (2014). Novel mutations in human and mouse SCN4A implicate AMPK in myotonia and periodic paralysis. Brain, 137(12), 3171–3185.

Corti, S., Bordoni, A., Ronchi, D., Musumeci, O., Aguennouz, M., Toscano, A., … Comi, G. P. (2008). Clinical features and new molecular findings in Carnitine Palmitoyltransferase II (CPT II) deficiency. Journal of the Neurological Sciences, 266(1), 97–103.

Cussó, R., Lerner, L. R., Cadefau, J., Gil, M., Prats, C., Gasparotto, M., & Krisman, C. R. (2003). Differences between glycogen biogenesis in fast- and slow-twitch rabbit muscle. Biochimica et Biophysica Acta (BBA) - General Subjects, 1620(1), 65–71.

Dainese, M., Quarta, M., Lyfenko, A. D., Paolini, C., Canato, M., Reggiani, C., … Protasi, F. (2009). Anesthetic- and heat-induced sudden death in calsequestrin-1-knockout mice. The Federation of American Societies for Experimental Biology (FASEB) Journal, 23(6), 1710–1720.

Davis, M., Brown, R., Dickson, A., Horton, H., James, D., Laing, N., … Stowell, K. (2002). Malignant hyperthermia associated with exercise-induced rhabdomyolysis or congenital abnormalities and a novel RYR1 mutation in New Zealand and Australian pedigrees. Br J Anaesth, 88(4), 508–515.

Dehbi, M., Uzzaman, T., Baturcam, E., Eldali, A., Ventura, W., & Bouchama, A. (2012). Toll-Like Receptor 4 and High-Mobility Group Box 1 Are Critical Mediators of Tissue Injury and Survival in a Mouse Model for Heatstroke. PLOS ONE, 7(9), e44100.

Denborough, M. A. (1979). Etiology and pathophysiology of malignant hyperthermia. International Anesthesiology Clinics, 17(4), 11–23.

Denborough, M. A., Dennett, X., & Anderson, R. M. (1973). Central-core disease and malignant hyperpyrexia. British Medical Journal, 1(5848), 272–273.

Denborough, M., & Lovell, R. (1960). Anaesthetics deaths in family. Lancet, 34, 395-3396.

Dennis, G., Sherman, B. T., Hosack, D. A., Yang, J., Gao, W., Lane, H. C., & Lempicki, R. A. (2003). DAVID: Database for Annotation, Visualization, and Integrated Discovery. Genome Biology, 4(9), R60.

des Georges, A., Clarke, O. B., Zalk, R., Yuan, Q., Condon, K. J., Grassucci, R. A., … Frank, J. (2016). Structural Basis for Gating and Activation of RyR1. Cell, 167(1), 145–157.e17.

Deschauer, M., Wieser, T., & Zierz, S. (2005). Muscle carnitine palmitoyltransferase ii deficiency: Clinical and molecular genetic features and diagnostic aspects. Archives of Neurology, 62(1), 37–41.

Deuster, P. A., Contreras-Sesvold, C. L., O'Connor, F. G., Campbell, W. W., Kenney, K., Capacchione, J. F., … Heled, Y. (2013). Genetic polymorphisms associated with exertional rhabdomyolysis. European Journal of Applied Physiology, 113(8), 1997–2004.

Dheda, K., Huggett, J., Bustin, S., A Johnson, M., Rook, G., & Zumla, A. (2004). Validation of housekeeping genes for normalizing RNA expression in Real-time PCR. BioTechniques, 37(1), 112-119.

Di Blasi, C., Sansanelli, S., Ruggieri, A., Moriggi, M., Vasso, M., D'Adamo, A. P., … Mora, M. (2015). A CASQ1 founder mutation in three Italian families with protein aggregate myopathy and hyperCKaemia. Journal of Medical Genetics, 52(9),617-26.

Dias, J. M., & Vogel, P. D. (2009). Effects of small molecule modulators on ATP binding to skeletal ryanodine receptor. The Protein Journal, 28(5), 240–246.

Dimauro, I., Mercatelli, N., & Caporossi, D. (2016). Exercise-induced ROS in heat shock proteins response. Free Radical Biology and Medicine, 98, 46–55.

Disease Control and Prevention. (2011). Nonfatal Sports and Recreation Heat Illness Treated in Hospital Emergency Departments — United States, 2001–2009. Morbidity and Mortality Weekly Report, 60(29), 977–1008.

Divet, A., Paesante, S., Grasso, C., Cavagna, D., Tiveron, C., Paolini, C., … Zorzato, F. (2007). Increased Ca2+ storage capacity of the skeletal muscle sarcoplasmic reticulum of transgenic mice over-expressing membrane bound calcium binding protein junctate. Journal of Cellular Physiology, 213(2), 464–474.

Dlamini, N., Voermans, N. C. C., Lillis, S., Stewart, K., Kamsteeg, E.-J. J., Drost, G., … Jungbluth, H. (2013). Mutations in RYR1 are a common cause of exertional myalgia and rhabdomyolysis. Neuromuscular Disorders, 23(7), 540–548.

Doudna, J. A., & Charpentier, E. (2014). The new frontier of genome engineering with CRISPR-Cas9. Science, 346(6213), 1258096.

Dowling, J. J., Lillis, S., Amburgey, K., Zhou, H., Al-Sarraj, S., Buk, S. J. A., … Jungbluth, H. (2011). King–Denborough syndrome with and without mutations in the skeletal muscle ryanodine receptor (RYR1) gene. Neuromuscular Disorders, 21(6), 420–427.

Downs, C. A., & Heckathorn, S. A. (1998). The mitochondrial small heat-shock protein protects NADH:ubiquinone oxidoreductase of the electron transport chain during heat stress in plants. Federation of European Biochemical Societies Letters, 430(3), 246–250.

Draznin, B. (1988). Intracellular calcium, insulin secretion, and action. The American Journal of Medicine, 85(5, Supplement 1), 44–58.

Du, G. G., Khanna, V. K., Guo, X., & MacLENNAN, D. H. (2004). Central core disease mutations R4892W, I4897T and G4898E in the ryanodine receptor isoform 1 reduce the Ca(2+) sensitivity and amplitude of Ca(2+)-dependent Ca(2+) release. Biochemical Journal, 382(Pt 2), 557–564.

Duarte, S. T., Oliveira, J., Santos, R., Pereira, P., Barroso, C., Conceição, I., & Evangelista, T. (2011). Dominant and recessive RYR1 mutations in adults with core lesions and mild muscle symptoms. Muscle & Nerve, 44(1), 102–108.

DuBose, D. A., Wenger, C. B., Flinn, S. D., Judy, T. A., Dubovtsev, A. I., & Morehouse, D. H. (2003). Distribution and mitogen response of peripheral blood lymphocytes after exertional heat injury. Journal of Applied Physiology, 95(6), 2381 LP-2389. Retrieved from

Ducreux, S., Zorzato, F., Müller, C., Sewry, C., Muntoni, F., Quinlivan, R., … Treves, S. (2004). Effect of Ryanodine Receptor Mutations on Interleukin-6 Release and Intracellular Calcium Homeostasis in Human Myotubes from Malignant Hyperthermia-susceptible Individuals and Patients Affected by Central Core Disease. Journal of Biological Chemistry, 279(42), 43838–43846.

Duke, A. M., Hopkins, P. M., Calaghan, S. C., Halsall, J. P., & Steele, D. S. (2010). Store-operated Ca2+ entry in malignant hyperthermia-susceptible human skeletal muscle. Journal of Biological Chemistry, 285(33), 25645–25653.

Duno, M., Colding-Jorgensen, E., Grunnet, M., Jespersen, T., Vissing, J., & Schwartz, M. (2004). Difference in allelic expression of the CLCN1 gene and the possible influence on the myotonia congenita phenotype. European Journal of Human Genetics, 12(9), 738–743.

Durham, W. J., Aracena-Parks, P., Long, C., Rossi, A. E., Goonasekera, S. A., Boncompagni, S., … Hamilton, S. L. (2008). RyR1 S-Nitrosylation Underlies Environmental Heat Stroke and Sudden Death in Y522S RyR1 Knockin Mice. Cell, 133(1), 53–65.

El-Orabi, N. F., Rogers, C. B., Gray Edwards, H., & Schwartz, D. D. (2011). Heat-induced inhibition of superoxide dismutase and accumulation of reactive oxygen species leads to HT-22 neuronal cell death. Journal of Thermal Biology, 36(1), 49–56.

Eltit, J. M., Bannister, R. A., Moua, O., Altamirano, F., Hopkins, P. M., Pessah, I. N., … Allen, P. D. (2012). Malignant hyperthermia susceptibility arising from altered resting coupling between the skeletal muscle L-type Ca2+ channel and the type 1 ryanodine receptor. Proceedings of the National Academy of Sciences, 109(20), 7923–7928.

Eltit, J. M., Ding, X., Pessah, I. N., Allen, P. D., & Lopez, J. R. (2013). Nonspecific sarcolemmal cation channels are critical for the pathogenesis of malignant hyperthermia. Federation of European Biochemical Societies Journal, 27(3).

EMHG. (1984). A protocol for the investigation of malignant hyperpyrexia (MH) susceptibility. British Journal of Anaesthesia., 56, 1267–1269.

Endo, Y., Noguchi, S., Hara, Y., Hayashi, Y. K., Motomura, K., Miyatake, S., … Nishino, I. (2015). Dominant mutations in ORAI1 cause tubular aggregate myopathy with hypocalcemia via constitutive activation of store-operated Ca2+ channels. Human Molecular Genetics, 24(3), 637–648.

Epstein, Y., & Roberts, W. O. (2011). The pathopysiology of heat stroke: an integrative view of the final common pathway. Scandanavian Journal of Medicine & Science in Sports, 21(6), 742–748.

Estève, E., Eltit, J. M., Bannister, R. A., Liu, K., Pessah, I. N., Beam, K. G., … López, J. R. (2010). A malignant hyperthermia–inducing mutation in RYR1 (R163C): alterations in Ca(2+) entry, release, and retrograde signaling to the DHPR. The Journal of General Physiology, 135(6), 619–628.

European Malignant Hyperthermia Group. (2017). Retrieved from: https://emhg.org/genetics.

Evgrafov, O. V, Mersiyanova, I., Irobi, J., Van Den Bosch, L., Dierick, I., Leung, C. L., … Timmerman, V. (2004). Mutant small heat-shock protein 27 causes axonal Charcot-Marie-Tooth disease and distal hereditary motor neuropathy. Nature Genetics, 36(6), 602–606.

F Wallace, R., Kriebel, D., Punnett, L., H Wegman, D., Bruce Wenger, C., W Gardner, J., & A Kark, J. (2006). Risk factors for recruit exertional heat illness by gender and training period. Aviation, space, and environmental medicine, 77(4), 415-421.

Febbraio, M. A. (2001). Alterations in Energy Metabolism During Exercise and Heat Stress. Sports Medicine, 31(1), 47–59.

Feng, W., Barrientos, G. C., Cherednichenko, G., Yang, T., Padilla, I. T., Truong, K., … Pessah, I. N. (2011). Functional and Biochemical Properties of Ryanodine Receptor Type 1 Channels from Heterozygous R163C Malignant Hyperthermia-Susceptible Mice. Molecular Pharmacology, 79(3), 420 LP-431.

Feriotto, G., Finotti, A., Volpe, P., Treves, S., Ferrari, S., Angelelli, C., … Gambari, R. (2005). Myocyte Enhancer Factor 2 Activates Promoter Sequences of the Human AβH-J-J Locus, Encoding Aspartyl-β-Hydroxylase, Junctin, and Junctate. Molecular and Cellular Biology, 25(8), 3261–3275.

Ferradini, V., Cassone, M., Nuovo, S., Bagni, I., D'Apice, M. R., Botta, A., … Sangiuolo, F. (2017). Targeted Next Generation Sequencing in patients with Myotonia Congenita. Clinica Chimica Acta, 470, 1–7.

Ferreiro, A., Monnier, N., Romero, N. B., Leroy, J.-P., Bönnemann, C., Haenggeli, C.-A., … Guicheney, P. (2002). A recessive form of central core disease, transiently presenting as multi-minicore disease, is associated with a homozygous mutation in the ryanodine receptor type 1 gene. Annals of Neurology, 51(6), 750–759.

Figarella-Branger, D., Kozak-Ribbens, G., Rodet, L., Aubert, M., Borsarelli, J., Cozzone, P. J., & Pellissier, J. F. (1993). Pathological findings in 165 patients explored for malignant hyperthermia susceptibility. Neuromuscular Disorders, 3(5), 553–556.

Figarella-Branger, D., Machado, A. M. B., Putzu, G. A., Malzac, P., Voelckel, M. A., & Pellissier, J. F. (1997). Exertional rhabdomyolysis and exercise intolerance revealing dystrophinopathies. Acta Neuropathologica, 94(1), 48–53.

Fill, M., Coronado, R., Mickelson, J. R., Vilven, J., Ma, J. J., Jacobson, B. A., & Louis, C. F. (1990). Abnormal ryanodine receptor channels in malignant hyperthermia. Biophysical Journal, 57(3), 471–475.

Fiszer, D., Shaw, M.-A., Fisher, N. A., Carr, I. M., Gupta, P. K., Watkins, E. J., … Hopkins, P. M. (2015). Next Generation Sequencing of RYR1 and CACNA1S in Malignant Hyperthermia and Exertional Heat Illness. Anesthesiology, 122(5), 1033–1046.

Fittipaldi, S., Mercatelli, N., Dimauro, I., Jackson, M. J., Paronetto, M. P., & Caporossi, D. (2015). Alpha B-crystallin induction in skeletal muscle cells under redox imbalance is mediated by a JNK-dependent regulatory mechanism. Free Radical Biology and Medicine, 86, 331–342.

Flucher, B. E., Conti, A., Takeshima, H., & Sorrentino, V. (1999). Type 3 and Type 1 Ryanodine Receptors Are Localized in Triads of the Same Mammalian Skeletal Muscle Fibers. The Journal of Cell Biology, 146(3), 621 LP-630.

Fokkema, I. F., Taschner, P. E., Schaafsma, G. C., Celli, J., Laros, J. F., & den Dunnen, J. T. (2011). LOVD v.2.0: the next generation in gene variant databases. Human Mutation, 32(5), 557–563.

Fortunato, G., Carsana, A., Tinto, N., Brancadoro, V., Canfora, G., & Salvatore, F. (1999). A case of discordance between genotype and phenotype in a malignant hyperthermia family. European Journal of Human Genetics, 7(4), 415-20.

Fryer, M. W., & Stephenson, D. G. (1996). Total and sarcoplasmic reticulum calcium contents of skinned fibres from rat skeletal muscle. The Journal of Physiology, 493(Pt 2), 357–370.

Fujii, J., Otsu, K., Zorzato, F., de Leon, S., Khanna, V. K., Weiler, J. E., … MacLennan, D. H. (1991). Identification of a mutation in porcine ryanodine receptor associated with malignant hyperthermia. Science, 253(5018), 448-451.

Fujino, T., Kondo, J., Ishikawa, M., Morikawa, K., & Yamamoto, T. T. (2001). Acetyl-CoA Synthetase 2, a Mitochondrial Matrix Enzyme Involved in the Oxidation of Acetate. Journal of Biological Chemistry, 276(14), 11420–11426.

Furuichi, T., Furutama, D., Hakamata, Y., Nakai, J., Takeshima, H., & Mikoshiba, K. (1994). Multiple types of ryanodine receptor/Ca2+ release channels are differentially expressed in rabbit brain. The Journal of Neuroscience, 14(8), 4794 LP-4805.

Ganeshan, K., & Chawla, A. (2017). Warming the mouse to model human diseases. Nature Reviews Endocrinology, 13(8), 458–465.

Gershome, C., Lin, E., Kashihara, H., Hove-Madsen, L., & Tibbits, G. F. (2010). Colocalization of voltage-gated Na+ channels with the Na+/Ca2+ exchanger in rabbit cardiomyocytes during development. American Journal of Physiology-Heart and Circulatory Physiology, 300(1), H300–H311.

Gillard, E. F., Otsu, K., Fujii, J., Khanna, V. K., de Leon, S., Derdemezi, J., … MacLennan, D. H. (1991). A substitution of cysteine for arginine 614 in the ryanodine receptor is potentially causative of human malignant hyperthermia. Genomics, 11(3), 751–755.

Girard, T., Cavagna, D., Padovan, E., Spagnoli, G., Urwyler, A., Zorzato, F., & Treves, S. (2001). B-lymphocytes from Malignant Hyperthermia-susceptible Patients Have an Increased Sensitivity to Skeletal Muscle Ryanodine Receptor Activators. Journal of Biological Chemistry, 276(51), 48077–48082.

Giulivi, C., Ross-Inta, C., Omanska-Klusek, A., Napoli, E., Sakaguchi, D., Barrientos, G., … Pessah, I. N. (2011). Basal Bioenergetic Abnormalities in Skeletal Muscle from Ryanodine Receptor Malignant Hyperthermia-susceptible R163C Knock-in Mice. Journal of Biological Chemistry, 286(1), 99–113.

Glazer, J. L. (2005). Management of Heatstroke and Heat Exhaustion. American Family Physician Journal, 71(11), 2133–2140.

Glover, L., Culligan, K., Cala, S., Mulvey, C., & Ohlendieck, K. (2001). Calsequestrin binds to monomeric and complexed forms of key calcium-handling proteins in native sarcoplasmic reticulum membranes from rabbit skeletal muscle. Biochimica et Biophysica Acta (BBA) - Biomembranes, 1515(2), 120–132.

Goeman, J. J. (2010). L1 Penalized Estimation in the Cox Proportional Hazards Model. Biometrical Journal, 52(1), 70–84.

Gordon, C. J. (2017). The mouse thermoregulatory system: Its impact on translating biomedical data to humans. Physiology & Behaviour, 179, 55–66.

Görlach, A., Bertram, K., Hudecova, S., & Krizanova, O. (2015). Calcium and ROS: A mutual interplay. Redox Biology, 6, 260–271.

Goto, K., Okuyama, R., Sugiyama, H., Honda, M., Kobayashi, T., Uehara, K., … Yoshioka, T. (2003). Effects of heat stress and mechanical stretch on protein expression in cultured skeletal muscle cells. Pflügers Archive, 447(2), 247–253.

Gouzi, F., Maury, J., Molinari, N., Pomiès, P., Mercier, J., Préfaut, C., & Hayot, M. (2013). Reference values for vastus lateralis fiber size and type in healthy subjects over 40 years old: a systematic review and metaanalysis. Journal of Applied Physiology, 115(3), 346–354.

Graier, W. F., Trenker, M., & Malli, R. (2008). Mitochondrial Ca(2+), the secret behind the function of uncoupling proteins 2 and 3? Cell Calcium, 44(1), 36–50.

Grayson, B. L., Wang, L., & Aune, T. M. (2011). Peripheral blood gene expression profiles in metabolic syndrome, coronary artery disease and type 2 diabetes. Genes & Immunity, 12(5), 341–351.

Green, J. H., Ellis, F. R., Halsall, P. J., Campbell, I. T., Currie, S., & Caddy, J. (1987). Thermoregulation, plasma catecholamine and metabolite levels during submaximal work in individuals susceptible to malignant hyperpyrexia. Acta Anaesthesiologica Scandinavica, 31(2), 122–126.

Grievink, H., & Stowell, K. M. (2010). Allele-specific differences in ryanodine receptor 1 mRNA expression levels may contribute to phenotypic variability in malignant hyperthermia. Orphanet Journal of Rare Diseases, 5(10), 1750-1172.

Grijalba, M. T., Vercesi, A. E., & Schreier, S. (1999). Ca2+-Induced Increased Lipid Packing and Domain Formation in Submitochondrial Particles. A Possible Early Step in the Mechanism of Ca2+-Stimulated Generation of Reactive Oxygen Species by the Respiratory Chain. Biochemistry, 38(40), 13279–13287.

Gronke, R. S., Welsch, D. J., VanDusen, W. J., Garsky, V. M., Sardana, M. K., Stern, A. M., & Friedman, P. A. (1990). Partial purification and characterization of bovine liver aspartyl beta-hydroxylase. Journal of Biological Chemistry, 265(15), 8558–8565.

Groom, L., Muldoon, S. M., Tang, Z. Z., Brandom, B. W., Bayarsaikhan, M., Bina, S., … Dirksen, R. T. (2011). Identical de novo Mutation in the Type 1 Ryanodine Receptor Gene Associated with Fatal, Stress-induced Malignant Hyperthermia in Two Unrelated Families. Anesthesiology, 115(5), 938–945.

Gross, M., Rötzer, E., Kölle, P., Mortier, W., Reichmann, H., Goebel, H. . H., … Sabina, R. . L. (2002). A G468-T AMPD1 mutant allele contributes to the high incidence of myoadenylate deaminase deficiency in the Caucasian population. Neuromuscular Disorders, 12(6), 558–565.

Grzybowski, M., Schänzer, A., Pepler, A., Heller, C., Neubauer, B. A., & Hahn, A. (2017). Novel STAC3 Mutations in the First Non-Amerindian Patient with Native American Myopathy. Neuropediatrics, 48(6), 451–455.

Guglielmi, V., Vattemi, G., Gualandi, F., Voermans, N. C., Marini, M., Scotton, C., … Tomelleri, G. (2013). SERCA1 protein expression in muscle of patients with Brody disease and Brody syndrome and in cultured human muscle fibers. Molecular Genetics and Metabolism, 110(1–2), 162–169.

Guo, W., & Campbell, K. P. (1995). Association of Triadin with the Ryanodine Receptor and Calsequestrin in the Lumen of the Sarcoplasmic Reticulum. Journal of Biological Chemistry, 270(16), 9027–9030.

Györke, I., Hester, N., Jones, L. R., & Györke, S. (2004). The Role of Calsequestrin, Triadin, and Junctin in Conferring Cardiac Ryanodine Receptor Responsiveness to Luminal Calcium. Biophysical Journal, 86(4), 2121–2128.

Haddad, F., Zaldivar, F., Cooper, D. M., & Adams, G. R. (2005). IL-6-induced skeletal muscle atrophy. Journal of Applied Physiology, 98(3), 911-917.

Hall, D. M., Buettner, G. R., Matthes, R. D., & Gisolfi, C. V. (1994). Hyperthermia stimulates nitric oxide formation: electron paramagnetic resonance detection of .NO-heme in blood. Journal of Applied Physiology, 77(2), 548-553.

Hamanaka, R. B., & Chandel, N. S. (2010). Mitochondrial reactive oxygen species regulate cellular signaling and dictate biological outcomes. Trends in Biochemical Sciences, 35(9), 505–513.

Hartley, S. W., & Mullikin, J. C. (2016). Detection and visualization of differential splicing in RNA-Seq data with JunctionSeq. Nucleic Acids Research, 44(15), e127–e127.

Haslbeck, M., Franzmann, T., Weinfurtner, D., & Buchner, J. (2005). Some like it hot: the structure and function of small heat-shock proteins. Nature Structural & Molecular Biology, 12(10), 842–846.

Hedberg, C., Niceta, M., Fattori, F., Lindvall, B., Ciolfi, A., D'Amico, A., … Bertini, E. (2014). Childhood onset tubular aggregate myopathy associated with de novo STIM1 mutations. Journal of Neurology, 261(5), 870–876.

Henstridge, D. C., Bruce, C. R., Drew, B. G., Tory, K., Kolonics, A., Estevez, E., … Febbraio, M. A. (2014). Activating HSP72 in Rodent Skeletal Muscle Increases Mitochondrial Number and Oxidative Capacity and Decreases Insulin Resistance. Diabetes, 63(6), 1881 LP-1894.

Hepner, A., & Greenberg, M. (2017). 95 Safety and Efficacy of Dantrolene Sodium (250 mg/5 mL) in Patients With Exertional Heat Stroke. Annals of Emergency Medicine, 70(4), S39.

Hirst, J., King, M. S., & Pryde, K. R. (2008). The production of reactive oxygen species by complex I. Biochemical Society Transactions, 36(5), 976-980.

Hong, C.-S., Kwon, S.-J., & Kim, D. H. (2007). Multiple functions of junctin and junctate, two distinct isoforms of aspartyl beta-hydroxylase. Biochemical and Biophysical Research Communications, 362(1), 1–4.

Hopkins, P. M. (2007). Is there a link between malignant hyperthermia and exertional heat illness? British Journal of Sports Medicine, 41(5), 283–284.

Hopkins, P. M. (2008). Malignant hyperthemia. Current Anaesthesia & Critical Care, 19(1), 22–33.

Hopkins, P. M., Ellis, F. R., & Halsall, P. J. (1991). Evidence for related myopathies in exertional heat stroke and malignant hyperthermia. The Lancet, 338(8781), 1491–1492.

Hopkins, P. M., Rüffert, H., Snoeck, M. M., Girard, T., Glahn, K. P. E., Ellis, F. R., … Urwyler, A. (2015). European Malignant Hyperthermia Group guidelines for investigation of malignant hyperthermia susceptibility. British Journal of Anaesthesia, 115(4), 531-539.

Horstick, E. J., Linsley, J. W., Dowling, J. J., Hauser, M. A., McDonald, K. K., Ashley-Koch, A., … Kuwada, J. Y. (2013). Stac3 is a component of the excitation-contraction coupling machinery and mutated in Native American myopathy. Nature Communications, 4, 1952.

Hosoi, E., Nishizaki, C., Gallagher, K. L., Wyre, H. W., Matsuo, Y., & Sei, Y. (2001). Expression of the Ryanodine Receptor Isoforms in Immune Cells. The Journal of Immunology, 167(9), 4887 LP-4894.

Huang, C., Jiao, H., Song, Z., Zhao, J., Wang, X., & Lin, H. (2015). Heat stress impairs mitochondria functions and induces oxidative injury in broiler chickens1. Journal of Animal Science, 93, 2144–2153.

Huang, D. W., Sherman, B. T., & Lempicki, R. A. (2008). Systematic and integrative analysis of large gene lists using DAVID bioinformatics resources. Nature Protocols, 4(1), 44–57.

Hubbard, R. W., Bowers, W. D., Matthew, W. T., Curtis, F. C., Criss, R. E., Sheldon, G. M., & Ratteree, J. W. (1977). Rat model of acute heatstroke mortality. Journal of Applied Physiology, 42(6), 809–816.

Hwang, H., Bowen, B. P., Lefort, N., Flynn, C. R., De Filippis, E. A., Roberts, C., … Mandarino, L. J. (2010). Proteomics Analysis of Human Skeletal Muscle Reveals Novel Abnormalities in Obesity and Type 2 Diabetes. Diabetes, 59(1), 33 LP-42.

Ibarra, C. A., Wu, S., Murayama, K., Minami, N., Ichihara, Y., Kikuchi, H., … Nishino, I. (2006). Malignant Hyperthermia in Japan Mutation Screening of the Entire Ryanodine Receptor Type 1 Gene Coding Region by Direct Sequencing. Anesthesiology, 104(6), 1146–54.

Inouye, S., Fujimoto, M., Nakamura, T., Takaki, E., Hayashida, N., Hai, T., & Nakai, A. (2007). Heat Shock Transcription Factor 1 Opens Chromatin Structure of Interleukin-6 Promoter to Facilitate Binding of an Activator or a Repressor. Journal of Biological Chemistry, 282(45), 33210–33217.

Irobi, J., Impe, K. Van, Seeman, P., Jordanova, A., Dierick, I., Verpoorten, N., … Timmerman, V. (2004). Hot-spot residue in small heat-shock protein 22 causes distal motor neuropathy. Nature Genetics, 36(6), 597–601.

Isackson, P. J., Bennett, M. J., & Vladutiu, G. D. (2006). Identification of 16 new disease-causing mutations in the CPT2 gene resulting in carnitine palmitoyltransferase II deficiency. Molecular Genetics and Metabolism, 89(4), 323–331.

Iyoho, A., Laurel, N., & Macfadden, L. (2017). Modeling of Gender Differences in Thermoregulation. Military Medicine, 182, 295-303.

Jacobs, R. A., Díaz, V., Meinild, A.-K., Gassmann, M., & Lundby, C. (2013). The C57Bl/6 mouse serves as a suitable model of human skeletal muscle mitochondrial function. Experimental Physiology, 98(4), 908–921.

Jain, D., Sharma, M. C., Sarkar, C., Suri, V., Sharma, S. K., Singh, S., & Das, T. K. (2008). Tubular aggregate myopathy: A rare form of myopathy. Journal of Clinical Neuroscience, 15(11), 1222–1226.

Jekabsone, A., Ivanoviene, L., Brown, G. C., & Borutaite, V. (2003). Nitric oxide and calcium together inactivate mitochondrial complex I and induce cytochrome c release. Journal of Molecular and Cellular Cardiology, 35(7), 803–809.

Jensen, P. K. (1966). Antimycin-insensitive oxidation of succinate and reduced nicotinamide-adenine dinucleotide in electron-transport particles I. pH dependency and hydrogen peroxide formation. Biochimica et Biophysica Acta (BBA) - Enzymology and Biological Oxidation, 122(2), 157–166.

Jiang, D., Chen, W., Xiao, J., Wang, R., Kong, H., Jones, P. P., … Chen, S. R. W. (2008). Reduced Threshold for Luminal Ca(2+) Activation of RyR1 Underlies a Causal Mechanism of Porcine Malignant Hyperthermia. Journal of Biological Chemistry, 283(30), 20813–20820.

Jones, L. R., Zhang, L., Sanborn, K., Jorgensen, A. O., & Kelley, J. (1995). Purification, Primary Structure, and Immunological Characterization of the 26-kDa Calsequestrin Binding Protein (Junctin) from Cardiac Junctional Sarcoplasmic Reticulum. Journal of Biological Chemistry, 270(51), 30787–30796.

Jungbluth, H. (2007). Central core disease. Orphanet Journal of Rare Diseases, 2(25), 1750-1172.

Jungbluth, H., Lillis, S., Zhou, H., Abbs, S., Sewry, C., Swash, M., & Muntoni, F. (2017). Late-onset axial myopathy with cores due to a novel heterozygous dominant mutation in the skeletal muscle ryanodine receptor (RYR1) gene. Neuromuscular Disorders, 19(5), 344–347.

Jungbluth, H., Zhou, H., Sewry, C. A., Robb, S., Treves, S., Bitoun, M., … Muntoni, F. (2007). Centronuclear myopathy due to a de novo dominant mutation in the skeletal muscle ryanodine receptor (RYR1) gene. Neuromuscular Disorders, 17(4), 338–345.

Kaciuba-Uscilko, H., & Grucza, R. (2001). Gender differences in thermoregulation. Current Opinion in Clinical Nutrition & Metabolic Care, 4(6), 533-536.

Kammoun, M., Cassar-Malek, I., Meunier, B., & Picard, B. (2014). A Simplified Immunohistochemical Classification of Skeletal Muscle Fibres in Mouse. European Journal of Histochemistry, 58(2)2254, 163-168.

Kanno, T., Sudo, K., Maekawa, M., Nishimura, Y., Ukita, M., & Fukutake, K. (1988). Lactate dehydrogenase M-subunit deficiency: a new type of hereditary exertional myopathy. Clinica Chimica Acta, 173(1), 89–98.

Karki, R., Pandya, D., Elston, R. C., & Ferlini, C. (2015). Defining “mutation” and “polymorphism” in the era of personal genomics. BMC Medical Genomics, 8, 37.

Kawasaki, T., & Kasai, M. (1994). Regulation of Calcium Channel in Sarcoplasmic Reticulum by Calsequestrin. Biochemical and Biophysical Research Communications, 199(3), 1120–1127.

Kazman, J. Ben, Heled, Y., Lisman, P. J., Druyan, A., Deuster, P. A., & O’Connor, F. G. (2013). Exertional Heat Illness: The Role of Heat Tolerance Testing. Current Sports Medicine Reports, 12(2), 101-105.

Keller, C., A, S., Pilegaard, H., Osada, T., Saltin, B., Pedersen, B. K., & Neufer, P. D. (2001). Transcriptional activation of the IL-6 gene in human contracting skeletal muscle: influence of muscle glycogen content. The Federation of American Societies for Experimental Biology (FASEB) Journal, 15(14), 2748–2750.

Kerr, Z. Y., Casa, D. J., Marshall, S. W., & Comstock, R. D. (2013). Epidemiology of Exertional Heat Illness Among U.S. High School Athletes. American Journal of Preventive Medicine, 44(1), 8–14.

Khassaf, M., Child, R. B., McArdle, A., Brodie, D. A., Esanu, C., & Jackson, M. J. (2001). Time course of responses of human skeletal muscle to oxidative stress induced by nondamaging exercise. Journal of Applied Physiology, 90(3), 1031-1035.

Kho, A. T., Kang, P. B., Kohane, I. S., & Kunkel, L. M. (2006). Transcriptome-scale similarities between mouse and human skeletal muscles with normal and myopathic phenotypes. BMC Musculoskeletal Disorders, 7, 23.

Kim, J., Wei, Y., & Sowers, J. R. (2008). Role of Mitochondrial Dysfunction in Insulin Resistance. Circulation Research, 102(4), 401 LP-414.

Kimlicka, L., Lau, K., Tung, C.-C., & Van Petegem, F. (2013). Disease mutations in the ryanodine receptor N-terminal region couple to a mobile intersubunit interface. Nature Communications, 4(1506).

King, A., Selak, M. A., & Gottlieb, E. (2006). Succinate dehydrogenase and fumarate hydratase: linking mitochondrial dysfunction and cancer. Oncogene, 25(34), 4675–4682.

King, M. A., Leon, L. R., Mustico, D. L., Haines, J. M., & Clanton, T. L. (2015). Biomarkers of multiorgan injury in a preclinical model of exertional heat stroke. Journal of Applied Physiology, 118(10), 1207-1220.

Kingma, B. R. M., Frijns, A. J. H., Schellen, L., & van Marken Lichtenbelt, W. D. (2014). Beyond the classic thermoneutral zone: Including thermal comfort. Temperature: Multidisciplinary Biomedical Journal, 1(2), 142–149.

Kircher, M., Witten, D. M., Jain, P., O'Roak, B. J., Cooper, G. M., & Shendure, J. (2014). A general framework for estimating the relative pathogenicity of human genetic variants. Nature Genetics, 46(3), 310–315.

Knochel, J. (1996). Modeling of Gender Differences in Thermoregulation. In P. M. Hopkins & F. R. Ellis (Eds.), Hyperthermic and Hypermetabolic Disorders. (pp. 42–62). Cambridge University Press.

Kobayashi, T., Tonai, S., Ishihara, Y., Koga, R., Okabe, S., & Watanabe, T. (2000). Abnormal functional and morphological regulation of the gastric mucosa in histamine H2 receptor–deficient mice. Journal of Clinical Investigation, 105(12), 1741–1749.

Kobzik, L., Reid, M. B., Bredt, D. S., & Stamler, J. S. (1994). Nitric oxide in skeletal muscle. Nature, 372(546).

Kochling, A., Wappler, F., Winkler, G., & Schulte am Esch, J. (1998). Rhabdomyolysis following severe physical exercise in a patient with predisposition to malignant hyperthermia. Anaesthesia & Intensive Care, 26(3), 315–8.

Koussounadis, A., Langdon, S. P., Um, I. H., Harrison, D. J., & Smith, V. A. (2015). Relationship between differentially expressed mRNA and mRNA-protein correlations in a xenograft model system. Scientific Reports, 5(10775).

Kraeva, N., Heytens, L., Jungbluth, H., Treves, S., Voermans, N., Kamsteeg, E., … Riazi, S. (2015). Compound RYR1 heterozygosity resulting in a complex phenotype of malignant hyperthermia susceptibility and a core myopathy. Neuromuscular Disorders, 25(7), 567–576.

Kraeva, N., Zvaritch, E., Rossi, A. E., Goonasekera, S. A., Zaid, H., Frodis, W., … Riazi1, S. (2013). Novel Excitation-Contraction Uncoupled RYR1 Mutations in Patients With Central Core Disease. Neuromuscular Disorders, 23(2), 120–132.

Kregel, K. C., & Moseley, P. L. (1996). Differential effects of exercise and heat stress on liver HSP70 accumulation with aging. Journal of Applied Physiology, 80(2), 547 LP-551.

Krustrup, P., Ferguson, R. A., Kjær, M., & Bangsbo, J. (2003). ATP and heat production in human skeletal muscle during dynamic exercise: higher efficiency of anaerobic than aerobic ATP resynthesis. The Journal of Physiology, 549(Pt 1), 255–269.

Kuppevelt, T. H. van, Veerkamp, J. H., Fishbein, W. N., Ogasawara, N., & Sabina, R. L. (1994). Immunolocalization of AMP-deaminase isozymes in human skeletal muscle and cultured muscle cells: concentration of isoform M at the neuromuscular junction. Journal of Histochemistry & Cytochemistry, 42(7), 861–868.

Kurebayashi, N., & Ogawa, Y. (2001). Depletion of Ca2+ in the sarcoplasmic reticulum stimulates Ca2+ entry into mouse skeletal muscle fibres. The Journal of Physiology, 533(1), 185–199.

Laforêt, P., Acquaviva-Bourdain, C., Rigal, O., Brivet, M., Penisson-Besnier, I., Chabrol, B., … Vianey-Saban, C. (2009). Diagnostic assessment and long-term follow-up of 13 patients with Very Long-Chain Acyl-Coenzyme A dehydrogenase (VLCAD) deficiency. Neuromuscular Disorders, 19(5), 324–329.

Lahat, H., Pras, E., & Eldar, M. (2003). RYR2 and CASQ2 Mutations in Patients Suffering from Catecholaminergic Polymorphic Ventricular Tachycardia. Circulation, 107(3), e29 LP-e29.

Lahat, H., Pras, E., Olender, T., Avidan, N., Ben-Asher, E., Man, O., … Eldar, M. (2001). A Missense Mutation in a Highly Conserved Region of CASQ2 Is Associated with Autosomal Recessive Catecholamine-Induced Polymorphic Ventricular Tachycardia in Bedouin Families from Israel. The American Journal of Human Genetics, 69(6), 1378–1384.

Lanner, J. T., Georgiou, D. K., Joshi, A. D., & Hamilton, S. L. (2010). Ryanodine Receptors: Structure, Expression, Molecular Details, and Function in Calcium Release. Cold Spring Harbor Perspectives in Biology, 2(11), a003996.

Lavezzi, W. A., Capacchione, J. F., Muldoon, S. M., Sambuughin, N., Bina, S., Steele, D., & Brandom, B. W. (2013). Death in the Emergency Department: An Unrecognized Awake Malignant Hyperthermia-Like Reaction in a Six-Year-Old. Anesthesia & Analgesia, 116(2).

Law, C. W., Chen, Y., Shi, W., & Smyth, G. K. (2014). Voom: precision weights unlock linear model analysis tools for RNA-seq read counts. Genome Biology, 15(R29).

Lee, J. M., Rho, S.-H., Shin, D. W., Cho, C., Park, W. J., Eom, S. H., … Kim, D. H. (2004). Negatively Charged Amino Acids within the Intraluminal Loop of Ryanodine Receptor Are Involved in the Interaction with Triadin. Journal of Biological Chemistry, 279(8), 6994–7000.

Leipold, E., Lu, S., Gordon, D., Hansel, A., & Heinemann, S. H. (2004). Combinatorial Interaction of Scorpion Toxins Lqh-2, Lqh-3, and LqhαIT with Sodium Channel Receptor Sites-3. Molecular Pharmacology, 65(3), 685-691.

Leite, A., Oliveira, N., & Rocha, M. (2012). McArdle disease: a case report and review. International Medical Case Reports Journal, 5, 1–4.

Lek, M., Karczewski, K. J., Minikel, E. V, Samocha, K. E., Banks, E., Fennell, T., … Consortium, E. A. (2016). Analysis of protein-coding genetic variation in 60,706 humans. Nature, 536(7616), 285–291.

Leon, L. R., DuBose, D. A., & Mason, C. W. (2004). Heat stress induces a biphasic thermoregulatory response in mice. American Journal of Physiology - Regulatory, Integrative and Comparative Physiology, 288(1), R197-R204.

Leon, L. R., Gordon, C. J., Helwig, B. G., Rufolo, D. M., & Blaha, M. D. (2010). Thermoregulatory, behavioral, and metabolic responses to heatstroke in a conscious mouse model. American Journal of Physiology - Regulatory, Integrative and Comparative Physiology, 299(1), R241-R248.

Levano, S., Vukcevic, M., Singer, M., Matter, A., Treves, S., Urwyler, A., & Girard, T. (2009). Increasing the number of diagnostic mutations in malignant hyperthermia. Human Mutation, 30(4), 590–598.

Li, H., Handsaker, B., Wysoker, A., Fennell, T., Ruan, J., Homer, N., … Subgroup, 1000 Genome Project Data Processing. (2009). The Sequence Alignment/Map format and SAMtools. Bioinformatics, 25(16), 2078–2079.

Li, L., Tan, H., Yang, H., Li, F., He, X., Gu, Z., … Su, L. (2017). Reactive oxygen species mediate heat stress-induced apoptosis via ERK dephosphorylation and Bcl-2 ubiquitination in human umbilical vein endothelial cells. Oncotarget, 8(8), 12902–12916.

Li, L., Wei, Y., Van Winkle, L., Zhang, Q.-Y., Zhou, X., Hu, J., … Ding, X. (2011). Generation and Characterization of a Cyp2f2-Null Mouse and Studies on the Role of CYP2F2 in Naphthalene-Induced Toxicity in the Lung and Nasal Olfactory Mucosa. The Journal of Pharmacology and Experimental Therapeutics, 339(1), 62–71.

Liao, Y., Erxleben, C., Abramowitz, J., Flockerzi, V., Zhu, M. X., Armstrong, D. L., & Birnbaumer, L. (2008). Functional interactions among Orai1, TRPCs, and STIM1 suggest a STIM-regulated heteromeric Orai/TRPC model for SOCE/Icrac channels. Proceedings of the National Academy of Sciences of the United States of America, 105(8), 2895-2900.

Lin, T.-K., Hughes, G., Muratovska, A., Blaikie, F. H., Brookes, P. S., Darley-Usmar, V., … Murphy, M. P. (2002). Specific Modification of Mitochondrial Protein Thiols in Response to Oxidative Stress: A PROTEOMICS APPROACH. Journal of Biological Chemistry, 277(19), 17048–17056.

Loh, E., Rebbeck, T. R., Mahoney, P. D., DeNofrio, D., Swain, J. L., & Holmes, E. W. (1999). Common Variant in *AMPD1*; Gene Predicts Improved Clinical Outcome in Patients with Heart Failure. Circulation, 99(11), 1422-1425.

Lonsdale, J., Thomas, J., Salvatore, M., Phillips, R., Lo, E., Shad, S., … Moore, H. F. (2013). The Genotype-Tissue Expression (GTEx) project. Nature Genetics, 45(6), 580-585.

Love, M. I., Huber, W., & Anders, S. (2014). Moderated estimation of fold change and dispersion for RNA-seq data with DESeq2. Genome Biology, 15(12), 550.

Loy, R. E., Orynbayev, M., Xu, L., Andronache, Z., Apostol, S., Zvaritch, E., … Dirksen, R. T. (2010). Muscle weakness in I4895T knock-in mice as a result of reduced ryanodine receptor Ca2+ ion permeation and release from the sarcoplasmic reticulum. The Journal of General Physiology, 137(1), 43-57.

Lu, K.-C., Wang, J.-Y., Lin, S.-H., Chu, P., & Lin, Y.-F. (2004). Role of circulating cytokines and chemokines in exertional heatstroke. Critical Care Medicine, 32(2), 399-403.

Lyfenko, A. D., & Dirksen, R. T. (2008). Differential dependence of store-operated and excitation-coupled Ca2+ entry in skeletal muscle on STIM1 and Orai1. The Journal of Physiology, 586(20), 4815-4824.

MacLennan Zorzarto, F., Fujii, J., Otsu, K., Phillips, M., Lai, F. A., Meissner, G., … Korneluk, R. G. (1989). Cloning and localization of the human calcium release channel (ryanodine receptor) gene to the proximal long arm (cen-q13.2) of human chromosome 19. American Journal of Human Genetics, 45(suppl.), A205.

Madamanchi, N. R., Li, S., Patterson, C., & Runge, M. S. (2001). Reactive Oxygen Species Regulate Heat-Shock Protein 70 via the JAK/STAT Pathway. Arteriosclerosis, Thrombosis, and Vascular Biology, 21(3), 321-326.

Magee, K., & Shy, G. (1956). A new congenital non-progressive myopathy. Brain, 79(4), 610–21.

Mane, V. P., Heuer, M. A., Hillyer, P., Navarro, M. B., & Rabin, R. L. (2008). Systematic Method for Determining an Ideal Housekeeping Gene for Real-Time PCR Analysis. Journal of Biomolecular Techniques, 19(5), 342–347.

Mangoni, M. E., & Barrère-Lemaire, S. (2004). Adenosine receptors, heart rate, and cardioprotection. Cardiovascular Research, 62(3), 447-449.

Marí, M., Morales, A., Colell, A., García-Ruiz, C., & Fernández-Checa, J. C. (2009). Mitochondrial Glutathione, a Key Survival Antioxidant. Antioxidants & Redox Signaling, 11(11), 2685-2700.

Marioni, J. C., Mason, C. E., Mane, S. M., Stephens, M., & Gilad, Y. (2008). RNA-seq: An assessment of technical reproducibility and comparison with gene expression arrays. Genome Research, 18(9), 1509–1517.

Maron, B. J., Doerer, J. J., Haas, T. S., Tierney, D. M., & Mueller, F. O. (2009). Sudden Deaths in Young Competitive Athletes: Analysis of 1866 Deaths in the United States, 1980–2006. Circulation, 119(8), 1085–1092.

Martin, M. (2011). Cutadapt removes adapter sequences from high-throughput sequencing reads. EMBnet Journal, 17(1).

Matsumoto, H., Hayashi, S., Hatashita, M., Ohnishi, K., Ohtsubo, T., Kitai, R., … Kano, E. (1999). Nitric Oxide Is an Initiator of Intercellular Signal Transduction for Stress Response after Hyperthermia in Mutant p53 Cells of Human Glioblastoma. Cancer Research, 59(13), 3239–3244.

Matthews, E., Labrum, R., Sweeney, M. G., Sud, R., Haworth, A., Chinnery, P. F., … Hanna, M. G. (2009). Voltage sensor charge loss accounts for most cases of hypokalemic periodic paralysis. Neurology, 72(18), 1544–1547.

McArdle, B. (1951). Myopathy due to a defect in muscle glycogen breakdown. Clinical Science, 10(1), 13–35.

McCormack, J. G., & Denton, R. M. (1979). The effects of calcium ions and adenine nucleotides on the activity of pig heart 2-oxoglutarate dehydrogenase complex. Biochemical Journal, 180(3), 533–544.

McCormack, J. G., & Denton, R. M. (1993). Mitochondrial Ca2+ Transport and the Role of Intramitochondrial Ca2+ in the Regulation of Energy Metabolism. Developmental Neuroscience, 15(3–5), 165–173.

McCormack, J. G., Halestrap, A. P., & Denton, R. M. (1990). Role of calcium ions in regulation of mammalian intramitochondrial metabolism. Physiological Reviews, 70(2), 391–425.

McCue, M. E., Valberg, S. J., Lucio, M., & Mickelson, J. R. (2008). Glycogen Synthase 1 (GYS1) Mutation in Diverse Breeds with Polysaccharide Storage Myopathy. Journal of Veterinary Internal Medicine, 22(5), 1228–1233.

McLellan, T. M., Jacobs, I., & Bain, J. B. (1993). Influence of temperature and metabolic rate on work performance with Canadian Forces NBC clothing. Aviation, Space, and Environmental Medicine, 64(7), 587–594.

McMillan, D. R., Xiao, X., Shao, L., Graves, K., & Benjamin, I. J. (1998). Targeted Disruption of Heat Shock Transcription Factor 1 Abolishes Thermotolerance and Protection against Heat-inducible Apoptosis. Journal of Biological Chemistry, 273(13), 7523–7528.

McPherson, P. S., & Campbell, K. P. (1990). Solubilization and biochemical characterization of the high affinity [3H]ryanodine receptor from rabbit brain membranes. Journal of Biological Chemistry, 265(30), 18454–18460.

Melli, G., Chaudhry, V., & Cornblath, D. R. (2005). Rhabdomyolysis: An Evaluation of 475 Hospitalized Patients. Medicine, 84(6). 377-385.

Merry, T. L., & McConell, G. K. (2009). Skeletal muscle glucose uptake during exercise: A focus on reactive oxygen species and nitric oxide signalling. International Union of Biochemistry and Molecular Biology (IUBMB) Life, 61(5), 479–484.

Metro. (2015). “I saw him take his last breath”: Walking the Nile shows last moments of journalist Matt Power. Metro. Retrieved from http://metro.co.uk/2015/01/05/i-saw-him-take-his-last-breath-walking-the-nile-shows-last-moments-of-journalist-matt-power-5009273/

Mickelson, J. R., & Louis, C. F. (1996). Malignant hyperthermia: excitation-contraction coupling, Ca2+ release channel, and cell Ca2+ regulation defects. Physiological Reviews, 76(2), 537–592.

Miller, J. (2003). Malignant Hyperthermia. Anesthesia & Analgesia, 96(2), 635-635.

Ministry of Defence. (2017). Heat illness and cold injury: prevention and management. Joint Service Protocol (JSP) 539, V3.0.

MoD. (2010). Treating Injury and Illness arising on Military Operations. National Audit Office.

MoD. (2012). CLIMATIC ILLNESS AND INJURY IN THE ARMED FORCES: FORCE PROTECTION AND INITIAL MEDICAL TREATMENT. Retrieved from https://www.gov.uk/government/uploads/system/uploads/attachment_data/file/245226/JSP_539_v2_1.pdf

Moniz, M., Mascarenhas, M., Escobar, C., Nunes, P., Abadesso, C., Loureiro, H., & Almeida, H. (2017). Rhabdomyolysis as a manifestation of a metabolic disease: A case report. Revista Brasileira de Terapia Intensiva, 29(1), 111-114.

Monnier, N., Krivosic-Horber, R., Payen, J.-F., Kozak-Ribbens, G., Nivoche, Y., Adnet, P., … Lunardi, J. (2002). Presence of Two Different Genetic Traits in Malignant Hyperthermia Families: Implication for Genetic Analysis, Diagnosis, and Incidence of Malignant Hyperthermia Susceptibility. Anesthesiology, 97(5), 1067–1074.

Monnier, N., Romero, N. B., Lerale, J., Nivoche, Y., Qi, D., MacLennan, D. H., … Lunardi, J. (2000). An autosomal dominant congenital myopathy with cores and rods is associated with a neomutation in the RYR1 gene encoding the skeletal muscle ryanodine receptor. Human Molecular Genetics, 9(18), 2599–2608.

Moore, A. C., Stacey, M. J., Bailey, K. G. H., Bunn, R. J., Woods, D. R., Haworth, K. J., … Folkes, S. E. F. (2016). Risk factors for heat illness among British soldiers in the hot Collective Training Environment. Journal of the Royal Army Medical Corps, 162(6), 434–439.

Mora-Rodriguez, R. (2012). Influence of Aerobic Fitness on Thermoregulation During Exercise in the Heat. Exercise and Sport Sciences Reviews, 40(2), 79-87.

Moran, D., Heled, Y., Still, L., Loar, A., & Shapiro, Y. (2004). Assessment of heat tolerance for post exertional heat stroke individuals. Medical Science Monitor: International Medical Journal of Experimental and Clinical Research, 10(6), 252–257.

Moran, D. S., Erlich, T., & Epstein, Y. (2007). The Heat Tolerance Test: An Efficient Screening Tool for Evaluating Susceptibility to Heat. Journal of Sport Rehabilitation, 16(3), 215–221.

Morisaki, T., Gross, M., Morisaki, H., Pongratz, D., Zöllner, N., & Holmes, E. W. (1992). Molecular basis of AMP deaminase deficiency in skeletal muscle. Proceedings of the National Academy of Sciences of the United States of America, 89(14), 6457–6461.

Mortazavi, A., Williams, B. A., McCue, K., Schaeffer, L., & Wold, B. (2008). Mapping and quantifying mammalian transcriptomes by RNA-Seq. Nature Methods, 5(7), 621–628.

Morton, J. P., Kayani, A. C., McArdle, A., & Drust, B. (2009). The Exercise-Induced Stress Response of Skeletal Muscle, with Specific Emphasis on Humans. Sports Medicine, 39(8), 643–662.

Morton, J. P., MacLaren, D. P. M., Cable, N. T., Bongers, T., Griffiths, R. D., Campbell, I. T., … Drust, B. (2006). Time course and differential responses of the major heat shock protein families in human skeletal muscle following acute non-damaging treadmill exercise. Journal of Applied Physiology, 101(1), 176-182.

Mueller, F. O., & Cantu, R. C. (2009). Catastrophic Sports Injury Research. Retrieved from http://www.unc.edu/depts/nccsi/2009ALLSPORT.pdf

Mujahid, A., Sato, K., Akiba, Y., & Toyomizu, M. (2006). Acute heat stress stimulates mitochondrial superoxide production in broiler skeletal muscle, possibly via downregulation of uncoupling protein content. Poultry Science, 85(7), 1259–1265.

Muldoon, S., Bunger, R., Deuster, P., & Sambuughin, N. (2007). Identification of risk factors for exertional heat illness: a brief commentary on genetic testing. Journal of Sports Rehabilitation, 16(3), 222–226.

Muldoon, S., Deuster, P., Brandom, B., & Bunger, R. (2004). Is there a link between malignant hyperthermia and exertional heat illness? Exercise and Sport Science Reviews, 32(4), 174–179.

Muldoon, S., Deuster, P., Voelkel, M., Capacchione, J., & Bunger, R. (2008). Exertional heat illness, exertional rhabdomyolysis, and malignant hyperthermia: is there a link? Current Sports Medicine Reports, 7(2), 74–80.

Muñoz-Cánoves, P., Scheele, C., Pedersen, B. K., & Serrano, A. L. (2013). Interleukin-6 myokine signaling in skeletal muscle: a double-edged sword? The Federation of European Biochemical Societies Journal, 280(17), 4131–4148.

Murayama, T., Kurebayashi, N., Ogawa, H., Yamazawa, T., Oyamada, H., Suzuki, J., … Sakurai, T. (2016). Genotype–Phenotype Correlations of Malignant Hyperthermia and Central Core Disease Mutations in the Central Region of the RYR1 Channel. Human Mutation, 37(11), 1231–1241.

Murayama, T., & Ogawa, Y. (1996). Properties of Ryr3 Ryanodine Receptor Isoform in Mammalian Brain. Journal of Biological Chemistry, 271(9), 5079–5084.

Murphy, M. P. (2009). How mitochondria produce reactive oxygen species. Biochemical Journal, 417(Pt 1), 1–13.

Nabben, M., Hoeks, J., Briedé, J. J., Glatz, J. F. C., Moonen-Kornips, E., Hesselink, M. K. C., & Schrauwen, P. (2008). The effect of UCP3 overexpression on mitochondrial ROS production in skeletal muscle of young versus aged mice. Federation of European Biochemical Societies (FEBS) Letters, 582(30), 4147–4152.

Nadel, E., Pandolf, K., Roberts, M., & Stolwijk, J. (1974). Mechanisms of thermal acclimation to exercise and heat. Journal of Applied Physiology, 37(4), 515–520.

Nakai, J., Imagawa, T., Hakamata, Y., Shigekawa, M., Takeshima, H., & Numa, S. (1990). Primary structure and functional expression from cDN A of the cardiac ryanodine receptor/calcium release channel. Federation of European Biochemical Societies (FEBS) Letters, 271(1–2), 169–177.

Narum, S. R. (2006). Beyond Bonferroni: Less conservative analyses for conservation genetics. Conservation Genetics, 7(5), 783–787.

Neal, R. A., Corbett, J., Massey, H. C., & Tipton, M. J. (2016). Effect of short-term heat acclimation with permissive dehydration on thermoregulation and temperate exercise performance. Scandinavian Journal of Medicine & Science in Sports, 26(8), 875–884.

Neal, R. C., Ferdinand, K. C., Yčas, J., & Miller, E. (2009). Relationship of Ethnic Origin, Gender, and Age to Blood Creatine Kinase Levels. The American Journal of Medicine, 122(1), 73–78.

Nelson, D. A., Deuster, P. A., Carter, R., Hill, O. T., Wolcott, V. L., & Kurina, L. M. (2016). Sickle Cell Trait, Rhabdomyolysis, and Mortality among U.S. Army Soldiers. New England Journal of Medicine, 375(5), 435–442.

Nichols, A. W. (2014). Heat-related illness in sports and exercise. Current Reviews in Musculoskeletal Medicine, 7(4), 355–365.

Nielsen, A. R., & Pedersen, B. K. (2007). The biological roles of exercise-induced cytokines: IL-6, IL-8, and IL-15. Applied Physiology, Nutrition, and Metabolism, 32(5), 833–839.

Nishio, H., Sato, T., Fukunishi, S., Tamura, A., Iwata, M., Tsuboi, K., & Suzuki, K. (2009). Identification of malignant hyperthermia-susceptible ryanodine receptor type 1 gene (RYR1) mutations in a child who died in a car after exposure to a high environmental temperature. Legal Medicine (Tokyo), 11(3), 142–143.

Nogales-Gadea, G., Brull, A., Santalla, A., Andreu, A. L., Arenas, J., Martín, M. A., … Pinós, T. (2015). McArdle Disease: Update of Reported Mutations and Polymorphisms in the PYGM Gene. Human Mutation, 36(7), 669–78.

Nogales-Gadea, G., Rubio, J. C., Fernandez-Cadenas, I., Garcia-Consuegra, I., Lucia, A., Cabello, A., … Martín, M. A. (2008). Expression of the muscle glycogen phosphorylase gene in patients with McArdle disease: the role of nonsense-mediated mRNA decay. Human Mutation, 29(2), 277–283.

Norman, B., Sabina, R. L., & Jansson, E. (2001). Regulation of skeletal muscle ATP catabolism by AMPD1 genotype during sprint exercise in asymptomatic subjects. Journal of Applied Physiology, 91(1), 258-264.

O'Brien, J. J., Feng, W., Allen, P. D., Chen, S. R. W., Pessah, I. N., & Beam, K. G. (2002). Ca2+ Activation of RyR1 Is Not Necessary for the Initiation of Skeletal-Type Excitation-Contraction Coupling. Biophysical Journal, 82(5), 2428–2435.

Observer. (2014). Remembering Journalist Matthew Power. Observer. Retrieved from http://observer.com/2014/03/remembering-journalist-matthew-power/

Oliveira, S. F., Pinho, L., Rocha, H., Nogueira, C., Vilarinho, L., Dinis, M. J., & Silva, C. (2013). Rhabdomyolysis as a Presenting Manifestation of Very Long-Chain Acyl-Coenzyme A Dehydrogenase Deficiency. Clinics and Practice, 3(2), e22.

Ørstavik, K., Wallace, S. C., Torbergsen, T., Abicht, A., Erik Tangsrud, S., Kerty, E., & Rasmussen, M. (2015). A de novo Mutation in the SCN4A Gene Causing Sodium Channel Myotonia. Journal of Neuromuscular Diseases, 2(2), 181–184.

Pan, Z., Yang, D., Nagaraj, R. Y., Nosek, T. A., Nishi, M., Takeshima, H., … Ma, J. (2002). Dysfunction of store-operated calcium channel in muscle cells lacking mg29. Nature Cell Biology, 4, 379.

Paolini, C., Quarta, M., Nori, A., Boncompagni, S., Canato, M., Volpe, P., … Protasi, F. (2007). Reorganized stores and impaired calcium handling in skeletal muscle of mice lacking calsequestrin-1. The Journal of Physiology, 583(2), 767–784.

Park, H. J., Chang, Y., Lee, J. E., Koo, H., Oh, J., Choi, Y.-C., & Park, K. D. (2016). Recurrent Episodes of Rhabdomyolysis after Seizures in a Patient with Glycogen Storage Disease Type V. Journal of Clinical Neurology (Seoul, Korea), 12(3), 373–375.

Peng, T.-I., & Jou, M.-J. (2010). Oxidative stress caused by mitochondrial calcium overload. Annals of the New York Academy of Sciences, 1201(1), 183–188.

Périard, J. D., Ruell, P., Caillaud, C., & Thompson, M. W. (2012). Plasma Hsp72 (HSPA1A) and Hsp27 (HSPB1) expression under heat stress: influence of exercise intensity. Cell Stress and Chaperones, 17(3), 375–383.

Pessah, I. N., Waterhouse, A. L., & Casida, J. E. (1985). The calcium-Ryanodine receptor complex of skeletal and cardiac muscle. Biochemical and Biophysical Research Communications, 128(1), 449–456.

Pestov, N. B., Ahmad, N., Korneenko, T. V, Zhao, H., Radkov, R., Schaer, D., … Modyanov, N. N. (2007). Evolution of Na,K-ATPase βm-subunit into a coregulator of transcription in placental mammals. Proceedings of the National Academy of Sciences, 104(27), 11215–11220.

Petitprez, S., Tiab, L., Chen, L., Kappeler, L., Rösler, K. M., Schorderet, D., … Burgunder, J.-M. (2008). A novel dominant mutation of the Nav1.4 α-subunit domain I leading to sodium channel myotonia. Neurology, 71(21), 1669-1675.

Pirone, A., Schredelseker, J., Tuluc, P., Gravino, E., Fortunato, G., Flucher, B. E., … Grabner, M. (2010). Identification and functional characterization of malignant hyperthermia mutation T1354S in the outer pore of the $Ca_v1.1$-subunit. American Journal of Physiology - Cell Physiology, 299(6), C1345-C1354.

Pollard, P. J., Brière, J. J., Alam, N. A., Barwell, J., Barclay, E., Wortham, N. C., … Tomlinson, I. P. M. (2005). Accumulation of Krebs cycle intermediates and over-expression of HIF1α in tumours which result from germline FH and SDH mutations. Human Molecular Genetics, 14(15), 2231–2239.

Potts, L. E., Longwell, J. J., Bedocs, P., Sambuughin, N., Bina, S., Cooper, P. B., … Capacchione, J. F. (2014). Improving Awareness of Nonanesthesia-Related Malignant Hyperthermia Presentations: A Tale of Two Brothers. A&A Case Reports, 3(2), 23-26.

Powers, S. K., & Jackson, M. J. (2008). Exercise-Induced Oxidative Stress: Cellular Mechanisms and Impact on Muscle Force Production. Physiological Reviews, 88(4), 1243–1276.

Proenza, C., O'Brien, J., Nakai, J., Mukherjee, S., Allen, P. D., & Beam, K. G. (2002). Identification of a Region of RyR1 That Participates in Allosteric Coupling with the α1S (CaV1.1) II–III Loop. Journal of Biological Chemistry, 277(8), 6530–6535.

Protasi, F., Paolini, C., & Dainese, M. (2009). Calsequestrin-1: a new candidate gene for malignant hyperthermia and exertional/environmental heat stroke. The Journal of Physiology, 587(13), 3095–3100.

Pusch, M. (2002). Myotonia caused by mutations in the muscle chloride channel gene CLCN1. Human Mutation, 19(4), 423–434.

Radi, R., Cassina, A., & Hodara, R. (2002). Nitric Oxide and Peroxynitrite Interactions with Mitochondria. Biological Chemistry, 383(3-4), 401-409.

Radich, J. P., Mao, M., Stepaniants, S., Biery, M., Castle, J., Ward, T., … Linsley, P. S. (2004). Individual-specific variation of gene expression in peripheral blood leukocytes. Genomics, 83(6), 980–988.

Rebbeck, R. T., Karunasekara, Y., Board, P. G., Beard, N. A., Casarotto, M. G., & Dulhunty, A. F. (2014). Skeletal muscle excitation-contraction coupling: who are the dancing partners? International Journal of Biochemistry & Cell Biology, 48, 28–38.

Reed, L. J. (1974). Multi-enzyme complexes. Accounts of Chemical Research, 7(2), 40–46.

Reiken, S., Lacampagne, A., Zhou, H., Kherani, A., Lehnart, S. E., Ward, C., … Marks, A. R. (2003). PKA phosphorylation activates the calcium release channel (ryanodine receptor) in skeletal muscle: defective regulation in heart failure. The Journal of Cell Biology, 160(6), 919–928.

Ren, J. M., & Hultman, E. (1990). Regulation of phosphorylase a activity in human skeletal muscle. American Physiological Society, 69(3), 919–923.

Robinson, R., Carpenter, D., Shaw, M. A., Halsall, J., & Hopkins, P. (2006). Mutations in RYR1 in malignant hyperthermia and central core disease. Human Mutation, 27(10), 977–989.

Robinson, R., Hopkins, P., Carsana, A., Gilly, H., Halsall, J., Heytens, L., … Shaw, M.-A. (2003). Several Interacting genes influence the malignant hyperthermia phenotype. Human genetics, 112(2), 217-218.

Robinson, R. L., Brooks, C., Brown, S. L., Ellis, F. R., Halsall, P. J., Quinnell, R. J., … Hopkins, P. M. (2002). RYR1 mutations causing central core disease are associated with more severe malignant hyperthermia in vitro contracture test phenotypes. Human Mutation, 20(2), 88–97.

Robinson, R. L., Curran, J. L., Ellis, F. R., Halsall, P. J., Hall, W. J., Hopkins, P. M., … Shaw, M. A. (2000). Multiple interacting gene products may influence susceptibility to malignant hyperthermia. Annals of Human Genetics, 64(4), 307–320.

Rogers, R. S., Morris, E. M., Wheatley, J. L., Archer, A. E., McCoin, C. S., White, K. S., … Geiger, P. C. (2016). Deficiency in the Heat Stress Response Could Underlie Susceptibility to Metabolic Disease. Diabetes, 65(11), 3341-3351.

Roiz de Sa, D., & House, C. (2015). Exercise heat tolerance assessment following a diagnosis of heat illness in UK military personnel. Extreme Physiology & Medicine, 4(Suppl 1), A105–A105.

Rooryck, C., Kydnt, F., Bozon, D., Rouz-Buisson, N., Sacher, F., Probst, V., & Thambo, J.-B. (2015). New Family with Catecholaminergic Polymorphic Ventricular Tachycardia Linked to the Triadin Gene. Journal of Cardiovascular Electrophysiology, 26(10), 1146–1150.

Rosenberg, H., Pollock, N., Schiemann, A., Bulger, T., Stowell, K. (2015). Malignant hyperthermia: a review. Orphanet Journal of Rare Diseases, 10, 93.

Rossi, D., Simeoni, I., Micheli, M., Bootman, M., Lipp, P., Allen, P. D., & Sorrentino, V. (2002). RyR1 and RyR3 isoforms provide distinct intracellular Ca2+ signals in HEK 293 cells. Journal of Cell Science, 115(12), 2497–2504.

Rossi, D., Vezzani, B., Galli, L., Paolini, C., Toniolo, L., Pierantozzi, E., … Sorrentino, V. (2014). A Mutation in the CASQ1 Gene Causes a Vacuolar Myopathy with Accumulation of Sarcoplasmic Reticulum Protein Aggregates. Human Mutation, 35(10), 1163–1170.

Roth, S. M., Ferrell, R. E., Peters, D. G., Metter, E. J., Hurley, B. F., & Rogers, M. A. (2002). Influence of age, sex, and strength training on human muscle gene expression determined by microarray. Physiological Genomics, 10(3), 181–190.

Roux-Buisson, N., Cacheux, M., Fourest-Lieuvin, A., Fauconnier, J., Brocard, J., Denjoy, I., … Marty, I. (2012). Absence of triadin, a protein of the calcium release complex, is responsible for cardiac arrhythmia with sudden death in human. Human Molecular Genetics, 21(12), 2759–2767.

RStudio. (2016). RStudio: Integrated Development Environment for R. Boston, MA. Retrieved from http://www.rstudio.com/

Ryan, J. F., & Tedeschi, L. G. (1997). Sudden unexplained death in a patient with a family history of malignant hyperthermia. Journal of Clinical Anesthesia, 9(1), 66–68.

Sahlin, K., Gorski, J., & Edstrom, L. (1990). Influence of ATP turnover and metabolite changes on IMP formation and glycolysis in rat skeletal muscle. American Journal of Physiology-Cell Physiology, 259(3), C409–C412.

Salin, K., Auer, S. K., Rey, B., Selman, C., & Metcalfe, N. B. (2015). Variation in the link between oxygen consumption and ATP production, and its relevance for animal performance. Proceedings of the Royal Society B: Biological Sciences, 282(1812).

Sambuughin, N., Capacchione, J., Blokhin, A., Bayarsaikhan, M., Bina, S., & Muldoon, S. (2009). The ryanodine receptor type 1 gene variants in African American men with exertional rhabdomyolysis and malignant hyperthermia susceptibility. Clinical Genetics, 76(6), 564–568.

Sambuughin, N., Zvaritch, E., Kraeva, N., Sizova, O., Sivak, E., Dickson, K., … MacLennan, D. H. (2014). Exome analysis identifies Brody myopathy in a family diagnosed with malignant hyperthermia susceptibility. Molecular Genetics & Genomic Medicine, 2(6), 472–483.

Samorodnitsky, E., Datta, J., Jewell, B. M., Hagopian, R., Miya, J., Wing, M. R., … Roychowdhury, S. (2015). Comparison of Custom Capture for Targeted Next-Generation DNA Sequencing. The Journal of Molecular Diagnostics, 17(1), 64–75.

Sanchez, E. J., Lewis, K. M., Danna, B. R., & Kang, C. (2012). High-capacity Ca2+ Binding of Human Skeletal Calsequestrin. Journal of Biological Chemistry, 287(14), 11592–11601.

Savarese, M., Di Fruscio, G., Mutarelli, M., Torella, A., Magri, F., Santorelli, F. M., … Nigro, V. (2014). MotorPlex provides accurate variant detection across large muscle genes both in single myopathic patients and in pools of DNA samples. Acta Neuropathologica Communications, 2(1), 100.

Sawka, M. N., Leon, L. R., Montain, S. J., & Sonna, L. A. (2011). Integrated Physiological Mechanisms of Exercise Performance, Adaptation, and Maladaptation to Heat Stress. In Comprehensive Physiology. Comprehensive Biology, 1(4), 1883-928.

Sawka, M. N., Wenger, C. B., & Pandolf, K. B. (2010). Thermoregulatory Responses to Acute Exercise-Heat Stress and Heat Acclimation. Comprehensive Physiology, Suppl. 14, 157-185

Scalco, R. S., Snoeck, M., Quinlivan, R., Treves, S., Laforét, P., Jungbluth, H., & Voermans, N. C. (2016). Exertional rhabdomyolysis: physiological response or manifestation of an underlying myopathy? British Medical Journal Open Sport & Exercise Medicine, 2(1), e000151.

Scheller, J., Chalaris, A., Schmidt-Arras, D., & Rose-John, S. (2011). The pro- and anti-inflammatory properties of the cytokine interleukin-6. Biochimica et Biophysica Acta (BBA) - Molecular Cell Research, 1813(5), 878–888.

Schermann, H., Heled, Y., Fleischmann, C., Ketko, I., Schiffmann, N., Epstein, Y., & Yanovich, R. (2017). The validity of the heat tolerance test in prediction of recurrent exertional heat illness events. Journal of Science and Medicine in Sport, 21(6), 549-552.

Schiemann, A. H., & Stowell, K. M. (2016). Comparison of pathogenicity prediction tools on missense variants in RYR1 and CACNA1S associated with malignant hyperthermia. British Journal of Anaesthesia, 117(1), 124–128.

Schlingmann, K. P., Waldegger, S., Konrad, M., Chubanov, V., & Gudermann, T. (2007). TRPM6 and TRPM7—Gatekeepers of human magnesium metabolism. Biochimica et Biophysica Acta (BBA) - Molecular Basis of Disease, 1772(8), 813–821.

Schmittgen, T. D., & Livak, K. J. (2008). Analyzing real-time PCR data by the comparative CT method. Nature Protocols, 3(6), 1101–1108.

Senior, A. E. (1988). ATP synthesis by oxidative phosphorylation. Physiological Reviews, 68(1), 177-231.

Sharma, P., Ishiyama, N., Nair, U., Li, W., Dong, A., Miyake, T., … Gramolini, A. O. (2012). Structural Determination of the Phosphorylation Domain of the Ryanodine Receptor. The Federation of European Biochemical Societies (FEBS) Journal, 279(20), 3952–3964.

Shen, X., Franzini-Armstrong, C., Lopez, J. R., Jones, L. R., Kobayashi, Y. M., Wang, Y., … Perez, C. F. (2007). Triadins Modulate Intracellular Ca2+ Homeostasis but Are Not Essential for Excitation-Contraction Coupling in Skeletal Muscle. Journal of Biological Chemistry, 282(52), 37864–37874.

Shepherd, R. K., Checcarelli, N., Naini, A., De Vivo, D. C., DiMauro, S., & Sue, C. M. (2006). Measurement of ATP production in mitochondrial disorders. Journal of Inherited Metabolic Disease, 29(1), 86–91.

Sherry, S. T., Ward, M.-H., Kholodov, M., Baker, J., Phan, L., Smigielski, E. M., & Sirotkin, K. (2001). dbSNP: the NCBI database of genetic variation. Nucleic Acids Research, 29(1), 308–311.

Shin, D. W., Pan, Z., Kim, E. K., Lee, J. M., Bhat, M. B., Parness, J., … Ma, J. (2003). A Retrograde Signal from Calsequestrin for the Regulation of Store-operated Ca2+ Entry in Skeletal Muscle . Journal of Biological Chemistry, 278(5), 3286–3292.

Shuaib, A., Paasuke, R. T., & W. Brownell, A. K. (1987). Central Core Disease: CLINICAL FEATURES IN 13 PATIENTS. Medicine, 66(5), 389-396.

Sigauke, E., Rakheja, D., Kitson, K., & Bennett, M. J. (n.d.). Carnitine Palmitoyltransferase II Deficiency: A Clinical, Biochemical, and Molecular Review. Labatory Investigation, 83(11), 1543–1554.

Sim, N.-L., Kumar, P., Hu, J., Henikoff, S., Schneider, G., & Ng, P. C. (2012). SIFT web server: predicting effects of amino acid substitutions on proteins. Nucleic Acids Research, 40(1), 452–457.

Sinert, R., Kohl, L., Rainone, T., & Scalea, T. (1994). Exercise-Induced Rhabdomyolysis. Annals of Emergency Medicine, 23(6), 1301–1306.

Snoeck, M., van Engelen, B. G. M., Küsters, B., Lammens, M., Meijer, R., Molenaar, J. P. F., … Kamsteeg, E.-J. (2015). RYR1-related myopathies: a wide spectrum of phenotypes throughout life. European Journal of Neurology, 22(7), 1094–1112.

Soneson, C., & Delorenzi, M. (2013). A comparison of methods for differential expression analysis of RNA-seq data. BMC Bioinformatics, 14(1), 91.

Soneson C, L. M. and R. M. (2016). Differential analyses for RNA-seq: transcript-level estimates improve gene-level inferences [version 2; referees: 2 approved]. F1000Research, 4, 1521.

Sonna, L. A., Sawka, M. N., & Lilly, C. M. (2007). Exertional heat illness and human gene expression. In H. S. B. T.-P. in B. R. Sharma (Ed.), Neurobiology of Hyperthermia, 162, 321–346.

Sonna, L. A., Wenger, C. B., Flinn, S., Sheldon, H. K., Sawka, M. N., & Lilly, C. M. (2004). Exertional heat injury and gene expression changes: a DNA microarray analysis study. Journal of Applied Physiology, 96(5), 1943-1953.

Speakman, J. R. (2013). Measuring Energy Metabolism in the Mouse – Theoretical, Practical, and Analytical Considerations. Frontiers in Physiology, 4, 34.

Stamm, D. S., Powell, C., Stajich, J., Zismann, V., A Stephan, D., Chesnut, B., … C Speer, M. (2008). Novel congenital myopathy locus identified in Native American Indians at 12q13.13-14.1. Neurology, 71(22), 1764-1769.

Starkie, R. L., Hargreaves, M., Rolland, J., & Febbraio, M. A. (2005). Heat stress, cytokines, and the immune response to exercise. Brain, Behavior, and Immunity, 19(5), 404–412.

Steele, D. S., & Duke, A. M. (2007). Defective Mg2+ regulation of RyR1 as a causal factor in malignant hyperthermia. Archives of Biochemistry and Biophysics, 458(1), 57–64.

Stenson, P. D., Mort, M., Ball, E. V, Shaw, K., Phillips, A., & Cooper, D. N. (2014). The Human Gene Mutation Database: building a comprehensive mutation repository for clinical and molecular genetics, diagnostic testing and personalized genomic medicine. Human Genetics, 133(1), 1–9.

Stiber, J., Hawkins, A., Zhang, Z.-S., Wang, S., Burch, J., Graham, V., … Rosenberg, P. (2008). STIM1 signaling controls store operated calcium entry required for development and contractile function in skeletal muscle. Nature Cell Biology, 10(6), 688–697.

Storey, J. D., & Tibshirani, R. (2003). Statistical significance for genomewide studies. Proceedings of the National Academy of Sciences, 100(16), 9440–9445.

Sugiura, Y., Aoki, T., Sugiyama, Y., Hida, C., Ogata, M., & Yamamoto, T. (2000). Temperature-sensitive sodium channelopathy with heat-induced myotonia and cold-induced paralysis. Neurology, 54(11), 2179-2181.

Tang, Y., Lu, A., Ran, R., Aronow, B. J., Schorry, E. K., Hopkin, R. J., … Sharp, F. R. (2004). Human blood genomics: distinct profiles for gender, age and neurofibromatosis type 1. Molecular Brain Research, 132(2), 155–167.

Tate, C. A., Hyek, M. F., & Taffet, G. E. (1991). The Role of Calcium in the Energetics of Contracting Skeletal Muscle. Sports Medicine, 12(3), 208–217.

Terentyev, D., Cala, S. E., Houle, T. D., Viatchenko-Karpinski, S., Gyorke, I., Terentyeva, R., … Gyorke, S. (2005). Triadin Overexpression Stimulates Excitation-Contraction Coupling and Increases Predisposition to Cellular Arrhythmia in Cardiac Myocytes. Circulation Research, 96(6), 651-658.

The Guardian. (2015). Defence minister apologises for SAS test march deaths. The Guardian. Retrieved from http://www.theguardian.com/uk-news/2015/jul/15/defence-minister-apologises-sas-test-march-deaths.

The Times. (2015). SAS deaths were a result of catalogue of gross failures by MoD. The Times Defence. Retrieved from http://www.thetimes.co.uk/tto/news/uk/defence/article4497530.ece.

Thermo Fisher Scientific. (2017). Retrieved from https://www.thermofisher.com/uk/en/home/life-science/pcr/real-time-pcr/qpcr-education/taqman-assays-vs-sybr-green-dye-for-qpcr.html

Thomas, J., & Crowhurst, T. (2013). Exertional heat stroke, rhabdomyolysis and susceptibility to malignant hyperthermia. Internal Medicine Journal, 43(9), 1035–1038.

Thomas, K. C., Zheng, X. F., Garces Suarez, F., Raftery, J. M., Quinlan, K. G. R., Yang, N., … Houweling, P. J. (2014). Evidence Based Selection of Commonly Used RT-qPCR Reference Genes for the Analysis of Mouse Skeletal Muscle. PLOS ONE, 9(2), e88653.

Thompson, H. S., Maynard, E. B., Morales, E. R., & Scordilis, S. P. (2003). Exercise-induced HSP27, HSP70 and MAPK responses in human skeletal muscle. Acta Physiologica Scandinavica, 178(1), 61–72.

Thompson, S. J., Riazi, S., Kraeva, N., Noseworthy, M. D., Rayner, T. E., Schneiderman, J. E., … Wells, G. D. (2017). Skeletal Muscle Metabolic Dysfunction in Patients with Malignant Hyperthermia Susceptibility. Anesthesia & Analgesia, 125(2), 434-441.

Tibshirani, R. (1996). Regression Shrinkage and Selection via the Lasso. Journal of the Royal Statistical Society, 58(1), 267–288.

Tibshirani, R. (2011). Regression shrinkage and selection via the lasso: a retrospective. Journal of the Royal Statistical Society: Series B (Statistical Methodology), 73(3), 273–282.

Tobin, J. R., Jason, D. R., Challa, V. R., Nelson, T. E., & Sambuughin, N. (2001). MAlignant hyperthermia and apparent heat stroke. JAMA, 286(2), 168–169.

Tomasi, M., Canato, M., Paolini, C., Dainese, M., Reggiani, C., Volpe, P., … Nori, A. (2012). Calsequestrin (CASQ1) rescues function and structure of calcium release units in skeletal muscles of CASQ1-null mice. American Journal of Physiology-Cell Physiology, 302(3), C575-86.

Tong, J., McCarthy, T. V, & MacLennan, D. H. (1999). Measurement of Resting Cytosolic Ca2+ Concentrations and Ca2+ Store Size in HEK-293 Cells Transfected with Malignant Hyperthermia or Central Core Disease Mutant Ca2+ Release Channels. Journal of Biological Chemistry, 274(2), 693–702.

Tong, J., Oyamada, H., Demaurex, N., Grinstein, S., McCarthy, T. V, & MacLennan, D. H. (1997). Caffeine and halothane sensitivity of intracellular Ca2+ release is altered by 15 calcium release channel (ryanodine receptor) mutations associated with malignant hyperthermia and/or central core disease. Journal of Biological Chemisry, 272(42), 26332-26339.

Toyama, K., Morisaki, H., Kitamura, Y., Gross, M., Tamura, T., Nakahori, Y., … Morisaki, T. (2004). Haplotype analysis of human AMPD1 gene: origin of common mutant allele. Journal of Medical Genetics, 41(6), e74-e74.

Trapnell, C., Roberts, A., Goff, L., Pertea, G., Kim, D., Kelley, D. R., … Pachter, L. (2012). Differential gene and transcript expression analysis of RNA-seq experiments with TopHat and Cufflinks. Nature Protocols, 7(3), 562–578.

Trenker, M., Malli, R., Fertschai, I., Levak-Frank, S., & Graier, W. F. (2007). Uncoupling proteins 2 and 3 are fundamental for mitochondrial Ca(2+) uniport. Nature Cell Biology, 9(4), 445–452.

Treves, S., Vukcevic, M., Jeannet, P.-Y., Levano, S., Girard, T., Urwyler, A., … Zorzato, F. (2011). Enhanced excitation-coupled Ca2+ entry induces nuclear translocation of NFAT and contributes to IL-6 release from myotubes from patients with central core disease. Human Molecular Genetics, 20(3), 589–600.

Treves, S., Vukcevic, M., Maj, M., Thurnheer, R., Mosca, B., & Zorzato, F. (2009). Minor sarcoplasmic reticulum membrane components that modulate excitation–contraction coupling in striated muscles. The Journal of Physiology, 587(13), 3071–3079.

Tsujino, S., Shanske, S., & DiMauro, S. (1993). Molecular Genetic Heterogeneity of Myophosphorylase Deficiency (McArdle's Disease). New England Journal of Medicine, 329(4), 241–245.

Tulapurkar, M. E., Asiegbu, B. E., Singh, I. S., & Hasday, J. D. (2009). Hyperthermia in the febrile range induces HSP72 expression proportional to exposure temperature but not to HSF-1 DNA-binding activity in human lung epithelial A549 cells. Cell Stress & Chaperones, 14(5), 499–508.

Valko, M., Leibfritz, D., Moncol, J., Cronin, M. T. D., Mazur, M., & Telser, J. (2007). Free radicals and antioxidants in normal physiological functions and human disease. The International Journal of Biochemistry & Cell Biology, 39(1), 44–84.

van den Maagdenberg, A. M. J. M., Schepens, J. T. G., Schepens, M. T. M., Pepers, B., Wieringa, B., Geurts van Kessel, A., & Hendriks, W. J. A. J. (1998). Assignment of Ptprn2, the gene encoding receptor-type protein tyrosine phosphatase IA-2β, a major autoantigen in insulin-dependent diabetes mellitus, to mouse chromosome region 12F. Cytogenetic and Genome Research, 82(3–4), 153–155.

Vandesompele, J., De Preter, K., Pattyn, F., Poppe, B., Van Roy, N., De Paepe, A., & Speleman, F. (2002). Accurate normalization of real-time quantitative RT-PCR data by geometric averaging of multiple internal control genes. Genome Biology, 3(7), 1–12.

Vanuxem, P., Vanuxem, D., Raharison, L., Aubert, M., Pouliquen, G., & Deslangles, O. (2001). Maximal exercise and muscle energy metabolism after recovery from exercise hyperthermia syndrome. Muscle & Nerve, 24(8), 1071–1077.

Vattemi, G., Gualandi, F., Oosterhof, A., Marini, M., Tonin, P., Rimessi, P., … Tomelleri, G. (2010). Brody Disease: Insights into Biochemical Features of SERCA1 and Identification of a Novel Mutation. Journal of Neuropathology & Experimental Neurology, 69(3), 246–252.

Vicario, S. J., Okabajue, R., & Haltom, T. (1986). Rapid cooling in classic heatstroke: Effect on mortality rates. The American Journal of Emergency Medicine, 4(5), 394–398.

Vladutiu, G. D., Bennett, M. J., Smail, D., Wong, L.-J., Taggart, R. T., & Lindsley, H. B. (2000). A Variable Myopathy Associated with Heterozygosity for the R503C Mutation in the Carnitine Palmitoyltransferase II Gene. Molecular Genetics and Metabolism, 70(2), 134–141.

Voermans, N. C., Laan, A. E., Oosterhof, A., van Kuppevelt, A., Drost, G., Lammens, M., … van Engelen, B. G. M. (2012). G.P.103 Brody syndrome: a clinically heterogeneous entity distinct from Brody disease: A review of literature and a cross-sectional clinical study in 17 patients. Neuromuscular Disorders, 22(9), 899.

Voermans, N. C., Snoeck, M., & Jungbluth, H. (2016). RYR1-related rhabdomyolysis: A common but probably underdiagnosed manifestation of skeletal muscle ryanodine receptor dysfunction. Revue Neurologique, 172(10), 546–558.

Walder, R. Y., Landau, D., Meyer, P., Shalev, H., Tsolia, M., Borochowitz, Z., … Sheffield, V. C. (2002). Mutation of TRPM6 causes familial hypomagnesemia with secondary hypocalcemia. Nature Genetics, 31(2), 171–174.

Wang, L., Mo, X., Xu, Y., Zuo, B., Lei, M., Li, F., … Xiong, Y. (2008). Molecular characterization and expression patterns of AMP deaminase1 (AMPD1) in porcine skeletal muscle. Comparative Biochemistry and Physiology Part B: Biochemistry and Molecular Biology, 151(2), 159–166.

Wang, L., Zhang, L., Li, S., Zheng, Y., Yan, X., Chen, M., … Luo, D. (2015). Retrograde regulation of STIM1-Orai1 interaction and store-operated Ca(2+) entry by calsequestrin. Scientific Reports, 5, 11349.

Wang, S., Trumble, W. R., Liao, H., Wesson, C. R., Dunker, A. K., & Kang, C. (1998). Crystal structure of calsequestrin from rabbit skeletal muscle sarcoplasmic reticulum. Nature Structural Biology, 5, 476.

Wang, Z., Gerstein, M., & Snyder, M. (2009). RNA-Seq: a revolutionary tool for transcriptomics. Nature Reviews Genetics, 10(1), 57–63.

Wappler Frank, M. D., Fiege Marko, M. D., Steinfath Markus, M. D., Agarwal Kamayni, M. D., Scholz Jens, M. D., Singh Surjit, P. D., … Schulte am Esch Jochen, M. D. (2001). Evidence for Susceptibility to Malignant Hyperthermia in Patients with Exercise-induced Rhabdomyolysis. Anesthesiology, 94(1), 95–100.

Wehner, M., Rueffert, H., Koenig, F., Neuhaus, J., & Olthoff, D. (2002). Increased sensitivity to 4-chloro-m-cresol and caffeine in primary myotubes from malignant hyperthermia susceptible individuals carrying the ryanodine receptor 1 Thr2206Met (C6617T) mutation. Clinical Genetics, 62(2), 135–146.

Wei, L., Gallant, E. M., Dulhunty, A. F., & Beard, N. A. (2009). Junctin and triadin each activate skeletal ryanodine receptors but junctin alone mediates functional interactions with calsequestrin. The International Journal of Biochemistry & Cell Biology, 41(11), 2214–2224.

Weiss, R. G., O'Connell, K. M. S., Flucher, B. E., Allen, P. D., Grabner, M., & Dirksen, R. T. (2004). Functional analysis of the R1086H malignant hyperthermia mutation in the DHPR reveals an unexpected influence of the III-IV loop on skeletal muscle EC coupling. American Journal of Physiology - Cell Physiology, 287(4), C1094-C1102.

Welc, S. S., Clanton, T. L., Dineen, S. M., & Leon, L. R. (2013). Heat stroke activates a stress-induced cytokine response in skeletal muscle. Journal of Applied Physiology, 115(8), 1126–1137.

Welc, S. S., Phillips, N. A., Oca-Cossio, J., Wallet, S. M., Chen, D. L., & Clanton, T. L. (2012). Hyperthermia increases interleukin-6 in mouse skeletal muscle. American Journal of Physiology - Cell Physiology, 303(4), C455-C466.

Whitney, A. R., Diehn, M., Popper, S. J., Alizadeh, A. A., Boldrick, J. C., Relman, D. A., & Brown, P. O. (2003). Individuality and variation in gene expression patterns in human blood. Proceedings of the National Academy of Sciences, 100(4), 1896–1901.

Wilhelm, B. T., Marguerat, S., Watt, S., Schubert, F., Wood, V., Goodhead, I., … Bähler, J. (2008). Dynamic repertoire of a eukaryotic transcriptome surveyed at single-nucleotide resolution. Nature, 453, 1239.

Wilmshurst, J. M., Lillis, S., Zhou, H., Pillay, K., Henderson, H., Kress, W., … Jungbluth, H. (2010). RYR1 mutations are a common cause of congenital myopathies with central nuclei. Annals of Neurology, 68(5), 717–726.

Worley, P. F., Zeng, W., Huang, G. N., Yuan, J. P., Kim, J. Y., Lee, M. G., & Muallem, S. (2007). TRPC channels as STIM1-regulated store-operated channels. Cell Calcium, 42(2), 205–211.

Wu, J., Yan, Z., Li, Z., Qian, X., Lu, S., Dong, M., … Yan, N. (2016). Structure of the voltage-gated calcium channel Cav1.1 at 3.6 Å resolution. Nature, 537(7619), 191–196.

Wu, S., Ibarra, M. C. A., Malicdan, M. C. V, Murayama, K., Ichihara, Y., Kikuchi, H., … Nishino, I. (2006). Central core disease is due to RYR1 mutations in more than 90% of patients. Brain, 129(6), 1470–1480.

Xiao, B., Coste, B., Mathur, J., & Patapoutian, A. (2011). Temperature-dependent STIM1 activation induces Ca(2+) influx and modulates gene expression. Nature Chemical Biology, 7(6), 351–358.

Xu, L., Wang, Y., Yamaguchi, N., Pasek, D. A., & Meissner, G. (2008). Single Channel Properties of Heterotetrameric Mutant RyR1 Ion Channels Linked to Core Myopathies. The Journal of Biological Chemistry, 283(10), 6321–6329.

Yan, Z., Bai, X., Yan, C., Wu, J., Li, Z., Xie, T., … Yan, N. (2015). Structure of the rabbit ryanodine receptor RyR1 at near-atomic resolution. Nature, 517(7532), 50–55.

Yang, T., Esteve, E., Pessah, I. N., Molinski, T. F., Allen, P. D., & López, J. R. (2007). Elevated resting Ca2+ in myotubes expressing malignant hyperthermia RyR1 cDNAs is partially restored by modulation of passive calcium leak from the SR. American Journal of Physiology - Cell Physiology, 292(5), C1591-C1598.

Yang, T., Riehl, J., Esteve, E., Matthaei, K. I., Goth, S., Allen, P. D., … Lopez, J. R. (2006). Pharmacologic and functional characterization of malignant hyperthermia in the R163C RyR1 knock-in mouse. Anesthesiology, 105(6), 1164–1175.

Yang, T., Ta, T. A., Pessah, I. N., & Allen, P. D. (2003). Functional Defects in Six Ryanodine Receptor Isoform-1 (RyR1) Mutations Associated with Malignant Hyperthermia and Their Impact on Skeletal Excitation-Contraction Coupling. Journal of Biological Chemistry, 278(28), 25722–25730.

Yao, M., Cai, M., Yao, D., Xu, X., Yang, R., Li, Y., … Yao, D. (2015). Abbreviated Half-Lives and Impaired Fuel Utilization in Carnitine Palmitoyltransferase II Variant Fibroblasts. PLOS ONE, 10(3), e0119936.

Yarotskyy, V., & Dirksen, R. T. (2012). Temperature and RyR1 Regulate the Activation Rate of Store-Operated Ca2+ Entry Current in Myotubes. Biophysical Journal, 103(2), 202–211.

Yarotskyy, V., Protasi, F., & Dirksen, R. T. (2013). Accelerated Activation of SOCE Current in Myotubes from Two Mouse Models of Anesthetic- and Heat-Induced Sudden Death. PLOS ONE, 8(10), e77633.

Yasuno, T., Kaneoka, H., Tokuyasu, T., Aoki, J., Yoshida, S., Takayanagi, M., … Saito, T. (2008). Mutations of carnitine palmitoyltransferase II (CPT II) in Japanese patients with CPT II deficiency. Clinical Genetics, 73(5), 496–501.

Ylänen, K., Poutanen, T., Hiippala, A., Swan, H., & Korppi, M. (2010). Catecholaminergic polymorphic ventricular tachycardia. European Journal of Pediatrics, 169(5), 535–542.

Yoshinaga, H., Sakoda, S., Good, J.-M., Takahashi, M. P., Kubota, T., Arikawa-Hirasawa, E., … Ohtsuka, Y. (2012). A novel mutation in SCN4A causes severe myotonia and school-age-onset paralytic episodes. Journal of the Neurological Sciences, 315(1), 15–19.

Yuan, Q., Fan, G.-C., Dong, M., Altschafl, B., Diwan, A., Ren, X., … Kranias, E. G. (2007). Sarcoplasmic Reticulum Calcium Overloading in Junctin Deficiency Enhances Cardiac Contractility but Increases Ventricular Automaticity. Circulation, 115(3), 300-309.

Yuen, B., Boncompagni, S., Feng, W., Yang, T., Lopez, J. R., Matthaei, K. I., … Pessah, I. N. (2012). Mice expressing T4826I-RYR1 are viable but exhibit sex- and genotype-dependent susceptibility to malignant hyperthermia and muscle damage. The Federation of American Societies for Experimental Biology (FASEB) Journal, 26(3), 1311–1322.

Zhang, J., George, A. L., Griggs, R. C., Fouad, G. T., Roberts, J., Kwiecinski, H., … Ptacek, L. J. (1996). Mutations in the human skeletal muscle chloride channel gene (CLCN1) associated with dominant and recessive myotonia congenita. Neurology, 47(4), 993-998.

Zhang, L., Franzini-Armstrong, C., Ramesh, V., & Jones, L. R. (2001). Structural Alterations in Cardiac Calcium Release Units Resulting from Overexpression of Junctin. Journal of Molecular and Cellular Cardiology, 33(2), 233–247.

Zhang, L., Kelley, J., Schmeisser, G., Kobayashi, Y. M., & Jones, L. R. (1997). Complex Formation between Junctin, Triadin, Calsequestrin, and the Ryanodine Receptor: Proteins of the cardiac junctional sarcoplasmic reticulum. Journal of Biological Chemistry, 272(37), 23389–23397.

Zhao, X., Min, C. K., Ko, J.-K., Parness, J., Kim, D. H., Weisleder, N., & Ma, J. (2010). Increased Store-Operated Ca(2+) Entry in Skeletal Muscle with Reduced Calsequestrin-1 Expression. Biophysical Journal, 99(5), 1556–1564.

Zhou, H., Jungbluth, H., Sewry, C. A., Feng, L., Bertini, E., Bushby, K., … Muntoni, F. (2007). Molecular mechanisms and phenotypic variation in RYR1-related congenital myopathies. Brain, 130(8), 2024–2036.

Zhou, H., Lillis, S., Loy, R. E., Ghassemi, F., Rose, M. R., Norwood, F., … Jungbluth, H. (2010). Multi-minicore disease and atypical periodic paralysis associated with novel mutations in the skeletal muscle ryanodine receptor (RYR1) gene. Neuromuscular Disorders, 20(3), 166–173.

Zhou, L. Z.-H., Johnson, A. P., & Rando, T. A. (2001). NFκB and AP-1 mediate transcriptional responses to oxidative stress in skeletal muscle cells. Free Radical Biology and Medicine, 31(11), 1405–1416.

Zullo, A., Klingler, W., De Sarno, C., Ferrara, M., Fortunato, G., Perrotta, G., … Carsana, A. (2009). Functional characterization of ryanodine receptor (RYR1) sequence variants using a metabolic assay in immortalized B-lymphocytes. Human Mutation, 30(4), E575–E590.

Zvaritch, E., Depreux, F., Kraeva, N., Loy, R. E., Goonasekera, S. A., Boncompagni, S., … MacLennan, D. H. (2007). An Ryr1 I4895T mutation abolishes Ca2+ release channel function and delays development in homozygous offspring of a mutant mouse line. Proceedings of the National Academy of Sciences, 104(47), 18537–18542.

Zvaritch, E., Kraeva, N., Bombardier, E., McCloy, R. A., Depreux, F., Holmyard, D., … MacLennan, D. H. (2009). Ca2+ dysregulation in Ryr1 I4895T/wt mice causes congenital myopathy with progressive formation of minicores, cores, and nemaline rods. Proceedings of the National Academy of Sciences, 106(51), 21813–21818.

Appendix A: Fluidigm® SNP Type™ genotyping primer sequences

ASSAY	ASP1_SEQ	ASP2_SEQ	LSP_SEQ	STA_SEQ
ACADVL_H259Q	CCAAACCTTCCATTGTTGAGGATG	CCAAACCTTCCATTGTTGAGGATT	GAGTGGCTTCAAGGTTGCCAT	TCATGGTACCTGCCAGGG
ACADVL_V207A	GAAGGAGAAGATCACAGCTTTTGC	TGAAGGAGAAGATCACAGCTTTTGT	ACTGGGTAATGCCCCCGA	AGATCCAGCCACAGGAGC
AMPD1_M340I	ACGCAGCAGATGTTTCTGGTTA	CGCAGCAGATGTTTCTGGTTC	CCATATCCATGCAGCCGCTT	CTCTGTCAGCATCAATTTGGTAAGA
AMPD1_R104H	ACAGTCTTCCGTCCTTGGAAAC	ACAGTCTTCCGTCCTTGGAAAT	CGCCTGATGAAGACAAAATTAACTCTTACTT	GATGTTTCACTTAGTGGAATGGACA
AMPD1_R64C	AAAGGGGGAAATCTCCTGACG	CAAAGGGGGAAATCTCCTGACA	GCAATGCGCAACTTTGCTGAA	CGGACAGATCTCATCCACATCA
ASPH_K88T	CAGTGGGGTAGCCAAGAGAAA	AGTGGGGTAGCCAAGAGAAC	AGGCTAATTTGAAAAAATGAAAATACCTTTAGCCT	TTGTAAATGTCAACAGAAGGACCC
ASPH_A85P	CCTTTAGCCTTAGTTTTTCTCTTGGC	CCTTTAGCCTTAGTTTTTCTCTTGGG	ACAGAAGGACCCAGTGGGG	ACTTGATTCACTCAAGGCTAATTTGA
ASPH_V84G	CCTTTAGCCTTAGTTTTTCTCTTGGCTA	CTTTAGCCTTAGTTTTTCTCTTGGCTC	TGTAAATGTCAACAGAAGGACCCAGT	ACTTGATTCACTCAAGGCTAATTTGA
ASPH_R397C	GAAATTGTTGCCTGTCTGAGCA	GAAATTGTTGCCTGTCTGAGCG	TGCAGACCTGCTGAAGCTGA	TGAATTACCTTTGATTGCATCTTACCT
ATP2A1_D650N	CCCGTGTAGGCGCGATC	CCCGTGTAGGCGCGATT	CTGCCGGCGAATTGGCAT	AGGTCGTCGAACTCTCGG
ATP2A1_P540L	GCCATGATCTTTTCCTTCACCG	GCCATGATCTTTTCCTTCACCA	CGAGTTGGCACCACCCG	AGTGCCCCACTCCTTGATC
ATP2A1_T538M	GCGCAGGGTGTCCCG	GCGCAGGGTGTCCCA	TCATGGCGGTGATCAAGGAGT	GCCAGGGCCAAGCAG
CACNA1S_G258D	CCGGTGCACCATCAATGG	GCCGGTGCACCATCAATGA	GCCATGGTTGGGCCCTG	GCCAGGACGGGCTCAG
CACNA1S_R498H	ACCACGAAGCAGTCGAAGC	ACCACGAAGCAGTCGAAGT	GGGCCTGCGCCAGTAC	ATCTCCAGGATACCGCTACAC
CACNA1S_R683C	TCACTTGGACATCTTCCTGCG	TCACTTGGACATCTTCCTGCA	AGAGCCTGACTTCTGCCCAG	CCTTCCTGCTAAGGAAGCAC
CACNA1S_S606N	TTCCCCAAGCCCTCATCAG	TTTCCCCAAGCCCTCATCAA	CACGCAGAGGGAGAGCCTAC	GAAGTACGGCGCAGCAA
CACNA2D1_D1045A	CCAAGACATTGTTATCAAAGCAGACAT	CCAAGACATTGTTATCAAAGCAGACAG	GGTCCAAATCCTTGTGACATGGT	TCCAGTAGAAGTGTGATCTTACCAA
CALR_P245A	TCGGGCTTCTTAGCATCAGG	TCGGGCTTCTTAGCATCAGC	ACTGGGACAAGCCCGAGC	TCTCCGTCCATCTCTTCATCC
CASQ1_D44N	GCTGGACTTCCCTGAGTACG	GCTGGACTTCCCTGAGTACA	TGATCACACGGTCCACACCA	AGGGACACCCAAGTCAGG
CASQ1_F186Y	CGCTCTGAGTCTTTGCTCTTGA	CGCTCTGAGTCTTTGCTCTTGT	CGAGAGCTGCAGGCGTTT	GGAGTCTGAGGGTTACCCA
CLCN1_R300Q	CCTCCACCTACTTTGCTGTTCA	CCTCCACCTACTTTGCTGTTCG	TGTTCCACACTGCCAGCACT	AGGTCACCTCCACCTACT
HOMER1_P142L	TCTGTCCCGTTGATACTTTCCG	CATCTGTCCCGTTGATACTTTCCA	CAGGCGGGGATCTTCAGTCT	GTCACATCAGGTGTTCTTTCATCA
HSPB1_T151S	CCGGTGTGGACCCCAC	CCGGTGTGGACCCCAG	GGGACAGGGAGGAGGAAACTT	CCTCTCTGCACGTCCAGG
NEB_S164L	CTTACCTTACTGACTTGCTGCG	CCTTACCTTACTGACTTGCTGCA	AGCAAAGGATATTGAACATGCAAAGAAAGT	ACCCCAGCCATCCATATCAT
PYGM_427R>W	GGACGTAGACCGGCTGC	GGACGTAGACCGGCTGT	GCCATGTTGATGCGCTTCACT	CGGCCGCATTCCCAG
PYGM_A105S	GCAACCCCTGGGAGAAGT	GCAACCCCTGGGAGAAGG	CTGGTGTGCTCCACATGGC	CTGGCTTCGCTACGGC
PYGM_R50*	GCCAGAGCAAAGTAGTAGTCTCA	GCCAGAGCAAAGTAGTAGTCTCG	CCGGCACCTGCATTTCACA	GTCGCGCACGGTATGG
RYR1_D4505H	CCCCAAGGCCACTCACTC	CCCCAAGGCCACTCACTG	CAGAGCCCGAGCCGGAA	GGCTAGGCCCCTCAGC
RYR1_H3981Y	CGTCCCATAGGCGACTGTG	CGTCCCATAGGCGACTGTA	CTCTGCCTCCCAGGGTCC	CAGGAATCCCACCACTGC
RYR1_I3253T	GCGGCTCATGGCAGACAT	CGGCTCATGGCAGACAC	CTCTGTGTAGCGGGCACCT	CCGACATCCCGGTGCT
RYR1_R1622Q	CGTGCCGGCGAGCG	CGTGCCGGCGAGCA	GCAGCGCCATCATGGTCAG	CCTGCAGGTGGAGACGA
RYR1_R3366H	ATCGGGCGGCTGCG	CTATCGGGCGGCTGCA	GCTGCTCCTCCTCGGACA	AGTCCCACTTCATCCCAACTA
RYR1_R492H	AGCAGTGGTGTAGACATTTAGGC	CAGCAGTGGTGTAGACATTTAGGT	GGGATGCTCTCCATGGTCCT	TGCAAACTCAGCAAAGTGGG
RYR1_S2776F	CATCTCTAGATCCAGAACAACTGGTC	CATCTCTAGATCCAGAACAACTGGTT	TCTTCAGCTCCTCGTCTATGTT	CACCCTGCCTCCCCTC
RYR1_T3711M	CAAGAGTCTTCACCTCTTTTCCG	GCAAGAGTCTTCACCTCTTTTCCA	CCCCTGCACCAGTTGGTC	GGGCCCTGGCAAGAGT
SCN4A_D1435H	CACGAAGTACTTCTGGATCAGGTC	ACGAAGTACTTCTGGATCAGGTG	ACTAGCTTCTCCCCGCAGG	ACGGAACAGCGTGGGT
SCN4A_N591K	CCATCTGCATCGTGCTCAAC	ACCATCTGCATCGTGCTCAAA	GTCAAAGTGCTCCGTCATGGG	GTGGACCTGGGCATCAC
SCN4A_R1745C	CCGGCACCTGCTACAGC	CCGGCACCTGCTACAGT	GCTGCCGTCGTGGCT	CCAGAGGGCCTACCGC
SCN4A_V730M	GCAAGAGCTACAAGGAGTGCG	GCAAGAGCTACAAGGAGTGCA	CCAGCGCGGCAGGTT	GTGGGCATGCAGCTGTT

Appendix A table (continued)

ASSAY	ASP1_SEQ	ASP2_SEQ	LSP_SEQ	STA_SEQ
SLC8A3_P402S	CAGGCACTGGTAAGAACATGG	CCAGGCACTGGTAAGAACATGA	CACCGATGAGCCTGAGGACT	ACAGCCCCACAGTTCTCC
SLC8A3_R314G	CTTGAGAATCCGGATCATCTCTCC	CTTGAGAATCCGGATCATCTCTCT	ACCTGGTGCCCCTGGAA	TGGGTGTTTTTGCTTCAGATCC
SLC8A3_R355L	TCATCATACGAGTGGCTTGGATAC	GTCATCATACGAGTGGCTTGGATAA	TCCCACCAACAGAAGAGCCG	AGGATATTGCCTGCACCAGT
SLC8A3_V152M	ATTCAGTCACAGCTGTTGTTTTCG	GATTCAGTCACAGCTGTTGTTTTCA	ACCTCTCACTCTCACCTGGGA	CTGCACCATTGGTCTCAAAGA
SRL_R398C	GAAGTCCTTATAGGCCTCGCG	GAAGTCCTTATAGGCCTCGCA	CTGGCAAAGACCAATGTCAGCA	AAATGGGATTGATGCCGAAGAA
STIM1_S613Y	GGTGGCTCTCCACATTTGGATTA	GTGGCTCTCCACATTTGGATTC	CCCCAACTGGAGATGGTGTGT	CCCTCAGCCCCACCTG
STIM1_T504M	CCATGCTGTGGCTCCG	GCCATGCTGTGGCTCCA	TCCTTGCAGCCCCTAGCC	AACCTCTGAGATCCCAGGC
SYPL2_R65H	CTTGGCTTCGTTGTTGCAGT	TTGGCTTCGTTGTTGCAGC	CGGGTCCTGTGGCTCCT	GATGATGGAGCTCACGTCC
TRDN_E135K	CCTTTTTTTCTCAAGGGAGGCTC	CCTTTTTTTCTCAAGGGAGGCTT	CTAACTTTGTTTTTCTTTTAATCTTGGTCTAGGAGAAA	TCAAAGGTGAAAACAACTAACCTTTTTTT
TRDN_S339N	CATCAATGGCAGTTTCCTTCTCAT	CATCAATGGCAGTTTCCTTCTCAC	TCTTATTTTACCAGCAGAAAAAGAAGATATCAAAAAGAAAAGGAAACAAAGAAAGTGCAATACCT	
TRPM6_G166R	GCCTTCAGTTATTATCCACGCTCC	GCCTTCAGTTATTATCCACGCTCT	GCCAAGGTTTGGTTAAAGCTGCA	GGGAGCTTTACCTGTATTGATGC
TRPM6_M1088R	AATACAACCGCTATCGCTACATCAT	ACAACCGCTATCGCTACATCAG	CAGCCAGGGCTTCTCGTG	TGGAATCCATTTCAAATAACCTGTGG

All primer sequences are written in the 5’ to 3’ orientation.

Appendix B: Generic steps to RNA-seq analysis

1. Run .FASTQ files on FastQC to quality check using default settings.

2. Trim .FASTQ reads to remove adapter contamination using Cutadapt. Trims Illumina TruSeq index prefix in read 1 'AGATCGGAAGAGCACACGTCTGAACTCCAGTCAC' and the reverse compliment of TruSeq universal adapter in read 2 'AGATCGGAAGAGCGTCGTGTAGGGAAAGAGTGTAGATCTCGGTGGTCGCCGTATCATT'. The package also trims reads with quality less than 2 (-q 20) and short than 20 (-m 20).

3. Run trimmed .FASTQ files on FastQC using default settings.

4. Align reads using Kallisto v0.43.0 pseudo-aligner and either the downloaded human reference (GRCh38-ensembl85) or mouse reference GRCm38-ensembl85) genome.

5. RNA-seq data were analysed using DESeq2 version 1.15.2 according the developer's instruction manual, updated on 28th October 2016 and downloaded from Bioconductor.

6. Import abudance.tsv files into Rstudio using Tximport. Create a vector containing the file path directing the programme towards the Kallisto files. Create a data frame linking the transcript ID to the gene ID to allow gene-level summarisation.

7. A model is specified using the biological information for each sample, for example 'design= ~ status + timepoint + status:timepoint'. Factor levels are defined within the DESeq2 datset.

8. Differential gene expression analysis is performed using the DESEq2 function and model design.

9. Results for specific pair-wise comparisons or model terms can be extracted using the 'results' function.

10. Additional annotation information can be added to the results tables prior to export to Excel files.

11. Data can be transformed using the 'rlog' function, which transforms the counts using the regularised logarithm transformation to stabilise variance to remove high variance from low counts.

12. The ggplot2 package can be used to perform a principal component analysis (PCA) to measure genetic distance between the samples and identify sample outliers and groupings at the whole-transciptome level.

13. Individual genes counts can be extracted from DESeq2 and plotted using ggplot2.

Appendix C: Table of human immune response genes differentially expressed in response to heat.

Gene ID	Ensembl ID	LFC_2 hr	lfc_SE	*p* value	*p* adj	LFC_24hr	lfc_SE	*p* value	*p* adj
APOBEC3C	ENSG00000244509.3	-0.4079	0.1003	0.0000	0.0005	-0.3011	0.1002	0.0027	0.0108
APOBEC3D	ENSG00000243811.7	-0.3833	0.0757	0.0000	0.0000	-0.2771	0.0755	0.0002	0.0016
ATG12	ENSG00000145782.12	0.3338	0.1089	0.0022	0.0120	0.4163	0.1087	0.0001	0.0010
B2M	ENSG00000166710.17	0.4524	0.1688	0.0074	0.0326	0.7898	0.2923	0.0069	0.0233
BCL6	ENSG00000113916.17	1.3412	0.1302	0.0000	0.0000	0.3630	0.1302	0.0053	0.0187
BTNL8	ENSG00000113303.11	1.0355	0.1354	0.0000	0.0000	-0.3472	0.1357	0.0105	0.0328
C8G	ENSG00000176919.11	-0.6820	0.1738	0.0001	0.0008	-0.6152	0.1705	0.0003	0.0020
CACTIN	ENSG00000105298.13	-0.1748	0.0542	0.0013	0.0077	-0.2243	0.0540	0.0000	0.0004
CD300A	ENSG00000167851.13	0.2875	0.0904	0.0015	0.0086	-0.2881	0.0904	0.0014	0.0065
CD3E	ENSG00000198851.9	-0.3419	0.1006	0.0007	0.0045	-0.3218	0.1005	0.0014	0.0063
CD4	ENSG00000010610.9	-0.3743	0.1154	0.0012	0.0072	-0.3118	0.1154	0.0069	0.0232
CD46	ENSG00000117335.19	0.7694	0.1376	0.0000	0.0000	0.6594	0.1376	0.0000	0.0001
CD6	ENSG00000013725.14	-0.2611	0.0864	0.0025	0.0136	-0.2508	0.0864	0.0037	0.0141
CD7	ENSG00000173762.7	-0.5225	0.1197	0.0000	0.0002	-0.5081	0.1197	0.0000	0.0003
CD74	ENSG00000019582.14	-0.2774	0.1077	0.0100	0.0422	-0.4314	0.1077	0.0001	0.0006
CFP	ENSG00000126759.12	0.4291	0.1343	0.0014	0.0083	-0.5168	0.1343	0.0001	0.0010
CHID1	ENSG00000177830.17	-0.2654	0.0823	0.0013	0.0076	-0.3427	0.0821	0.0000	0.0004
CLEC6A	ENSG00000205846.3	0.9222	0.2236	0.0000	0.0004	0.7766	0.2230	0.0005	0.0028
CLEC7A	ENSG00000172243.17	0.4279	0.1181	0.0003	0.0022	0.3852	0.1181	0.0011	0.0053
CNPY3	ENSG00000137161.16	0.3485	0.1071	0.0011	0.0070	-0.4294	0.1071	0.0001	0.0006
CR1	ENSG00000203710.10	0.9548	0.1308	0.0000	0.0000	0.4791	0.1308	0.0003	0.0017
CYLD	ENSG00000083799.17	0.2679	0.1003	0.0075	0.0333	0.4566	0.1002	0.0000	0.0001
DBNL	ENSG00000136279.19	0.2998	0.1071	0.0051	0.0243	-0.3345	0.1072	0.0018	0.0079
DDX3X	ENSG00000215301.9	0.5722	0.1492	0.0001	0.0011	0.7681	0.1492	0.0000	0.0000
DHX58	ENSG00000108771.12	-0.2583	0.0814	0.0015	0.0089	-0.3431	0.0813	0.0000	0.0003
F2RL1	ENSG00000164251.4	0.5139	0.1387	0.0002	0.0017	0.4769	0.1386	0.0006	0.0032
FADD	ENSG00000168040.4	0.6014	0.1063	0.0000	0.0000	-0.3073	0.1064	0.0039	0.0146
FGR	ENSG00000000938.12	0.3666	0.0907	0.0001	0.0005	-0.2430	0.0907	0.0073	0.0245

Appendix C table continued (1)

Gene ID	Ensembl ID	LFC_2 hr	lfc_SE	*p* value	*p* adj	LFC_24hr	lfc_SE	*p* value	*p* adj
GZMM	ENSG00000197540.7	-0.7686	0.1162	0.0000	0.0000	-0.4082	0.1161	0.0004	0.0026
HCK	ENSG00000101336.12	0.4752	0.1078	0.0000	0.0001	-0.3355	0.1078	0.0019	0.0080
HMGB2	ENSG00000164104.11	0.7428	0.1742	0.0000	0.0002	0.4302	0.1742	0.0135	0.0405
IFIT2	ENSG00000119922.9	0.6321	0.1527	0.0000	0.0004	0.3630	0.1527	0.0174	0.0497
IFITM2	ENSG00000185201.16	0.7045	0.1586	0.0000	0.0001	-0.6141	0.1586	0.0001	0.0009
IL1RAP	ENSG00000196083.9	0.6327	0.1318	0.0000	0.0000	0.3396	0.1318	0.0100	0.0314
IRAK4	ENSG00000198001.13	0.2631	0.0971	0.0067	0.0302	0.4079	0.0971	0.0000	0.0003
ITCH	ENSG00000078747.13	0.3685	0.0999	0.0002	0.0018	0.3898	0.0999	0.0001	0.0008
ITK	ENSG00000113263.12	-0.2712	0.0996	0.0065	0.0293	0.3685	0.0995	0.0002	0.0015
LAT	ENSG00000213658.10	-0.3260	0.0900	0.0003	0.0022	-0.3624	0.0899	0.0001	0.0005
LAT2	ENSG00000086730.16	0.7094	0.0925	0.0000	0.0000	-0.2418	0.0925	0.0089	0.0288
LILRB5	ENSG00000274311.4	0.7447	0.2865	0.0094	0.0398	-0.5348	0.1608	0.0009	0.0044
LIME1	ENSG00000203896.9	-0.3412	0.1090	0.0017	0.0100	-0.3729	0.1089	0.0006	0.0034
LRMP	ENSG00000118308.15	0.6319	0.0876	0.0000	0.0000	0.3253	0.0876	0.0002	0.0014
LY96	ENSG00000154589.6	0.7585	0.2223	0.0006	0.0043	0.5325	0.2222	0.0166	0.0477
MIF	ENSG00000240972.1	-0.2960	0.0951	0.0019	0.0105	-0.3286	0.0950	0.0005	0.0031
MR1	ENSG00000153029.14	0.2080	0.0515	0.0001	0.0005	0.1499	0.0514	0.0035	0.0135
MSRB1	ENSG00000198736.11	0.8123	0.1346	0.0000	0.0000	-0.4339	0.1346	0.0013	0.0059
MYD88	ENSG00000172936.12	0.3361	0.1007	0.0008	0.0054	-0.2575	0.1007	0.0106	0.0330
MYO1G	ENSG00000136286.14	-0.3375	0.0949	0.0004	0.0028	-0.3999	0.0949	0.0000	0.0003
NLRP1	ENSG00000091592.15	0.2619	0.0906	0.0038	0.0191	-0.2184	0.0906	0.0159	0.0461
NLRX1	ENSG00000160703.15	0.6690	0.1252	0.0000	0.0000	-0.3722	0.1253	0.0030	0.0118
ORAI1	ENSG00000276045.2	-0.2179	0.0857	0.0110	0.0455	-0.3864	0.0857	0.0000	0.0001
PGLYRP1	ENSG00000008438.4	1.0491	0.1976	0.0000	0.0000	-0.4854	0.1977	0.0141	0.0418
PIK3CG	ENSG00000105851.10	0.5727	0.1172	0.0000	0.0000	0.3691	0.1172	0.0016	0.0073
POLR3C	ENSG00000186141.8	-0.2956	0.0534	0.0000	0.0000	-0.1407	0.0529	0.0078	0.0259
POLR3E	ENSG00000058600.15	-0.2017	0.0684	0.0032	0.0165	0.1648	0.0680	0.0154	0.0450
POLR3H	ENSG00000100413.16	-0.4081	0.0696	0.0000	0.0000	-0.1719	0.0692	0.0131	0.0393
PSTPIP1	ENSG00000140368.12	0.2815	0.1113	0.0114	0.0469	-0.3758	0.1113	0.0007	0.0039
PTK2B	ENSG00000120899.17	0.4912	0.0854	0.0000	0.0000	-0.2200	0.0854	0.0100	0.0315
RNF135	ENSG00000181481.13	0.3105	0.0676	0.0000	0.0001	-0.1791	0.0676	0.0081	0.0266

Appendix C table continued (2)

Gene ID	Ensembl ID	LFC_2 hr	lfc_SE	*p* value	*p* adj	LFC_24hr	lfc_SE	*p* value	*p* adj
SERINC3	ENSG00000132824.13	0.4858	0.0716	0.0000	0.0000	0.1950	0.0716	0.0065	0.0221
SFTPD	ENSG00000133661.15	-0.8969	0.1771	0.0000	0.0000	-0.4736	0.1713	0.0057	0.0199
SKAP1	ENSG00000141293.15	-0.4220	0.0855	0.0000	0.0000	-0.2103	0.0853	0.0137	0.0408
SPON2	ENSG00000159674.11	-1.1975	0.1805	0.0000	0.0000	-0.4713	0.1804	0.0090	0.0289
SRC	ENSG00000197122.11	-0.3685	0.1019	0.0003	0.0023	-0.4617	0.1018	0.0000	0.0001
TBK1	ENSG00000183735.9	0.4684	0.1520	0.0021	0.0115	0.4973	0.1519	0.0011	0.0051
TBKBP1	ENSG00000198933.9	0.4663	0.1350	0.0006	0.0038	-0.4556	0.1351	0.0007	0.0039
TFE3	ENSG00000068323.16	0.5427	0.0984	0.0000	0.0000	-0.3530	0.0985	0.0003	0.0021
TIRAP	ENSG00000150455.13	0.2774	0.0862	0.0013	0.0078	0.3034	0.0859	0.0004	0.0024
TLR1	ENSG00000174125.7	0.8818	0.1185	0.0000	0.0000	0.4042	0.1185	0.0006	0.0035
TLR10	ENSG00000174123.10	0.5817	0.1628	0.0004	0.0026	0.6078	0.1627	0.0002	0.0013
TLR4	ENSG00000136869.13	0.8991	0.1163	0.0000	0.0000	0.3920	0.1163	0.0008	0.0039
TLR6	ENSG00000174130.12	0.6699	0.1170	0.0000	0.0000	0.3917	0.1170	0.0008	0.0042
TLR8	ENSG00000101916.11	0.7555	0.1023	0.0000	0.0000	0.3302	0.1023	0.0012	0.0058
TNFAIP8L2	ENSG00000163154.5	0.2845	0.0900	0.0016	0.0091	-0.2919	0.0900	0.0012	0.0056
TRIM25	ENSG00000121060.15	0.8877	0.1201	0.0000	0.0000	0.3562	0.1202	0.0030	0.0120
TRIM56	ENSG00000169871.12	0.1750	0.0495	0.0004	0.0029	0.1295	0.0494	0.0088	0.0284
TRPM4	ENSG00000130529.15	0.6035	0.1326	0.0000	0.0001	-0.4264	0.1332	0.0014	0.0063
TXK	ENSG00000074966.10	-0.4111	0.1527	0.0071	0.0315	0.6158	0.1523	0.0001	0.0005
ZAP70	ENSG00000115085.13	-0.4950	0.0780	0.0000	0.0000	-0.3416	0.0780	0.0000	0.0002